University of Southampton

National Oceanography Centre

Variability of the Arctic freshwater export west of Greenland:

a proxy from 65 years of hydrographic observations on the Labrador Shelf

Thesis for the degree of Doctor of Philosophy

Author:
Cristian Florindo-López

Supervisors:
N. Penny Holliday,
Sheldon Bacon,
Yevgeny Aksenov, and
Eleanor Frajka-Williams

20th June 2018

UNIVERSITY OF SOUTHAMPTON

ABSTRACT

FACULTY OF NATURAL AND ENVIRONMENTAL SCIENCES

National Oceanography Centre

Doctor of Philosophy

Variability of the Arctic freshwater export west of Greenland:

a proxy from 65 years of hydrographic observations on the Labrador Shelf

by Cristian Florindo-López

The Arctic Ocean has increased significantly its storage of freshwater over the past two decades. It is a major source of freshwater to the subpolar North Atlantic, where it has the potential to freshen deep-water formation regions, disrupt the meridional overturning circulation and severely affect the European (and even global) climate. This manuscript describes, for the first time, the multidecadal (1950 to 2014) variability of the Arctic freshwater export west of Greenland from observations, with the purpose of investigating how the freshwater budgets of the Arctic and the North Atlantic connect through these fluxes. First, this thesis processes repeated hydrographic observations at the Seal Island section (on the Labrador shelf) and produces a multidecadal dataset of gridded summer sections of temperature, salinity and density. Then, a high-resolution coupled ice-ocean global general circulation model is used to describe the circulation on the Labrador shelf region and to put the observations in context. The regional circulation is dominated by the Labrador current, which presents a dual core with different dynamics. Its upper component carries the Arctic freshwater export west of Greenland and, at the Seal Island section, it fills the mid-shelf with this water. The newly named Labrador Coastal current is a continuation of the Hudson Strait outflow and contains the Hudson water inshore (in the first 50 km of the shelf). This makes it possible to identify the signal of Arctic freshwater at the Seal Island observations. The observed freshwater transport (referenced to salinity 35.0) of this Arctic signal is used as a proxy for the variability of the Arctic freshwater export west of Greenland over 65 years of data. Two periods of enhanced export (1955-1960 and 1968-1994) and two periods of decreased transport (1960-1968 and 1994-present)

are identified. The variability shown by the proxy is compared to observed and modelled changes in the Arctic and the North Atlantic freshwater budgets. This is to test the hypothesis that an increased storage of freshwater in the Arctic results in a decreased export and a reduction in the freshwater content of the subpolar North Atlantic, and otherwise. The transport shown by the proxy totals to an accumulated increase of ∼22000 km^3 from 1965 to 1995 and an accumulated decrease of ∼16000 km^3 from 1995 to 2014. This fully accounts for the magnitude of the changes observed in the Arctic and the North Atlantic budgets during the same periods, and comparable changes are also found throughout the full time series. This indicates that the advection of freshwater west of Greenland has a key role in the freshwater balance of these budgets. This also underlines the relevance of the freshwater export west of Greenland to the total magnitude of the export and the impacts on the North Atlantic.

Contents

List of Tables

List of Figures

Academic Thesis: Declaration Of Authorship

I, Cristian Florindo-López, declare that this thesis and the work presented in it are my own and has been generated by me as the result of my own original research.

I confirm that:

1. This work was done wholly or mainly while in candidature for a research degree at this University;

.

2. Where any part of this thesis has previously been submitted for a degree or any other qualification at this University or any other institution, this has been clearly stated;

3. Where I have consulted the published work of others, this is always clearly attributed;

4. Where I have quoted from the work of others, the source is always given. With the exception of such quotations, this thesis is entirely my own work;

5. I have acknowledged all main sources of help;

6. Where the thesis is based on work done by myself jointly with others, I have made clear exactly what was done by others and what I have contributed myself;

7. Either none of this work has been published before submission, or if parts of this work have been published this will be specified where applicable.

Signed:

Date: 12-05-2017

Acknowledgements

First, I would like to thank all my supervisors. I am really grateful for their endless help and expertise, and I feel really fortunate to have been supported by this team. Working with Sheldon has been captivating and thought-provoking. His broad expertise still keeps amazing me to date. I want to thank Yevgeny for our endless meetings, his patience showing me the ropes in how to deal with the model and troubleshooting the diverse programming issues. I am especially thankful to Penny. She has not only been extremely supportive through the tough years of pursuing this PhD, but she has also been a role model whom I admire. Her knowledge, wisdom and approach to science have forged my idea of what a researcher is.

I would also like to thank Eleanor for the work and the endless discussions outside of this PhD. Working together and demonstrating for her class has been an excellent experience. Thank you also to Eugene Colbourne, who has been a fundamental collaborator to this work and who has provided the data used here. I am looking forward to continue collaborating in the publications to follow this thesis. Thank you to George Nurser too, for his support as panel chair and to Bob Marsh and Stephen Dye for extensively examining this thesis.

I also greatly appreciate everyone who has helped throughout my PhD, although it is perhaps impossible to mention everyone. I want to thank my officemates for the mutual support and procrastination. To Lena Schulz and Liz Comer for their technical support trying to figure out a right colour scale for the Labrador Sea salinity. Thanks to Helen Burns, Maike Sonnewald and Jeff for their endless computing help. The team of students working with Ariane has also been hugely supportive: Lena again, Josie Robinson, Stephen Kelly and especially Zoe Jacobs. Thank you to Freya Garry for proof reading one of my chapters, and to Mary

Smith and Jonathan Wilkinson; two devoted and extremely valuable members of the university administration. I also want to thank Mathieu and Marzia, my flatmates, for their great support in the last days of writing this thesis, and also to the Mettricks team. They have also made possible this thesis and have provided me with a second office for my writing.

I want to especially thank Giulia and Silvia for their support and the great times in our writing retreat, and to Zoe for the endless help. They have been a huge support and great friends to have around during my PhD. I want to thank my family too, especially my mother and my brother. Without them I would have not been able to achieve this, or half the things I have done in my life.

Finally I want to thank Elena and Victor. For the endless support and help, for the physics and trigonometry discussions, for the gin supply, for the late dinners, for the coffee breaks, for the good times and for being two great friends whom this PhD has granted me.

Chapter 1

Introduction

In a globally warming planet, the North Atlantic has gained major attention in the study of oceanography and climate. It is a key component in the formation of deep waters, in the large scale circulation and in the redistribution of heat. As it will be fully described in the following chapter, the North Atlantic, and especially its subpolar regions, are sensitive to large salinity changes. These are thought to have the potential to severely impact large scale circulation and climate. The Arctic Ocean, directly connected to the subpolar North Atlantic, is a major source of freshwater and is also focus of recent research as a rapidly changing environment. How ongoing changes there will affect the North Atlantic and the sensitive subpolar regions is still an open question.

This thesis is an effort to better understand the connection between the Arctic Ocean and the North Atlantic, through the export of Arctic freshwater. It is this export, and in particular that flowing west of Greenland (through the Canadian Arctic Archipelago and Davis Strait), that becomes the main topic studied here. There are still many open questions. We don't fully understand the mechanisms controlling the storage and export of Arctic freshwater. We are unsure about how these connect the Arctic freshwater budget and the large-scale salinity changes in the subpolar North Atlantic. As it will be fully explained in the following chapter, we do know that the Arctic is currently accumulating unprecedented quantities of freshwater. As a major freshwater source to the North Atlantic, it becomes essential to investigate the Arctic export fluxes, how they vary in a multidecadal

time scale and what impact do they have on the subpolar North Atlantic. The work presented here tries to answer most of these ambitious questions.

We know little about the variability of the export, and most of what we know, it is from models. Observations in the Arctic and the subpolar regions are scarce; these are inaccessible regions, partly (or fully) covered in ice and hence hard to measure with long standing programs (repeated cruises or moorings). Programs observing the Arctic or its gateways to the Atlantic are only recent. We lack multidecadal observations there. This thesis, however, tries to characterise how the Arctic freshwater export has varied in the past 6 decades from observations, providing the first estimate of its kind. In order to do so, in this thesis I analyse this variability in a set of hydrographic observations that lie further south, on the Labrador Shelf. With the help of an ocean circulation model, I investigate how these observations can be used as a proxy for the Arctic freshwater export.

I present the work of this thesis in three main research chapters. The first one processes the observations into a regular dataset. The second one covers an extensive model study to put the observations in context. The third one combines the previous two chapters and analysis the variability of the Arctic freshwater export in the observations. The main findings will be discussed at the end of the document, covering three main topics: the role of coastal currents in the subpolar freshwater budget, the link between the Arctic and the North Atlantic through the export of freshwater, and the size or representativeness of the export west of Greenland with respect to the total export.

Chapter 2

Motivation, Background and Objectives

This chapter overviews the scientific context of this thesis. First, it covers the motivation behind this work in order to understand how this thesis fits in the bigger picture. It continues reviewing the background by offering a broad review of the state of the art knowledge. It provides with understanding of what it is already known, but most importantly, it points out to the missing gaps. The chapter follows indicating the main objectives and how this work aims to answer some of those open questions. Finally, the structure of this thesis is described at the end.

2.1 Motivation

This thesis is an effort to broaden our current knowledge of the Arctic and North Atlantic freshwater systems. It aims to better understand how those two systems link to each other through the export of Arctic freshwater towards the subpolar North Atlantic seas, to evaluate their current ongoing changes and how they interconnect. This is important in order to predict the impact that these changes will have in the buoyancy balance of deep water formation regions and, most importantly, the potential implications in the European climate and, ultimately, in the global climate system.

We now have the skill to measure the Arctic and North Atlantic freshwater budgets to a degree that allows us to assess their magnitude, monitor their current changes and speculate on the potential impacts of these changes. However, this ability is only recent; local observations (especially in the Arctic) are relatively new. This means that we lack of a consistent context beyond the last decade. Only model studies can estimate past regimes and the full amplitude of the variability. To predict the consequences of the current changes, it is essential to understand how significant they are in context of their long term variability. This study sets out to describe multi-decadal variability of Arctic freshwater export to the North Atlantic from observations and also to contextualise current changes with past ones.

Missing repeated measurements at the Arctic gateways over a long period does not necessarily preclude from analysing the Arctic freshwater export variability from hydrographic observations. Tools that allow understanding of the circulation and the export exist and can be employed to study this signal downstream. Given a better knowledge of the Arctic water pathways, is it possible to track and identify this water further south where other long-term observational programs exist? This thesis aims at describing the pathways of some of the Arctic freshwater export down to where sustained observations exist. This offers the potential to use those observations as a multi-decadal proxy for the Arctic freshwater export variability. Assuming this is possible, the multi-decadal time series of this export will help in relating the Arctic and North Atlantic freshwater budgets, the nature of their variability and the importance of the undergoing changes.

First, in order to address these open questions, it is essential to review the most advanced understanding about this topic. This identifies gaps in the knowledge and targets the objectives or which are the questions to answer. The following section covers a literature review of the most recent scientific work to set the background of this thesis. The review first inspects the importance of the Arctic freshwater fluxes into the North Atlantic and why buoyancy changes in the northern North Atlantic are important for climate. It continues examining the Arctic Ocean as a freshwater source, focusing on its circulation and its export pathways. Finally, this section reviews current observational programs and tools to investigate the long-term variability of the Arctic freshwater export.

2.2 Background

2.2.1 Buoyancy balance of the North Atlantic

The North Atlantic and its circulation are key elements of the climate system. It is characterised by the Atlantic meridional overturning circulation, which transports heat northward and thus controls the ocean heat content. By supplying heat to the atmosphere, it regulates the temperate northwestern European climates. Variations in the heat fluxes and sea surface temperature force atmospheric changes that impact the European climate (*Rodwell et al.*, 1999).

Circulation in the subpolar North Atlantic is driven by both wind stress and buoyancy fluxes. The wind component is more energetic, but limited to the upper layer of the ocean (scale circa 1000 m). This circulation is responsible for 35 to 50% of the overturning seasonal to inter-annual variability at 26°N (*Stepanov and Haines*, 2014). The formation of deep water formation accounts for another 30% of the upper layer variability at a lower frequency period (∼4 years).

The North Atlantic Ocean is an important driver of both regional and global climate variability on multi-decadal scale (*Sutton and Hodson*, 2005). As heat is released, water becomes denser, sinks and closes the density-driven circulation by returning south. At those deep-water formation regions, salinity mostly controls density (*Carmack*, 2007) and they are sensitive to the inputs of freshwater. Even relatively small increases of the freshwater fluxes can potentially increase the stability of the weakly stratified water column and alter or stop convection (*Aagaard and Carmack*, 1989). Hence, they may affect the magnitude of the overturning circulation, alter the global ocean circulation and impact the European climate (e.g. *Dickson et al.*, 1996; *Manabe and Stouffer*, 1995; *Schiller et al.*, 1997).

The hysteresis of the system (or whether those effects are irreversible) is still an open question; *Stommel* (1961) first introduced the idea that this density-driven circulation is bistable and the overturning can switch off beyond restoration. This is mainly due to the salt feedback. An addition of freshwater into regions of deep-water could stratify the water column and considerably diminish the sinking of

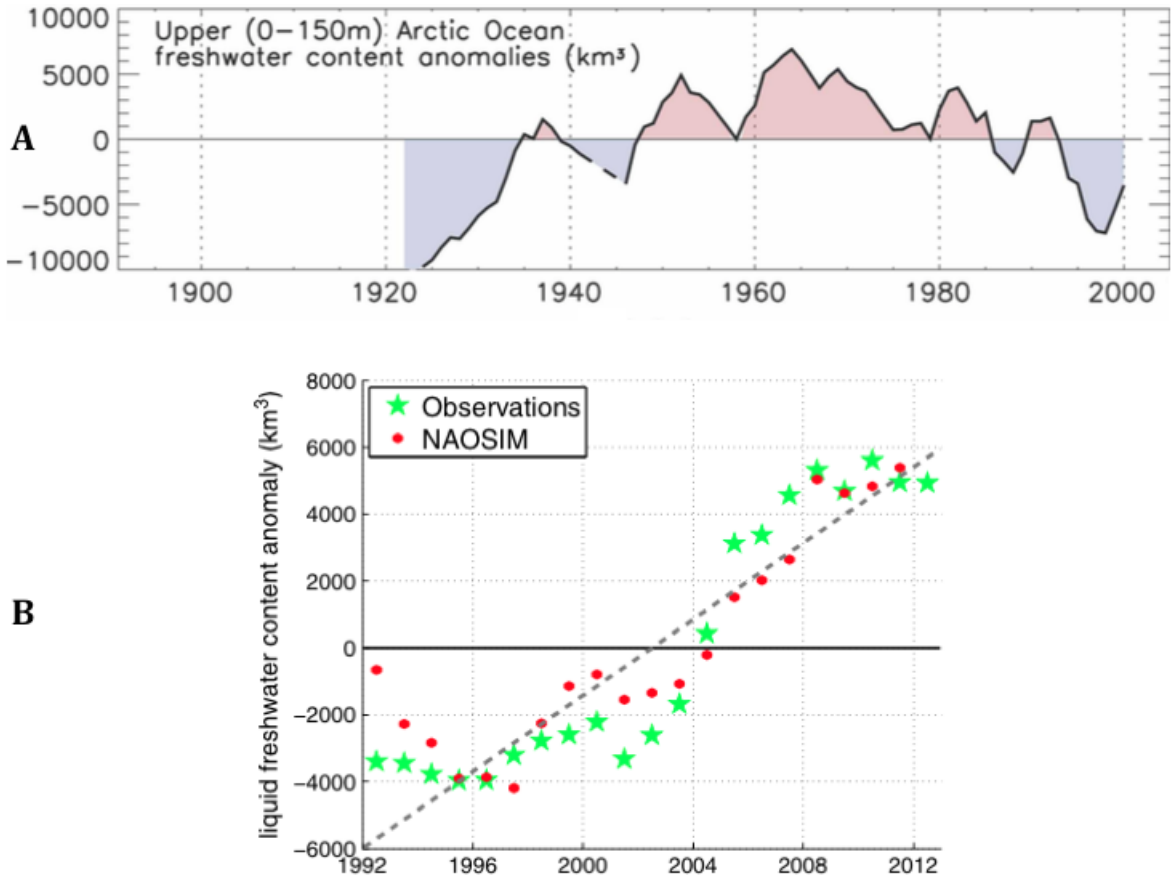

Figure 2.1: Two comparatives of the Arctic freshwater content variability, adapted from the literature. ***A****: Estimates of the upper (0-150m) Arctic freshwater content by Polyakov et al. (2008) from a set of sparse observations.* ***B:*** *Most recent changes observed and modelled in the Arctic freshwater storage by Rabe et al. (2014), showing a recent and constant increase.*

water and its return southwards. This would primarily slow down the overturning circulation. In turn, this would prevent the advection of surface saltier water northwards and hence it would further enhance the stratification of subpolar regions. The prevalence of those conditions are known as a stable off-state of the overturning circulation.

Paleoclimate records relate abrupt climate change to a stable off-state (*Broecker et al.*, 1985) and although most coupled general circulation models present a monostable overturning circulation (*Weaver et al.*, 2012), some do succeed to recreate a bistable regime (*Hawkins et al.*, 2011) when realistic freshwater fluxes are successfully simulated. Evaluating the fluxes of freshwater in the North Atlantic remains essential to understand the potential effects on the overturning circulation stability.

An important source of freshwater to the subpolar gyre comes in the form of ice. Recent observations quantify an addition of 510 Gt·year^{-1} of freshwater by icebergs from the Greenland ice sheet alone (*Enderlin and Hamilton*, 2014). Ice sheet mass loss in Greenland iceberg calving trends have increased in the past two decades and are expected to further increment in the coming years (*Rignot et al.*, 2011). A continued increase of freshwater addition by icebergs and their equatorward divergence could have an impact on the overturning circulation that models are expected to underestimate (*Wagner and Eisenman*, 2017). In addition to this, the western Labrador sea (Labrador and Newfoundland shelves) are seasonally covered in sea-ice. Local ice-drift has been observed in that region, with a weekly average rate of 18 km·day and up to 75 km·day during strong wind events (*Prinsenberg and Peterson*, 1992). The observed ice divergence favours the formation of sea-ice in the near-shore and its melt over the shelf break. These add local and seasonal (winter and spring) variability in the freshwater balance.

The low salinity of the surface Arctic Ocean means that it is also a vast reservoir of freshwater, with inputs from precipitation, oceanic inflow and river and melt-water run-off, and export to the subpolar North Atlantic (*Carmack*, 2000). Stored in the surface layers, within the complex halocline system and as sea ice, the total freshwater content is estimated to be 84000 ± 8400 km^3 (*Serreze et al.*, 2006). The budget is not in steady state, rather it is dominated by decadal to multi-decadal variability (*Polyakov et al.*, 2008), and over the past two decades it has been increasing by 600 ± 300 km^3 per year (*Rabe et al.*, 2014). Figures by those authors are adapted and shown here in figure 2.1. In total the Arctic freshwater content is estimated to have increased by an unprecedented 8000-8500 ± 2000 km^3, concentrated in the Beaufort Gyre (*Giles et al.*, 2012; *McPhee et al.*, 2009; *Rabe et al.*, 2011). Although the causes for the increased storage are still debated, it is thought that enhanced wind stress curl reinforced the convergence of surface waters at the Beaufort Gyre and thus increased the storage (*Giles et al.*, 2012). Decadal changes between different Arctic atmospheric regimes determine the strength and storage of the gyre, which is presently under an exceptionally long storing regime (*Proshutinsky et al.*, 2015).

The freshwater budget of the northern North Atlantic also presents a multi-

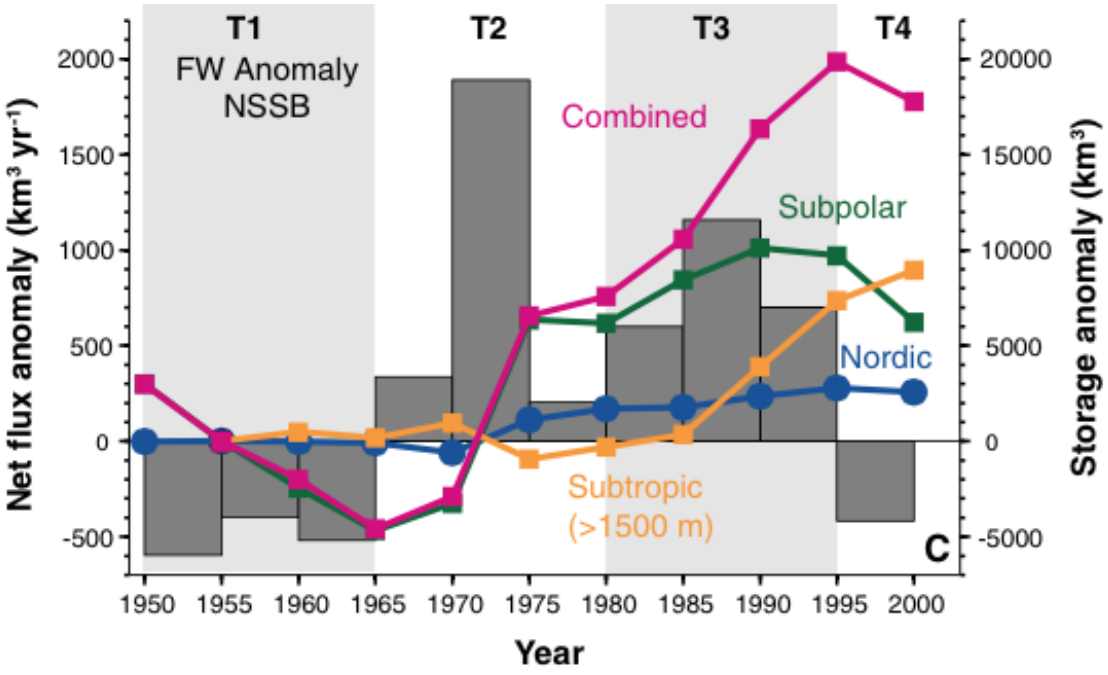

Figure 2.2: Changes in the freshwater content of the northern North Atlantic, shown as anomalies (lines) from the 1955 mean and also given as different components. The flux anomalies are shown as bars for the different time periods. This figure has been adapted from figure 3 of Peterson et al. (2006).

decadal variability characterised by periodic dilution events (*Curry and Mauritzen*, 2005). The "Great Salinity Anomaly" in the 1970s (*Dickson et al.*, 1988), characterised by exceptionally fresh conditions, caused decreased deep convection for some years after that period. This Atlantic dilution has been associated with anomalous Arctic freshwater export, both in the form of ice (*Häkkinen*, 1993) and liquid in the later years (*Karcher et al.*, 2005). The Arctic and the Atlantic freshwater budgets are linked and periods of lower Arctic salinity are associated with a saltier North Atlantic (*Peterson et al.*, 2006). The most recent changes in the freshwater content of the northern North Atlantic observed by these authors are also included here in figure 2.2, adapted from their original figure. However little is known about the processes by which this apparent redistribution of freshwater takes place. The current Arctic freshwater storage anomaly is large enough to cause an additional dilution of at least the magnitude of the Great Salinity Anomaly, verging towards a critical North Atlantic freshwater threshold (*Curry and Mauritzen*, 2005). This raises the question as to whether we have the skill to quantify the variability of Arctic freshwater export.

2.2.2 Arctic circulation and export pathways of the Arctic freshwater

One way to evaluate the variability of the Arctic freshwater fluxes affecting the salinity of the North Atlantic is by studying the variability of the processes that control them. A complete knowledge of these would help in predicting eventual transport changes and the impacts in the North Atlantic. There is a great research effort to identify the mechanisms behind the intricate system responsible for the Arctic freshwater export variability (e.g. *Haine et al.*, 2015). Although it is thought that large-scale atmospheric circulation plays an important role controlling the export (*Jahn et al.*, 2010), the lack of long-term observations means that these mechanisms are not yet fully understood. The export fluxes do not only concern to the buoyancy of the North Atlantic, but they are also the leading process controlling the freshwater content variability in the Arctic Ocean (*Lique et al.*, 2009). This means that, alternatively, current knowledge of the Arctic circulation may serve to identify the freshwater export pathways and allow measuring of the freshwater fluxes at the export gateways.

The general circulation of the Arctic Ocean has been described for over a century (*Nansen*, 1902). This ocean is the northern connection between the Pacific and the Atlantic oceans, working as an important exchange system (*Carmack*, 2007; *Macdonald*, 2000). The Atlantic hydrological deficit and the net advection of moisture towards the Pacific translate into a net inflow of water at Bering Strait and a net ouflow towards the Atlantic (*Aagaard and Carmack*, 1989), regardless of some inflow through the Barents Sea opening. Considering the freshwater fluxes within the Arctic (*Serreze et al.*, 2006), this means that Arctic freshwater is exported to the North Atlantic. This occurs via the Canadian Arctic Archipelago and Davis Strait (west of Greenland) and via Fram Strait (east of Greenland). The dichotomy of the export raises the question as to how important each branch is for the total Arctic export and whether a single route is representative of the total export.

The first estimates of the Arctic freshwater budget and export indicated a dominant role of the ice export via Fram Strait (two thirds of the total export; *Aagaard*

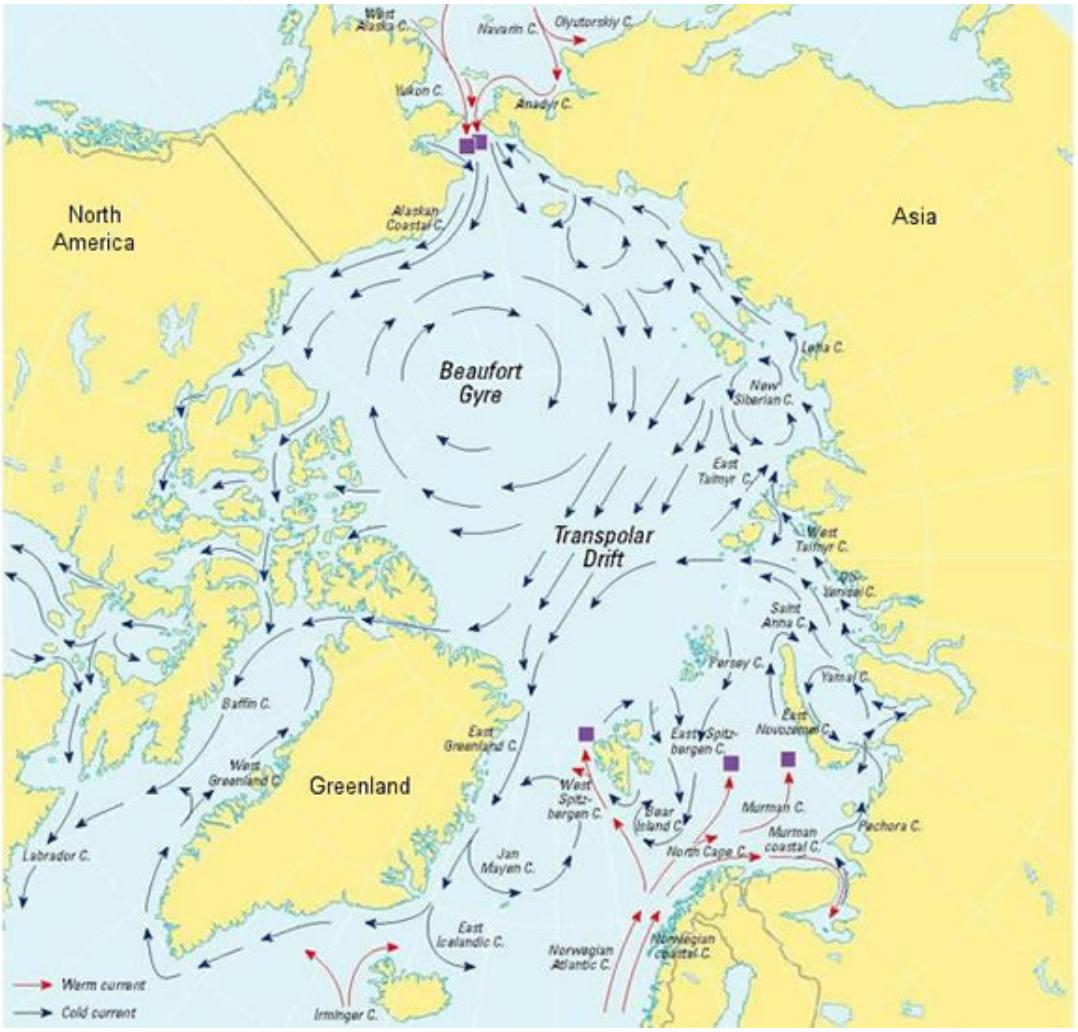

Figure 2.3: Map of the Arctic surface circulation, displaying the main surface circulation features (the Beaufort Gyre and the Transpolar Drift). Relatively cold/warm currents are shown in blue/red. Squares show where the warmer inflows submerge. This figure has been extracted from figure 3.29 of the Arctic Monitoring and Assessment Programme (AMAP, 1998).

and Carmack, 1989), controlled by the Transpolar Drift (a meridional surface current from the Eurasian basin to Greenland, see figure 2.3). However, more recent measurements of the velocity at Fram Strait (*Fahrbach et al.*, 2001) and of the meteoric component of the export (*Meredith et al.*, 2001) revealed that the sea-ice and liquid components of the freshwater export shared an equal size of the total (*Serreze et al.*, 2006). On the other side, the Canadian Arctic Archipelago is a complex system that leads the Arctic export west of Greenland towards Davis Strait. Its inaccessibility and the original concept of a freshwater export dominated by sea-ice export through Fram Strait have hindered the study of this export branch. *Steele et al.* (1996) suggested in a model study that this branch accounts for at least a

third of the total export, with a growing importance in a warmer climate scenario. Later, *Prinsenberg and Hamilton* (2005) provided the first extensive observations of the freshwater export through the Canadian Arctic Archipelago. They showed that this predominantly liquid transport is significantly larger than earlier estimates, accounting for the largest liquid component of the total export with a flux almost as important in size as that east of Greenland (*Serreze et al.*, 2006).

The estimates introduced here are point estimates; they show a snapshot and their long-term variability remains unclear. The magnitude of both export branches are expected to vary in a changing climate in different ways (*Koenigk et al.*, 2007). Their model study expects a relatively unchanging export east of Greenland (with the liquid component compensating for the ice loss). In contrast, they predict a large growth of the export west of Greenland. However, the variability of this diversification and future changes are not yet fully understood.

Profiling the Atlantic/Pacific fraction of the water being exported both ways around Greenland helps to determine the Arctic dynamics that may control the storage and export, as well as predicting changes in the export. *Lique et al.* (2010) used a lagrangian model study to analyse the water sources at both main gateways: Davis Strait (west of Greenland) and Fram Strait (east of Greenland). They showed that an important fraction of the Pacific inflow is exported through Davis Strait and that Atlantic water dominates the export at Fram Strait. These results, however, do not fully agree with the few available observations (*Jones et al.*, 1998; *Taylor et al.*, 2003) and point to a strong seasonal and interannual variability. The strength of the Beaufort Gyre (see figure 2.3), linked to the Arctic Oscillation, seems to have a significant role controlling the Pacific fraction in the Arctic freshwater export. A negative Arctic Oscillation strengthens the gyre (*Proshutinsky and Johnson*, 1997; *Zhang et al.*, 2003), enhances the transfer of Pacific water towards Davis Strait and constrains the Atlantic water and the Transpolar Drift towards the Eurasian Basin (*Lique et al.*, 2010; *Steele et al.*, 2004). A positive Arctic Oscillation intensifies the Transpolar Drift and directs it towards Greenland, enhancing the export on both sides of Greenland. This suggests that the mechanisms behind the freshwater storage and export are not only controlling these, but they may also be responsible for a variable partitioning between the two export routes.

The apparently variable composition of the freshwater export between the straits of Davis and Fram indicates that their relative impact on the North Atlantic may be different. Albeit the total freshwater transport by both branches is of similar size, it is essential to understand how their relative importance to the total transport varies. Do they mostly co-vary or do they present different dynamics? Is any of those routes representative of the total transport? Measuring the long-term variability of any of those individual export routes is already challenging, let alone obtaining simultaneous estimates of both. Differences between variability may limit the extent to which the overall export may be represented by a single branch, and this may limit information regarding the potential impacts on the North Atlantic buoyancy balance. A recent model study (*Lique et al.*, 2009) shows that the Arctic volume export fluctuates between both branches, alternating the export route between the east of Greenland and the west. Their variability is highly anti-correlated and shows a similar amplitude, meaning that the total volume transport is relatively steady regardless of the route. The main difference involves the factor that controls the freshwater transport. Whereas the export via Davis Strait is mostly dependent on the volume transport, the one through Fram Strait depends on the volume flux and also on salinity variations, linked to sea-ice interactions.

It is still unclear the extent to which the different routes of the export are responsible for the variability of the total Arctic freshwater transport. Their individual contributions to the North Atlantic freshwater budget are also unknown. This thesis will approach and discuss this issue. However, before doing this it is essential to assess which available resources offer the potential to inform about the variability of the Arctic freshwater export. This will allow us to identify whether any export route can be fully studied and used to inform the global Arctic freshwater export.

2.2.3 Obtaining long-term information of the Arctic freshwater export from existing observations

Directly measuring Arctic freshwater fluxes in key straits is difficult, and large-scale observational programs have been established only relatively recently. Currently a successful effort assessing the Arctic export fluxes is underway (e.g. *Dickson et al.*, 2007; *Haine et al.*, 2015); we now have year-round observations at both Arctic export gateways, Fram Strait (*Rabe et al.*, 2013) and Davis Strait (*Curry et al.*, 2014). Similarly, the Pacific inflow gateway; the Bering Strait, has been studied for longer, since 1990 (*Roach et al.*, 1995; *Woodgate and Aagaard*, 2005; *Woodgate et al.*, 2006). This has allowed for the first flux estimates at the Arctic gateways that are almost synoptic (*Tsubouchi et al.*, 2012). However, those observations do not yet capture multi-decadal variability, and so freshwater export variations that link the multi-decadal changes in the Arctic and subpolar North Atlantic storage remain elusive.

The lack of direct observations have lead to several model studies that have estimated the variability of these fluxes (e.g. *Häkkinen and Proshutinsky*, 2004; *Köberle and Gerdes*, 2007; *Lique et al.*, 2009). This information is very valuable, but models present several limitations and biases. They show a weak representation of the mesoscale processes, they lack of accurate riverine and precipitation estimates and there is insufficient knowledge about which processes control the variability and the feedbacks between the system's components (*Lique et al.*, 2015). Additionally, missing long-term observations of the export hinder the certainty analysis of those results and their validation. This points out to the need for future extended observational programs in the Arctic, but also to the convenience of estimates of the Arctic freshwater fluxes that go beyond the last decade. Past direct measurements in the Arctic that prove consistent in space and time do not exist, but this does not prevent us from using observations immediately downstream to study the variability of the Arctic system. With an accurate understanding of the export pathways of the Arctic freshwater, it may be possible to track and capture the export variability further south where long-term observations exist. Those data have the potential to serve as a proxy to measure the long-term variability of the

Arctic freshwater export from observations, for the first time.

Other than the only recent observational programs at the gateways of the Arctic export at Davis strait (*Curry et al.*, 2014) and Fram strait (*Rabe et al.*, 2013), the North Atlantic has a broad history of long-lasting observational schemes. The RAPID-MOCHA-WBTS array (e.g. *Smeed et al.*, 2016) is a pioneering array of sustained observations of the North Atlantic meridional circulation that spans for over a decade. This array, however, lies at 26°N and far from the Arctic. Similarly, the Extended Ellett Line has measured the upper limb of the Atlantic meridional circulation (from Scotland to Iceland) since 1996 (*Holliday et al.*, 2015). This section misses the transect closest to Greenland where the Arctic export through Fram strait circulates. Recently, the new UK-OSNAP array has been put in place (*Lozier et al.*, 2016). This new transect goes from Canada to Greenland, and continues to Scotland closing the upper North Atlantic. The array aims to provide with understanding of the circulation and fluxes of the North Atlantic Subpolar Gyre, but it only provides data from 2014 onwards.

One more extensive observational program lies on the Canadian continental platform in the Atlantic Ocean, a region directly below Davis strait and in the known pathway of the Arctic export west of Greenland (*Smith et al.*, 1937). The Canadian Department of Fisheries and Oceans stores a comprehensive dataset of oceanographic observations on the Labrador Shelf (*Colbourne*, 2004). These observations have been collected almost yearly under different purposes over a centennial time scale and, since 1950, they have been measured with remarkable consistency. They offer the potential to capture and inform about the multi-decadal variability. This thesis will be based in these observations and will focus on the Arctic freshwater export west of Greenland.

2.3 Objectives

The main aim of this thesis is to describe, for the first time, the multi-decadal variability of Arctic freshwater export to the North Atlantic from a very long record of hydrographic observations on the Labrador shelf (1950 to 2014). These results

set out to discuss the link between the Arctic and the North Atlantic freshwater budgets through the variability of this export, as well as to evaluate the importance of the export route west of Greenland to the total export. Finally it aims to introduce current and ongoing changes in the system. The general objectives are:

- To describe the pathways of the Arctic freshwater export beyond the Arctic boundaries.
- To provide a detailed description of the Labrador shelf circulation.
- To investigate the role of the different Labrador shelf features in the transport of freshwater and their link to the export west of Greenland.
- To obtain a dataset of hydrographic observations that proves consistent in time, resolution and space over a multi-decadal period.
- To identify the signal of Arctic freshwater export in such dataset.
- To compute a multi-decadal proxy for Arctic freshwater export from the Arctic signal on the observations.
- To analyse the variability of this export, including the identification of the predominant mode of variability.
- To study how the export variability and its accumulated trends relate to the long-term changes in the North Atlantic freshwater budget.
- To link the changes in the Arctic freshwater content with the export in order to better understand the possible mechanisms that control the export.
- To provide insight about the importance of the export route west of Greenland and its significance in the total export of Arctic freshwater.
- To finally point out the current ongoing changes, to place them in their multi-decadal context and to analyse their potential impact given the new knowledge provided by this thesis.

2.4 Thesis overview

The structure of this thesis is as follows; first the main methods and the different tools (a high-resolution ocean general circulation model and a long dataset of repeated hydrographic observations) are described in chapter 3. This is followed by the main analysis work, consisting of three connecting chapters: chapter 4 offers a preliminary evaluation of the dataset and processes it into a long time series that is consistent in time and space. Chapter 5 continues providing an extensive model analysis of the circulation on the Labrador Shelf and Baffin Bay. This puts the observations from the previous chapter in context of the Arctic freshwater export west of Greenland. The last main analysis section; chapter 6, combines the information from the two previous chapters to produce a proxy for the variability of the Arctic freshwater export. This provides the first multi-decadal estimates of the Arctic export, from observations. Finally, chapter 7 covers a summary of the work and results, the main conclusions and the general discussion of this thesis. This includes a description of the general implications for the Arctic and North Atlantic freshwater budgets, as well as a discussion about the role of the west of Greenland route in the overall Arctic freshwater export and a brief indication of current changes and future work directions.

Chapter 3

Data, Model and Methods

The research carried out in this thesis employs a set of tools that include hydrographic observations and an ocean general circulation model. Some analytical calculations are computed using both tools and are also described here. Before applying any of these for analysis, this chapter describes the details of the different tools and methods as follows: After a short introduction to the different instruments, it first covers the background of the dataset. Then it continues explaining the attributes of the model and finalises with the additional calculations.

The main core of this thesis investigates a large set of repeated hydrographic observations on the Labrador Shelf. Chapter 4 will cover the quality control and chapter 6 will document an extensive analysis. These data are provided by the Canadian Department of Fisheries and Oceans (DFO), and can be downloaded from the Canadian National data centre (`http://www.meds-sdmm.dfo-mpo.gc.ca`). In order to understand the regional context and the ocean boundary circulation affecting the observations, an ocean general circulation model will be used in chapter 5. The Nucleus for European Modelling of the Ocean (NEMO) is the modelling framework chosen for this study (`www.nemo-ocean.eu`). In addition to describing both the dataset and the model, this chapter also covers other relevant methods used in this thesis. These include the Montgomery streamfunction (chapter 5), which enables the analysis of the flow pathways of the Labrador Shelf currents; and the calculation of volume and freshwater transports (chapters 5 and 6), which allow the assessment of watermass origins.

3.1 The history of the Labrador and Newfoundland shelves

In an international effort, the physical properties of the Labrador and Newfoundland shelves have been studied since the early 20th century. Many oceanographic cruises have extensively observed the Labrador Shelf over time, but due to the varied purposes of the different projects, data present diverse characteristics (different variables, resolutions, instrumentation, etc.) and irregular distributions in space and time. The first observations tracked ice conditions for safer navigation, although the goal of most data sampling focused on assessing fish stocks. Comprehensive physical oceanography studies began towards the end of the 20th century. Several cruises aimed to study the variability of the physical properties on the shelf and the regional circulation. The most remarkable study is the analysis of the Cold Intermediate Layer (CIL)†, a shelf subsurface structure of very cold water. The measure of its magnitude has been tracked over decades (*Colbourne et al.*, 1995) and is used as an index of regional ocean climate variability. The varied motivations for data sampling in the region mean there is little consistency between observational datasets. They present different spatial distributions, varying resolutions and the inclusion of new variables with improving instrumentation. However most data include temperature and, to a lesser extent, salinity profiles. They therefore have the potential to be combined into a dataset to describe the variability of the shelf waters over the period that they span.

Colbourne (2004) describes the history and nature of the observations in the region. The first measurements were taken by the sailing boat Jubilee in 1894. After the sinking of the Titanic in 1912, observations in the region increased due to the interest of assessing the iceberg drift. This led to the foundation of the International Ice Patrol (IIP)†. After World War I, different nations carried out an extensive surveying of the Northwest Atlantic, including the historic expeditions Chance in 1926 (*Iselin*, 1930), Challenger in 1932 (*Glover*, 2004), Marion in 1928 (*Smith*, 1931) and General Greene in 1931-1935 (*Smith et al.*, 1937). Observations halted during World War 2, but resumed shortly after as hydrographic

†See glossary. From now on, † indicates that a word is defined at the glossary

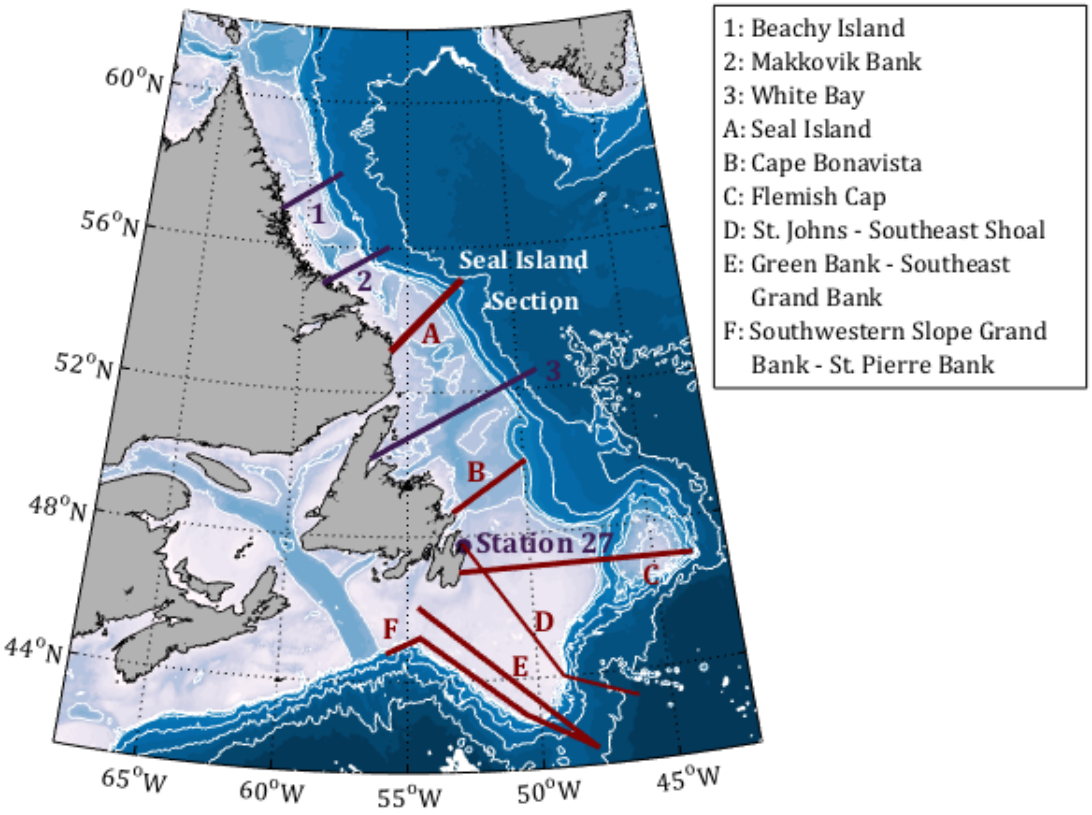

Figure 3.1: Distribution of the historical sections on the Labrador and Newfoundland shelves, inspired from figure 2 in Colbourne (2004). Station 27 has been repeatedly sampled for over 100 years. Sections A to F (maroon lines) are the longest standing transects, standardised in the 1950s. Sections 1 to 3 (indigo lines) were added in 1978.

cruises across the Atlantic Canadian shelves. In 1951 the Fisheries Research Board of Canada standardised 6 sections (A to F; figure 3.1). Later in 1978, the International Commission for the Northwest Atlantic Fisheries[†] added new standard sections (1 to 3; figure 3.1) and continued to sample them every summer. The first measurements were taken with bottle samples and reversing thermometers. During the late 20th century, observations were implemented with CTDs and several research programs began to include biological and chemical measurements. Measurements are now made yearly (mostly in the summer) and they record both physical and biochemical properties.

The standardisation of the hydrographic sections in the 1950s (*Templeman*, 1975) and their repeated measurements are a milestone in the Labrador Shelf oceanographic record. They include the Seal Island standard section, located in the southern Labrador Sea and extending from the coast to the edge of the continental

shelf. Of all the standard sections, the Seal Island section is the one that lies closest to the Arctic gateways and that comprises the longest continuous data record. For this reason, the observations at this transect have been chosen for the core of this study. The first measurements along the section date back to 1928, although they only become consistent shortly after World War II. All months of the year have been measured at some point throughout the whole record, but the observations are heavily weighted towards summer (July and August) and November. The record mainly contains temperature and salinity profiles, incorporating other biological and chemical variables in the late 1990s. The first measurements were from bottles with reversing thermometers. Then they introduced electronic bathythermographs in the 1960s and CTDs after the late 1970s. Reliable salinity measurements started in 1950, when conductivity was introduced rather than tritation methods (*Thomson and Emery*, 2014). This transitioning period marks the beginning of more accurate salinity measurements. Consequently, data quality varies according to the instrumentation. The temperature accuracy ranges from $\pm$ 0.02 °C (reversing thermometers) to $\pm$ 0.2 °C (bathythermographs) and $\pm$ 0.005 °C (CTDs). Salinity improved from $\pm$ 0.02 psu† for bottle titrations to $\pm$ 0.005 psu for CTD measurements (*Colbourne et al.*, 1995).

The data for this project was provided by the Canadian National data centre as a collection of every single profile ever sampled within a $\sim$0.5° degree margin around the Seal Island section. The profiles come from many sources and as such have varying levels of completeness, regularity or processing. The varied nature of the observations results in an uneven dataset. Consequently, processing the data to provide a reliable final product has been an extensive and challenging process that compromises a fundamental part of this thesis. Chapter 3 fully describes the course from unequal observations to a consistent dataset.

3.2 The 1/12° NEMO Model

NEMO is a modeling framework developed by a consortium of European research institutions that provides state of the art simulations of global ocean circulation, coupled to a sea-ice component. The model framework is projected onto a tripolar

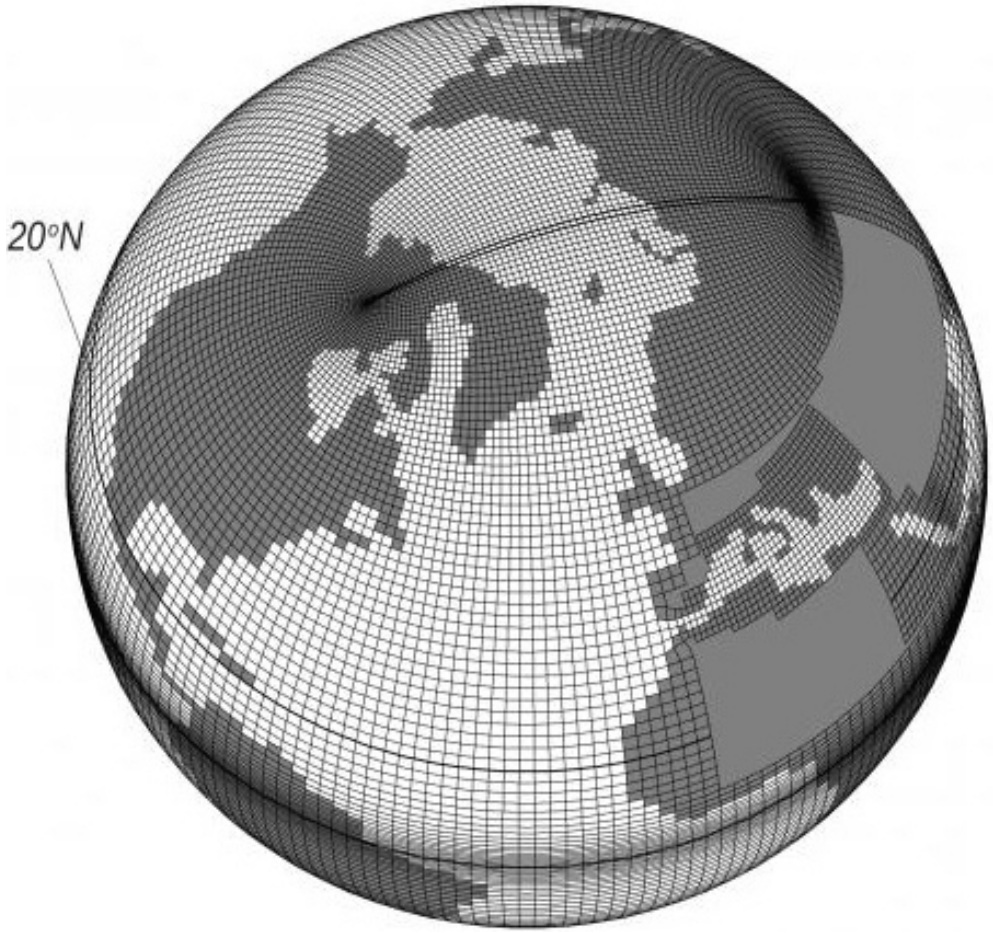

Figure 3.2: Figure from `http://www.nemo-ocean.eu/About-NEMO` *depicting the 1° ORCA tripolar grid. The North Pole is diverted into two continental poles, avoiding a singularity point on the ocean. The South Pole rests on the Antarctic continent, allowing the grid to follow a regular Mercator projection below* $20°N$.

Arakawa C-grid (figure 3.2) and allows for different resolutions (*Madec*, 2008). This three-poled grid avoids oceanic poles and prevents the development of mathematical singularities. The grid also curves near the North Pole to reduce the anisotropy of the cells (i.e. to keep gridcells square). Since the narrow currents that dominate the shelf dynamics have widths of about 10 km, the analysis requires a similar model resolution. The highest horizontal resolution available at the time of this study was of 1/12°. It is important to note that smaller resolutions (such as 1°, depicted in figure 3.2) fail to represent the narrow straits of the Canadian Arctic Archipelago, which are essential in the study of Arctic freshwater export. The 1/12° resolution renders a grid of 10 km at the Equator and 3.5 km at 75°N. The model is thus able to capture the mesoscale processes that characterise the shelf circulation, it resolves the Canadian Arctic Archipelago straits and also the eddies in deep

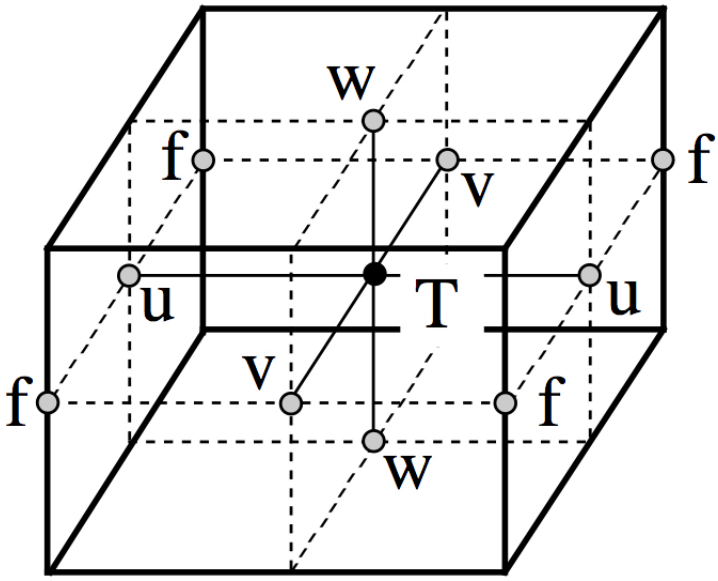

Figure 3.3: Figure 3.1 from Madec (2008) showing the distribution of variables within a C-grid cell. Tracer variables T (e.g. temperature, salinity) are placed at the center (i, j, k) of the cell, whereas u, v and w velocities are on the sides of the grid-box at $(i + 1/2)$, $(j + 1/2)$ and $(k + 1/2)$ respectively. Vorticity (both relative and planetary, and denoted by f) is given at the $(i + 1/2,\ j + 1/2,\ k)$ corners.

ocean regions, and it is eddy-permitting on the Arctic shelves. In the vertical, 75 levels of progressive depth represent the water column. They provide a higher resolution at the surface ($\sim 1\,\mathrm{m}$), which decreases with depth to approximately 200 m thick gridcells at the bottom. This resolution is shown in figure 3.4. The unequal vertical resolution allows for a better representation of the surface layers, where gradients are sharper. For a more realistic column structure, the model also adjusts to a non-linear free surface as a function of sea level. That is that the thickness of surface cells change to account for variations in the sea surface height. Similarly, it also allows for partial (shorter) bottom cells that adapt to the bathymetry, which is derived from the ETOPO2v2 global relief Earth Topography.

The employed Arakawa C-grid contains tracer variables within the grid-boxes while placing the velocities on the faces of the cube (*Arakawa and Lamb*, 1977), as shown in figure 3.3. This collocation provides the most suitable set-up to compute fluxes, divergence and pressure gradients. By staggering the velocities between grid positions, partial derivatives of velocity in space are given without need for averaging. The weakness of this distribution comes when computing non-linear velocity cross-products, as it is the case of the Coriolis component in the equations

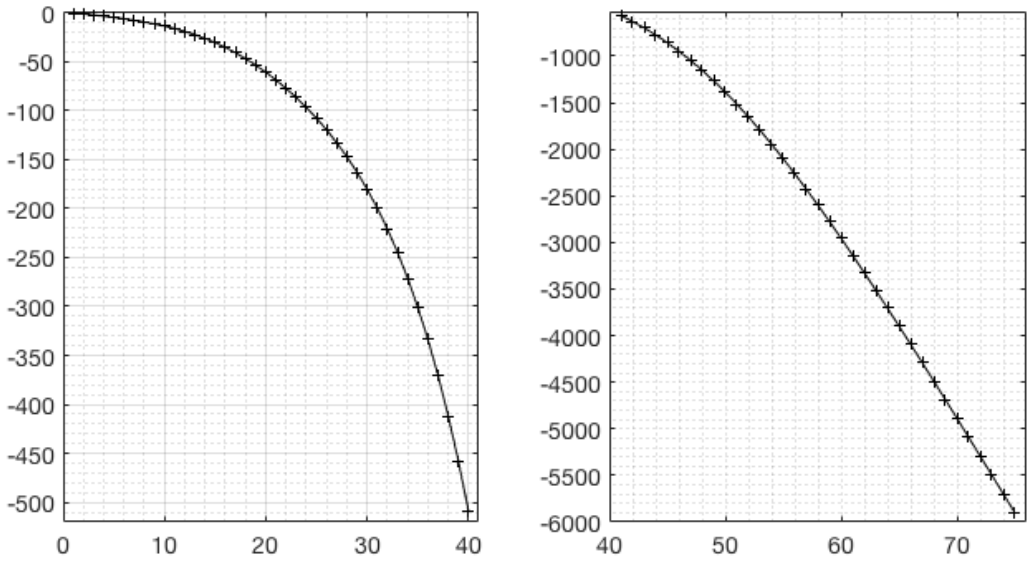

Figure 3.4: Depth (in meters, y axis) of the model 75 depth k-levels (x axis). The resolution near the surface (left) is enhanced, and decreases with depth (right).

of motion. In those situations, a mid-point velocity average is required. When the Rossby radius is larger than the grid, as it is the most common case, this does not become an issue and the C-grid remains suitable.

The model run, carried out by the National Oceanography Centre, started from resting conditions using the code version 3.2 and updated to the 3.3.1 version from the beginning of model year 1989 (run N001). The ocean time step was 200 seconds, calling the ice model component at every time step. A further description of this run, its strategy and its application in the North Atlantic subpolar region can be found in *Marzocchi et al.* (2015). The model run was initiated with climatological values of temperature and salinity in the same way as *Scheinert et al.* (2010) and *Lecointre et al.* (2011). They combine the World Ocean Atlas (*Levitus*, 1989) with the Polar Hydrographic Climatology (*Steele et al.*, 2001). An atmospheric forcing produced by the DRAKKAR consortium (`http://www.drakkar-ocean.eu/`) is then applied to the model. The forcing datasets vary depending on the time period: DFS4 (*Brodeau et al.*, 2010) from 1978 to 2005 and DFS5 (*Dussin et al.*, 2014) from 2006 to 2010. Both datasets combine air-sea fluxes derived from ERA40 reanalysis and the CORE forcing from *Large and Yeager* (2004). The simulation produced a broad output of physical fields that span from 1979 to 2010. The provided diagnostics come in 5-day means, but monthly and yearly averages

are also given. Finally, some climatologies are available as multiannual averages (e.g. 1997 to 2007). For the purposes of this study, monthly means are used; these products match the time resolution of the observations and also average out the high-frequency variability in time. The climatological average from 1997-2007 is also used to characterise regional surface characteristics.

3.3 Montgomery Streamfunction

The Montgomery function is used in chapter 5 to depict the pathways of the Labrador shelf currents. As a geostrophic streamfunction, the streamlines indicate the expected direction of the geostrophic flow. Thus, the lateral gradient of the Montgomery streamfunction serves to evaluate the pathways of the geostrophic flow. This section defines the Montgomery function, including a detailed mathematical description of its calculation and the reasons why this function has been chosen over other available streamfunctions. Finally, it explains how the streamfunction is adapted so that it can be used with the model data.

The streamfunction on a neutral surface provides a useful tool to analyse the flow pathway of a watermass. At those surfaces, a parcel of water can move short distances without experiencing work against buoyancy or gravity. Therefore, most of the mixing and advection occur along the streamlines. They provide a representation of the 3-dimensional flow onto a 2-dimensional surface. Although a streamfunction for neutral surfaces exists, we have not yet found a closed solution (*McDougall*, 1989) and thus we generally aim to work with surfaces that approximate to neutral ones and for which a closed solution can be obtained. The Montgomery function, in addition to being an exact streamfunction of the geostrophic flow on surfaces of constant steric anomaly (easily adapted to the model framework), also conserves linear potential vorticity. This makes it a preferable tool to other streamfunctions. If adapted using the Boussinesq approximation[†] as most ocean general circulation models do, the function can be applied to the NEMO model to provide visualisation of flow pathways. This section presents how this streamfunction is computed and adapted for the model.

When geostrophic balance holds, the Coriolis acceleration is in equilibrium with the horizontal pressure gradient, so that

$$\vec{k} \times -f\vec{u_g} = \frac{1}{\rho}\nabla_z p \begin{cases} +fv = \frac{1}{\rho}\frac{\delta p}{\delta x}\Big|_z \\ -fu = \frac{1}{\rho}\frac{\delta p}{\delta y}\Big|_z \end{cases}, \tag{3.1}$$

where $\vec{k}$ is the unit upward vector, $\vec{u_g}$ is the geostrophic velocity and $\frac{1}{\rho}\nabla_z p$ denotes the horizontal pressure gradient force per volume unit. Other variables use standard symbols; the Coriolis parameter (f), pressure (p), density (ρ) and zonal (u) and meridional (v) velocities, which are defined on a Cartesian framework (zonal or longitudinal, x; meridional or latitudinal, y; and depth, z). The expressions to the right of the bracket separate the equality in both horizontal (x and y) components.

In such balance, a geostrophic streamfunction ψ^r is given if the geostrophic velocity follows the streamlines of such function on a material surface r. The best way to prove that a geostrophic streamfunction exists is by demonstrating that its horizontal gradient on a r-surface ($\nabla_r \psi^r$) is equivalent to the geostrophic balance (equation 3.1). This identity is expressed in 3.2, where the geostrophic velocity ($\vec{u_g}$) is now referenced to the horizontal velocity at the sea surface ($\vec{v_0}$) given by the surface geopotential (Φ_0), which is the product of the sea surface height anomaly (η) and gravity (g), ($\Phi_0 = g\eta$),

$$\nabla_r \psi^r \equiv \vec{k} \times -f(\vec{v} - \vec{v_0}) = \frac{1}{\rho}\nabla_z p - \nabla\Phi_0. \tag{3.2}$$

Proving that the lateral gradient of the Montgomery function follows this expression will demonstrate that it is a streamfunction of the geostrophic flow.

The Montgomery streamfunction (M) was previously described as the acceleration potential by *Montgomery* (1937). It can be defined on surfaces of constant steric anomaly[†] (δ) as a function of pressure and the steric anomaly itself,

$$M = p\delta - \int_{p_a}^{p} \delta \mathrm{dp}. \tag{3.3}$$

The integral is evaluated vertically from a constant reference pressure in which δ varies (such as the surface atmospheric pressure, p_a) down to the steric anomaly

surface of concern, where pressure varies. The definition of δ (see glossary for steric anomaly) helps expanding this expression. It is described as a difference in specific volume, which is a function of potential temperature (θ), practical salinity (S) and pressure (p),

$$\delta = \frac{1}{\rho(\theta, S, p)} - \frac{1}{\widetilde{\rho}(\theta_0, S_0, p)}, \tag{3.4}$$

and referenced to seawater at the same pressure but at $\theta_0 = 0°C$ and $S_0 = 35psu$ ($1/\widetilde{\rho}$). It is important to note that the steric anomaly is more adequately defined as a function of absolute salinity and conservative temperature, as given by the Thermodynamic Equation of Seawater (*IOC et al.*, 2010). However, the use of potential temperature and practical salinity is more convenient and yields an equally valid result (*McDougall and Klocker*, 2010).

Continuing to show that M is a geostrophic streamfunction, the horizontal gradient of equation 3.3 on a surface of constant steric anomaly (∇_δ) gives:

$$\nabla_\delta M = \nabla_\delta p \cdot \delta + \cancel{\nabla_\delta \delta} \cdot p - \nabla_\delta \int_{p_a}^{p} \delta(p) \mathrm{dp}. \tag{3.5}$$

The change of δ over a surface of constant steric anomaly ($\nabla_\delta \delta$) is zero. By expanding δ using the definition given in equation 3.4 gets

$$\nabla_\delta M = \frac{1}{\rho}\nabla_\delta p - \frac{1}{\widetilde{\rho}}\nabla_\delta p - \nabla_\delta \int_{p_a}^{p} \frac{1}{\rho}\mathrm{dp} + \nabla_\delta \int_{p_a}^{p} \frac{1}{\widetilde{\rho}}\mathrm{dp}. \tag{3.6}$$

It is worth noting that by using the hydrostatic balance equation,

$$\begin{aligned} \frac{\mathrm{dp}}{\mathrm{dz}} &= -\rho g \\ \frac{1}{\rho}\mathrm{dp} &= -g\mathrm{dz}, \end{aligned} \tag{3.7}$$

it is possible to relate the third term of the right-hand side of equation 3.6 with the geopotential ($\Phi = gz$), so that

$$\nabla_\delta M = \frac{1}{\rho}\nabla_\delta p - \frac{1}{\widetilde{\rho}}\nabla_\delta p - \nabla_\delta \int_{z(p_a)}^{z(p)} -g\mathrm{dz} + \nabla_\delta \int_{p_a}^{p} \frac{1}{\widetilde{\rho}}\mathrm{dp}. \tag{3.8}$$

Gravity changes with depth (z) are infinitesimal. Is is possible to assume Earth as an ellipsoid (equipotential gravitational surface) and gravity can come out of the

integral. Equally, the second and last terms of the RHS balance each other out. That leaves

$$\nabla_\delta M = \frac{1}{\rho}\nabla_\delta p + g\nabla_\delta z(p) - \nabla_\delta(g\eta), \tag{3.9}$$

where $z(p_a)$ is the sea surface height (η) and $z(p)$ is just the height of the steric anomaly surface of concern, which can also be written as z.

Taking into account the definition of the geopotential at the surface ($\Phi_0 = g\eta$), the gradient of which only depends on x and y, equation 3.9 can be expressed as

$$\nabla_\delta M = \frac{1}{\rho}\nabla_\delta p + g\nabla_\delta z - \nabla\Phi_0, \tag{3.10}$$

The gradient of any property χ in a surface r can be expressed in a constant height (z) surface by using the general coordinate transformation,

$$\nabla_r \chi = \nabla_z \chi + \frac{\mathrm{d}\chi}{\mathrm{dz}}\nabla_r z, \tag{3.11}$$

and the gradient of pressure in a constant steric anomaly surface can hence be written as

$$\nabla_\delta p = \nabla_z p + \frac{\mathrm{dp}}{\mathrm{dz}}\nabla_\delta z. \tag{3.12}$$

Combining this definition with the hydrostatic balance (equation 3.7) and substituting in equation 3.10, we obtain that

$$\nabla_\delta M = \frac{1}{\rho}\nabla_z p - \cancel{\frac{1}{\rho}\rho g\nabla_\delta z} + \cancel{g\nabla_\delta z} - \nabla\Phi_0 \tag{3.13}$$

The gradient of the Montgomery function in δ-planes reduces to

$$\nabla_\delta M = \frac{1}{\rho}\nabla_z p - \nabla\Phi_0 \equiv \vec{k} \times -f\vec{u_g}, \tag{3.14}$$

so that it is proportional to the geostrophic balance in agreement with equation 3.2. This proves that the Montgomery is a geostrophic streamfunction on surfaces of constant steric anomaly.

Finally, to adapt the streamfunction to the Boussinesq approximation (most

models use this approximation), density is approximated as constant (ρ_0) when it is not a product with gravity. Equally, the steric anomaly surfaces are adapted to Boussinesq pseudo-potential density surfaces (r_B), where

$$r_B = \rho(\theta, S, p) - \widetilde{\rho}(\theta_0, S_0, p) + \sigma(\theta_0, S_0). \tag{3.15}$$

In this case, the pseudo-potential surfaces are calculated as $r_B = \delta^{-1} + \sigma(\theta_0, S_0)$, where $\sigma(\theta_0, S_0)$ is just a reference potential density anomaly added to provide r_B-surfaces with a physical meaning. Hence, r_B can be seen as pseudo-isopycnals.

The resulting Montgomery function, modified with the Boussinesq approximation (M_B) and represented on surfaces of constant r_B will provide a visualisation tool for the geostrophic flow. This is calculated in the same way as explained in section 2.3.1 in (*Aksenov et al.*, 2011), more specifically using their equation 6. By defining pseudo-potential density surfaces that are representative of the different currents, it is possible to analyse their expected route. This will be used in chapter 5 for the different shelf waters in order to understand the regional pathways of the Arctic freshwater export.

3.4 Transport Calculations

Comparing the freshwater transports between different sections serves to evaluate the continuity of a current and its evolution between the two sections. Chapter 5 uses this tool in the model to test the origins of the currents found on the Labrador Shelf, by the Seal Island transect. Additionally, chapter 6 employs the calculation of freshwater fluxes on the observations to compute a proxy for Arctic freshwater export West of Greenland. This section covers the background of the volume and freshwater transport calculations. It defines both transport types and it explains the preference for freshwater ones. The mathematical description includes how the calculations are adapted to the different arrangements of data in the model and the observations. Finally, this section overviews the concept of 'reference salinity' and the reasons behind the chosen one for this study.

Idealising the ocean as incompressible and considering the conservation of mass within a closed domain, the influx of water equals the outflow. This way, the mass transport by a current through a section or strait is balanced by a counterpart elsewhere in the defined region. Comparing the transport at different boundaries helps informing about the fate of such current. However, this analysis is fully dependant on the selected area. Whereas enclosed domains (i.e. straits and coast-to-coast sections) are easily defined, this is not the case for open-ocean regions such as a shelf. Additionally, mass (or volume) transports are a bulk measure and do not consider the complexity of the diverse components. Many factors impact in the velocity and the trajectory of the different inflows and outflows, and their variability has an individual repercussion in the net measure. In contrast, transports related to watermass properties, such as freshwater transports, provide a more reliable measure. When mixing and external local inputs (such as ice-melt or precipitation) are small, they remain fairly constant. Freshwater transports can provide a quasi-conservative tracer for a current. The work in this thesis has compared the freshwater transport by different currents, defined by the properties of the watermasses they carried, to relate their origin and fate. They have also been used to infer the magnitude of the Arctic freshwater export west of Greenland as seen in the Seal Island observations.

Transports are a flux measure of water flowing across a defined area. They inform about the mass or volume of water that crosses a section (or boundary) per unit of time. Mass and volume are related by density; the mass transport is the product of volume transport and density. In the ocean, volume transports (Q) are more useful as they can be calculated regardless of density. They can be computed as the velocity of the water $\mathbf{v}$ integrated across an area A of interest, in the form

$$Q = \int_A \mathbf{v} \, \mathrm{dA}. \tag{3.16}$$

The resulting flux has SI units of m^3/s, however they are more commonly expressed in Sverdrups[†] (Sv), where 1 Sv $= 10^6$ m^3/s. The sign is negative to the south and the west.

Data are defined differently in the model and the observations. As sketched in

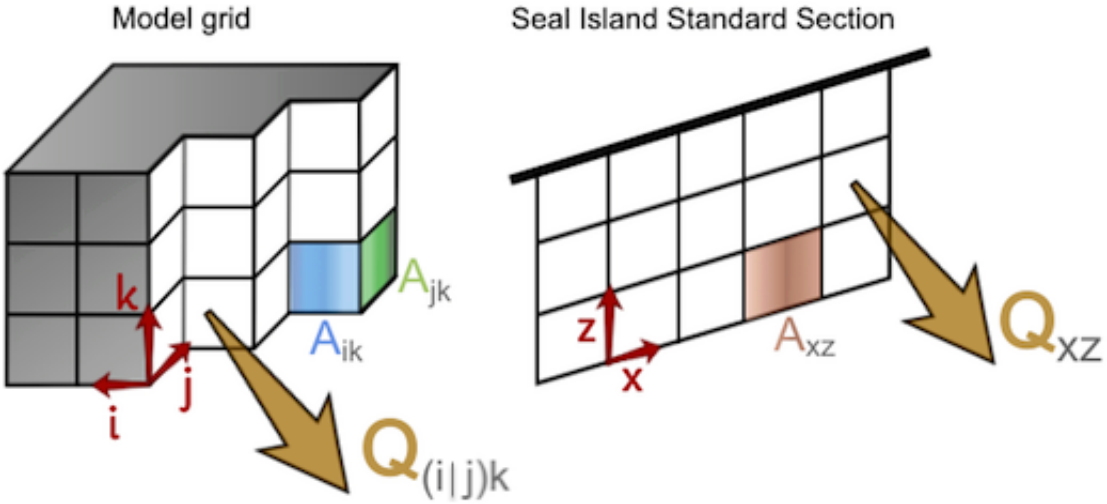

Figure 3.5: Sketch of the different grid frames for the model (left) and the observations (right). The model presents a 3-dimensional structure defined by i, j and k. Fluxes across a section (white squares) are given in both lateral faces (A_{ik} and A_{jk}). Observations are projected onto a 2-dimensional section defined by x and z. Transports are only given across A_{xz} faces. These distinctions yield different nomenclature; $Q_{(i|j)k}$ and Q_{xz} .

figure 3.5, model grid boxes present a 3-dimensional structure defined by the i, j and k indexes. The observations instead, are interpolated along the 2-dimensional grid (x and z axes) given by the Seal Island line. In both cases, Q is calculated individually at every grid cell as the product of the velocity and the area of the cell's face. This definition varies slightly according to the different frameworks and the cell areas they yield. In the model, the flux is across both the ik and the jk faces (Q_{ik} or Q_{jk}; so $Q_{(i|j)k}$). The transport in the observations is across the x and z plane. Q is then defined as

$$\begin{aligned} Q_{(i|j)k} &= \mathbf{v} \cdot A_{(i|j)k}, \\ &\textit{or} \\ Q_{xz} &= \mathbf{v} \cdot A_{xz} \end{aligned} \tag{3.17}$$

respectively. It is worth noting from figures 3.3 and 3.5 that model cells present u velocity across j faces (area A_{jk}) and v velocity across i faces (area A_{ik}). In the observations, the $\mathbf{v}$ components are calculated as orthogonal (across) or parallel (along) to the section. Only the orthogonal velocity v_{ort} has a role in computing the transport across the cell's area (A_{xz}). Finally, the total transport is computed as the summation of the transport by each individual cell within the established domain

(e.g. a complete section, or only those gridcells that belong to a certain watermass). Q is calculated using the 'cdfvhst' fortran program from the cdftools package, version 3.0 (`http://servforge.legi.grenoble-inp.fr/projects/CDFTOOLS`).

Freshwater transports (Q_{FW}) relate the volume flux with a salinity ratio. They can be understood as the salinity difference between the inflowing and outflowing waters, produced by surface fluxes (i.e. runoff, ice-melt and precipitation minus evaporation). In other words, they are a measure of the freshwater required to equilibrate a system's mean (or reference) salinity. They are defined as

$$Q_{FW} = Q\frac{S_{ref} - S}{S_{ref}}. \tag{3.18}$$

Here, the reference salinity S_{ref} denotes the freshening threshold for a certain boundary or section. Salinities below this reference produce a positive (freshening) ratio, and vice versa. The sign of the resulting transport also depends on the flow direction of Q (in or out of the system). This way, freshening may occur by inflows of lower salinity or by outflows saltier than the reference. In this study, freshwater transports are given positive when they freshen downstream, in the direction of the net flow across a section.

The choice of an appropriate reference salinity value is often a challenge and cause of discussion. A general approach is the stirred box system, where the reference salinity is averaged along a section or within a box. Other approaches use a characteristic salinity of an inflow, a current or a deep estuarine layer. Most of the Arctic research agrees on a reference salinity of 34.8, defined as the Arctic mean salinity by Aagaard and Carmack (1989). However, in Atlantic subpolar regions, a salinity of 35.0 is more commonly used as it is a common limit with Atlantic waters (e.g. *Dickson et al.*, 2007, 1988; *Holliday et al.*, 2007). Current research is heading towards a methodology centred in the physical meaning of freshwater fluxes, rather than the abstract sense of a reference salinity. As such, new formulation that avoids arbitrary reference salinities has been recently developed (*Bacon et al.*, 2015). They define freshwater fluxes as a function of stored salinity and the anomalies produced by boundary fluxes. To reconcile this emerging definition with the conventional methodology, in this study I choose to use a reference salinity of

35.0. This value is close to the established subarctic reference salinity and it is also a general mean salinity of the boundary; the surrounding Atlantic waters.

Chapter 4

The Labrador Shelf dataset: producing a consistent summer dataset

The first observations on the Labrador Shelf date back to the early 20th century, as introduced in section 3.1. The reasons for the collection of data and the technology of the instruments, have changed during the time over which the observations have been taken. This results in differing characteristics between profiles. The lack of consistency requires a challenging process to obtain a final, uniform dataset. This chapter covers the whole process from original observations to homogeneously gridded sections, required for the analysis in the following chapters. First, I introduce the formatting of the original data files and their basic characteristics. Secondly, I evaluate their distribution in time and space. After inspecting some of the problems in the observations, I continue explaining step by step all the profile processing. This quality control includes a batch of automated cleansing filters and further manual checks. I follow by designing a standard section grid on which to interpolate both observations and model data. Finally, I compute climatological products and use them to complete gaps at individual years. The main results and the Seal Island summer dataset product are summarised at the end of this chapter.

The Canadian Department of Fisheries and Oceans provides data as text files, which can be found at `http://www.meds-sdmm.dfo-mpo.gc.ca`. Each file contains

```
NAFC_Y2K_HEADER
84005746  53 45.00 -055 16.00 1928-07-22 00:00 0250 FAPBO 000 V     00125      1
84005746 000007 99.90 A 05 #DTSM---------------            D 999 0000 0250 000 4
84005746      -01    -999.9 -99.9 -99.9
-- CHANNEL STATS -->
# span     scan =      1.000,     8.000
# span     pres =      0.000,   250.000
# span     temp =     -1.450,     5.500
# span      sal =     32.160,    34.140
# span   sigmat =     25.370,    27.370
-- END --
-- HISTORY --> Sat Jan 29 16:02:48 2000
>REJECT_WITH 0 F C
>READ # T (DP) S M  scan temp pres sal sigmat
>HISTORY_ON
>SET_NEW_HEADER
>WRITEFILE .p???? scan pres temp sal sigmat
>END
-- END --
 scan     pres      temp      sal    sigmat
-- DATA --
    1    0.000    5.500   32.160   25.370
    2   25.000    3.170   32.380   25.780
    3   50.000   -1.340   32.400   26.060
    5  100.000   -1.450   32.800   26.380
    6  150.000   -1.060   33.530   26.960
    7  200.000    0.140   34.000   27.290
    8  250.000    0.730   34.140   27.370
```

Figure 4.1: Example of a text file showing the usual data display of a Seal Island profile. This profile belongs to the earliest cruise available, in July 1928. As is common in earlier cruises, only a few points of the water column could be sampled. In this case, only 8 data values are provided by presumably bottles with reversing thermometers.

a single profile. I collected all available profiles that were within approximately 2° from the Seal Island section. The original data at the time contained a total of **3905 profiles**, the first of which dates to 22-07-1928 and the most recent one is from 11-01-2015. Data files present a common structure given by the North Atlantic Fisheries Commission, as exemplified in figure 4.1. Although details about the observations are not explicitly provided, most information can be inferred from the metadata heading. The second line contains a numerical ID for the profile (84005746 in the given example), followed by latitude, longitude, date, time and, in some cases, information about the recording instrument. After the main heading, files describe which variables they contain and the limits of the measured data (minimum and maximum values). After the text headings, data are provided in a column for each variable.

Despite the common structure of the files, most headings and variables change from profile to profile. This is most clearly reflected in the resolution of the profiles and the number of variables. Tables 4.1 and 4.2 show the difference between an

scan	pres	temp	sal	sigmat
1	0.000	0.270	31.280	25.090
2	24.000	1.230	33.600	26.900
3	47.000	1.370	33.900	27.140
4	71.000	1.180	34.000	27.230
5	94.000	2.020	34.190	27.320
6	141.000	2.890	34.400	27.420
7	189.000	3.400	34.600	27.530
8	283.000	3.930	34.730	27.580

Table 4.1: Profile 84009836, recorded on 25-06-1940 during World War 2. This example shows data from a low-resolution profile with values at specific depths, presumably taken by bottles with reversing thermometers. The profile contains 8 data points down to a maximum pressure of 283 dbar. Earlier profiles only contain temperature and, in some cases, salinity and derived density.

earlier profile and a more recent one, respectively. The first table contains data from a full 1940 profile. Before the 1960s, observations were taken with bottles that contained reversing thermometers. As a consequence, and as shown by the pressure column, only a few data points sampled the water column at set depths. Additionally, data mostly contains temperature profiles and, to a lesser extent, salinity and derived variables like density. Other measurements are rare during the first decades of the record. Recent cruises present an opposite situation, as shown in table 4.2. This example from 2004 contains part of a processed CTD profile with a much higher resolution, presenting a few measurements within a unit of pressure. Because of its high resolution, the full profile is too long to be shown in the table completely. In this case, the measurements are not limited to temperature, salinity and density, but also include other variables. Recent CTD profiles contain biochemical parameters such as dissolved oxygen, pH, fluorescence and photosynthetically active radiation (PAR). The varied resolutions and variables, together with the different heading formats, made importing over 3000 profiles a challenging process.

The original name of the files was given by their profile's ID number, followed by the year in which they were measured. However, these ID tags (such as the ones showed in tables 4.1 and 4.2) do not follow an apparent logical meaning. To

scan	pres	temp	cond	sal	sigt	oxy	flor	par
43	0.856	10.707	3.316	29.425	22.488	6.437	0.231	288.900
80	1.170	10.690	3.316	29.443	22.505	6.433	0.230	269.090
88	1.293	10.688	3.316	29.438	22.501	6.426	0.216	258.440
130	1.452	10.560	3.321	29.598	22.647	6.401	0.214	225.780
196	1.689	10.395	3.324	29.761	22.801	6.380	0.227	221.350
200	1.887	10.352	3.325	29.803	22.841	6.393	0.229	208.650
203	2.062	10.302	3.327	29.860	22.893	6.409	0.231	205.320
208	2.325	10.213	3.328	29.947	22.975	6.436	0.233	235.430
211	2.468	10.225	3.328	29.934	22.963	6.444	0.233	225.810
214	2.624	10.112	3.327	30.016	23.046	6.468	0.234	210.280
...								

Table 4.2: Profile 10552075, recorded on 30-07-2004. This example shows data from a high-resolution profile with different physical and biochemical variables. Only the first 10 data values are shown. The original file contains 486 data points for a relatively shallow profile (maximum pressure of 134 dbar).

facilitate the data processing and analysis, I organised all profiles in chronological order and renamed them accordingly. The earliest profile being numbered as '1', and increasing the count to the latest profile; number '3905'. From this point, in this thesis I will only refer to the new profile numbering.

4.1 Distribution of data

Temporal distribution

One of the key attributes of the data to be exploited is their long time span. It is essential to understand their coverage, both as the total number of profiles every year and also as the seasonal or monthly distribution. Understanding the year to year distribution helps to determine the potential length of the time series that can be extracted. Similarly, the total number of profiles each month tells us about the seasonal weight of the data. This subsection clarifies these questions.

The overall distribution of profiles since 1928 is fairly consistent, in that there are data for almost every year until present (as shown in the top panel of figure

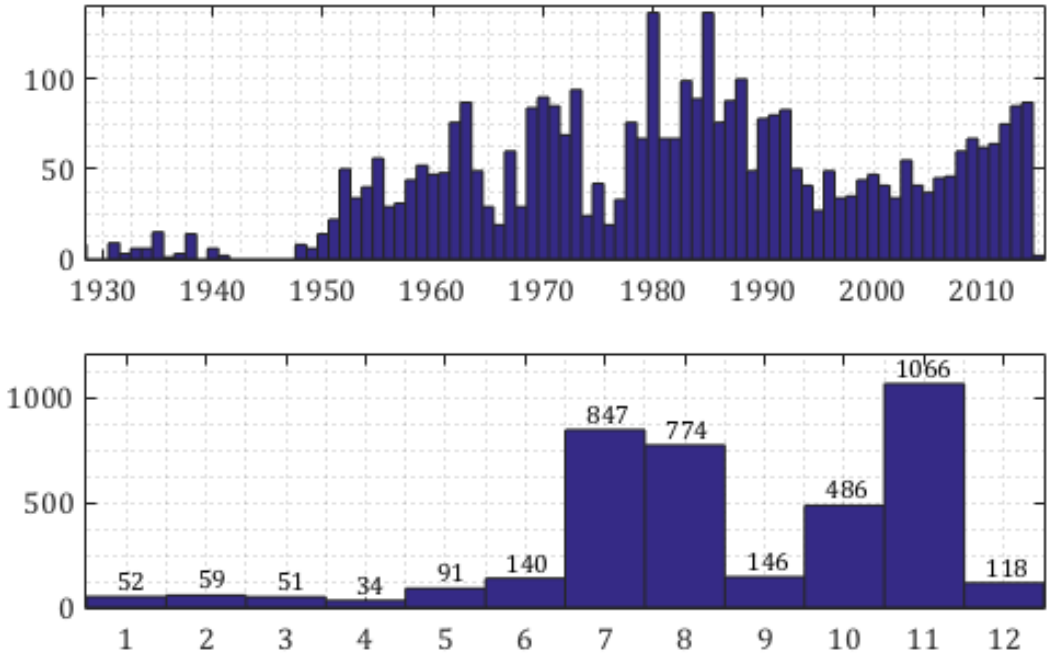

Figure 4.2: Histograms showing the total number of profiles initially available for every year (top) and each month of the year (bottom).

4.2). As can be expected, earlier years have considerably fewer measurements. The lack of international commissions and limited oceanographic resources make those data sparse, with poorer quality and resolution. The only gap in the whole time series coincides with World War 2, resuming shortly after it ended. Since then, the distribution is irregular, but there are samples every year. The 1980s are characterised by a high number of observations, containing also the years with most profiles (1980 and 1985, each with 137 data files). Finally, after the mid 1990s (when the sole use of CTDs was established), the number of measurements has grown almost yearly.

Regarding the seasonality, presented in the lower panel of figure 4.2, data concentrate in two peaks: one in the summer (July and August) with a total of 1621 profiles, and another in November with 1066. Those seasons are sea ice free, as opposed to winter and spring months. Other than weather conditions hindering the measurements, the varied reasons for sampling can also have an effect in their distribution over time (e.g. repeated sections in the summer, or fish stock analysis carried out generally in November).

The distribution is most clearly seen when the concentration of profiles is plotted

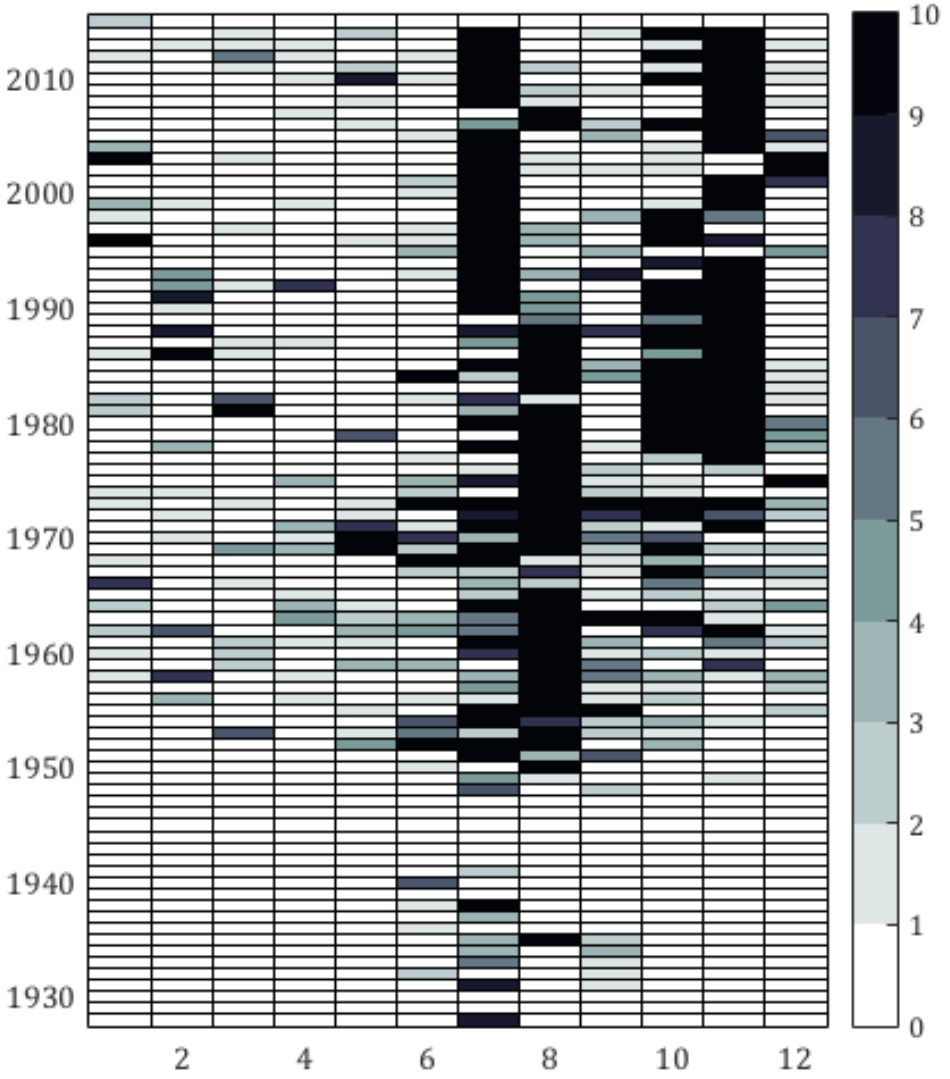

Figure 4.3: Hövmoller diagram presenting the number of profiles originally available for every month (x-axis) and year (y-axis). Months with 10 profiles or more are shown in black.

against months and years. The Hövmoller diagram in figure 4.3 shows how many profiles are available at each time. Darker colours denote a higher concentration, and black boxes indicate months where 10 or more profiles have been recorded. Again, it is rare to find high concentration of data in winter and spring months. However, it is worth noticing that all months of the year have been sampled at least once. If those data cover the whole section, they could provide with the means to compile a composite average for every month. Additionally, in 1973 there is a high concentration of profiles all the way from June to November. If their quality and spatial coverage are adequate, they could provide a half year of continuous data.

Despite the big potential offered by this dataset, this study will only focus

on summer observations (July-August months). If data in November are equally abundant, they only become consistent after late 1970s. The interest in this thesis is on multidecadal variability. It is only summer observations that can inform about long-term variability, for over 60 years. In addition to this, *Colbourne et al.* (1995) describe the seasonality of the water on the shelf. In autumn, more unstable weather conditions favour the mixing of the water column and by November this is fairly well mixed. An example is shown in figure 4.4, a November temperature section (2014) that can be compared to summer sections (for example, those in the appendix). That year, as in most November sections, temperature shows mixed water in the mid-shelf. It also shows how mixing transfers the heat of the summer warmer surface water to the bottom. This dissipates the very cold water signal (-1°C) that characterises the intermediate shelf water in the summer. This means that mixing on the shelf possibly hinders the identification of any Arctic water signal in the TS properties.

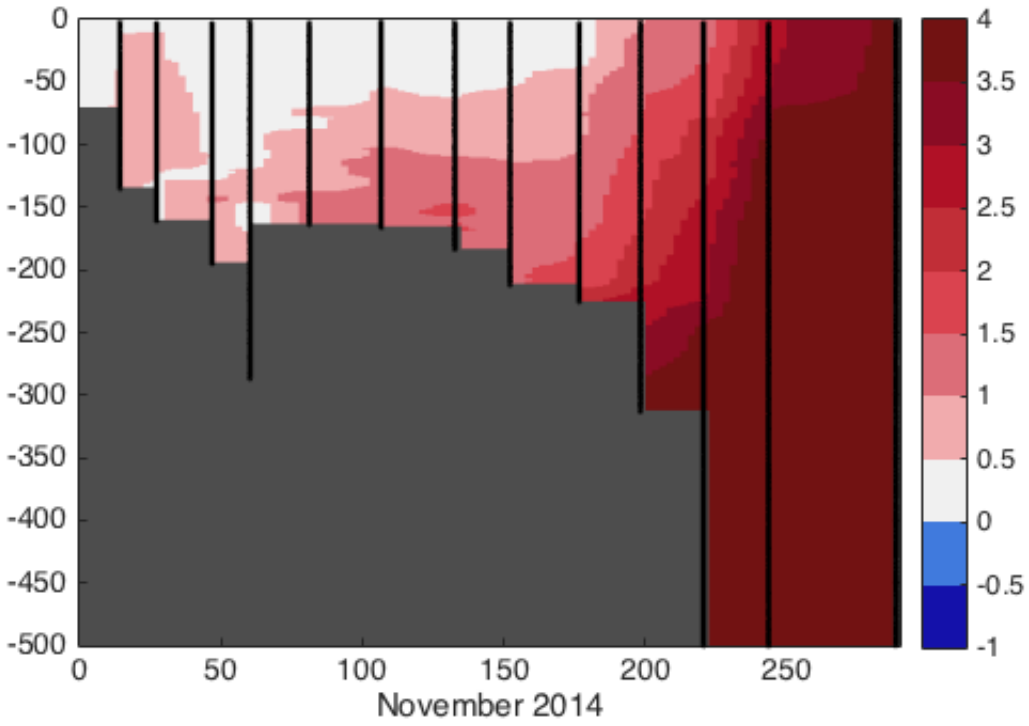

Figure 4.4: Seal Island temperature section in November 2014.

Spatial distribution

It is equally important to assess the spatial data coverage. Profiles may be abundant in certain months, but they also need to spread over the shelf. Some cruises may concentrate the observations locally or they may distribute them along the shelf, rather than across. This subsection evaluates the spatial coverage of the observations. Firstly as a whole and secondly by months in order to analyse the seasonal spread.

It is in the interest of this study to have as much data as possible distributed along the Seal Island Section. For this purpose, all data at around 0.5° from the section were pulled out from the database. The Seal Island transect is defined by the line traced by its standard stations. Table 4.3 indicates the position of the 9 standard locations. Although the 87 years of varied cruises allow for a big spread of data, most profiles are expected to concentrate at those standard locations. More recent cruises measured further stations along the Seal Island section and introduced new locations within the transect.

The positions of all initially available profiles are shown in figure 4.5, with the Seal Island standard stations plotted on top. Standard stations are depicted in blue. Later, from 1993, the section was implemented by 5 additional repeated stations (shown in red). The observations gather all over the selected region, and

Station	**Longitude**	**Latitude**
1	-55.65	53.23
2	-55.50	53.33
3	-55.00	53.62
4	-54.50	53.92
5	-54.00	54.20
6	-53.50	54.50
7	-53.25	54.63
8	-53.00	54.78
9	-52.50	55.07

Table 4.3: Standard stations of the Seal Island transect.

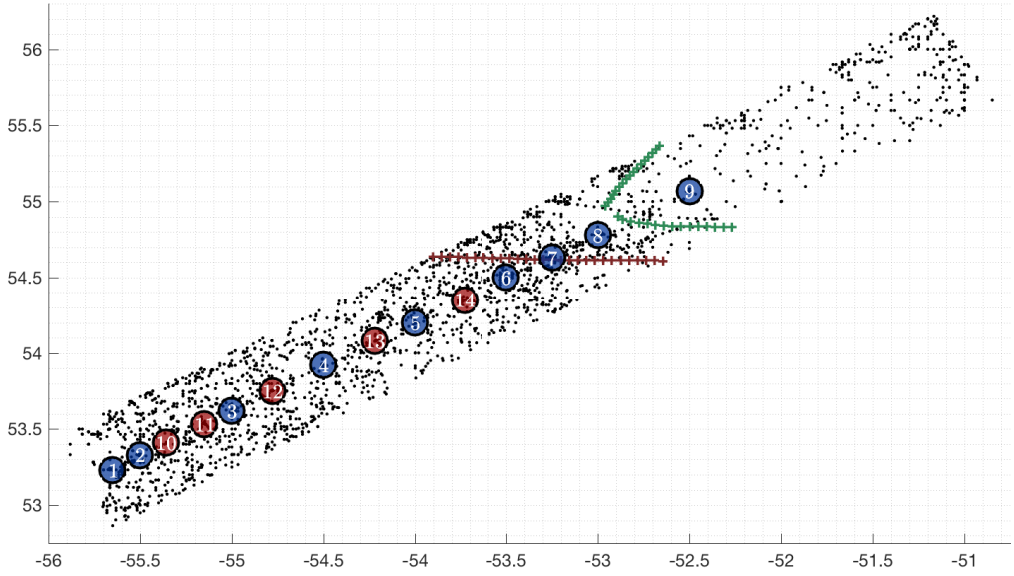

Figure 4.5: Distribution of all profiles initially available. Blue circles denote the position of the Seal Island standard stations and red circles indicate the addition of extra stations in 1993 (axes correspond with longitude and latitude).

even continue further offshore beyond the section (towards the north-west). However, there is a predominant concentration of profiles at the standard stations, and between them. Additionally, the same figure shows how some cruises present arrays different to the standard section. For example, this can be seen as a trail of profiles forming two horizontal lines between 54.5 and 55 °N (between stations 8 and 9). Those lines belong to two different cruises unrelated to the Seal Island section, which occurred to lie within the region. Overall there is a good spatial coverage. However, when working with these data, those profiles that depart from the official transect need to be looked at closely. If they lie away from the line, they may introduce irregularities or local anomalies in the final gridded sections.

The coverage of the observations by month is also presented in figure 4.6. The seasonal distribution is evident again, as seen in the previous subsection. Summer and autumn show a higher concentration of profiles. Colder seasons only accumulate a handful of profiles through the 87 years of data; especially April (with only 34 profiles) just after the maximum sea ice extent is reached. Despite the low concentration in those months, they still manage to cover most of the Seal Island section. It is worth noticing how some cruises at certain months cluster the observations locally. The 'cloud' of profiles in the middle of the section in February is an

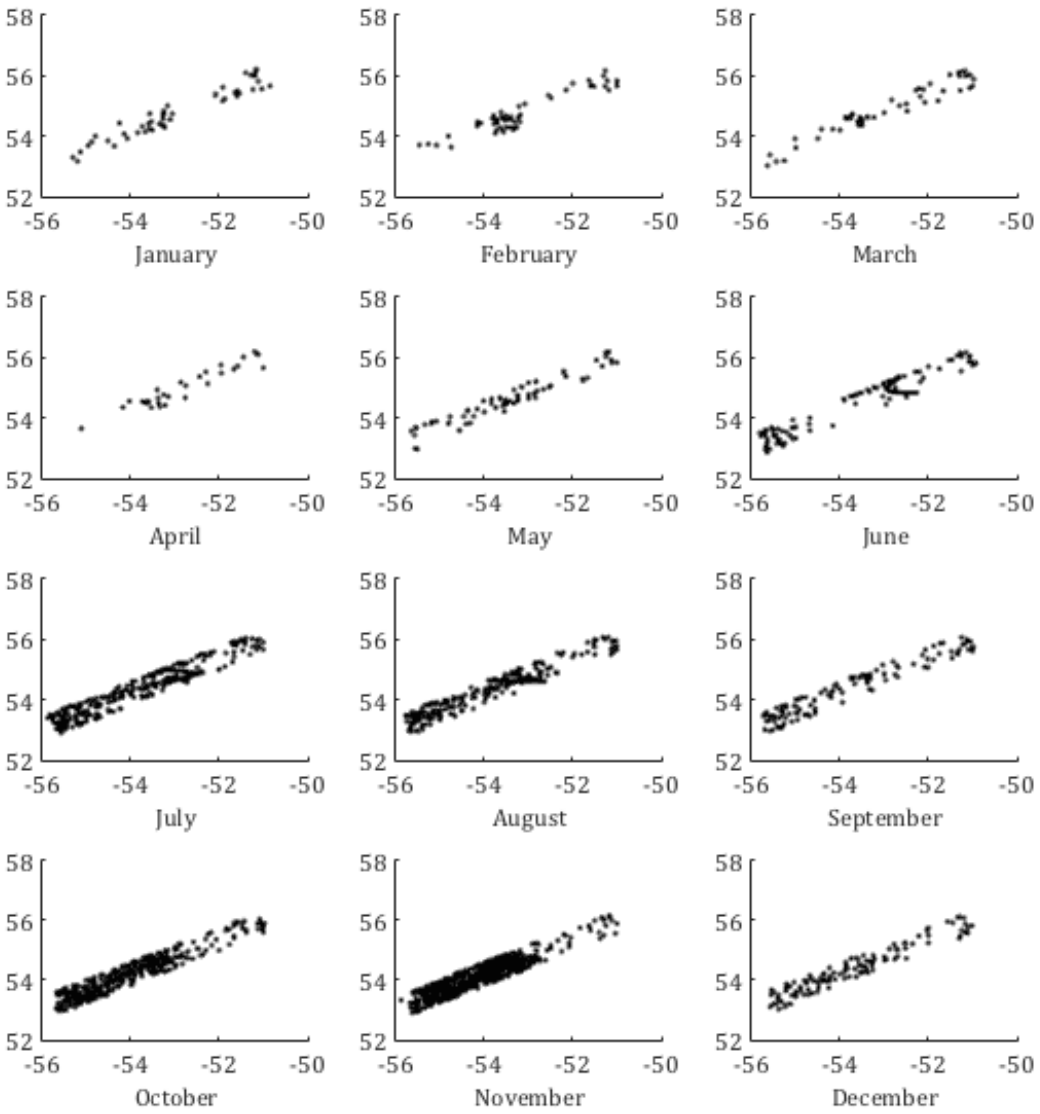

Figure 4.6: Seasonal distribution of all profiles initially available, grouped by months (axes correspond with longitude and latitude).

example. Again, this denotes how cruises with a different objective to measuring the Seal Island section contribute to an unequal distribution of observations and with potentially different characteristics. The effects of irregular characteristics or the anomalies resulting from outer stations are further discussed in the following section.

The spatial distribution of data shows that they do cover the Seal Island section, but also that further analysis is required to remove irregular profiles. For this purpose, a data quality control needs to be in place to select only suitable data.

4.2 Quality control

The observations at the Seal Island section have shown they have the potential to provide information about multidecadal variability on the Labrador Shelf. In order to ensure good data standards for the analysis, the observations require a thorough quality control, and in this section I examine the consistency of the data. It covers most of their general attributes, to find the flaws and potential of each profile. The ultimate goal is to only select those observations that comply with the quality standards.

First, I carry out a general assessment to identify the most evident issues hampering the use of the full record. Then I continue by flagging and rejecting all "bad" data. The processing starts with a step by step automated routine that removes most of the unusable profiles. It continues with a manual check of final yearly products, to finalise cleansing the record. At the end of this section, I present the resulting distribution of suitable profiles after the quality control.

4.2.1 Preliminary assessment

Yearly plots of the profile stations prove to be an ideal tool to approach to the dataset for the first time. They do not only inform about sparsity, as seen in the previous section, but they also help understanding the purposes of individual cruises. It is worth noticing that the profiles rarely provide with metadata about the aim of the cruises. Only in some cases they contain key words (e.g. *FISH*) or the names of the specific instruments used. By displaying the observations yearly with a monthly legend, the disposition of cruises is seen and they can hint at the purpose of individual observations. These yearly plots with a monthly legend have been used to understand the dataset and to point out some of the data issues and strengths. They can be found in appendix A, after page 203.

In addition to the annexed plots, figure 4.7 summarises some of the most relevant features. The observations focus on the Seal Island section at specific times. In other seasons, cruises often cluster around certain regions or trace across the transect. The top panel shows two good examples of clustered cruises, such as the

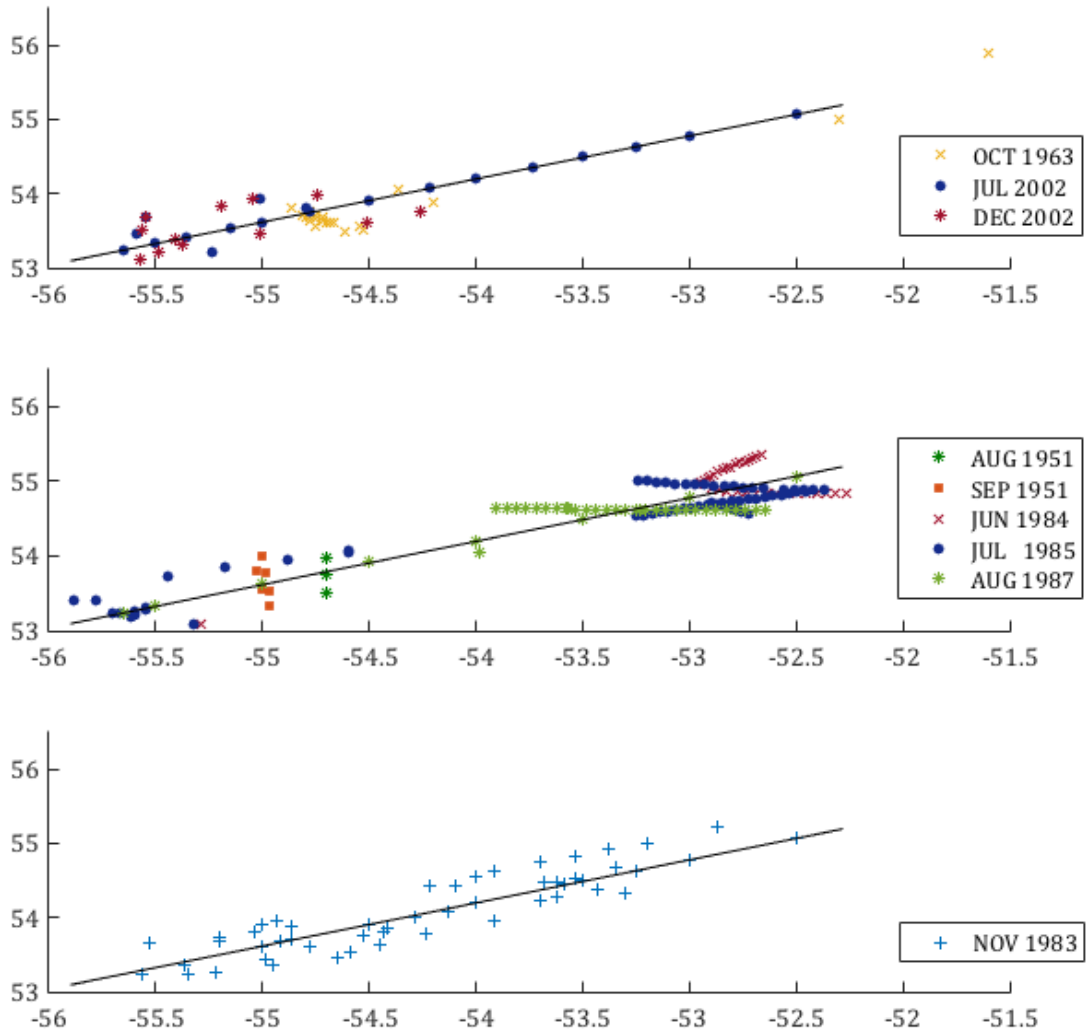

Figure 4.7: Different examples of how cruises do not always follow the standard Seal Island section, indicated by the black line. Markers depict the longitude and latitude of the stations by all the cruises within the times shown. Some cluster stations locally (top panel), other go across the section (middle panel) and some months recorded uncountable stations over the whole region (bottom panel).

one in December 2002 or, especially, the cruise in October 1963. Those months, the observations did not cover the whole section (depicted by the black line), but concentrated locally towards the west. It can then be seen that even though some months may contain abundant profiles, they do not necessarily cover the complete section. The same plot also overlies the stations recorded in July of one of those years. This layout of profiles clearly shows that the original purpose of that July cruise was to repeat the Seal Island hydrographic section. The three stations lying off the standard transect were recorded by a different cruise in a different week. Summer observations perfectly tracking along the Seal Island is a common fea-

ture repeated throughout the whole dataset, mostly during July or August. This reinforces the sole use of these profiles to compute a Seal Island time series.

Some cruises appear to be alien to the Seal Island section and seem to only measure the same region by coincidence. Sometimes they are completely perpendicular to the transect and cut it across. The middle panel in figure 4.7 presents some of those examples. Most of them appear incomplete; the initial sub-selection of data 0.5° around the transect crops cruises that track across the standard line. For example, the cruises in August and September of 1951 run orthogonal to the section, nearly parallel to each other. Those cases do not provide useful information and these profiles are disregarded. Other examples, like July 1985, show many different cruises around the transect at the same time. Despite those profiles may be taken under different circumstances and lie in a rather random pattern, they have the potential to produce a composite product for that month. Similar cases are found in the dataset. However, merging data from different cruises need particular care. On the one hand they can be measured weeks apart within the same month. This can cause irregularities when averaging along the section, especially at the surface if weather conditions differ considerably. On the other hand, some data points may lie fairly off the standard line. These stations need special attention to ensure they do not add spurious information or local anomalies.

Some months, the overwhelming concentration of data also contributes in the problem. An excessive number of profiles may obstruct interpolating the data into consistent sections. Data for August 1987 (middle panel in figure 4.7) shows a good example, with over 30 profiles from different cruises. Stations are arranged in two predominant layouts: the repeated Seal Island section and a cruise crossing the transect at a fixed latitude. In this case, it is more sensible to only use the measurements by the standard cruise. The additional observations could increase the resolution locally, but they would likely add irregularities. Some stations lie almost half degree away from the transect and, as mentioned above, they can introduce unreliable data. Also, when those profiles are projected into the standard line to interpolate the whole section, some can lie very close together. This can cause deceptive gradients, with consequences in derived properties such as the geostrophic velocity. Other than August 1987, several years commonly present an

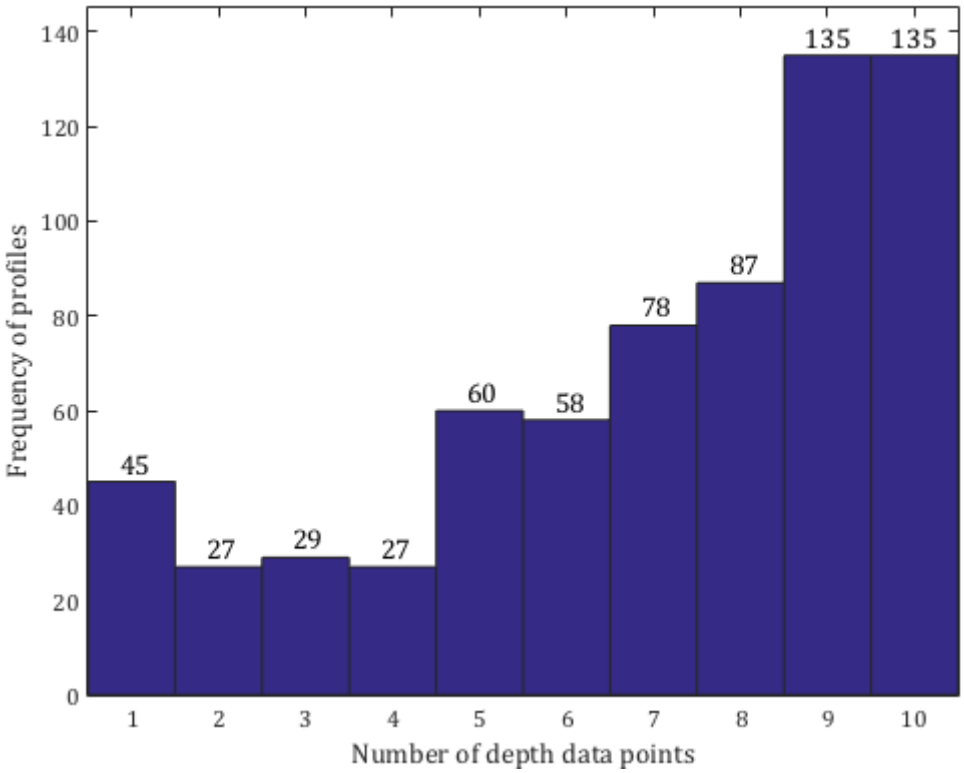

Figure 4.8: Histogram of profiles with poor vertical resolution. Bars display the total number of profiles with as many data points as specified in the x-axis. Only profiles with 10 or less values of pressure (or depth) are shown.

excess of observations in November, as shown in the bottom panel of figure 4.7. This is yet another example of how observations can overcrowd the section. In general, additional observations can help to improve the spatial resolution, however, care needs to be taken to avoid spurious gradient. Discerning which stations are adequate proves to be difficult and a fine filtering is required to guarantee the sole use of reasonable observations. This processing is developed in subsection 4.2.2.

Further to the varied nature of the cruises, some individual profiles can present problems. Their individual characteristics need to be considered during the data quality control. One of the most significant problems is their vertical coverage. Almost 5% of the profiles contain only 5 depth data values or less. From a total of 3905 profiles, 45 are single depth measurements at the surface or at a single depth level. The histogram in figure 4.8 displays the count of profiles that contain a poor vertical resolution, from a single datum up to 10 pressure (or depth) points. When selecting suitable profiles, a compromise between a reasonable vertical resolution and the coarser earlier measurements needs to be found. This is achieved

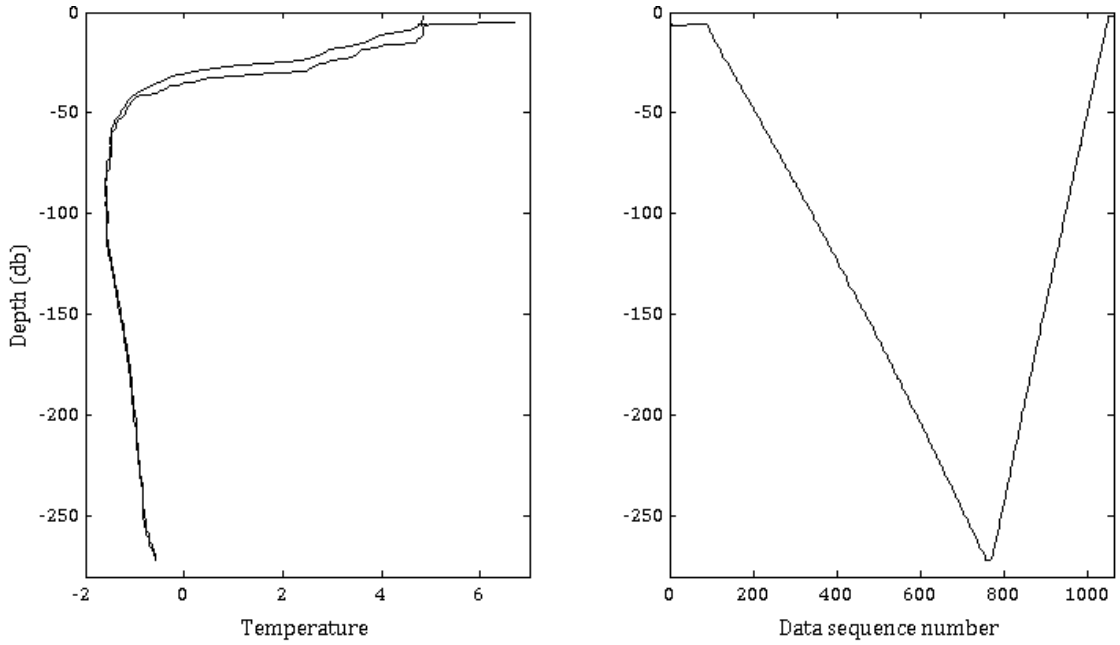

Figure 4.9: CTD profile number 2503, recorded on 19-07-1990. Temperature (left panel) and data sequence (right panel) are displayed with depth. This example shows a profile with uncompleted processing, where the upcast and downcast have not been separated.

in the following subsection.

Similarly, not all data provide the information required for the purpose of this study. In order to obtain the longest-possible yet consistent record, profiles must contain temperature and salinity data. Further information is useful but only those variables are essential. From the 3905 profiles, all contain temperature measurements. However, only 2450 files provide accompanying salinity data. That is, only 63.4% of the profiles contain both. Other than the profiles missing salinity, those before 1950 can also be disregarded. Salinity measurements only become reliable after 1950s, when the improved electrical conductivity measurements were introduced, replacing titration (*Thomson and Emery*, 2014). Any observations before then need to be disregarded for consistency.

Files are taken from a bulk data base and they carry other general issues. Some files seem to contain two different profiles merged together. Other provide repeated data under different file names. Sometimes with duplicated information, other times showing the same station after different levels of processing. Often, one is a version of the original profile, binned into a coarser vertical resolution.

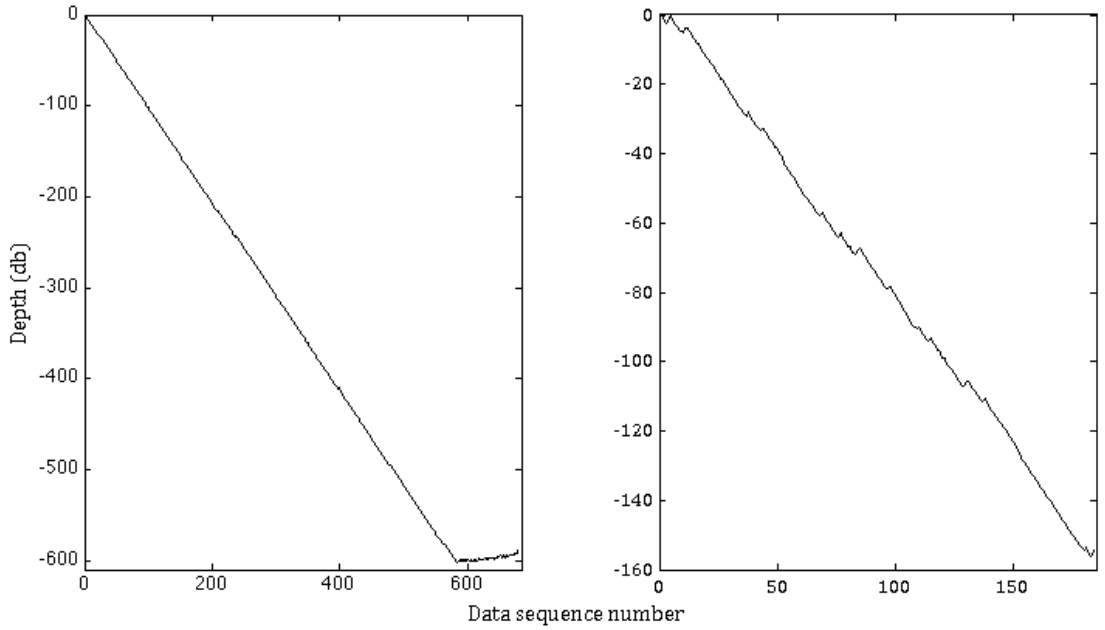

Figure 4.10: Profiles 1649 (left) and 1632 (right) are examples of uncompleted processing profiles. The former shows uncropped data when the CTD lay at the bottom. The profile in the right panel shows unbinned data, displaying the effect of waves (or looping effect).

An example of these varying levels of regularity and processing is shown in figure 4.9. The figure displays a summer temperature CTD profile. Generally, data are provided fully processed. In this example the upcast and the downcast have not been separated, which is part of any primary processing. Displaying the depth of consecutive data scans (shown in the right panel) also allows identifying parts of incomplete processing. For instance the initial surface soak, waiting for the sensors to adjust, has not been removed.

A similar example is presented in figure 4.10. It shows two different profiles from August 1980, which are not monotonic (i.e. data are not sorted or binned regularly with increasing depth). This poses a problem when vertically interpolating the data. The left panel displays a profile including the time that the CTD spent at the bottom. The right panel shows an unbinned profile. In this example the effect of the waves can be identified by the reversing directions of the CTD. This can also be seen as small loops in the temperature profiles. The different levels of completeness in the data also needs refining to achieve homogeneity between profiles.

The preliminary quality assessment of the data has shown that the observations

by different cruises and years can be very varied. However, it has also shown that the Seal Island section has good coverage in summer (July and August). The data have the potential to be compiled into a yearly time series that can span for at least 6 decades. Producing this consistent summer dataset is the main goal of this chapter. The unequal processing and the irregularity between profiles have also been highlighted in this section. These problems include, but are not limited to, the vertical resolution, the distribution of stations and the uneven completeness in the processing. The issues emphasised here corroborate the need to thoroughly filter the data before compiling the yearly time series of summer observation. Generating comparable profiles is the first step to assemble the necessary time series. Next subsection covers the filtering steps followed to obtain consistent profiles and comparable sections.

4.2.2 Data filtering

Some of the problems found in the data relate to individual profiles. Analysing one datafile at a time would require a vast amount of time and it would prevent us from completing a thorough quality check. For this reason, an automated filtering process was specifically designed for this dataset. Firstly, the computed processing assesses every profile individually and flags any assessed as unsuitable. Secondly, it evaluates their suitability to form summer sections. Lastly, the process is finalised by a manual check of the resulting sections. This ensures there are no other missed issues. This subsection explains how the data filtering was approached and describes the whole process step by step.

In order to keep track of the changes and which profiles remain valid, a binary array was devised. This "flag vector" contains 3905 rows, as many as profiles there are. Initially, all profiles are classified as suitable and they are given a value of 1. If, throughout the process, a profile is found misleading, the respective index in the flag vector is changed to 0. Questionable data are independently flagged to be manually checked at the end. After the automated processing is finished, the flag vector informs about which profiles remain valid and which are to be dismissed.

A. Selecting only summer data

One of the main points learnt from the preliminary assessment was that only summer months have the potential to compile a time series consistent over decades. This first step evaluates the month in which each profile was recorded. Those taken in July or August remain eligible. Any other data are flagged. From all data filtering steps, this one removes the largest bulk of data. From the original 3905 profiles, only **1649** remain. It is worth noticing this does not mean the dismissed months lack of any use. They still have the potential to inform about generic seasonal traits and about how well do summer months represent the whole year. Simply they are not used to compute the yearly Seal Island sections.

B. Considering data from 1950 onwards

Salinity measurements before 1950 are relatively unreliable (*Thomson and Emery*, 2014) and they may contribute with weak results. Additionally, observations become much more frequent during that decade and onwards. For these reasons, it is preferable to remove data prior to 1950. There is a handful of summer profiles before then. They can still be used to extend the time series, but always under careful considerations. After selecting data only from 1950 onwards, the available profiles add up to **1583**.

C. Disregarding profiles missing salinity data

Temperature and salinity are basic variables required for any oceanographic analysis. All profiles contain temperature information, but this is not the case for salinity. Those files missing these data can be disregarded. Some records may provide conductivity data and salinity can hence be inferred. For this reason, all files are checked for either salinity or conductivity and, if neither are available, the profile is then removed. Over 400 files miss salinity information and **1135** profiles remain after this filtering step.

D. Setting a suitable vertical resolution

The irregular vertical resolution between earlier profiles and the more recent CTD casts has been pointed out earlier in this chapter. Consistency in the vertical is essential to adequately represent the water column and a minimum resolution standard is required. However, it is not clear which is an appropriate number of vertical data points. The ideal case is to keep as many profiles as possible without affecting the quality of the final product. This requires removing single-depth profiles (or those with very few data points) without disregarding the earlier coarser resolution profiles.

To find this compromise, it is essential to consider the variety of instruments used at different times and the features of the shelf. The earliest measurements were taken with bottles and reversing thermometers. These only sample the water column every few tens of meters (or dbar). Taking into account that the inshore side of the shelf is between 50 to 100 m deep, shallow profiles with only **4 data points** would ensure vertical data every 12 to 25 m. Although such resolution is not ideal, it allows for the use of earlier data while removing the coarsest ones. Additionally, as previously shown in figure 4.8, profiles with 4 or more data points (but less than 10) only add up to less than a 6 % of total profiles. This means that the outcome will be overweighted by finer profiles.

Removing data with poor vertical resolution diminishes the number of available profiles down to **1110**. The manual check of yearly sections at the end of the cleansing process will ensure that the vertical resolution is not compromised by this set limit.

E. Removing profiles distant from the Seal Island

Data are not only located along the Seal Island section, but spread everywhere around the area. At the time of interpolating the profiles into sections, stations can incorporate errors if they lie too far off the transect line or if they cluster locally. To avoid spurious effects, this filter removes distant observations. By reducing further offshore profiles, observations from repeated Seal Island cruises

gain a greater weight in the interpolation. The closest adjacent profiles would then only serve to fill gaps and provide additional information.

An easy way to remove the profiles far from the section is by defining a distance limit. Observations farther away from a set boundary can be disregarded. Setting this maximum distance may be arbitrary, but the characteristics of the section help finding this limit. The closest distance between two standard stations is approximately 15 km (between stations 1 and 2; table 4.3 in page 44). Observations located farther away than this distance, in a perpendicular direction, could potentially incorporate spurious data between stations when projected onto the standard line. Thus, a distance of **15 km** makes a reasonable limit to avoid interferences while keeping the largest number of profiles. For convenience and once the automated data cleansing is complete, manually checking the final layout of stations will confirm whether this is an appropriate limit for every year.

Additionally, some years present high concentration of profiles clustered near the section. These are singular cases and can be given a stricter limit. Particularly, summer of 1985, 1987 and 1988 contain a large number of stations closer than 15 km. Some of these examples were depicted in figure 4.7 on page 48. A distance of 5 km proved to be more appropriate for those cruises. After removing all profiles outside the different distance boundaries, a total **857** profiles remain available.

F. Selecting pressure as the vertical axis

During the preliminary assessment it was noticed that some profiles were duplicated with different processing stages. Commonly, two or more profiles were found on the same position and time, but with different vertical binning. One of them would contain 'original' information without averaging, and with pressure defining the vertical axis (in dbar). In contrast, lower quality profiles (i.e. low resolution binning) were averaged to equidistant depth intervals, in metres, and they miss pressure information. Unbinned profiles provide more complete data and are preferable to averaged observations. Additionally, pressure is measured directly, whereas depth is computed secondarily and as a function of latitude. It is then preferable to keep pressure as the vertical axis until completing the interpolation

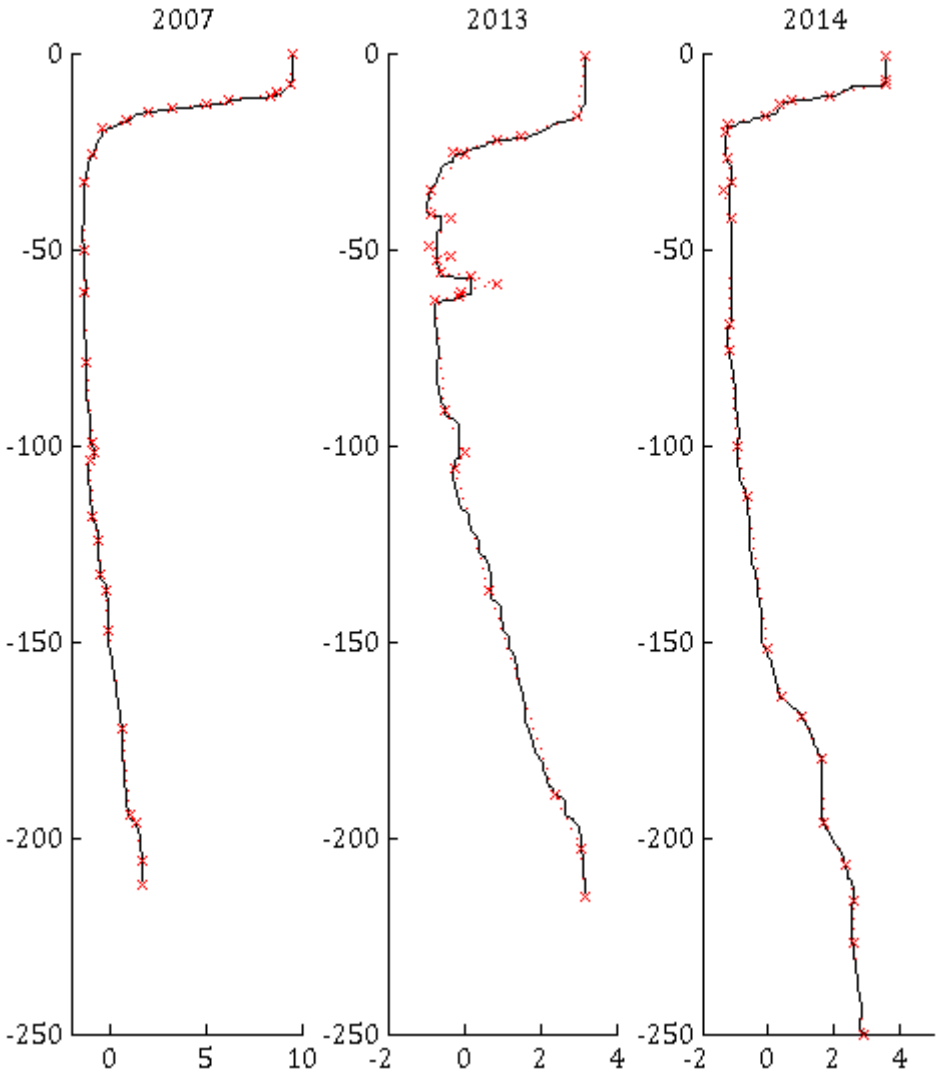

Figure 4.11: Examples of simultaneous temperature profiles at single stations in 2007 (profiles 3333 & 3334), 2013 (profiles 3711 & 3712) and 2014 (profiles 3787 & 3788). Black lines depict CTD casts and red dotted lines show the duplicated profiles. Red markers show the depth of the additional profiles' data points. The vertical is defined by pressure in dbar (black lines) or depth in m (red lines).

into sections.

Some stations in the latest cruises contain two simultaneous profiles for the same cast. One is a CTD profile, with high resolution and coherent with the other stations in the cruise. The additional profiles come from different instruments and they present a poorer resolution. Figure 4.11 shows some of these examples. The black lines depict CTD temperature profiles. The additional profiles are presented in red. Their lower resolution allows including the depth at which the data points were taken. The CTD profiles provide higher resolution, present a strong precision and are coherent with the other stations in the same cruise. For these reasons, CTD

profiles are preferred over other additional profiles. Since the additional profiles also provide data as a function of depth and not pressure, they are easily spotted.

This filtering step removes profiles that miss pressure data. The program additionally ensures that a full profile always remains in place. By doing this, most repeated profiles are removed without losing information at any station. At the end of this step, **813** profiles remained and in all cases an 'original' (or CTD) profile was preserved.

G. Deleting duplicated profiles

In addition to the previous case, which presented profiles repeated by different instruments or with varied stages of processing, it is also common to find duplicated data. Most times these are different files that contain the exact same information, but stored under different file names. Other times, they are the same station, immediately repeated by the same instrument on the same day. In both cases, only one file is useful. This processing step finds all remaining repeated stations and data, to keep only one sample.

When several identical files are found, the program keeps the first sample and dismisses any other after. If it is the case of a repeated station on the same day, it preventively keeps the first cast. However, both files are flagged in a list of profiles to manually check at the end of the data automated filtering. After running this step, **760** profiles remain. From those, 6 profiles were listed to be checked. These are profiles 98 and 99 (August 1950); 347 and 348 (August 1957); 1457, 1463 and 1465 (July 1978); 1612 and 1637 (July 1980); 2368 and 2381 (August 1988); and 2669 and 2670 (July 1992). They will be analysed in the manual checks section, in page 64.

H. Avoiding profiles far off in time

In order to produce a summer composite time series, it is a good approach to use observations taken in either July or August. However, this is not the case for individual years. Contiguous observations taken within a few weeks can present

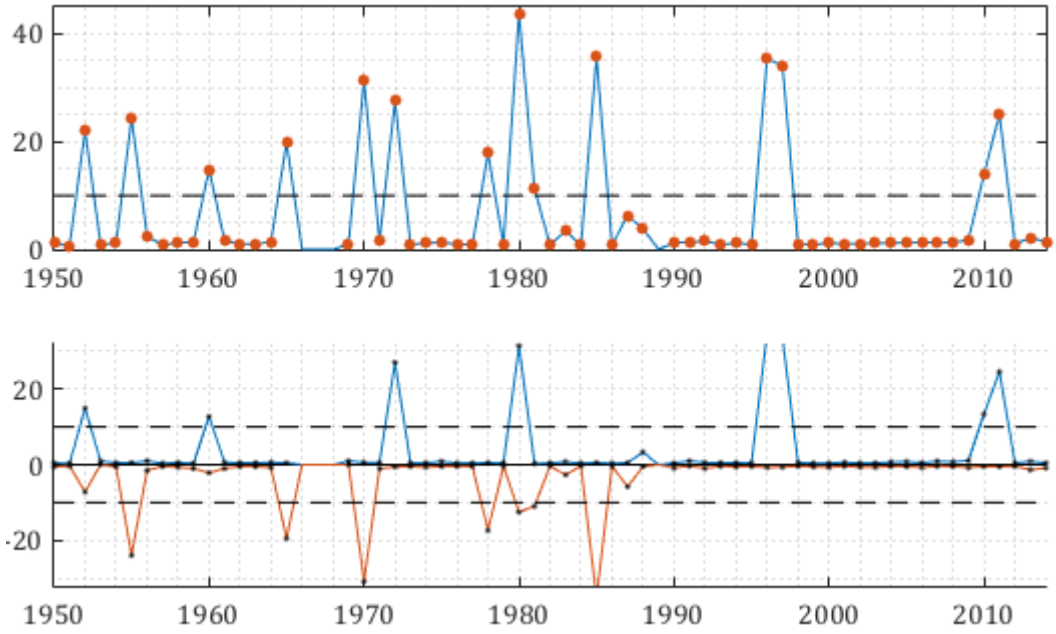

Figure 4.12: Yearly time spread of summer stations. The upper panel shows the difference in days between the earliest and latest profile for each year. The lower panel shows the difference in days between the median and the extremes. The dashed black lines depict the proposed 10-day limit.

small variations that magnify when interpolating the whole section. To prevent from factitious gradients, it is advisable to ensure that only continuous data are used at each yearly section. This processing step evaluates the time difference between the stations and removes those that differ considerably.

Finding a central time stamp of the observations helps setting a reference from which to evaluate each station. At this stage, the previous filtering steps have removed most of the interfering data and the repeated standard stations dominate the yearly records. For this reason, the median date provides an accurate measure of the core of the observations. Any remaining profiles lying far off in time can be disregarded.

Figure 4.12 shows the time spread of summer observations remaining every year at this processing step. The upper panel displays the total difference between the earliest and latest profiles. The most common time spread is under a week, and fully measuring the Seal Island section seems to require less than 5 days. This is more clearly seen from 1990s onwards, when the sole use of CTDs was common. Several peaks, from just above 10 days and ranging up to 44 days (in 1980) show how

the synopticity of the observations can be compromised. Additionally, displaying the same range but referenced to the median date (lower panel) helps to define a time limit of 10 days from the median. This boundary removes most of the peaks, yet offers a narrow margin to keep some useful additional observations. The effectiveness of this limit and any required fix can be identified when analysing the resulting stations at the end of the data cleansing.

Removing all stations that depart more than 10 days off the median leaves **726** profiles. It is worth noticing that this also removes the problematic profiles in 1978 and 1980, which were flagged in the previous step.

I. Disregarding nearly overlying stations

Sometimes, stations are repeated but not exactly at the same location. The precision used to record position and the drift of the ship can make repeated stations lie at slightly different positions. For this reason, some repeated stations cannot be identified in step 7. Additionally, different cruises can have stations that nearly overlap each other. As discussed in the preliminary assessment, this can pose a problem when projecting and interpolating profiles onto the standard line. This step filters nearly overlying stations as repeated stations, to keep only one sample.

Up to this point, all remaining profiles have passed the different quality filters. They are all presumed to be valid and any one profile within a set of nearly overlying observations could represent that station. To keep the final number of stations at a maximum, this program evaluates the observations in distance order from coast to the shelf edge. It compares the distance between consecutive stations and, if two are found within a small range, it keeps the one closest inshore. When three stations (or any odd number of stations) are found in a chain, disregarding the second cast (the middle one) maximises the distance between consecutive profiles. This enhances the likelihood of keeping a higher number of stations.

Setting a minimum distance between profiles to consider them as different stations can be an arbitrary selection. However, looking at different characteristics of the data can help finding a sensible distance. Figure 4.13 shows the distance

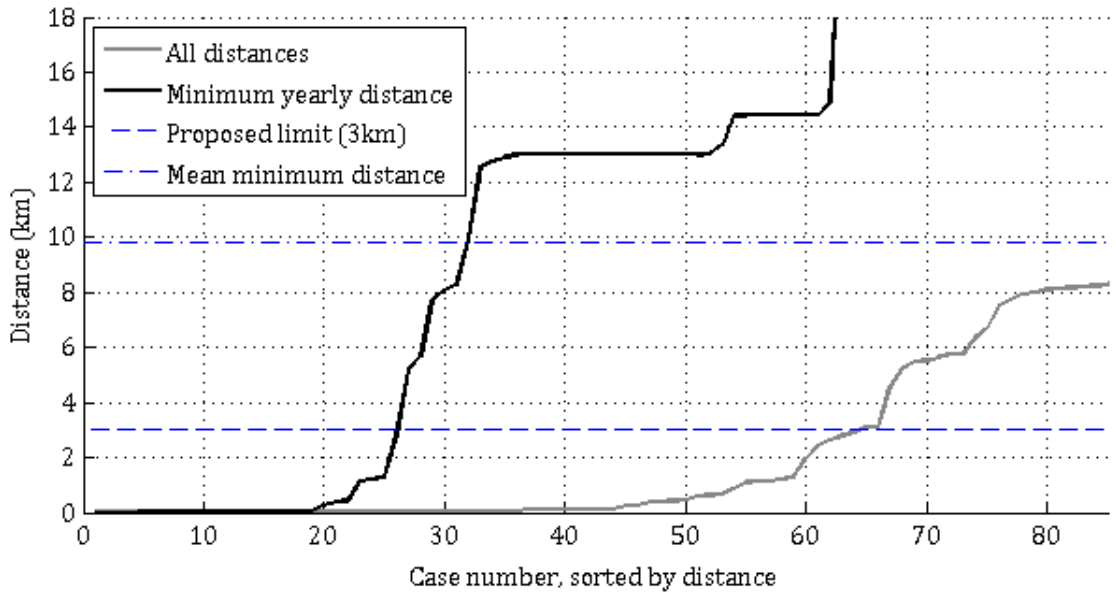

Figure 4.13: Distance between all summer stations within each year, remaining at this processing stage. Distances are sorted from smaller to larger. The grey line shows the distance difference between stations within a year. The black line displays only the smallest one found each year. They range beyond the axis. Horizontal lines show the distance limit used and the average minimum distance between 2 stations.

between summer yearly profiles, sorted in ascending order. The black line displays the minimum distance between two summer casts within the same year. The plateau of the line between 13 and 15 km shows this is a common minimum distance, which matches with the smallest distance between two Seal Island standard stations. It is also the median. The mean is slightly smaller, just below 10 km. The desired limit should be considerably smaller than these distances to allow for intermediate stations. At the same time, there is a large number of profiles separated by a very small distance, even smaller than 1 km. This is seen by the flat beginning of both lines. The chosen limit should disregard those almost overlapping profiles.

A distance limit of **3 km** proves to be adequate. It is approximately a quarter tenth of a degree (0.027°), a third of the average minimum distance and a quarter of the median. This still allows incorporating intermediate profiles between the standard stations, but removes nearly overlying casts. This boundary also accounts for a moderate ship drift and is a sensible range expected for stations repeated by different cruises. The limit, shown by the dashed blue line in figure 4.13, crops the observed distances at the beginning of their rapid increase. This only rejects less than 10% of the profiles, seen where the grey line (any distance between two

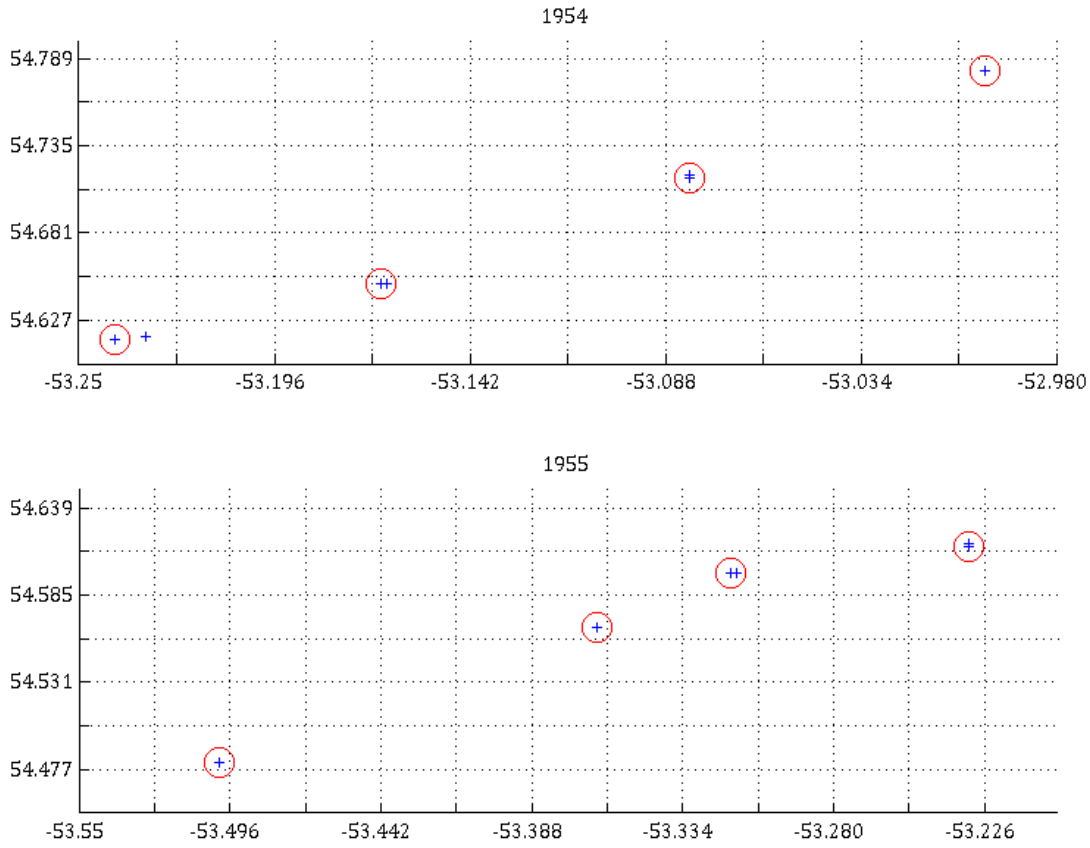

Figure 4.14: Example of two years presenting nearly overlying stations. Blue crosses show the position of the initially available casts. Red circles show the position of the final stations. When two casts lie with a grid box (dotted line), they are considered repeated stations and only one of them is kept. The grid is equidistant at 3 km to show the range of the imposed limit.

summer stations in the same year) meets the 3 km limit.

Displaying examples of how this limit affects the distribution of stations is a useful way to revise this boundary. Figure 4.14 partially shows the station distribution for 1954 and 1955, before and after this processing filter. The grid lines are at approximately 3 km, to show the range of the distance limit. Blue crosses show the initial locations. Repeated profiles can be seen as pairs lying within a grid box (three cases in 1954, two in 1955). When profiles lie very close together it is hard to spot them. The red circles indicate the final location of stations after this processing step, encircling the chosen profile. They show that this filter solves the nearly overlying stations problem and continues to preserve a fair distribution of stations. Removing these doubled casts reduces the number of available profiles down to **679 stations**.

J. Disregarding years with an incomplete spatial coverage

Individual profiles have undergone a thorough quality control. So far, from the initial 3905 profiles, only 651 still provide useful information for a summer composite time series. At this point, the automated filtering of single profiles is complete and only a more general analysis can improve the current set. The overall distribution of stations fully covers the Seal Island section (figures 4.5 and 4.6). However, this is not the case for every year with data. Some times very few stations sample the section. Even if there are abundant stations, they do not necessarily measure the full section. This is hinted in figure 4.13, where the black line (minimum distance between two summer stations within the same year) shoots out of range, up to 138 km. This final processing step evaluates summer yearly data as a whole. It analyses the number of stations and their extreme locations to ensure a consistent spatial coverage each year. Data from incomplete years are removed.

Figure 4.15 helps understanding of the variability in the yearly number of stations. The histogram shows two dominating distributions; 9 stations and 14. This is consistent with the original 9 standard stations, presumably implemented to 14 after the addition of CTDs. This gradual transition is also hinted in the time series. It is remarkable that, since 1950, only 4 years lack summer observations (1966, 1967, 1968 and 1989). Additionally, only two stations sample the transect in 1951, which is insufficient to compute a summer section and they can be disregarded. The remaining years have at least 6 stations. If equally spread along the section, this renders a minimum distance of approximately half degree. This is potentially a tolerable distribution, but only a final manual analysis can confirm it.

Other than the number of stations, it is important to ensure they provide a full sectional coverage. Observations need to capture the main shelf water features. *Smith et al.* (1937) provided with the first description of the circulation in the western Labrador Shelf and identified two jets; one near-shore and another over the shelf edge and slope. *Chapman and Beardsley* (1989) later included this in their proposed regional circulation pattern, in their figure 6. This sketch still remains being broadly used in Labrador shelf circulation studies and offers a reference

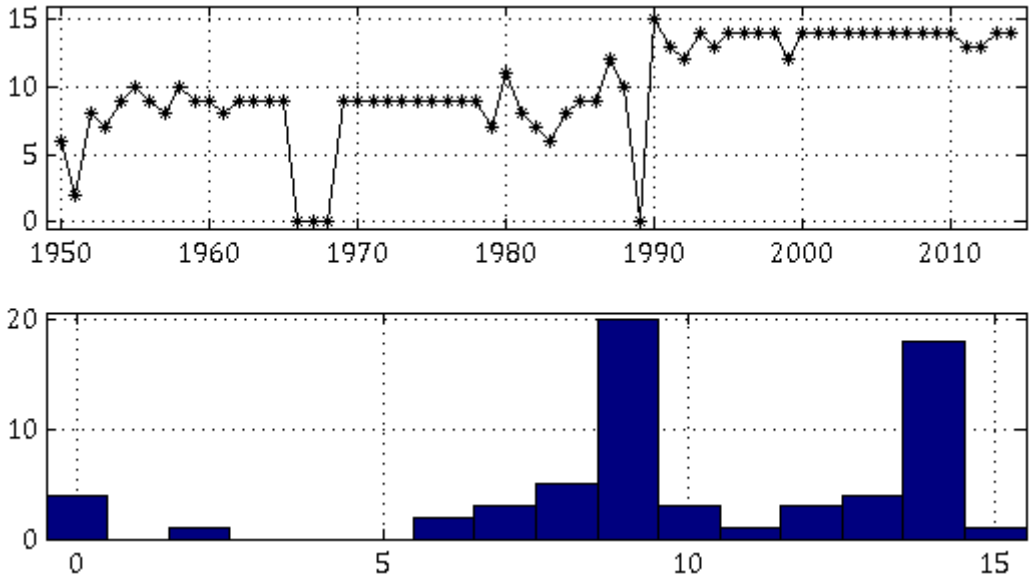

Figure 4.15: Number of summer stations available every year, after the main automated quality control. Data are presented as a yearly time series (upper panel) and as a frequency histogram (lower panel).

to establish the required stretch of the observations. Sections in which the first station lies further than 60 km from the coast miss the inshore current. Similarly, those which do not reach the edge, 250 km beyond the coast, fail to measure the Labrador Current. Sections that do not fulfil the spatial coverage set by these limits are removed from the dataset. Sections that start or finish within both of those boundaries are removed from the dataset.

This final processing step removes year 1951 due to its low number of stations. Equally, it dismisses years 1982 and 1983 because of their narrow coverage. After carrying out the full automated process of data filtering, **60** summer sections compose the dataset since 1950, with a total of **664** profiles.

K. Manual checks

Until this point, data cleansing has been devised as a set of programs that filtered observations to set standards. Throughout this process some profiles and issues have been flagged to be manually analysed. This section revises repeated stations with distinct data, it provides an overview of the resulting distribution of stations and evaluates the skill of the filtering parameters. It finishes by ensuring the

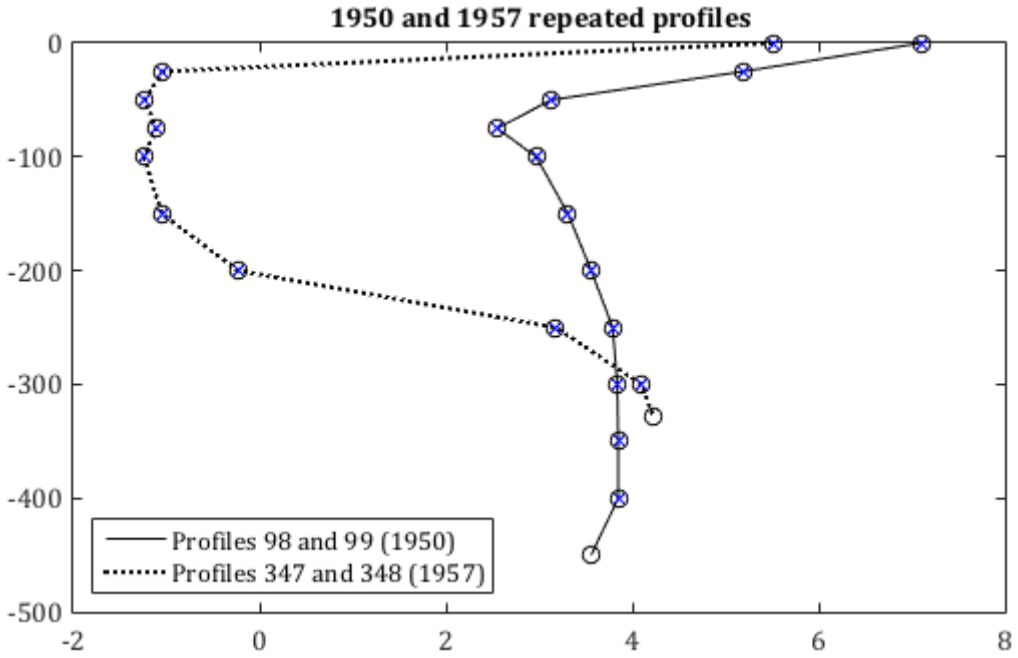

Figure 4.16: Conflicting profiles in 1950 and 1957. Both years present a pair of almost identical profiles at the same position. One profile is shorter (blue crosses) and the other has an additional bottom data point (black circles).

coherence of all profiles within each yearly section and by removing any remaining unsuitable profiles.

Several pairs of profiles were marked as 'conflictive' in step 7 of the processing. These pairs were located at the exact same position, but unlike other duplicated files, they presented different data. Here they are presented and compared in order to keep a single sample. The first highlighted profiles belong to years 1950 and 1957, as shown in figure 4.16. Each year has a station with a duplicated profile. However, their data are slightly different. Whereas all measurements are identical within each pair, one profile provides an additional data point at the bottom. This difference is depicted in the figure by the additional circle datum missing the blue crosses, which belong to the shorter sample. In these two cases, keeping one profile or the other does not account for a significant difference. Since it is preferable to conserve a larger amount of data, in both stations the deeper profile was kept (shown by the solid and dashed lines).

A different case is found in 1988. Two overlying profiles (2380 and 2368) show significantly different data. These are plotted in figure 4.17 (solid black and red lines), alongside all remaining summer profiles (grey lines). In the summer, en-

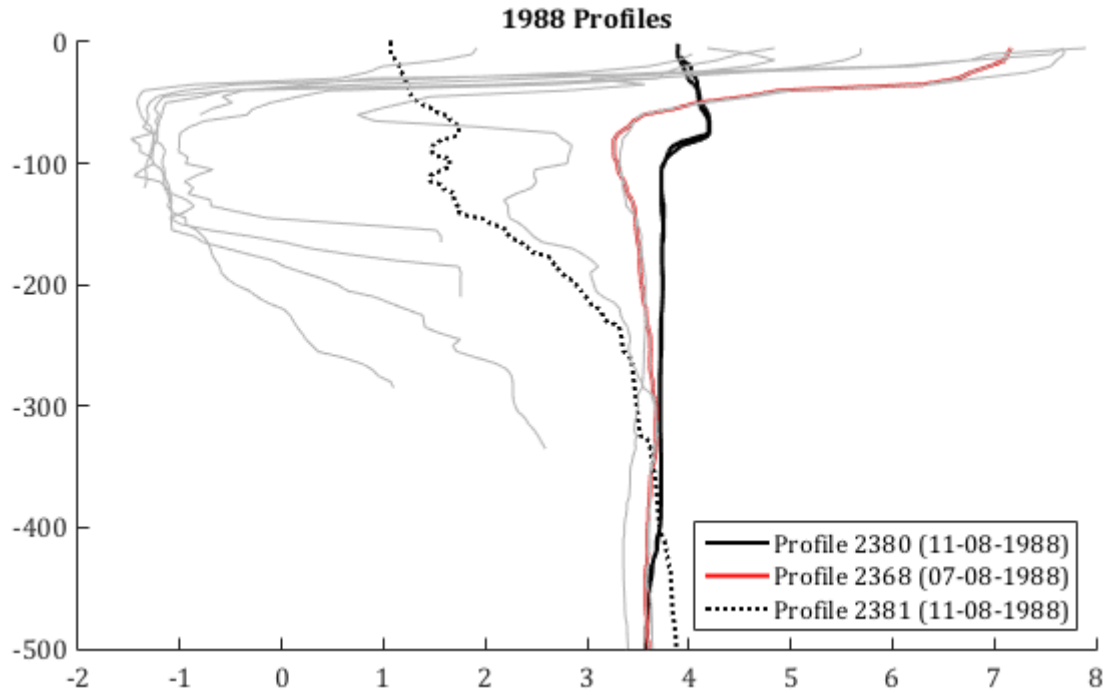

Figure 4.17: Summer temperature profiles in 1988 (grey lines). Profiles flagged as problematic are highlighted. Profiles 2380 and 2368 are different profiles, at the same position. Profile 2381 is inconsistent with summer profiles.

hanced irradiation warms up surface waters and profiles in this season are characterised by strong stratification. Profile 2368 (red) is consistent with all other summer profiles (grey). This is not the case for the repeated-position profile (2380; solid black) and the additionally highlighted profile (2381, dashed black). Their structure is distinctive of autumn, with enhanced mixing and surface cooling (*Colbourne et al.*, 1995). Comparing the dates helps finding a potential explanation for this anomaly. Although the date stamp is the 11th of August (11-08), these two profiles are presumably from the 8th of November (08-11). A date formatting confusion (day-month or month-day) is a plausible mistake. Additionally, the time stamp for all other profiles is from a few days earlier (7th and 8th of August). For these reasons, profile 2368 is kept and the pair of dubious profiles are removed.

In 1992, profiles 2669 and 2670 also inform about a repeated station. They were recorded just 90 minutes apart. The second cast is noisier and thus discarded, keeping profile 2669. This decision, however, does not have an impact in the study of shelf waters. This station is the furthest one offshore, over the slope and well beyond the latest standard station.

Other than repeated profiles, additional flawed data identified in the process were corrected at this point. Firstly, full up-down casts were split and only the downcast was kept. Secondly, those stations with incomplete processing were fixed (e.g. removing surface soak or time at the bottom). This includes sorting non-monotonic profiles vertically. They are casts presenting negative increments in pressure data due to waves reversing the CTD direction (such as the examples in figure 4.10).

After completing the analysis of individual profiles, sections can be studied as a whole. By displaying the distribution of summer stations remaining for every year, it is possible to ensure the spatial coverage is adequate. It also serves to confirm that the parameters used in the filtering process produce acceptable results. A full set of plots in annex 1.2 presents the final layout of summer stations, yearly. Overall, the resulting distribution of stations is remarkable most years, including the earlier ones. The dominating role of the Seal Island section in the regional observations is emphasised by the repetition of the standard stations year after year. Recent transects; after 1993, include what seems new standard locations. Also, additional observations beyond the line show how some sections can be implemented with measurements from additional cruises. Examples can be seen in 1980 and 1981. These years do not present data at the standard stations, but different observations along the line serve to compute a composite. In turn, their distribution is more irregular and the coherence between profiles will need to be further studied. Finally, the consistent distribution of data for all years confirms the appropriateness of the spatial limits used in the data cleansing process. Unlike other highly measured years, 1950 is the only section that provides with just 6 profiles; the minimum required number of stations. Even so, they are fairly distributed along the shelf and sample both ends of the section.

Further to the position of the stations, their interpolation into sections helps completing the quality control of grouped profiles. Data cleansing ultimately seeks to guarantee the coherence between remaining profiles. This is required in order to produce the yearly sections needed to analyse the observations, but also pinpoints inconsistencies in the data. These are commonly inconsistent profiles that show spurious or incomplete data. They include profiles with a resolution significantly

coarser than adjacent casts and also incomplete profiles that miss to measure the full water column. Section 4.3 fully covers the interpolation of profiles into consistent summer sections of temperature, salinity and other derived variables. Those were used retrospectively to identify and remove another 6 profiles with suspect data.

L. Final remarks

The different steps of the quality control conveyed a large and varied number of temperature and salinity profiles into a data set of summer observations. From the original 3905 files, the final number of accepted profiles is **654**. They cover a total of **60** different years from 1950 to 2014. Table 4.4 summarises all the filtering steps and the number of profiles remaining after each one. The finalised filtering leaves data organised into yearly sections, ready to be gridded into a common structure.

Filtering step	Remaining profiles
Initial number of profiles	3905
A. Selecting summer data only	1649
B. Limiting the time range from 1950 to present	1583
C. Excluding profiles that miss salinity data	1135
D. Minimum vertical resolution of 4 data points	1110
E. Narrowing horizontal spread to 15 km	857
F. Removing depth-binned repeated profiles	813
G. Disregarding repeated files and stations	760
H. Forcing a ±10 days synopticity range	726
I. Setting a 3 km separation between stations	679
J. Guaranteeing full spatial coverage of sections	664
K. Final visual checks of sections	654

Table 4.4: Summary of the quality control process and the number of remaining profiles after each filtering step.

4.3 A consistent yearly summer dataset

The analysis of the observations at the Seal Island and their variability requires consistent sections. They need to transform the unequal distribution of data into a standard structure. To achieve this, profiles are projected and interpolated into a regular 2 dimensional grid (depth and distance). This common framework makes

sections comparable from year to year, and also allows contrasting them with the model. Other than data gridding, it is equally important that the observations cover the same space. Earlier cruises and coarser profiles may compromise with small data gaps at the edges. To account for an equal sectional area throughout the dataset, a climatology is used to fill in these small gaps.

This section describes the confluence of the processed profiles into a yearly product of summer sections of temperature, salinity and density. First, I devise the standard structure onto which the profiles are projected and interpolated. I compile climatological sections with those years that present an extensive spatial coverage, in order to produce a composite of the section and to complete small gaps in coarser sections. Finally, I present the resulting product: a dataset of summer sections at the Seal Island from 1950 to present, with a gridded and consistent coverage.

4.3.1 Gridding into standard sections

Arranging data onto a two dimensional framework in order to obtain equally-structured sections is standard practice. This includes projecting the available profiles onto the standard line defined by the Seal Island stations. A regular line allows us to define the horizontal axis as a distance to a reference point, such as the beginning of the section or the coast. Similarly, binning profiles into equidistant depth intervals aligns the observations into a standard vertical axis. To finally complete the sections, data are interpolated horizontally along grid cells between profiles.

Projection to the standard line

The standard Seal Island stations, previously shown in table 4.3, are almost perfectly aligned. For this reason, their best fitting line provides a standard measure of the section. By extracting the slope and intercept from the line equation ($y = mx + n$), it is then possible to project the observations onto the standard transect.

The position of the original Seal Island stations is shown in figure 4.18. The best fitting line is plotted on top and its equation shown above. The standard line of the transect is defined by a slope of 0.5818 and a meridional intercept of 85.6152° (at the Greenwich Meridian; where longitude is 0). In addition to the line fitting the standard stations, the one fitting all the available observations only differs in slope and intercept by -0.0013 and -0.0744 respectively (not shown in the figure). This small difference assures the appropriate use of this line and also indicates again that most observations aim to measure the Seal Island section.

The orthogonal projection of data onto the line yields the shortest transposition. This is given by the distance between a station and the standard line in a perpendicular (or orthogonal) direction. The projected position of a profile is obtained by finding the intersect between the standard line and the perpendicular one that crosses the profile's position. Considering the line equation again, the orthogonal line is given by the negative reciprocal of the slope (see glossary for negative reciprocal) and the crossing point given by the position of the profile.

The translation of stations does not involve big changes to the original positions. Previous processing ensured that the selected profiles lie fairly close to the line. The maximum allowed departure was of 15 km and, in some special cases, this limit was smaller (5 km). Together with the imposed 3 km minimum separation between different stations, this means that the projected data are free from profiles that may lie too close together and that could generate irregular gradients. To provide an idea of how the projection changes the original positions, and how this change is much smaller than the distance between stations, figure 4.19 shows the projection for an example year. The chosen example year is 1980; according to appendix 1.2, the profiles in this year show the maximum misalignment with the standard line (the profiles lie away from the standard line). The figure shows that, although this year contains the largest projection distances (seen by the black lines, orthogonal to the section), it still preserves the order and relative distance between stations. It is worth noticing that this specific year was previously highlighted as a composite year; it contains data from different cruises that took place over summer that year. This explains why the distribution of stations in 1980 is more irregular than other years. Although this can compromise the quality of the gridded section, a full

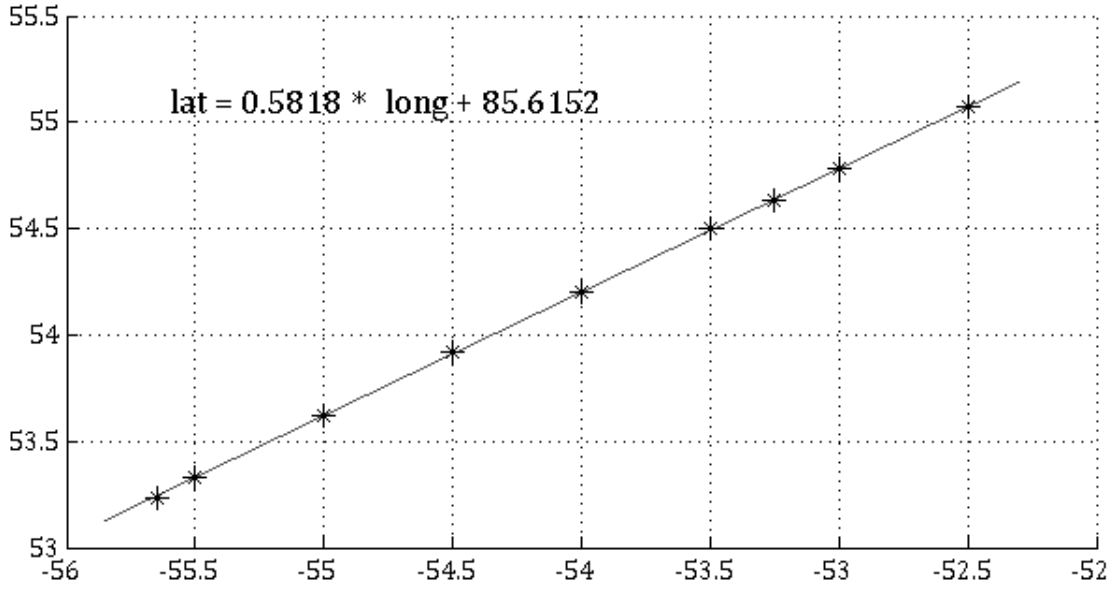

Figure 4.18: Best fitting line to the standard Seal Island stations. Stars show the position of the original Seal Island stations and the line depicts their best fit. The equation above displays the resulting line equation relating the longitude (x axis) with the latitude (y axis).

analysis of the final interpolated sections will serve to ensure the standards of 1980 and other composite years.

After projecting the data onto the line, all profiles are now arranged on the same plane, which is defined by the standard line and the depth. This allows gridding data into two-dimensional sections.

Vertical binning of profiles

The vertical resolution of profiles is varied. Bottles fitted with reversing thermometers present a much coarser sampling than current CTD casts. For example, the first profile in 1950 has a measure every 25 dbar, from surface to 125 dbar. In contrast, the latest profile in 2014 provides 2 to 4 datapoints per dbar. Equally distributed data are required to achieve consistent sections. Additionally, depth (in metres) is a more comprehensible variable than pressure (it is easier to understand depth changes). In this case it is also preferred to define the vertical dimension by depth in order to facilitate eventual calculations of cross-sectional area and transport. Prior to binning the profiles, depth is calculated as a function of pressure and latitude. The 1983 Unesco Algorithms for computation of fundamental properties

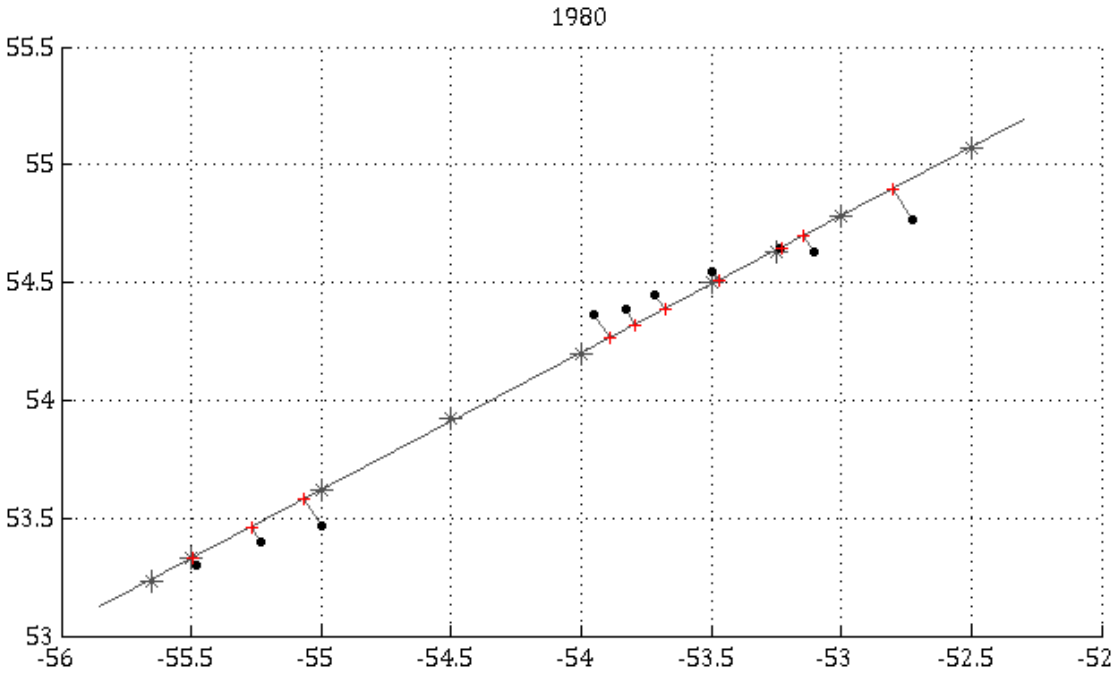

Figure 4.19: Projection of the 1980 summer profiles onto the standard line. Stars and the black line show the Seal Island stations and the standard line. Black dots indicate the original position of profiles, connected to their projected position (shown by the red crosses).

of seawater (*Fofonoff and Millard Jr*, 1983) are used for this conversion.

The chosen bin size needs to convey these different resolutions to a common vertical interval. Averaging data to **1 m** bins smooths out the profiles and provides a unitary and intelligible scale. This bin size smooths out the high-frequency measurements of CTDs, while keeping a reasonable resolution. Figure 4.20 shows an estimate of the resolution loss by averaging. Both histograms show the frequency of the temperature and salinity gradients every two consecutive data points. This helps visualizing the expected changes in the data by averaging to 1 m bins. The medians are smaller (or approximately equal) to the CTD accuracy ranges for temperature (and salinity), described earlier in section 3.1. Furthermore, over 95% of the data is within only ± 0.2 units, a much smaller vertical variation than the one offered by coarser bottle profiles. This indicates that the chosen bin size will homogenise all profiles while preserving the resolution of CTD casts to a reasonable standard. Other profiles with sampling coarser than 1 m are not sensitive to this measure. Instead, they are interpolated linearly along intermediate bins.

Finally, profiles are extended to the surface (0 m depth) in order to complete

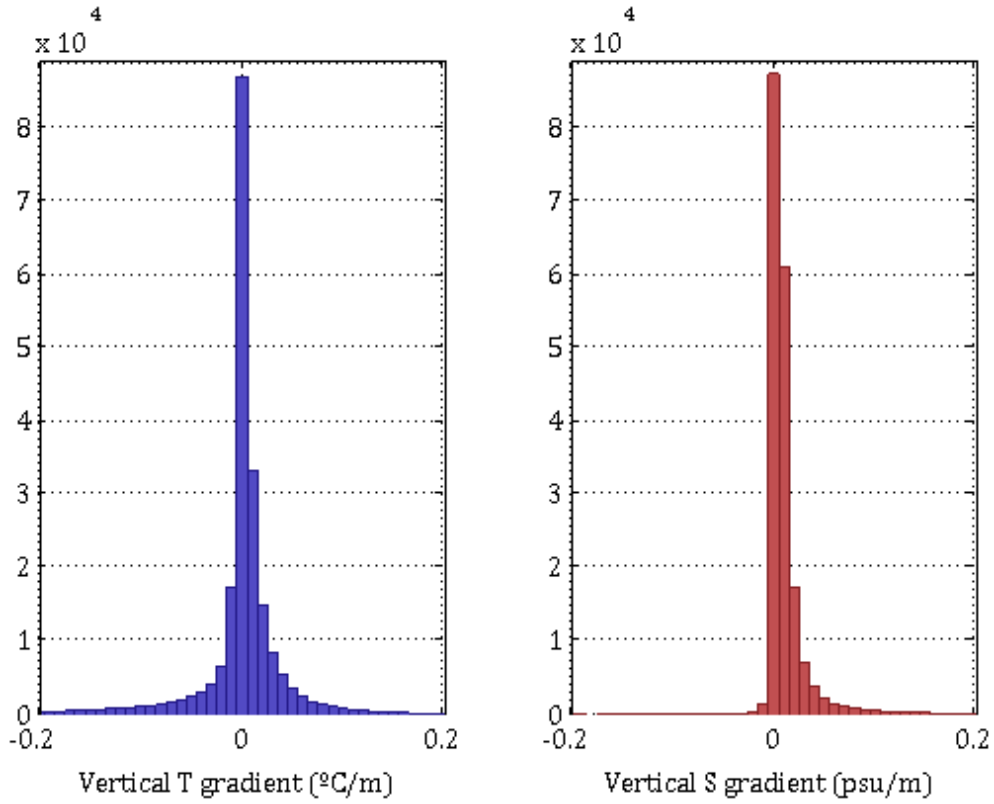

Figure 4.20: Histograms of all vertical temperature (left) and salinity (right) gradients from all valid summer profiles, at 0.01 intervals. Medians of 0.0014 °C/m and 0.0056 psu/m respectively. Repeated values (e.g. well-mixed layers) that render null gradients have been removed to emphasise vertical variations.

consistency. CTD casts acclimatise in the surface and profiles generally miss the first few meters. This is solved by assuming well-mixed water, finding the shallowest data values and replicating those as a constant in the bins above.

Horizontal interpolation

Equally gridded profiles can now be interpolated to yearly summer sections. The horizontal axis is defined by distance from a reference point. The coastline or the first Seal Island standard station are examples of possible references. In this case, the origin has been determined by the most inshore station of all the profiles that have been projected on the standard line. With a longitude of -55.66° and a latitude of 53.23°, it almost overlaps with the first standard station (see table 4.3). This position lies at approximately 30 km from the Canadian shore and, as a reference, it is given a distance value of 0 km. Other stations are sorted by their offshore

distance from the reference position. For every yearly section, the space between profiles is completed by linear interpolation.

It is important to select a horizontal resolution that it is coherent with the spatial distribution of data. A horizontal spacing larger than the distance between two consecutive stations would induce to unnecessary smoothing. On the other hand, an excess of intermediate interpolated bins increases the size of the dataset without providing any additional information. A horizontal grid size of **2.5 km** provides a concise resolution smaller than the distance between two adjacent profiles. The minimum distance between two standard stations is 15 km, giving at least 5 bins between them and an average of 10 intermediate data points in the whole dataset. Most importantly, this value is below the 3 km limit used in section 4.2.2 to differentiate nearly-overlying stations. This ensures that two different stations will never be averaged together. Finally, the chosen grid also sub-samples the model resolution (1/12° or approximately 8 km). This allows the use of the same framework for the model and the observations.

The resulting grid is $2.5km \times 1m$. All selected summer profiles are interpolated into sections of temperature, salinity and density. These provide sections over 58 years, from 1950.

4.3.2 Using climatology to fill gaps

In order to study the variability of integrated products, such as transports, it is important to work with consistent sections (i.e. equal area). The distribution of profiles and their sampled depth vary from year to year, covering a varying area. To preserve the coherence throughout the time series, gaps are filled with an averaged product. Here, a climatology of high-resolution (CTD) cruises is computed and used to complete all sections. The high-resolution of those cruises allow for the best representation of the gradients found at the Seal Island section. This subsection briefly describes the climatology sections, it covers the process to fill those missing gaps and it presents the final Seal Island dataset at the end.

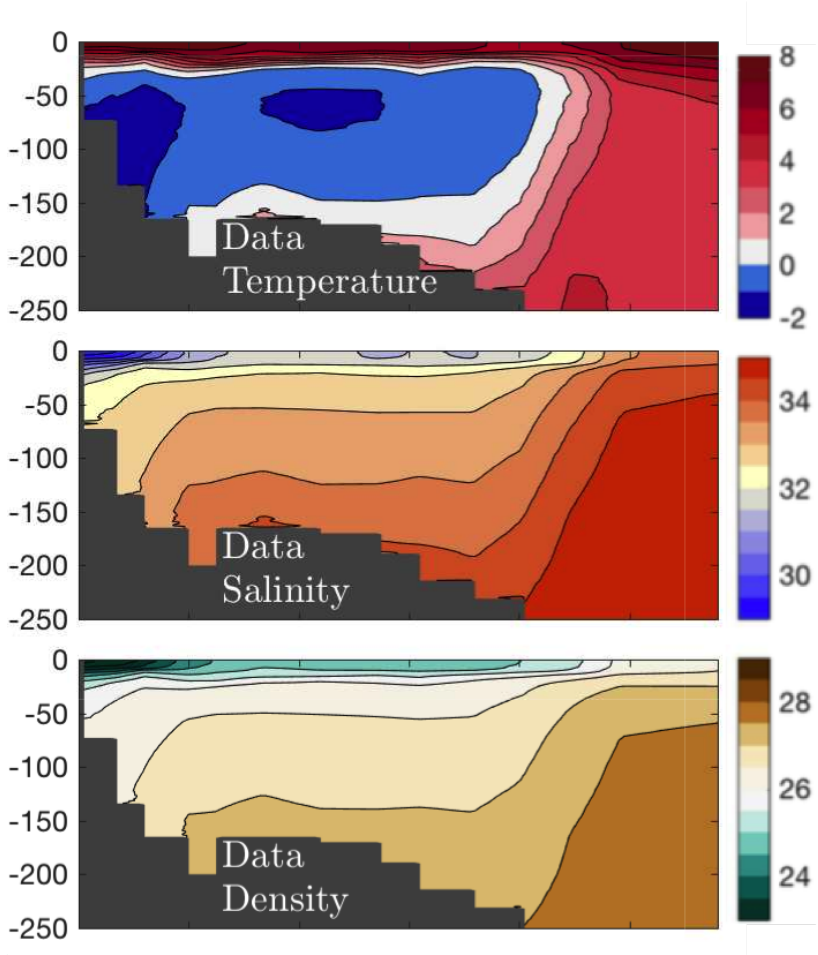

Figure 4.21: Seal Island climatology sections of temperature (top), salinity (middle) and density (bottom). Averaged summer sections from 1995 to 2010.

Climatology sections

Climatological sections allow us to describe the average conditions of the Seal Island section as well as to complete missing data. It is essential to only use those years that offer a good representation of the transect (from coast to slope) and of the bathymetry (by having abundant and full profiles). Although high vertical resolution profiles sections start in 1980, it is only since 1993 that they present an extensive coverage of the shelf (around 14 equidistant repeated stations, from surface to bottom). This would invite to compute the climatology sections from 1993 to 2016. However, to make this comparable with the model's time span, this climatology averages data from 1995 to 2010.

The climatology sections of temperature, salinity and density are shown in figure 4.21 and briefly described here. The temperature section reflects the strong

stratification due to enhanced heating in the summer, as it was also seen in the individual profiles. Furthermore, a subsurface core of very cold water ($< 0°C$) surrounded by warmer waters can be identified, depicted by blue colours. This is the Cold Intermediate Layer (CIL), a characteristic structure of the Labrador and Newfoundland shelves (*Petrie et al.*, 1988).

Other than vertical stratification, the salinity section also shows a horizontal structure in the form of two fronts. Salinity contours are flat in the mid-shelf, but they strongly tilt towards the bottom/surface at the inshore/shelf-break sides of the section. This means that, at those fronts, water at the same depth is fresher towards the continent. It is worth noticing that water with a very low salinity (< 30 psu) forms an inshore wedge at the surface. The combination of these salinity and temperature structures are responsible of the density distribution. This is very similar to the salinity section; in the cold waters found at high latitudes the salinity acquires a larger role controlling density.

To understand the variability of these sections and the error (variation from the climatology), the mean standard deviation of each section is calculated and shown in figure 4.22. These account for 0.56°C in the temperature section, 0.13 psu for salinity and 0.10 $kg{\cdot}m^{-3}$ for σ. The uncertainty in temperature lies at 20 m depth, near the thermocline, and reaches a single point maximum of 2.9°C. Here is where most interanual differences are found, depending on what depth the CIL begins. This is followed by the shelf-edge waters, showing the range area of the offshore CIL limit and with values around 1.5°C. The rest of the water shows near-zero standard deviations.

Salinity displays a different pattern of variability. Most of it is concentrated in the near coast freshwater wedge, reaching a maximum of 1.46 psu. Surface waters (up to 20 m) show mean differences between 0.6 and 0.8 psu. The rest of the section shows small errors, particularly in the offshore deep waters. This pattern is repeated in the density section, which is mainly controlled by salinity at this latitude.

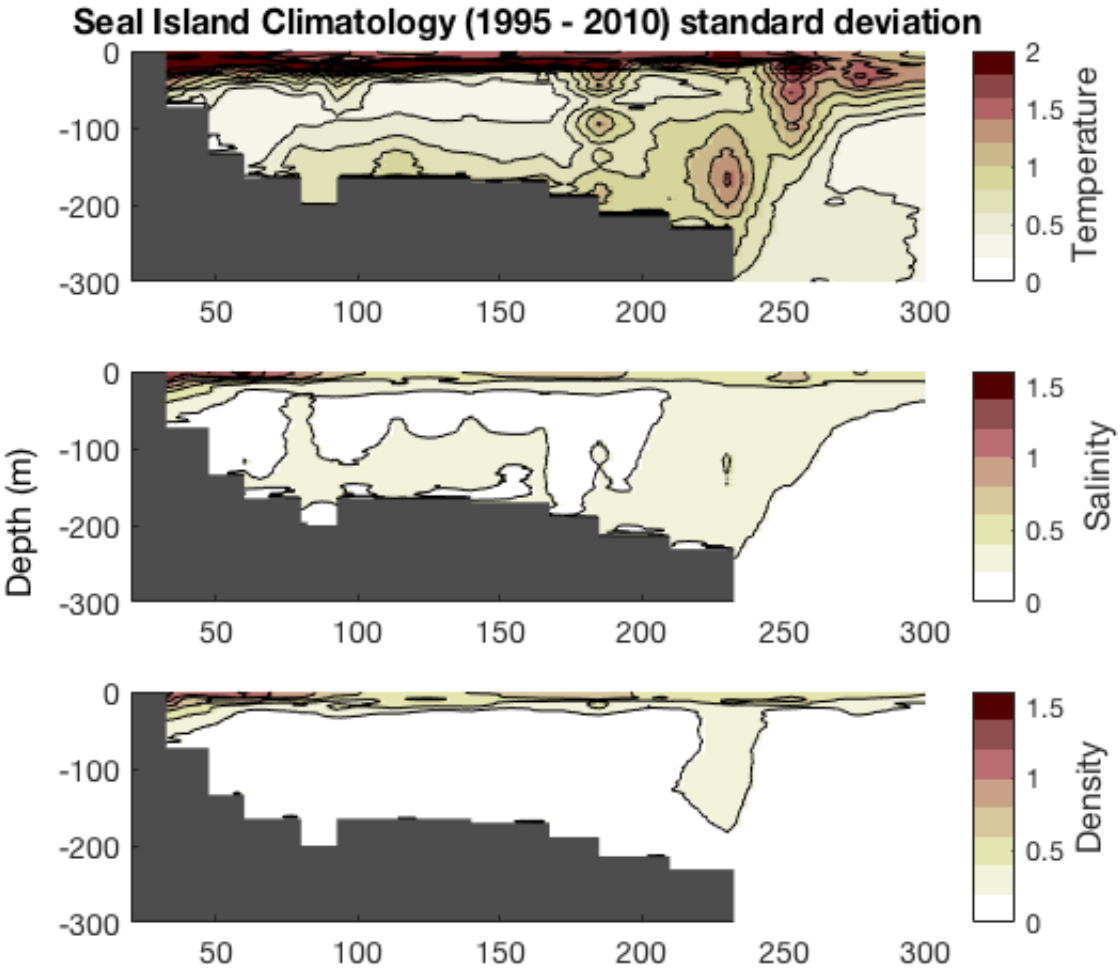

Figure 4.22: Standard deviation of the Seal Island climatology sections of temperature (top), salinity (middle) and density (bottom). Averaged summer sections from 1995 to 2010.

Filling gaps

The newly computed sections now help completing yearly sections. In most cases, this is only at the bottom of the sections where a coarse spacing between profiles prevents from accurately interpolating data towards the seabed. Filling sections can be a significant source of error in places with strong gradients; these are locations where water can present a relevant inter-annual variability. The fronts seen near shore and at the shelf break are the most sensitive regions of the section. The earlier quality control has removed those yearly sections with a poor spatial coverage and now this reflects as gaps at the sides of the section being small. This means that completing sections with the climatology does not compromise the sensitive front

regions.

In addition to this, the previous study of the climatology sections' standard deviation showed that most of the variability lies at the surface and at the fronts. The infilling of sections happens at the bottom and at the very edges of the sections. These areas all display little variability (i.e. near-zero standard deviations). In further sections where these sections are used to calculate other variables (e.g. transport), the results will be compared to not-filled sections to fully understand the added uncertainty.

One particular case has emerged in 1981. This year, summer profiles miss the first 50 m of the surface and no explanation for this has been found. In this case, as shown in figure 4.23, extrapolating the first values up to the surface (top panel) does not offer a satisfactory solution. Again, the climatological sections can provide a useful tool to fill this gap. In this particular case, the surface waters have been interpolated using the surface climatological values (result shown in the bottom panel). The section appears more consistent now. Other missing parts at the bottom and the sides have been replaced with the climatological values (no interpolation involved).

The particular data distribution of this section highlights its higher uncertainty compared to the other sections. This is to be considered when using this year's data in further analysis. The following subsection further explains this and also evaluates which other years may present a higher uncertainty.

The Seal Island yearly summer dataset

The final summer temperature, salinity and density sections at the Seal Island from 1950 to 2016 are presented in appendixes 1.3 to 1.5. They include the position of the profiles that remained after the data quality control and the depths they measured. Sections are shown after being completed with the climatologies.

These sections consistently convey the different resolutions and distributions into a standard grid regardless of the evolving technology. Earlier years present blunter shapes due to their coarser resolution, yet they do represent the main features found

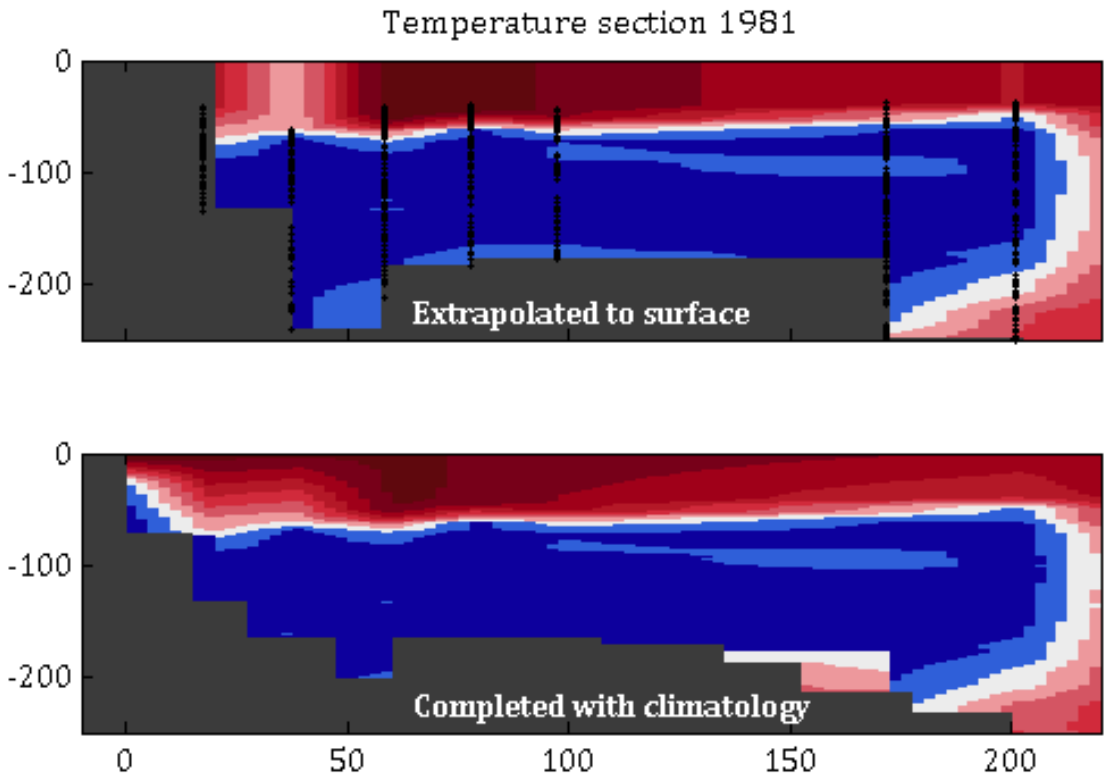

Figure 4.23: The 1981 temperature before and after completion with the climatology. The top panel shows the section before completion, where the missing surface values were completed by extrapolating the first datum of each profile. The bottom panel shows the corrected section, interpolating profiles to the climatological value at the surface and completing gaps with the climatological section.

in the Seal Island region. Some incomplete sections show discontinuities where gaps have been filled with the climatologies, that can generate sharp gradients. Where secondary variables are calculated (such as velocities and transports), they only use original data to avoid spurious values. New climatological values of those derived variables will complete those gaps later. In this way, the regions filled with the climatology can be understood as a background correction to account for inconsistent areas. For instance, this can be useful to calculate the mean salinity of the section without fearing that a year may be apparently fresher because it does not reach so far beyond the shelf break (where water is saltier). Another example is the volume transport. A smaller section will usually constrain a smaller transport, but by filling these gaps this is compensated by a background or mean transport.

This is useful where the relevance of the filled areas is small. That is mostly regions that are fairly constant and do not show important gradients, as it is the case for most sections. Some years, however, present weaker resolution or a

more irregular distribution and can present a higher uncertainty. These data are highlighted here. The first example is year 1981. It was studied in the previous subsection as the set of data that missed the top 50 m. Variability in the surface is high and observations of the top layer are essential to account for this. However, the processed section shows values and gradients that are coherent with the rest of the time series. Despite the larger uncertainty in this year, it still provides with valuable data. Other examples of conflicting years are 1950, 1979 and 1980. All three cases show a significant (higher than average) distance between two consecutive stations. These gaps always occur at the mid-shelf, where isolines have been observed to be flat and where general variability is smallest. Temperature, salinity and density structures do not seem to be significantly affected by this spread and these sections can be used with reasonable certainty.

4.4 Summary

This chapter has covered the thorough process to assemble a long time series of yearly summer sections of hydrographic data at the Seal Island section, on the south Labrador Shelf. It included a primary analysis of the observations, covering their basic characteristics and distribution in time and space. The plethora of profiles have been sorted through a comprehensive quality control and discrepancies have been removed. Data have been finally merged onto a regular dataset. The main findings and results are as follows:

- Originally, 3905 hydrographic profiles were retrieved from the Seal Island.
- As shown by their distribution, the greatest potential of the data is to obtain a yearly dataset of summer sections.
- The quality control categorised 630 valid profiles.
- Data are used to compute gridded sections of temperature, salinity and density.
- The sections span from 1950 to 2016 and sample 60 of the 67 years.
- Enhanced uniformity since 1993 allows to compute climatological sections for the 1995 to 2010 period. This is used to fill missing data gaps in some sections.
- The long time spread of the data is reflected in varying resolutions and quality.
- Their different characteristics have been successfully conveyed into consistent sections.
- Years 1950, 1979, 1980 and 1981 present higher uncertainty but still provide valuable data.

This finishes the general data processing and their quality study. The computed sections can now be used to evaluate the performance of the model (chapter 5), to derive further variables (e.g. velocity and transports) and to study the variability of the waters on the shelf (chapter 6).

Chapter 5

Model study of the Labrador Shelf circulation

The intricate circulation on the Labrador Shelf challenges the analysis of the observations at the Seal Island. An exhaustive description of the circulation is essential to put the observations in context, to unveil the sources of the water on the shelf and to inform about the multidecadal variability of its components. This chapter provides a comprehensive model study to develop detailed understanding of the upstream sources and pathways of freshwater on the Labrador Shelf. This is used to specifically identify the Arctic-origin water in order to divide the shelf water into source regions. In chapter 6, this new knowledge will allow isolation of the Arctic components in the observations to describe their multidecadal variability at annual resolution.

It is already known that the Labrador Shelf circulation features a complex interaction of Arctic currents, Atlantic water and freshwater from run-off and ice melt (*Loder et al.*, 1998). The southward-flowing Labrador Current (figure 5.1), formed as the Baffin Island Current joins the recirculating West Greenland Current, dominates the circulation over the shelf's edge and slope with an estimated total transport of 11 Sv (*Lazier and Wright*, 1993). A near-coast jet called the inshore Labrador Current has been observed (e.g. *Lazier and Wright*, 1993; *Mertz et al.*, 1993; *Smith et al.*, 1937) and described in models (Wang et al. 2015; Wu et al. 2012). However there remain gaps in our knowledge that limit our understanding

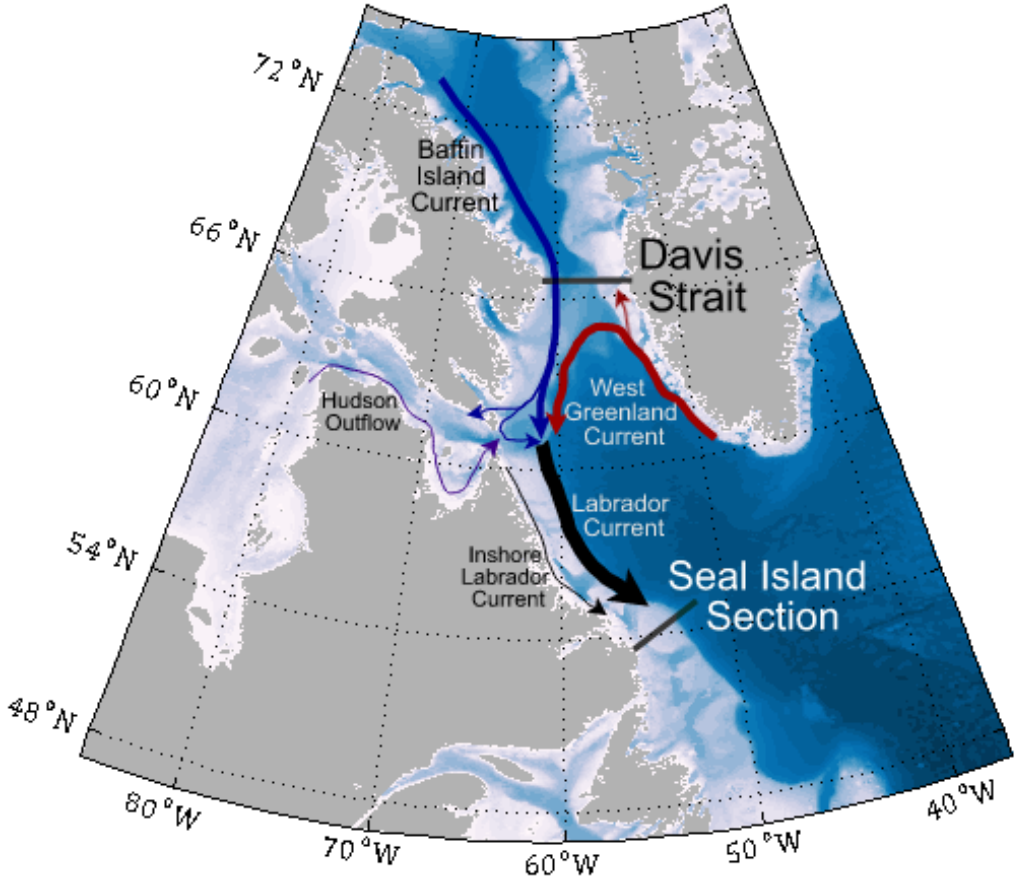

Figure 5.1: Sketch of the known circulation on the Labrador Shelf. Other than the main currents, sections with repeated observations at Davis Strait and the Seal Island are shown.

of the sources of the freshwater on the shelf. For example, the nature and origin of the inshore jet is not clear, and the fate of the Hudson Strait outflow (including the extent of exchange with the Labrador current) remains uncertain (*Dickson et al.*, 2007). Additionally, we know that the main sources of Arctic water are through export to the west and east of Greenland, carried by the Baffin Island Current(*Ingram and Prinsenberg*, 1998; *Jones et al.*, 2003) and the West Greenland Current (*Cuny et al.*, 2002; *Dickson et al.*, 2007; *Myers et al.*, 2009) respectively. But there are potentially additional large inputs of freshwater from the Hudson outflow that could confuse the signal of Arctic export variability in the observations (*Straneo and Saucier*, 2008).

The NEMO model, with its current highest resolution available (1/12°), provides an adequate tool to address these open questions. In this chapter, I first evaluate the model performance to validate further results. For this, I compare hydro-

graphic observations at different sections with their model analogue. I complete the evaluation contrasting the regional circulation and surface properties with the available literature. I then continue by identifying the different freshwater sources and their pathway to the Seal Island section. This analysis sheds light on the fate of the Hudson Strait outflow, includes a description of the dynamics of the shelf jets and uses the Montgomery function to determine the flow pathways. Finally, I employ this new knowledge to divide the shelf water into source regions in order to compute freshwater transports and test their degree of preservation at the Seal Island section. The results of this chapter, summarised at the end, will provide the required understanding to investigate the Seal Island observations in the following chapter.

5.1 Model performance

General circulation models provide extensive representations of the oceans in a scale (both in time and space) that observations do not achieve. This makes them a useful tool for precise examination of the system. However, their skill needs to be continuously assessed. This section revises the general accuracy of the NEMO model to replicate the Labrador Shelf features. The analysis comprises a model comparison with available observations at standard sections and in the surface Labrador region (see section 3.2 for more information about the model and the run).

Co-localisation of model sections

To study the representativeness of the model, comparable data first need to be co-localised in the model framework. This process involves the discretisation of stations in the model grid in order to find the closest-lying grid cells. Then, intermediate gaps are completed by the shortest route between grid points. This way, the extracted model section provides the most representative data.

For a certain section, the position of every standard station is first found in the model framework. This is given by the grid cell that presents the shortest

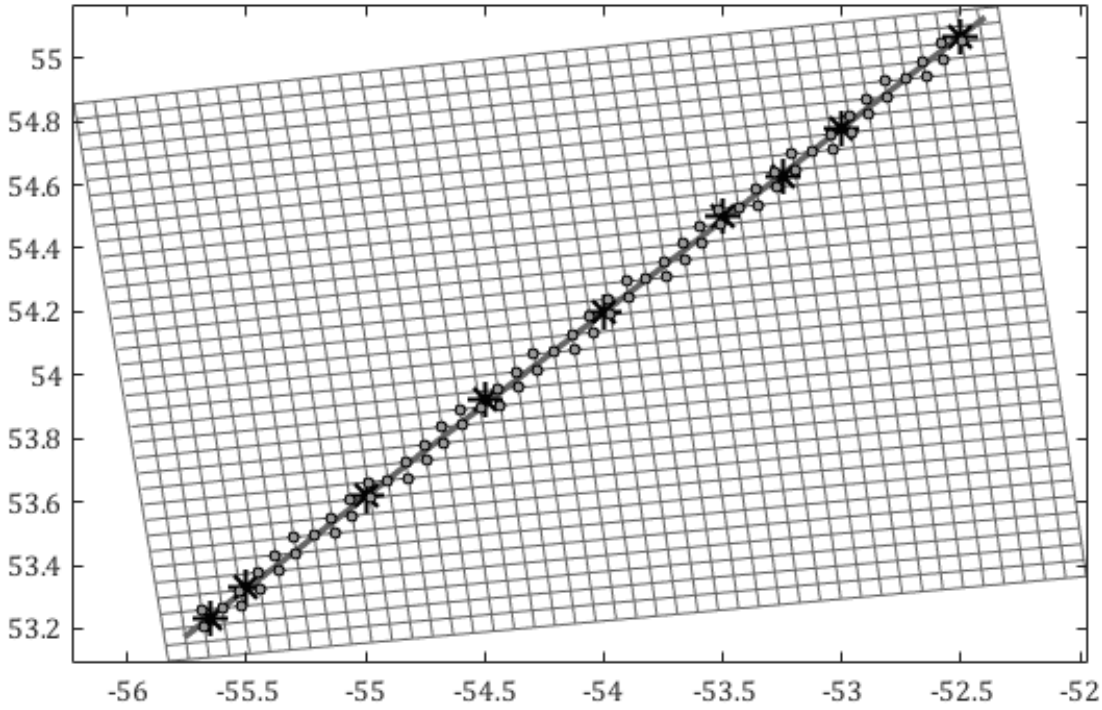

Figure 5.2: Co-localisation of the Seal Island section in the model framework. The grid shows the centre of the model cells in a longitude-latitude reference. The Seal Island standard stations are shown by the black stars, including their fitting line. The grid cells that best represent the section, which result from the colocalisation process, are displayed by the grey circles.

distance to the original coordinates of the station. Once the standard positions are translated to the model reference, the section is completed by the grid cells that yield the shortest path. This is done following a 'grid staircase' approach. Starting by the first co-localised station, the grid cells around it are assessed. The one displaying the shortest linear distance to the second standard station is selected as the consecutive point of the section. This process is then iterated for every newly incorporated position until reaching the second standard position. Finally, this is repeated for every station, following the section until the last standard position. The resulting grid emulates the given section in the model framework.

Figure 5.2 displays the Seal Island section and its co-localisation in the NEMO framework. The model horizontal reference is given by i and j positions (shown by the grid) and the circles show the model positions that render the best fit. Stations are devised in geographical coordinates. Because models are not generally defined in a longitude-latitude frame, the staggering of the model positions with respect to the geographical grid results in the displayed staircase-like layout. This can also

produce small aliasing (examples can be seen as winding lines in figure 5.4, left column). In order to smooth out this effect, model stations can also be projected onto a standard line following the same method as section 4.3.1. The co-localised Seal Island section has been projected onto the standard line for this reason.

Comparison with standard sections

The accuracy of the model is investigated at the Seal Island section; where we have the set of observations, and a realistic performance is required for the analysis. The climatology sections produced in the previous chapter (figure 4.21) stand as a first approach to test the model performance. The standard stations (table 4.3) have been co-localised in the model and sections of temperature, salinity and density have been produced. They are monthly model products for July and August, from 1995 to 2010, to match most of the time span of the observational climatologies and to capture their summer imprint. This period is the closest one in the available model diagnostic files described in section 3.2. It excludes the first two years (1993 and 1994; salinity data in the model prior to 1995 is unreliable). Model data span to the end of 2010, thus they also exclude the last years of the climatology. Results are shown in figure 5.3.

The overall performance of the model at the Seal Island section is in very good agreement with the climatology. The sections of all three variables are remarkably similar between model and observations. The properties show near-identical structure with matching distribution of isolines and, most importantly, equally located fronts. This is especially visible in the density distribution. Isopycnals are flat in the mid-shelf and significant horizontal gradients appear inshore and at the shelf break. The coarser resolution in the data, compared to the model, can explain the more rugged aspect of the observations. This is particularly seen off the shelf, where fewer profiles are available and more sudden gradients are present. However, the analysis here focuses only on the shelf and hence it is not affected adversely by this characteristic. Additionally, mixing in the model is parametrised, and forcing in the real world is different to that of the model. Over-represented mixing can cause a smoothing of gradient. However, the model represents both shelf fronts

and at the same position than the observations.

The modelled temperature successfully represents the Cold Intermediate Layer (CIL), in the same way it is evident in the climatology. Although the structure is well represented, temperature in the model appears to be about one degree warmer than the observations and slightly cooler at the surface. The salinity sections match instead, displaying almost identical structure and magnitude. Because salinity mainly controls density at low temperatures, the small offset between the temperature sections does not seem to have a significant effect in the density structure. The way properties are distributed along the section will have a major role describing the circulation and the processes found on the shelf. For this reason, correctly representing the structure is more important than the precise values of the properties. At the Seal Island, the model shows a great structural agreement throughout and a fair match of mean values. It thus provides a useful tool to represent the long-term means of this section.

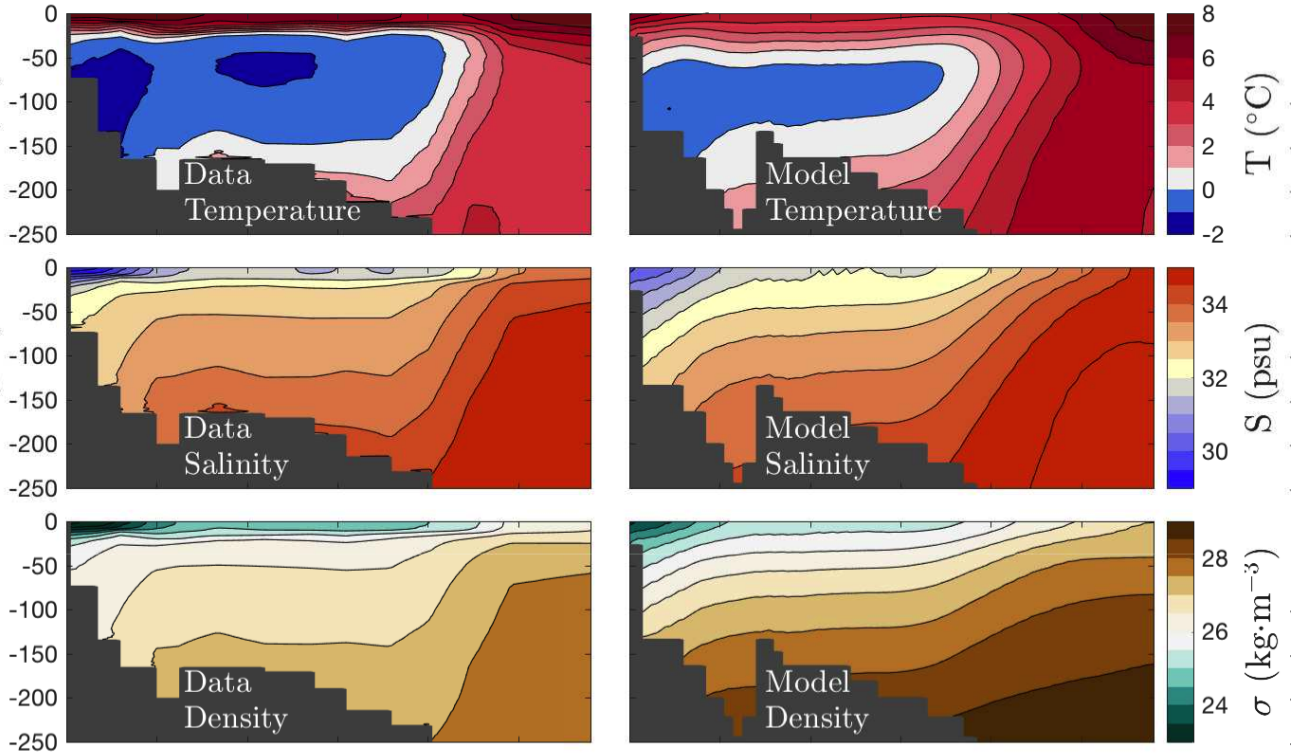

Figure 5.3: Temperature (°C; top), salinity (psu; middle) and σ (kg/m^3; bottom) summer climatology sections (July and August 1995 - 2010) at the Seal Island, in the observations (left) and the model (right).

To ensure that the skill of the model does not only apply to climatological means, this assessment is completed with an example of a single year. Figure 5.4 compares the temperature and salinity sections in July 2010 with an analogue from the literature. *Colbourne et al.* (2011) provide an oceanographic report of the region, including analysis of the Seal Island section using the same set of observations. The results show the same attributes described in the previous example. Temperature in the model remains approximately 1 °C warmer. The stratification at the surface, however, is better represented in this specific year. Salinity shows a good agreement again, especially on the shelf. Both variables also represent the structures off the shelf, though to a lesser extent. The differences are small and are found beyond the slope. They do not have an impact on the Labrador Shelf and, overall, the model proves to be a useful tool to analyse the circulation at the Seal Island section.

On the north side of the Labrador Sea lies Davis Strait, as displayed in figure 5.1. Arctic freshwater export west of Greenland occurs through this gateway, which has

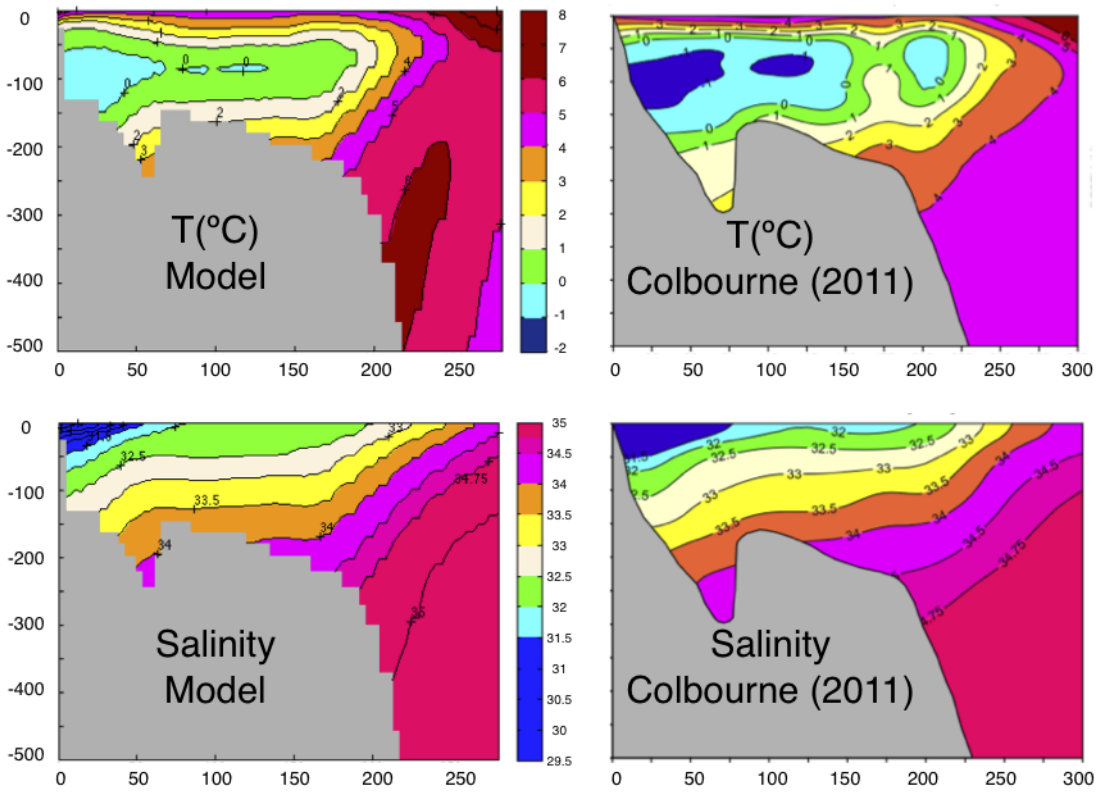

Figure 5.4: Model-observations comparison of the temperature and salinity sections at the Seal Island in July 2010. The observed sections have been modified from figure 10 in Colbourne et al. (2011). They use the same dataset. The model sections emulate the colour scale to make them comparable.

been continuously measured by a mooring array from 2004 to 2010 (*Curry et al.*, 2014). As such, it also provides data to test the performance of the model at the other end of the region. The temperature and salinity sections in August 2005 by *Curry et al.* (2011) are compared with the model results for the same month in figure 5.5.

Again, the representative skill of the model is high. All main structures found in the observations are accurately represented in the model. This includes the southwards flowing Arctic water (the subsurface core of cold water) and the shelf and slope components of the northwards flowing West Greenland current (warmer waters in the east). The 27 kg/m^3 isopycnal, density of Arctic water at its freezing/melting point (*Curry et al.*, 2011), lies in the same position. In this comparison,

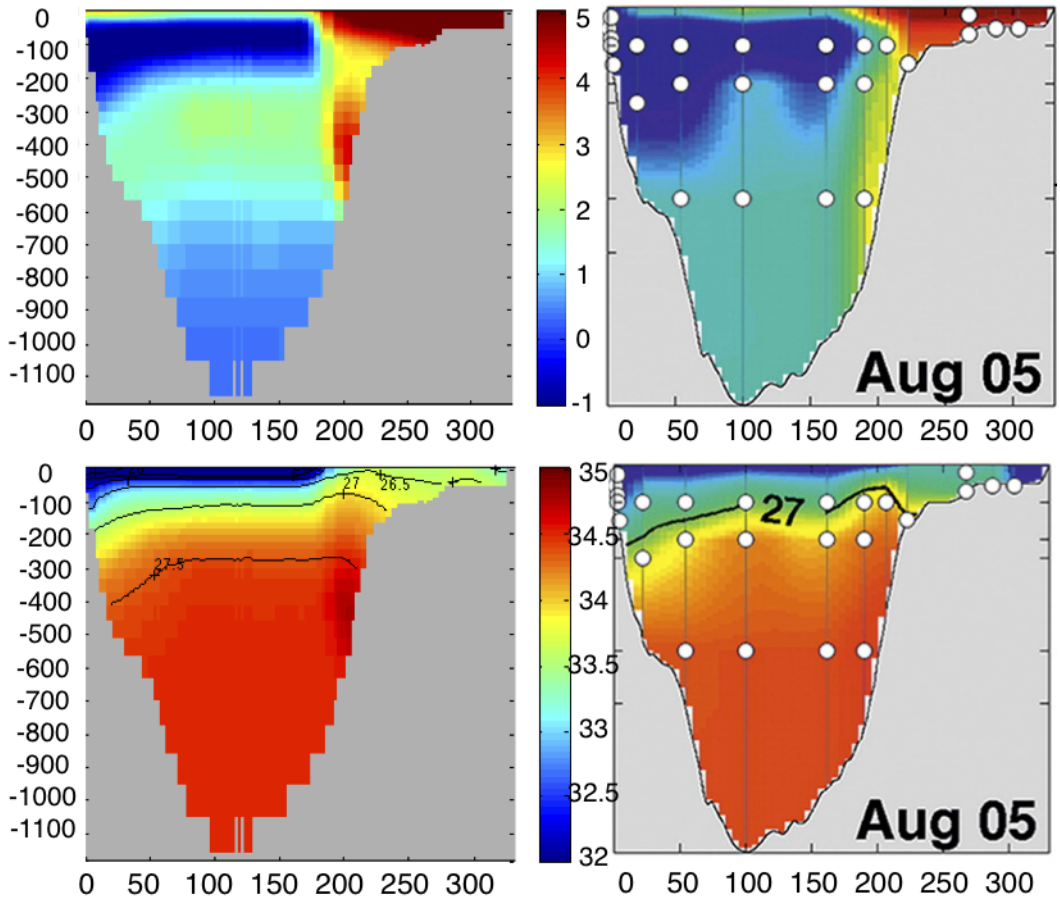

Figure 5.5: Model-observations comparison of the temperature and salinity sections at Davis Strait in August 2005. The observed sections have been extracted from figure 2 in Curry et al. (2011). Contours display σ and white dots the locations of the moored instruments. The x-axis displays distance from west (Baffin Island) to east (Greenland). The model sections emulate the colour scale for comparability.

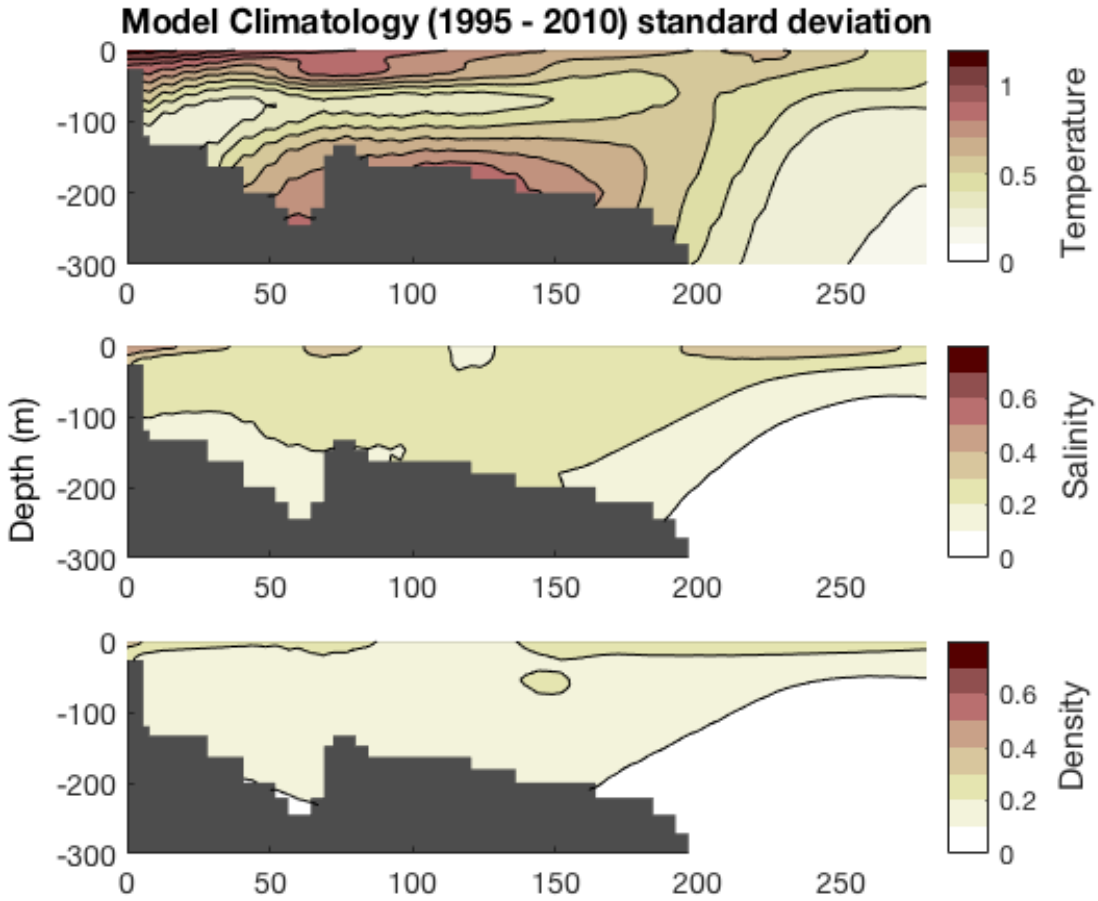

Figure 5.6: Standard deviation of the Seal Island model climatology sections of temperature (top), salinity (middle) and density (bottom). Averaged summer sections from 1995 to 2010.

it is important to consider the different resolutions. Observations are measured at the noted instrument positions, the intermediate gaps are then linearly interpolated and depths below 500 m are held constant with the values at that depth. The regions where discrepancies arise coincide with areas that miss instrumentation; waters deeper than 500 m, upper Greenland slope and mid-depths (∼400 m). The points where the mooring measures the water column display a strong agreement between both tools. This shows again that the model represents accurately the water column properties (temperature, salinity and hence density) in the shelf regions around the Labrador Sea.

Similar to the climatology sections in the observations, here the standard deviation of the model climatology sections is calculated and shown in figure 5.6. The distribution of the uncertainty in the model is in agreement with that in the

observations (in figure 4.22). However, the standard deviation in the model appear smoother and about half the size of the observations error. The temperature in the model shows a fairly constant temperature in the core of the CIL, displaying most of the error at the surface and at the bottom of the shelf, as well as the position of the shelf edge front. Salinity, as in the observations, gathers most of the error at the surface and at the coastal freshwater wedge. Finally, density shows a similar pattern to the salinity one, with larger standard deviations at the surface and some over the shelf.

Surface properties of the region

In addition to analysing the model performance with section-based products, the extensively studied surface properties of the region also serve to complete this analysis. Comparing the model's climatological surface properties to the current knowledge of the shelf continues the assessment of its overall performance, but also serves to shed light on some of the unanswered questions. So far the analysis has focused on the density structures at the Seal Island section. These can inform about geostrophic velocities and the geostrophic circulation. The model, however, also provides net velocities of the region. Surface circulation can then be compared with the literature in order to test the reliability of the model beyond geostrophy. This subsection briefly evaluates the skill of NEMO representing the surface properties of the Labrador region, focusing in the velocity and salinity on the shelf. It finishes by hypothesising about the fate of the Hudson Strait outflow and its relation with the Labrador shelf components.

Surface net velocity averaged over 11 years, as shown in figure 5.7, displays the climatological features in the model circulation. The velocity map shows that the model properly represents all the currents expected on the Labrador shelf, mostly following bathymetric features. The Baffin Island current lies on the 500-m isobath in agreement with *Tang et al.* (2004), bifurcates at 63N and follows the same trajectories as the floats by *LeBlond et al.* (1981). Moreover, most of the West Greenland current detaches along the 2000-m isobath in the same way as the drifters by *Cuny et al.* (2002). It then joins the Baffin Island current, south

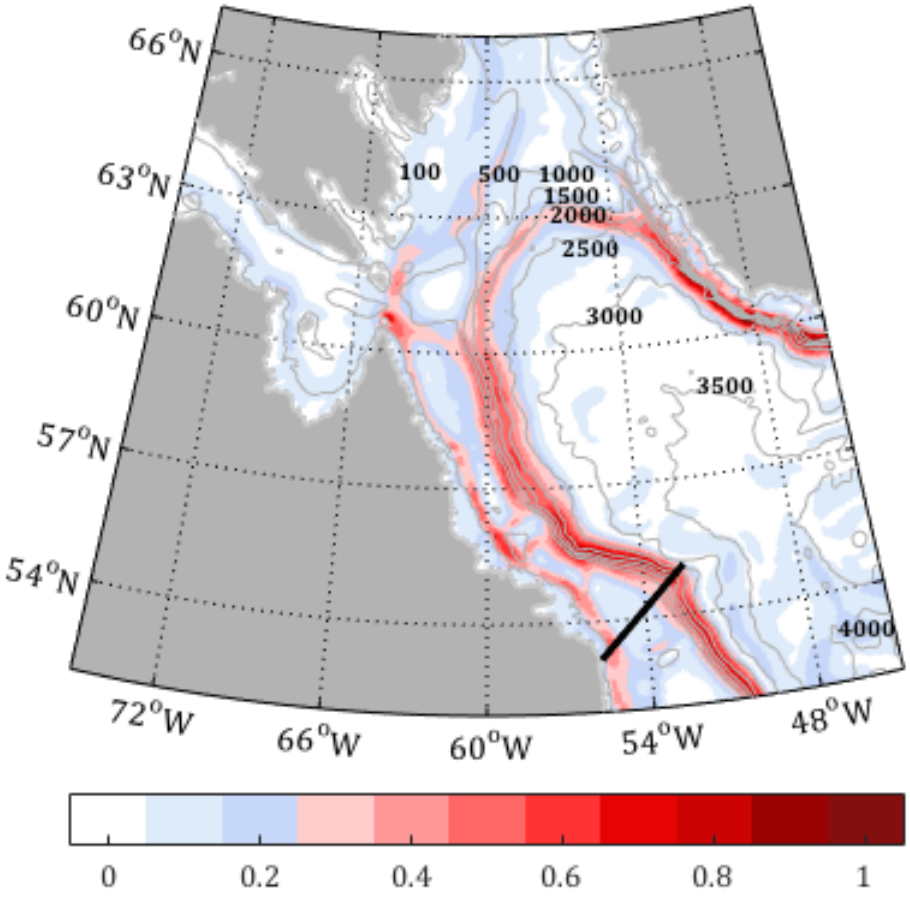

Figure 5.7: Sea surface absolute velocity (m/s) in the Labrador Sea from the NEMO $1/12^{\circ}$ *model, averaged from 1997 to 2007. Contour lines denote the model bathymetry and the thick line shows the location of the Seal Island Section.*

of Hudson Strait, to form the Labrador current. An inshore current on the Labrador shelf is also observed close to the coast and parallel to the Labrador Current proper. This coincides with the expected trajectory of the inshore branch of the Labrador Current (*Smith et al.*, 1937), though this branch is less well described in the literature.

The Hudson Strait outflow, with surface salinities lower than 30 psu, is found at the 150-m isobath (figure 5.8). It runs on the southern side of the Hudson strait, following the trajectory described by *Drinkwater* (1986). There is limited understanding of the pathways of the real-world outflow once it leaves the strait, but the model shows that the outflow is deflected to the south. It then remains constrained to the coast, feeding the inshore jet found on the shelf rather than joining the Labrador Current on the shelf's edge. This is seen by the plume of very fresh water (<30.5 psu, blue colours) that, after leaving Hudson Strait, continues

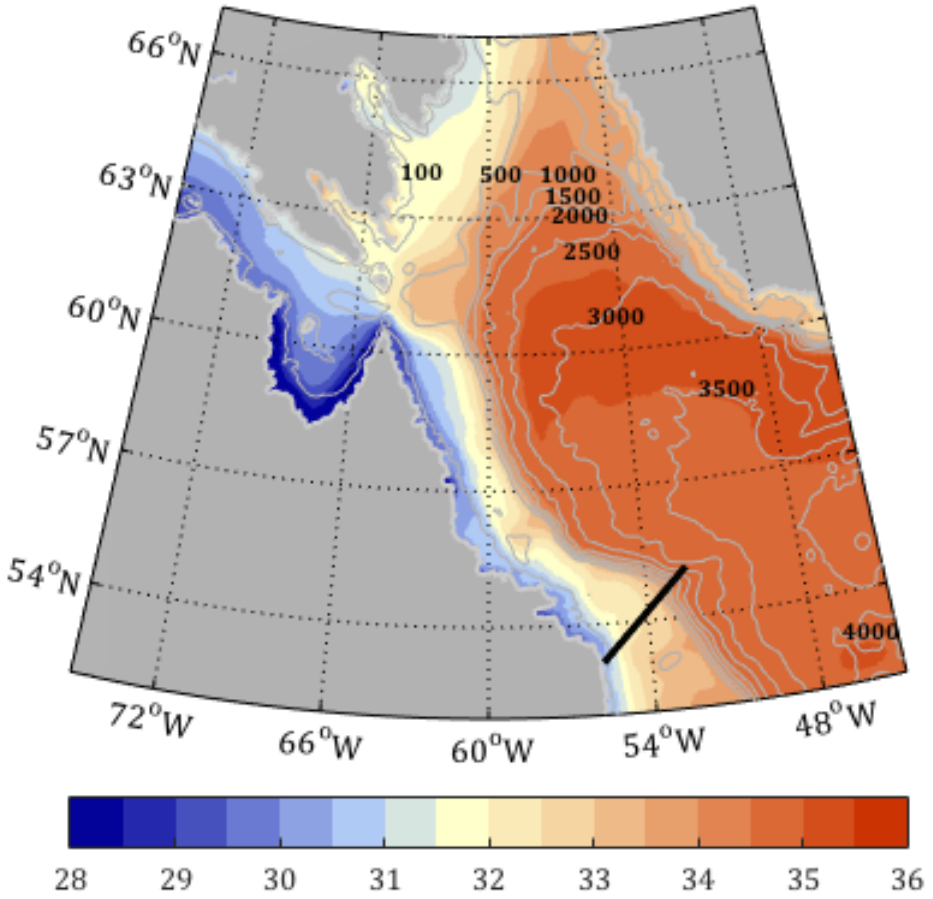

Figure 5.8: Sea surface salinity in the Labrador Sea from the NEMO 1/12° model, averaged from 1997 to 2007. Contour lines denote the model bathymetry and the thick line shows the location of the Seal Island Section.

southwards along the velocity trace of the inshore jet on the Labrador shelf. The Arctic water flowing south through the western Davis Strait (salinities $\sim$ 31 to 32.5, yellow colours) seems to continue and fill the open Labrador shelf up to the edge. The distinction in salinity seems to be bounded by the two currents on the shelf, as seen in figure 5.7.

This suggests that the inshore current observed on the Labrador shelf may possibly be partially or fully related to the Hudson Strait outflow, rather than being strictly a branch of the Labrador Current. This distinction is important for the purpose of looking at multi-decadal variability of Arctic water export. The Hudson Strait outflow, which is dominated by river run-off (with a small Arctic component), needs to be distinguished from the Arctic export through Davis Strait within the Labrador Current proper.

There is some observational evidence to support the hypothesis. The freshwater

transport of the outflow is 44 mSv (*Straneo and Saucier*, 2008), which is comparable to the 41 mSv carried by the inshore jet (*Mertz et al.*, 1993). However this does not preclude exchange of freshwater with the rest of the shelf. Further analysis is required to trace the pathway of the outflow and to understand the degree of isolation of the Hudson water. To achieve this, the following section; 5.2, assesses the differences between these two shelf currents. It focuses in their velocity, dynamics and pathways. Section 5.3 completes the study by comparing the currents to their origins, to analyse the degree of preservation of the Arctic signal on the shelf.

5.2 Two independent shelf currents?

The understanding of the Labrador shelf circulation remains incomplete. Little is known about the inshore Labrador current, its relationship with the main Labrador current and their link with the Hudson Strait outflow. Here, a detailed study of this double jet system completes the shelf circulation description and facilitates understanding the transport of water from upstream sources. It aims to provide the first full study of the inshore current, helping to uncover the fate of the Hudson outflow. This section analyses the nature of the two shelf currents. It also inspects the degree of connection between both jets and evaluates whether they are two geographically and dynamically different currents.

To begin, the basic characteristics of the circulation are analysed. A study of the cross-sectional velocities at the Seal Island section looks into how they vary along the shelf and how this relates to different bathymetric features. This will inform whether there are any geographical or lateral distinctions between the shelf currents. The section continues with a brief study of the dynamics. It includes an analysis of the mechanisms behind both jets and the application of a theoretical model for buoyancy-driven currents. After providing new knowledge about the circulation and dynamics of the two currents, this study concludes by using the Montgomery function to link the currents to their source region and to describe the transport pathways of the waters found on the shelf.

5.2.1 Circulation and velocity at the Seal Island section

In addition to the distinction seen in the surface velocity map (figure 5.7), studying the cross-sectional velocities at the Seal Island section can help to confirm whether the currents are geographically different. Here the climatological net velocity across the Seal Island section are computed first from the model. This includes a description of how the model zonal and meridional velocities are rotated to a sectional reference (across and along the section). The subsection continues by describing the bathymetric features of the shelf and it analyses whether the direction of the jets relates to these. In conclusion, the average velocity at the bottom of the section is computed. This will describe the velocity shear in the vertical and introduce the dynamics underpinning the currents.

Rotation of velocities to the perpendicular component

Velocity in the model is given as zonal (u) and meridional (v) components, as displayed in figure 3.3. However, the flow can be interpreted more easily if it is represented as components across and along the section. This setting reconciles the model with the observational framework. Figure 5.9 sketches the trigonometrical relationship between both frames and provides the required identities to rotate the model velocity. The shown velocity vector ($\mathbf{V}$) is decomposed as u and v in the model. For the interest of the analysis, I want to represent the velocity in a single component; across the section ($v_{orthogonal}$). This component can be achieved considering the trigonometric identities. The orthogonal velocity is given by

$$\sin(\gamma) = \frac{v_{orthogonal}}{|\mathbf{V}|}, \tag{5.1}$$

where γ is the angle between the Seal Island section and the velocity vector $\mathbf{V}$. This angle is calculated as $\gamma = \beta - \alpha$, which is the x-angle of the velocity (β) minus the deviation of the section from x (α, constant). It is worth noticing that α and β are referenced to x and are positive in a counter-clockwise direction. In this example, α is positive, β is negative and the resulting γ is also negative, yielding negative velocities south-eastwards from the section.

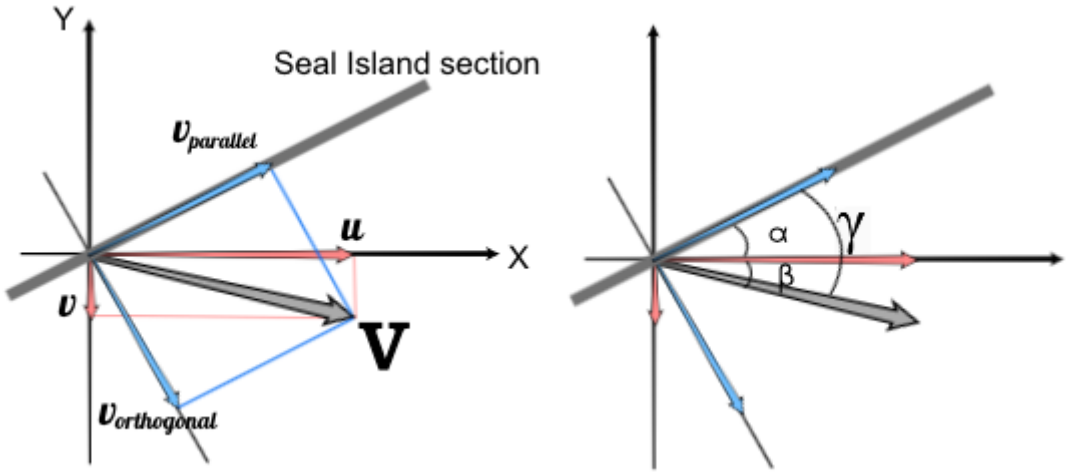

Figure 5.9: Sketch of the velocity rotation. A velocity vector $\boldsymbol{V}$ *(grey arrow) at the Seal Island section (grey thick line) can be decomposed in an* $x - y$ *framework (*u *and* v *components, red lines) or as along and across the section (*$v_{parallel}$ *and* $v_{orthogonal}$*, blue lines).* α *is the angle of the section with* x*,* β *is the angle between the velocity vector and the same axis.* γ *is the angle between the velocity vector and the Seal Island section.*

The deviation of the section from the x-axis (α) is constant and it is given by the inverse tangent of the section's slope (m). Regarding β, it can be obtained from

$$\sin(\beta) = \frac{v}{|\mathbf{V}|}. \tag{5.2}$$

Finally, combining equations 5.1 and 5.2, and knowing that the velocity module is $|\mathbf{V}| = \sqrt{u^2 + v^2}$, the velocity referenced to the section can be calculated as

$$v_{orthogonal} = \sin\left(\arcsin(\frac{v}{\sqrt{u^2+v^2}}) - \arctan(m)\right) \cdot \sqrt{u^2+v^2}, \tag{5.3}$$

$$v_{parallel} = \cos\left(\arcsin(\frac{v}{\sqrt{u^2+v^2}}) - \arctan(m)\right) \cdot \sqrt{u^2+v^2}. \tag{5.4}$$

Net velocity across the Seal Island section

The resulting net velocity across the Seal Island section is shown in figure 5.10, which displays July and August model data averaged for the same 1995 to 2010 period. As displayed by the blue colours, the water speed throughout the section is negative. Considering the orientation of the section and the orthogonal/parallel framework, negative values indicate a south-eastwards flowing direction. The two

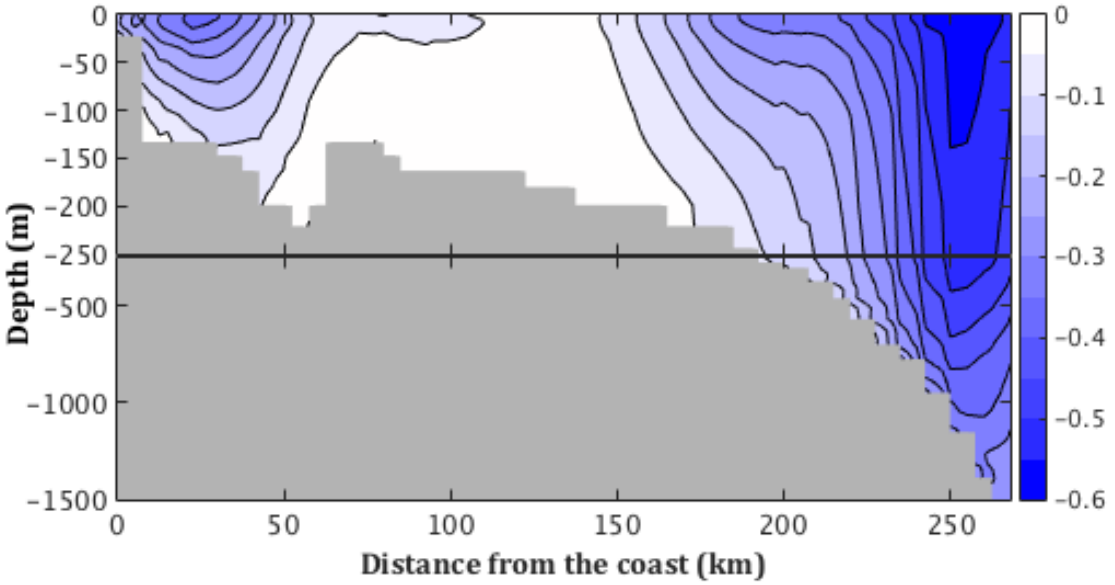

Figure 5.10: Model net velocity (m/s) across the Seal Island section for July and August, 1993 to 2014 climatology. Contours every 0.05 m/s. The vertical axis focuses on the top 250 m. The scale on the slope is 1:5 that of the shelf. The discontinuity in the vertical scale is denoted by the black line.

shelf jets are clearly identified as two distinct cores of relatively high velocities (near 0.5 m/s). They are separated by a mid-shelf region of low activity; zero or near zero velocity. Although not displayed, this structure is identified at all times in the model, both interannually and seasonally. Some recirculation is sometimes seen as very small positive velocities in the mid-shelf. The clear separation of the currents by a quasi-steady region, consistent throughout time, indicates that the two currents are geographically separate at this location; they follow a distinct pathway.

Analysing the depths over which the two currents flow further supports this distinction. At the Seal Island, the inshore current lies approximately on the 140 m isobath. The wider Labrador current presents an extended velocity core. Some flow at the shelf edge, at about 270 m, while intensified flow hugs the full slope. These features are also apparent in the sea surface net velocity (figure 5.7) throughout the Labrador Shelf, indicating that the shelf currents follow the topography. This raises the question of what are the mechanisms behind these currents. Their low salinities, as seen in figure 5.3 and 5.4, also indicate that they may be driven by density gradients related to buoyancy fluxes. Significant freshwater fluxes can generate sharp density gradients, which in turn control the circulation by the resultant

cross-shore pressure gradients, as described in the region (*Smith and Schwing*, 1991). Further analysing the shelf's topography will help determine the extent to which the currents relate to the bathymetry and provide information about the mechanisms behind them.

Bathymetry and vertical structure

The slope of the shelf at the Seal Island is displayed in figure 5.11 as the bathymetry gradient orthogonal to the section, together with the vertically-integrated velocity at the same positions. The bathymetry gradient has been calculated considering an area of 3×3 gridcells around each point in the section. The orthogonal component (perpendicular to the section) has been obtained rotating the gradient 90° clockwise. This displays the magnitude of the slope in a comparable direction to the velocity vectors. As shown in the figure, the relationship between both variables is evident. This is evidenced by both matching magnitude and direction. Bathymetry seems to confine velocity within distinct ranges. The cores of the two currents coincide with the two separate regions of intensified slope, denoting again they are geographically distinct.

The vertical structure and shear further inform us about the baroclinicity of the currents and their relationship with topography. Baroclinic currents, given by density gradients, are depth-dependent and display vertical-shear. The barotropic component is depth-averaged and responds to different forcing. The bottom velocity at the section gives further information about the characteristics of the shelf currents; it provides an estimate of the vertical shear, and a numerical magnitude (or reference velocity) for the barotropic component. The mean (July-August, 1995 to 2010) velocity at the bottom of the section is shown in figure 5.12. Velocity contours are negative and displayed at 0.1 m/s intervals. The bottom velocities shown in the bottom panel are decomposed in the two different frameworks, geographical (u and v) and sectional (across and along the section). Here, the velocity orthogonal to the section is the variable of interest. It has relatively low values (below 15% of the surface maxima) throughout the shelf, with zero or near zero values at the mid-shelf. Its magnitude increases exponentially through the slope to a maximum

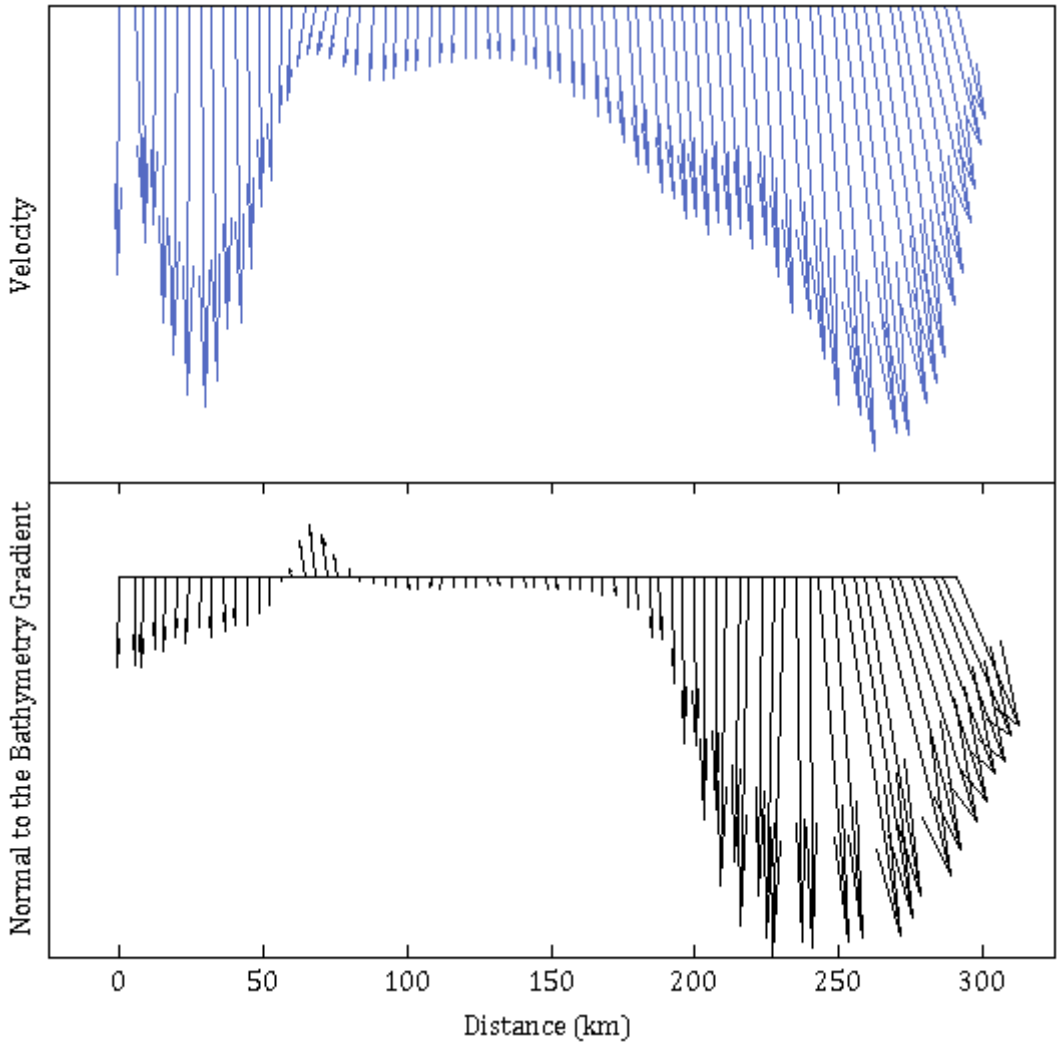

Figure 5.11: Quiver plots of vertically-integrated velocity (top panel) and bathymetry gradient (bottom panel) at the Seal Island section. Data from the available model multiannual average (1997 to 2007). The vertical axes display qualitative magnitudes. The bathymetry gradient has been rotated clockwise by 90° *so that it is displayed normal to the section.*

absolute value of 28 cm/s, indicating a significant increase of the barotropic role towards the open ocean. This can be further explained by comparing the vertical shear in the velocity.

The inshore current on the shelf (figures 5.10 and 5.12) shows a clear decrease in velocity with depth. The velocity is reduced to just 15% of its surface maximum at the seafloor. The current is co-located with steep pycnoclines (figure 5.3) and bathymetry (figure 5.11), suggesting a high degree of baroclinicity. In contrast, the Labrador current instead is more complex and displays a dual structure; a shelf edge component and a slope one. The shelf edge part has a vertical shear

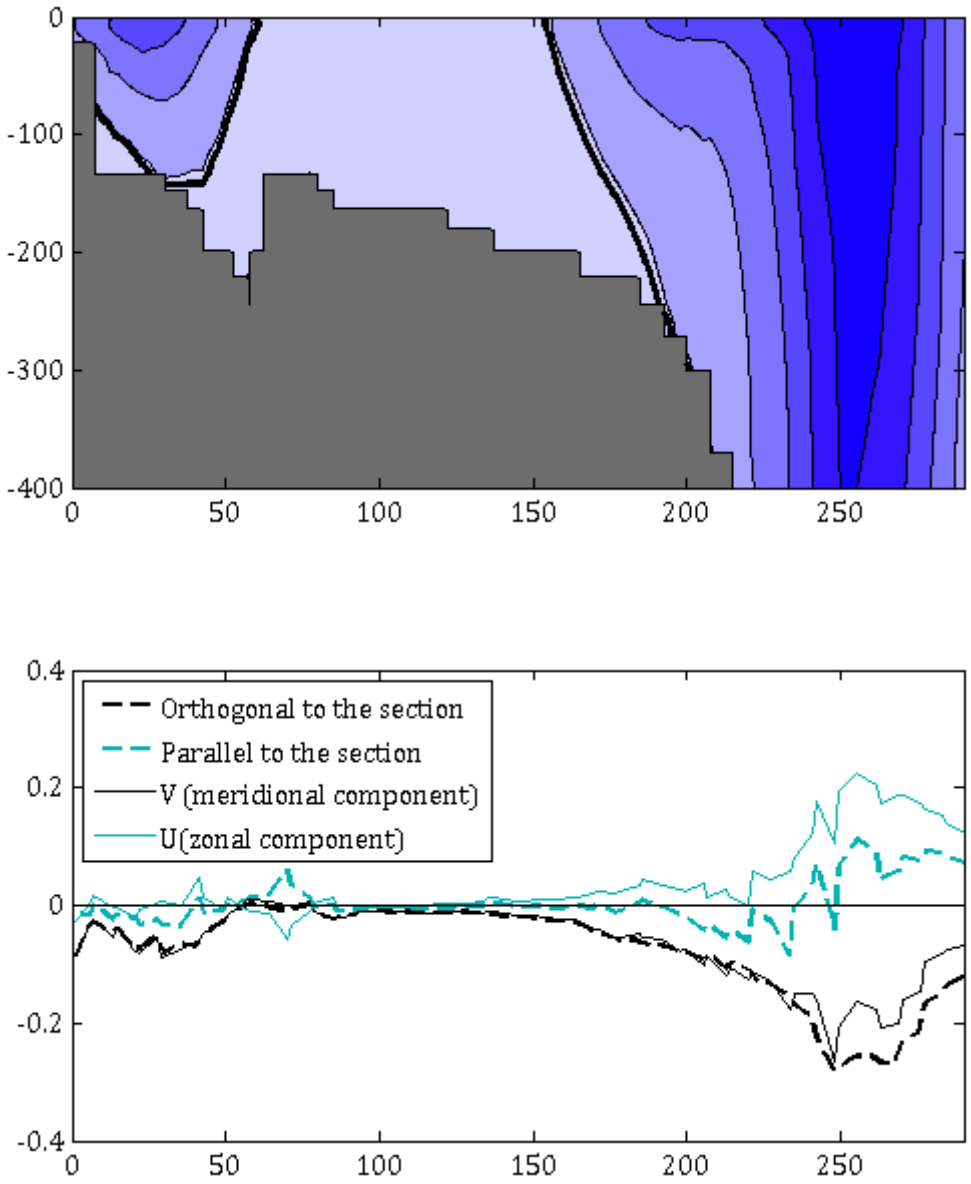

Figure 5.12: Model bottom velocity at the Seal Island. Velocity across the section (top) and bottom velocity values along the shelf (bottom). The thick contour in the section denotes where the velocity is 15% of the each jet's maximum velocity at the surface.

structure that is similar to the inshore current, and shows low bottom velocities ($\sim$ 15cm/s). This shelf edge part of the Labrador current is adjacent to a stronger core of velocity on the slope, with velocity contours that are almost vertical and that extend deep into the water column. The bottom velocity (i.e. barotropic component) of the slope component of the Labrador current is significantly larger ($\sim$ 30cm/s) than the bottom velocity along the full shelf. It is half the speed at the surface. This distinction can be explained by the composition of the Labrador current. It is formed by two components: the Baffin Island current (Arctic water

exported west of Greenland) and the West Greenland current (modified Arctic water exported east of Greenland). They are separated by a distinct temperature front (*Smith et al.*, 1937). This dual composition provides the current with an equal bimodal nature: a buoyancy-driven component over the shelf break and a more barotropic component over the slope; the West Greenland current part of the Subpolar gyre (*Lazier and Wright*, 1993).

The analysis of this subsection has shown that the two currents on the shelf are geographically distinct. Furthermore, there are indications that the dynamics driving these currents might be different. Buoyancy fluxes seem to control the inshore current and the shelf break part of the Labrador current. Its slope component presents a significant barotropic component (part of the Subpolar Gyre). However, the full dynamics of the circulation remain unclear at this stage. I the next section I investigate the processes driving the currents and assess whether they are dynamically different.

5.2.2 Basic dynamics of the currents

Studying the seasonality of both currents will help understand their dynamics too. If their variability differ, it may indicate that they are driven by different mechanisms. This subsection starts by comparing the general seasonal traits in the surface density and velocity of the section (where velocity and gradients are greatest). It continues by comparing the jets to changes in the density field. This assesses the baroclinicity of the currents and informs us about the importance of the buoyancy fluxes in the circulation. Finally, the dynamics of the inshore jet are studied by modelling it as buoyancy coastal current using the theoretical approach by *Lentz and Helfrich* (2002).

Variability of the surface velocity and the density gradient

The variability in the surface density and velocity is shown in figure 5.13, which displays monthly model data as a Hövmoller diagram from 1995 to 2010. The surface density distribution has its lowest values in the summer, especially near the coast

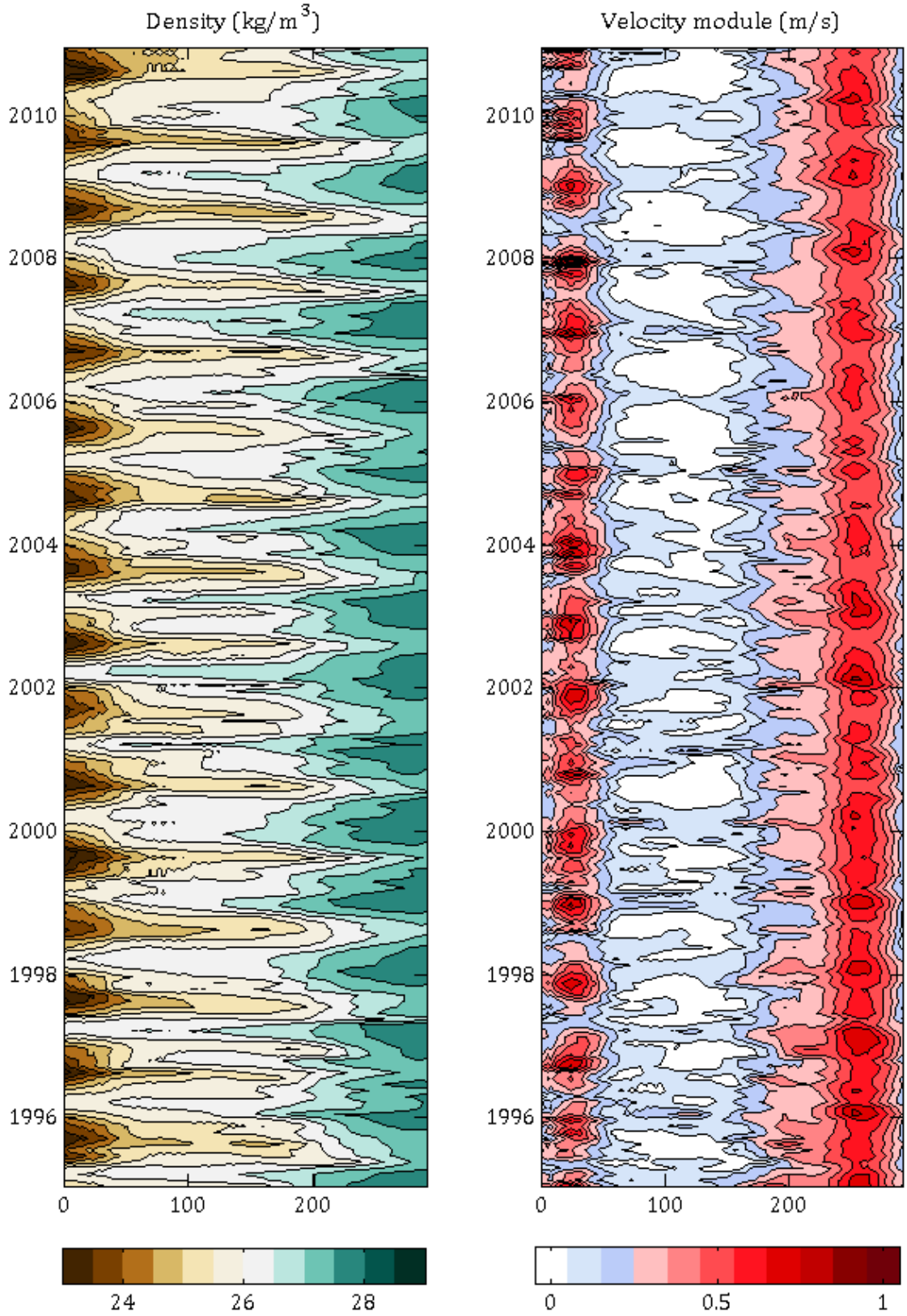

Figure 5.13: Hövmoller diagram of the model surface σ-density (left, kg/m^3) and speed (right, m/s). Monthly data at the Seal Island section (x-axis, distance in Km) from 1995 to 2010 (y-axis).

(the time where the inshore current is freshest and warmest). A general increase in the density occurs in autumn, which propagates coast-wards and further confines the fresh plume of water inshore. This coincides with the maximum velocities of the inshore current. In winter, surface density is at its highest values throughout the section. The velocity of the inshore current decreases through the winter and reaches a minimum in spring. It starts increasing again when the plume of fresh water intensifies in the summer.

The Labrador current, on the shelf edge and slope, can be seen to have the bimodal nature described earlier. The shelf component (seen as the lighter red colours in the velocity diagram, $\sim$ 0.4 m/s) centres around the 200 km mark of the shelf. The slope component has the largest velocities ($\sim$ 0.8 m/s) at around 250 km. Some years they show separate cores of maximum velocity (e.g. 1995, 1999 or 2003). In contrast with the inshore jet, the Labrador current velocity peaks a few months later in mid-winter. The peak in the velocity is better seen in the slope component. The shelf break part of the Labrador current does not show a clear seasonality. Minimum velocities for the inshore current are found in spring ($\sim$ 0.25 m/s). The Labrador current minimum velocities ($\sim$ 0.5 m/s over the slope, $\sim$ 0.3 m/s on the shelf break) are seen in autumn.

The inshore jet and the Labrador current (as a whole) present different timings in their seasonality. Their interannual variability also seem unrelated (there is no evidence of coinciding years with high or low velocities). Additionally, the shelf edge and slope components of the Labrador current present different regimes. This indicates that different mechanisms may be forcing the separate jets and also the different components of the Labrador current. Examining their velocity variability and the horizontal density gradients on the shelf will help understand the role of buoyancy fluxes. This will complete the study of the vertical structure and determine their degree of baroclinicity.

Where buoyancy fluxes are important in controlling the circulation, horizontal density gradients are closely related to the strength of the velocity. In an ideal baroclinic case, currents have vertical shear with zero bottom velocity. A previous section (5.2.1) presented some results about the baroclinicity of the shelf features.

The inshore current and the shelf edge component of the Labrador Current displayed considerable vertical shear and low bottom velocity. The slope component showed the opposite case. This section completes this analysis by further relating these differences to the buoyancy forcing.

Figure 5.14 shows a Hövmoller diagram similar to figure 5.13. This time, density is displayed as a zonal gradient (the magnitude of the horizontal changes in density) and compared again with net surface velocity. Data are plotted at each grid cell rather than interpolated with contours, as it was the case in figure 5.13. This is to show more evidently how strong density gradients (sometimes shown by a single grid cell) relate to the velocity. The position of the inshore jet fully coincides with the location of the maximum density gradient found in the time series. The relationship between the magnitude of the gradient and the strength of the current is also evident; small/large gradients correlate with a slower/faster current. This is seen by a density gradient seasonality that matches in space and time the seasonality of the inshore jet velocity. Sometimes, this velocity seems to respond to the changes in density gradient with a small lag (ranging from 0 to 2 months), fading away shortly after the gradient diminishes in winter-spring. The Labrador current displays its bimodal regime again. The shelf edge part lies where the Labrador current density gradients are highest (at around 200 km off the coast). Furthermore, peaks in its velocity relate to periods of enhanced zonal density gradient (e.g. 1995, early 2000 and 2002, 2005, late 2006, etc.). Similar events of unusual velocity highs in the mid-shelf also match equivalent density changes (1996, 2001, 2007). All these features indicate that buoyancy forcing is important controlling the circulation on the shelf. In contrast, circulation on the slope cannot be explained by these fluxes. Although the slope component of the Labrador current ($\sim$ 250 km offshore) presents the highest velocities, density gradients in this position are marginal. In combination with the significant bottom velocities found on the slope (figure 5.12), this indicates that the slope part is highly barotropic and controlled by different mechanisms.

This picture is further inspected in figure 5.15. All months of the time series (1995 to 2010) are plotted independently. The general aspects discussed above are displayed again. The inshore current coincides with strong density gradients

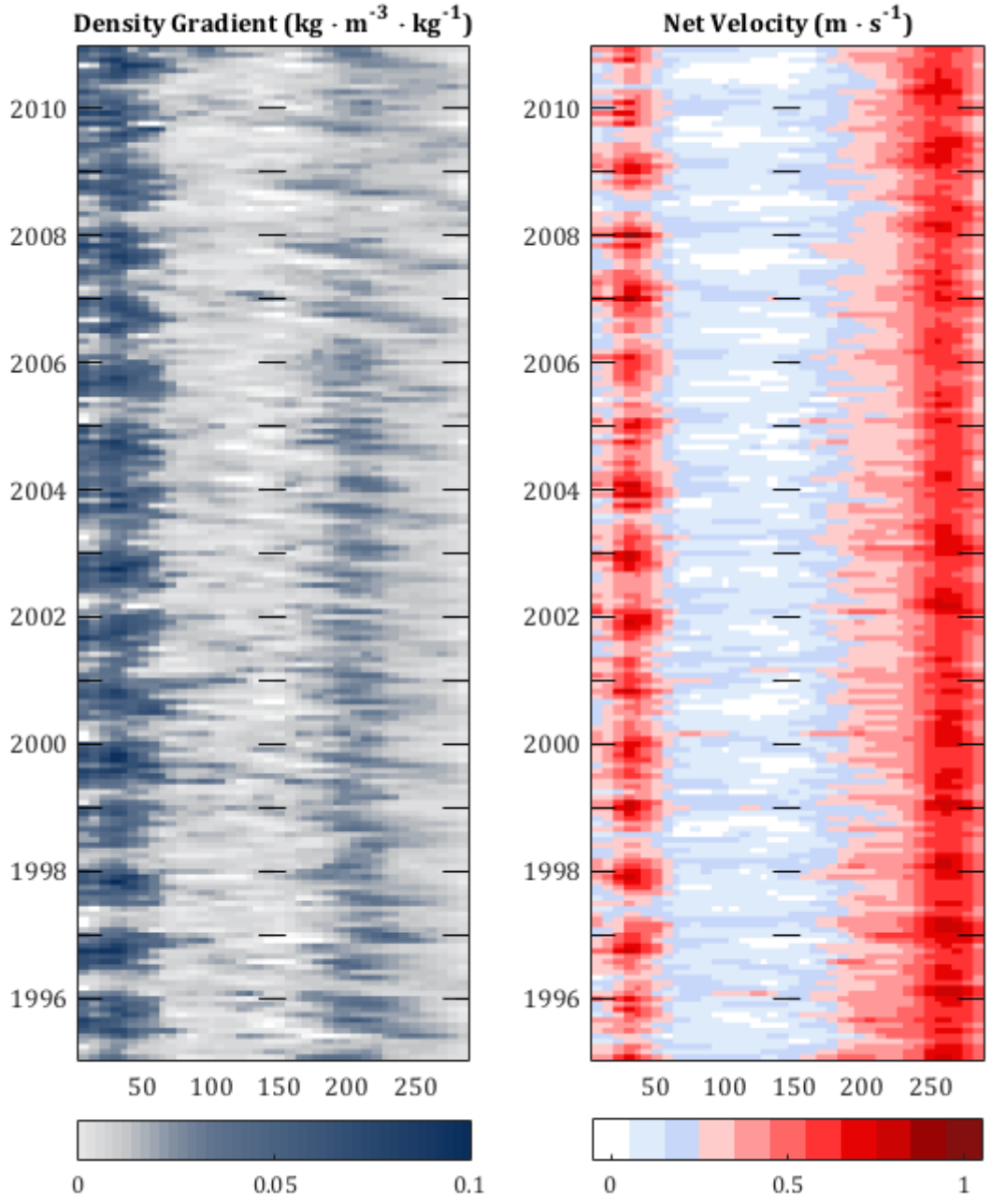

Figure 5.14: Hövmoller diagram of the model surface σ-density gradient (left, $kg{\cdot}m^{-3}{\cdot}km^{-1}$) and net velocity (right, m/s). Monthly data at the Seal Island section (x-axis, distance in Km) from 1995 to 2010 (y-axis).

and the Labrador current shows a double core structure. The shelf component is appreciated as a plateau in velocity at around 200 km, followed by an adjacent peak on the slope (250 km). Density gradients on the slope are small. On the shelf edge, however, they relate to the variability in velocity. The pairs of lowest and highest density gradient on the shelf edge are highlighted in the figure. In all cases, the position and magnitude of the gradient is matched by an equal velocity distribution.

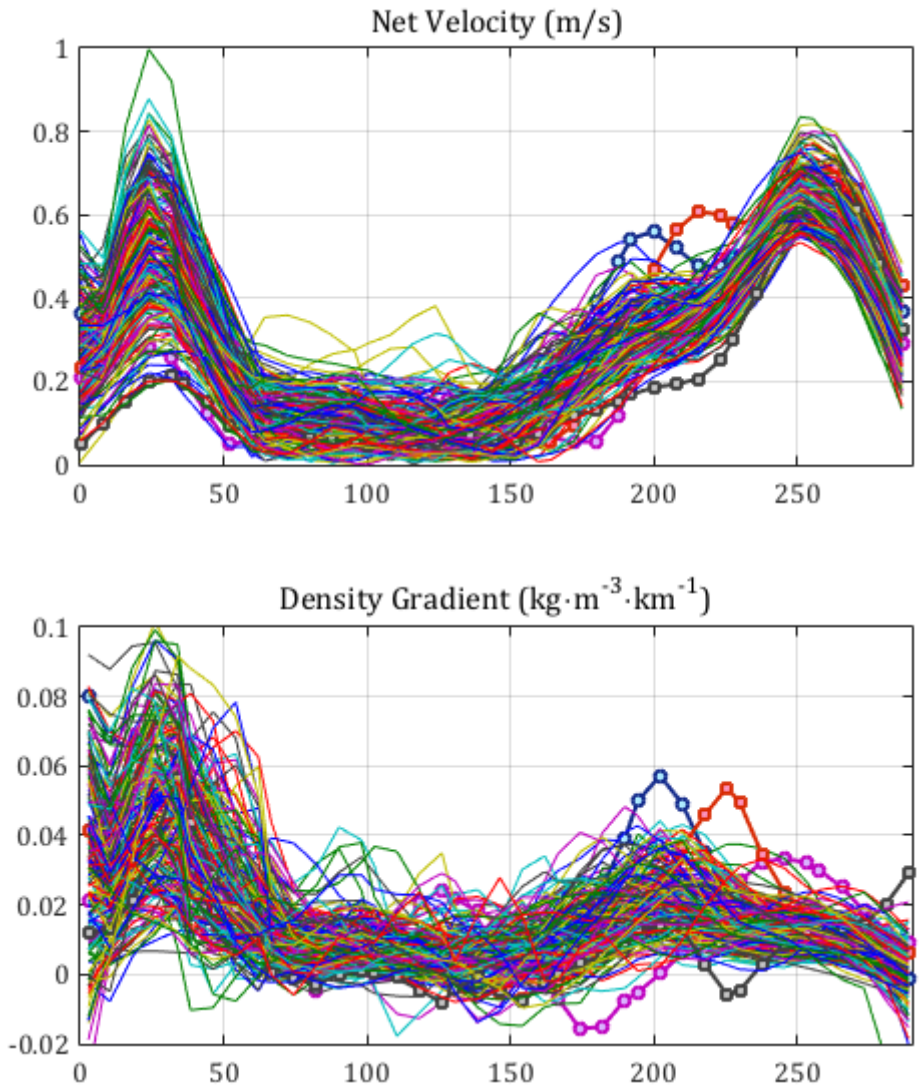

Figure 5.15: Monthly model distribution of surface net velocity (top) and surface density gradient (bottom), from 1995 to 2010 at the Seal Island. The pairs of months with lowest and highest density gradient on the shelf edge are highlighted by circular markers.

To better understand the seasonality, figure 5.16 shows the monthly averages for the 1995-2010 period. These averages are computed from the surface speed (same as figure 5.15), at the velocity core of the coastal jet and the core of the shelf edge component of the Labrador current. The coastal core shows a clear seasonality, with maximum speed in December-January and minimum in spring to summer. The density gradient shows a similar pattern with a coherent amplitude. However, there is a difference in the phase (a lag of 3 months, as observed in figure 5.14). The shelf edge component of the Labrador current shows a different seasonality. In this case, there are two peaks in the speed, in January and in August, with lower speeds the rest of the year. It is interesting to note that again, the density gradient

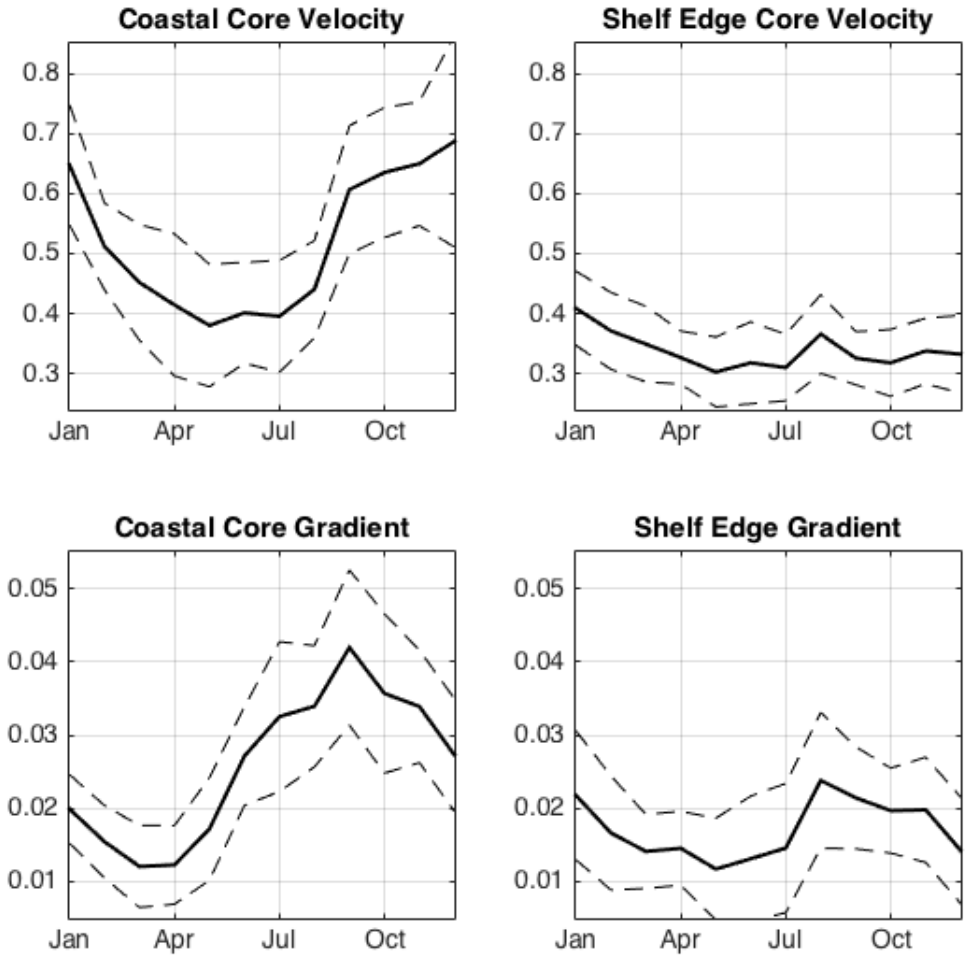

Figure 5.16: Model 1995-2010 monthly averages of speed (top) and density gradient (bottom) at the cores of the coastal jet (left) and the shelf edge component of the Labrador current (right). The thick lines show the mean and the dashed lines show the standard deviation.

shows a similar seasonality, with a similar amplitude of change. In this case, they show the same phase; there is no lag.

These results indicate that the mechanisms behind the circulation on the shelf are different to those on the slope. Implicitly buoyancy fluxes appear important for the inshore current and the shelf edge part of the Labrador current. Yet their seasonality varies across the shelf, suggesting that the buoyancy fluxes controlling circulation elsewhere are different. The slope component instead presents a barotropic behaviour, which is characteristic of the Subpolar Gyre. The strong baroclinic behaviour of the inshore current coincides with very low salinities (fig-

ures 5.3 and 5.8), following the shape of a freshwater plume. This suggests that the dynamics of this jet could follow the structure of a buoyancy-driven coastal current. Parametrising this current as such will help evaluating its dynamics and relating them to hypothesised sources.

JEBAR in the control of the Labrador current's seasonal variability

The dynamics of the shelf currents show that the shelf currents are mainly buoyancy-driven. However, can this buoyancy forcing explain the seasonal variability described above? In principle, in the geostrophic adjustment after buoyancy forcing changes, it is expected to observe a deeper current in opposite direction with a compensating opposite transport. This has not been observed or described in the Labrador shelf or slope. Here, following the study by *Lazier and Wright* (1993), I describe how the joint effect of baroclinicity and relief (JEBAR) helps determining whether buoyancy forcing can explain the observed variability in the upper Labrador current.

Lazier and Wright (1993) hypothesise and test two possible explanations for the lack of a compensating deep current flowing northwards as a consequence of the shelf buoyancy forcing. They consider that either bottom friction suppresses the expected deep circulation, or that it is JEBAR that produces a counter-acting barotropic circulation. JEBAR is the combined effect of bottom stress with flow originated by along-isobaths density gradients. This circulation can overrun the deep compensating flow and can explain why upstream buoyancy forcing can determine the seasonal variability.

In their study, Lazier and Wright idealise a simple diagnostic model of the Labrador shelf and test the effect of bottom stress and of JEBAR in the variability. In their results, they reject the hypothesis that bottom stress alone can account for buoyancy-driven variability, as it is not enough to account for the $\sim$ 4 Sv of observed annual variability. However, when the JEBAR term is taken into account, they observe that buoyancy fluxes upstream account for an annual variability of $\sim$ 5 Sv, consistent with the Labrador current transport annual variability. Furthermore, they observe that the transport is mostly obtained from the deep offshore region,

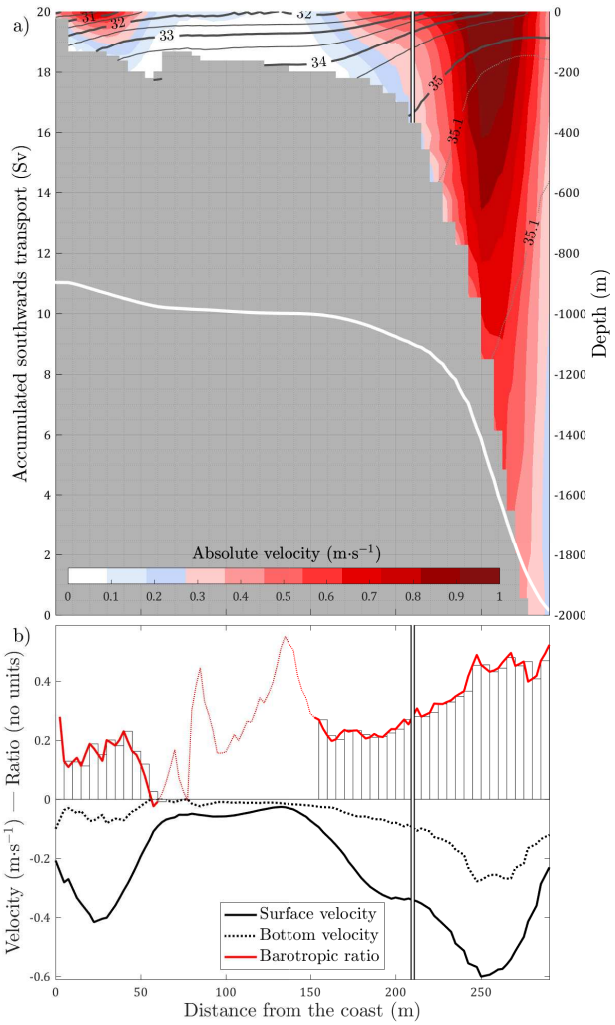

Figure 5.17: Velocity dynamics at the Seal Island section from the NEMO 1997-2010 summer mean. Panel 'a' shows speed (colour contours) and salinity contours. The light gray line (left axis) shows the accumulated transport from the bottom of the slope to the coast. Panel 'b' shows surface and bottom velocity, and the barotropic ratio (fraction of the bottom velocity relative to the surface velocity).

rather than from the shelf. The flow over the upper slope is nearly not affected. The authors conclude that JEBAR is the main feature allowing buoyancy-driven variability by the addition of a barotropic component to the Labrador current that mostly impacts on the slope part of the current.

In order to understand how the NEMO model results at the Seal Island compare with the study by *Lazier and Wright* (1993), figure 5.17 shows the speed section (panel a), it estimates the accumulated transport from the bottom of the slope to the coast (grey line at the bottom of panel a) and shows the barotropic influence along the section (panel b). The velocity shown by the NEMO model displays the

same structure than that observed by Lazier and Wright. If the accumulated transport is calculated the same way than the authors' method (accumulated transport from the bottom of the slope to the coast, referenced at 1500 m and adding the barotropic component), it yields the same total transport: 11.0 Sv. Note that the NEMO is a July-August climatology (1995 to 2010) and the results by Lazier and Wright are from observations from August 1988. This evidences the agreement between both tools.

Additionally, the barotropic influence at the Seal Island section in the NEMO model is shown in panel b of figure 5.17. The barotropic ratio (bar plots and red line) is calculated as the fraction of the bottom velocity (dashed black line) relative to the surface velocity (black line). The ratio is depicted by a red dashed line at the mid-shelf where velocities are residual (<0.08 m·s^{-1}) and hence the ratio tends to inaccurate large numbers. Finally, the vertical line shows the approximate surface position of the offshore front between the shelf edge part of the Labrador current and the offshore part. The barotropic component is below a 25% along the section, and it rapidly increases to account for almost half of the velocity seaward of the shelf edge front. This is also seen in the velocity section (panel a), where velocity vertical shear decreases beyond the front and velocity becomes rather constant in the vertical. This is in agreement with the results by Lazier and Wright, who concluded that the barotropic influence generated by the JEBAR was mostly found over the slope.

Parametrisation of the inshore current as a coastal current

Lentz and Helfrich (2002) show idealised buoyancy gravity currents over a sloping bottom (e.g. continental shelves) with a simple two-layer model. *Lentz* (2012) later reviewed this topic and focused on buoyant coastal currents. By assuming the flow is hydrostatic (equation 3.7) and in geostrophic balance (equation 3.1), the frictional forces balance the horizontal density gradients. This equality allows scaling the basic features of the current, including geometry (width and thickness) and velocity. The model only takes as inputs the transport of the current, Q; the Coriolis parameter, f; the bottom slope, α; and the reduced gravity, g', which

is given by the density gradient of the front between the two layers. The given outputs are the thickness (depth) of the current, h_p; and the width of the current, W_p, which is the sum of the offshore distance to the foot of the current (W_α) and the surface extension to the edge of the plume (W_w) as shown in figure 5.18. Similarly, the propagation speed of the current (c_p) can also be calculated.

In this subsection, the inshore jet is scaled in order to compare the current in the NEMO model with the structure expected for a buoyant coastal current of the same characteristics. The required inputs for the *Lentz and Helfrich* (2002) model have been extracted from the velocity summer climatology (figure 5.10). It is worth noticing that scaling exercises compare gross magnitudes, thus mean values are sufficient to represent the required magnitudes for this purpose. The values extracted from NEMO are explained here. The Coriolis parameter assumes a constant f-plane†, valid when the study region is constrained in latitude. The Seal Island Section barely extends 2° meridionally and averages to a latitude (θ) of 54°. This yields $f = 1.2 \times 10^{-4}$ s^{-1}. The slope of the bottom, in this case the slope of the shelf, is also considered constant. The current of interest is found on the inshore side of the shelf, which reaches a depth of 150 m in about 40 km. This approximates the slope to $\alpha = \Delta y/\Delta x = 3.75 \times 10^{-3}$. The remaining variables require more detailed considerations.

The Lentz and Helfrich model assumes a uniform gradient between two homogeneous layers with different densities. This constrains the velocity and transport to just above the interface. In reality, the layers are not uniform. The density front and velocity are diffused laterally. For this reason, the transport of the current as observed in the NEMO model is given by the width of the full current and not just that above the front. This follows the same approach as *Straneo and Saucier* (2008). Here the center of the current has been found by the maximum surface velocity ($c_p = 0.37$ m/s), at a distance of 22.5 km. Considering the apparent symmetric shape of the current, its total width can be estimated as 45 km. The transport given by those limits totals to 1.05 Sv. Finally, the density gradient ($\Delta\rho$) is given by the density difference between the coastal and the shelf layers. Because these are not homogeneous, their densities have been averaged over each full layer. This yields an inshore density of $\rho_0 = 1025.93$ kg/m^3, an offshore density of $\rho_0 = 1024.43$

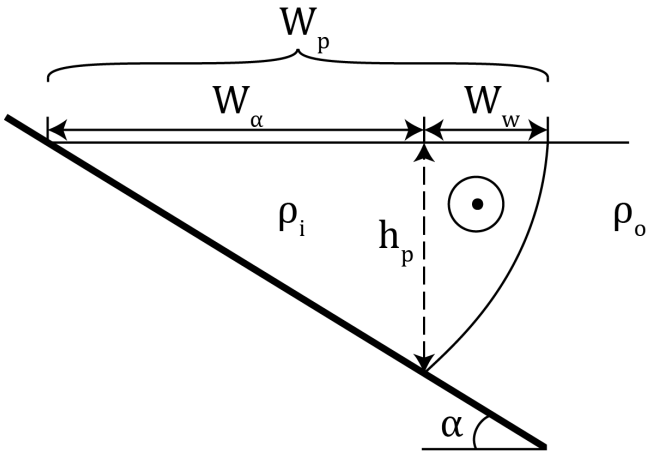

Figure 5.18: Sketch displaying the main variables of the Lentz and Helfrich model for buoyancy driven coastal currents, adapted from Lentz (2012). The curved line shows the front ($\Delta\rho$) between the inshore plume of fresher water (ρ_i) and the offshore environmental water (ρ_o). In the northern hemisphere this yields a cross-flow outwards from the plane.

kg/m^3 and thus a difference, $\Delta\rho$ of 1.50 kg/m^3. Section 5.3 provides a detailed description of how the different shelf layers are separated.

These initial parameters allow us to compute the expected geometry and velocity of a buoyant coastal current following the *Lentz and Helfrich* (2002) model. This model first obtains the thickness of the current as

$$h_p = \sqrt{\frac{2Qf}{g'}}. \tag{5.5}$$

This depth equation is obtained from *Yankovsky and Chapman* (1997) and it depicts the point where the density front intersects with the ground. This is also referred to as the foot of the current, and where the velocity core is found. The reduced gravity term is given by the gravitational acceleration (g) and the density difference ratio;

$$g' = g\Delta\rho/\rho_o. \tag{5.6}$$

The thickness of the current also determines the distance between the foot of the current and the coast. Considering the constant slope, this W_α term is given by the distance that allows for such h_p. The total width of the current includes a

Inputs	**NEMO** $^1/_{12}$	**Outputs**	**NEMO** $^1/_{12}$	**Lentz & Helfrich**
Q (Sv)	1.05	h_p (m)	134	134
f ($\theta = 54°N$)	1.2×10^{-4}	W_α (km)	—	36
α	3.75×10^{-3}	W_w (km)	—	11
ρ_0 (kg/m^3)	1025.93	W_p (km)	45	47
ρ_i (kg/m^3)	1024.43	c_α (m/s)	—	0.44
$\Delta\rho$ (kg/m^3)	1.50	c_w (m/s)	—	1.37
g' (m/s^2)	1.4×10^{-2}	c_p (m/s)	0.37	0.33

Table 5.1: Summary of the parametrisation of the Labrador inshore jet as a coastal current. It includes the chosen input values (left), the magnitude of the current as seen on NEMO (centre) and the values expected from the Lentz and Helfrich model (right).

second term, W_w, to account for the distance between W_α and the surface limit of the current. In geostrophic balance this is given by the isopycnal tilt, which is in turn determined by the deformation radius. The total width of the current is then computed as

$$W_p = W_\alpha + W_w = \frac{h_p}{\alpha} + \frac{\sqrt{g' h_p}}{f}. \tag{5.7}$$

Finally, the propagation speed of the buoyancy-driven current is determined by the transport of the current over the cross-sectional area (A),

$$c_p = Q/A \sim \frac{c_w}{1 + c_w/c_\alpha}. \tag{5.8}$$

This is proportional to the propagation speed of a gravity current along a vertical wall (c_w) and the velocity in a slope-controlled (small α) regime. The speed of a gravity current against a wall is given by

$$c_w = \sqrt{g' h_p}, \tag{5.9}$$

and that relative of a small bottom slope is

$$c_\alpha = \frac{\alpha g'}{f}. \tag{5.10}$$

Table 5.1 summarises the input variables extracted from NEMO (first two columns)

and the output results from the Lentz and Helfrich model. The geometry and velocity calculated from this coastal current model are shown in the final column of the table. The equivalent and relevant variables observed in the NEMO model have also been included in the fourth column of the same table, to allow comparison. It is worth noticing that the slope (α) or wall (w) components are not specified for NEMO. Those are calculated variables, rather than observed magnitudes. They also lack of consistency in NEMO, where density is continuous in contrast with the two distinct homogeneous layers of the Lentz and Helfrich model. The basic geometry features (expected total width and thickness), together with the propagation speed of the current, are the main comparable variables.

The results of the Lentz and Helfrich model strongly agree with the observed magnitudes in the NEMO model. The thickness of the inshore current coincides exactly with the expected depth of a coastal buoyant current; 134 m. It is noted that the thickness in NEMO is the observed depth at the core of the jet and it is not constrained to a constant slope. The resulting width of the current (47 km) also lies very close to the width observed in NEMO (45 km). Similarly, the propagation speed as seen above the density front (c_p) displays a close agreement between the observed (0.37 m/s) and the expected (0.33 m/s) values.

It is worth noting that the width of the current in NEMO was initially considered symmetric and of 45 km. The offshore limit of the current, however, is not sharply defined and it may also be variable. For this reason, it is convenient to consider a width range rather that a single value. From figure 5.15, it is inferred to be from 45 to 60 km. The limits of this range still remain comparable with the magnitude of the calculated thickness. Furthermore, considering a slightly wider current would imply an increase in transport and area. This would compensate the calculations and result in a wider coastal current (equation 5.7) yet with a similar speed (equation 5.8).

The characteristics of the inshore current (a plume of freshwater) and the results of the scaling study highly support the hypothesis that the inshore current is a buoyancy-driven coastal current. Combined with the described dynamics, it is concluded that the two currents on the shelf are also dynamically different. The in-

shore branch behaves as a coastal current with different variability to the Labrador current proper. The latter presents two cores, a baroclinic buoyant flow on the shelf break and a baroclinic component over the slope, part of the Subpolar Gyre. These results, however, only provide a snapshot at the Seal Island section. In order to provide a general view of the shelf, the next section employs the Montgomery function to study the flowing pathways upstream of the Seal Island section. This serves to explore the source regions of the shelf waters and to link the currents to the mechanisms controlling their different dynamics.

5.2.3 Flow pathways of the shelf waters

The Montgomery function allows us to evaluate the expected pathways of the geostrophic flow, as described in section 3.3. By representing this function over density surfaces, it is possible to determine the continuity of the currents north of the Seal Island section. The Montgomery function is calculated over different pseudo-potential density (r_B) surfaces, chosen according to the density of the fronts at the Seal Island section, as given by the climatology (figure 5.3). To reduce the impact of the summer surface warming, the density below the thermocline (at 25m deep) is used. The first surface is defined at $r_B = 25.00$ kg/m^3. This is the climatological front density at the inshore jet and sets the offshore limit of the water at the first kilometres of the shelf. The second surface is defined at $r_B = 26.50$ kg/m^3. Similarly, this density is found at the shelf edge front and sets the limit of the mid-shelf water. Figure 5.19 shows the Montgomery function values at those surfaces, and figure 5.20 shows their *in situ* temperature. The analysis in this section is based on those figures.

The shown data is from the model, from the 1997 to 2007 multiannual average. The Montgomery streamlines (figure 5.19) show the pathways for each watermass, with the flow being orthogonal to the Montgomery gradient. This means that water follows the streamlines with a magnitude proportional to their gradient. In the Northern Hemisphere that is from high to low Montgomery, to the right of the gradient. Inconsistencies where the streamfunction outcrops at the surface or with the bathymetry at the bottom are shown as data gaps.

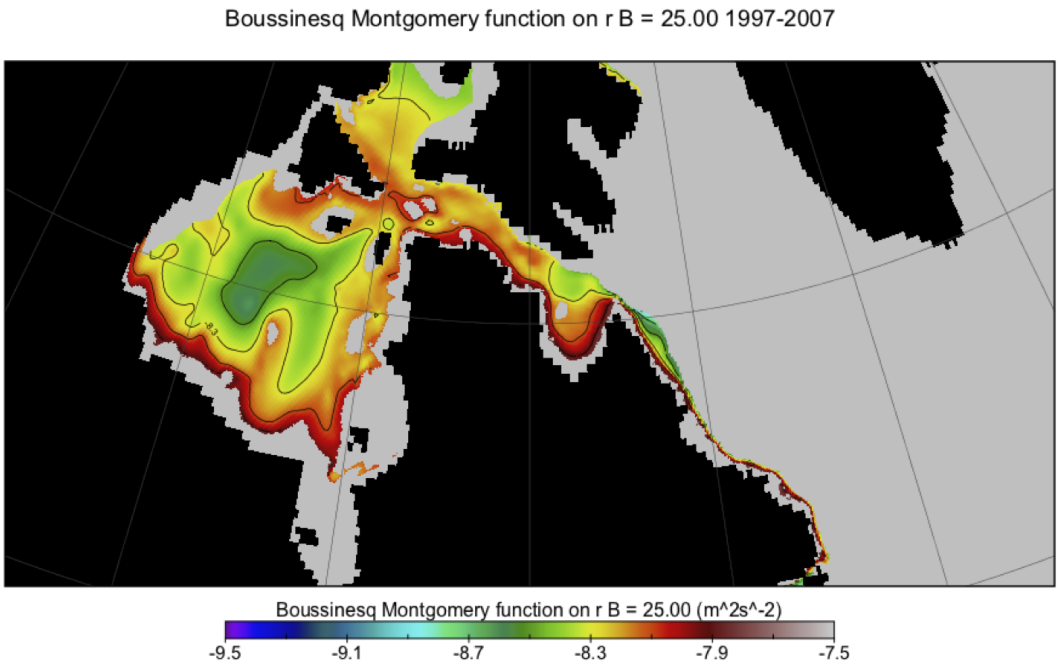

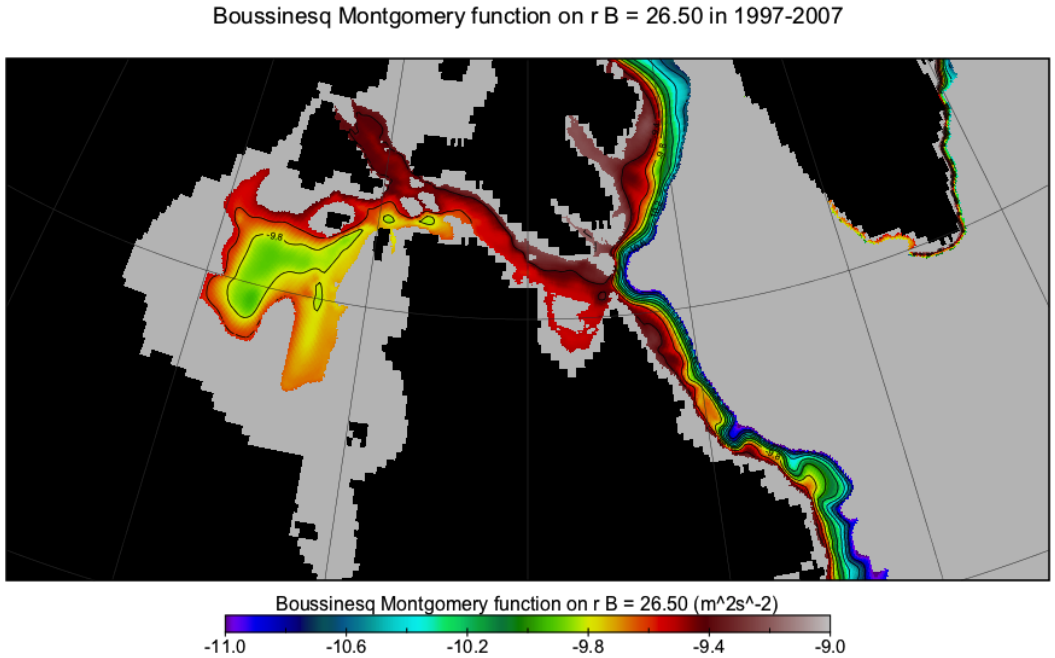

Figure 5.19: Montgomery streamfunction at the inshore front ($r_B = 25.0$ surface, top panel) and the offshore one ($r_B = 26.5$ surface, lower panel).

The Montgomery function in figure 5.19 links the currents seen at the Seal Island section with their tracks north of the section, and inform us about their source regions. Overall, the streamlines follow the same path inferred from the salinity and velocity structures described in figures 5.7 and 5.8. The lower panel in the Montgomery figure displays the function for the mid-shelf waters. The isolines show a clear continuation of the Baffin Current as the Labrador Current at the

shelf edge, south of the Hudson Strait mouth. The Baffin Current carries Arctic water southwards, at the west side of Baffin Bay (*Ingram and Prinsenberg*, 1998). The water temperature at this r_B, shown in figure 5.20, is consistent with this. Arctic water is characterised by temperatures below 0°C and close to their freezing point. In the Baffin side, the multiannual average shows water below -1.4°C. It warms up on the way south, but remains below 0 in most of the Labrador Shelf.

The r_B surface for the inshore waters (upper panel, figure 5.19) displays a different picture. All the streamlines for the inshore current front flow out of the southern part of the Hudson Strait. This means that the waters between the coast and this front virtually contain no water coming directly from Davis Strait or Baffin Bay. Accompanying the inshore Montgomery function are temperatures that are marginally below zero, yet they are about a degree warmer than their mid-shelf Arctic counterpart (figure 5.20). They become positive shortly after entering the Labrador Shelf. Where the Hudson Outflow enters the Labrador shelf, the streamlines merge close together and appear constrained in space, showing a clear boundary. Then the flow continues as a thin and well defined inshore current.

These new results shed light on the unknown fate of the Hudson outflow and its link to the Labrador shelf. They also inform qualitatively about the exchange between both parts. Most of the Baffin/Labrador Current system circulates outside Hudson Strait and continues south at the shelf edge. A small part flows into the strait along the north side and recirculates back towards the shelf, following the paths observed by drifters in the region (*LeBlond et al.*, 1981). This branch interacts with the Hudson outflow and forms a front between both waters at the inner shelf. This allows the Arctic water flowing south through Davis Strait with the Baffin Current to fill most of the Labrador shelf between both fronts. In contrast, the Hudson Strait outflow deflects south-east as soon as it meets the denser shelf waters and continues as an inshore coastal current. The narrowing of the streamlines on the shelf, associated with the observed strong density gradient, indicates a clear boundary between the Hudson and the Labrador waters. The Hudson water is constrained inshore, in the first 40-50 km of the shelf. This indicates that the strong boundary prevents the Hudson water from reaching the Labrador Current proper or from mixing with the shelf water.

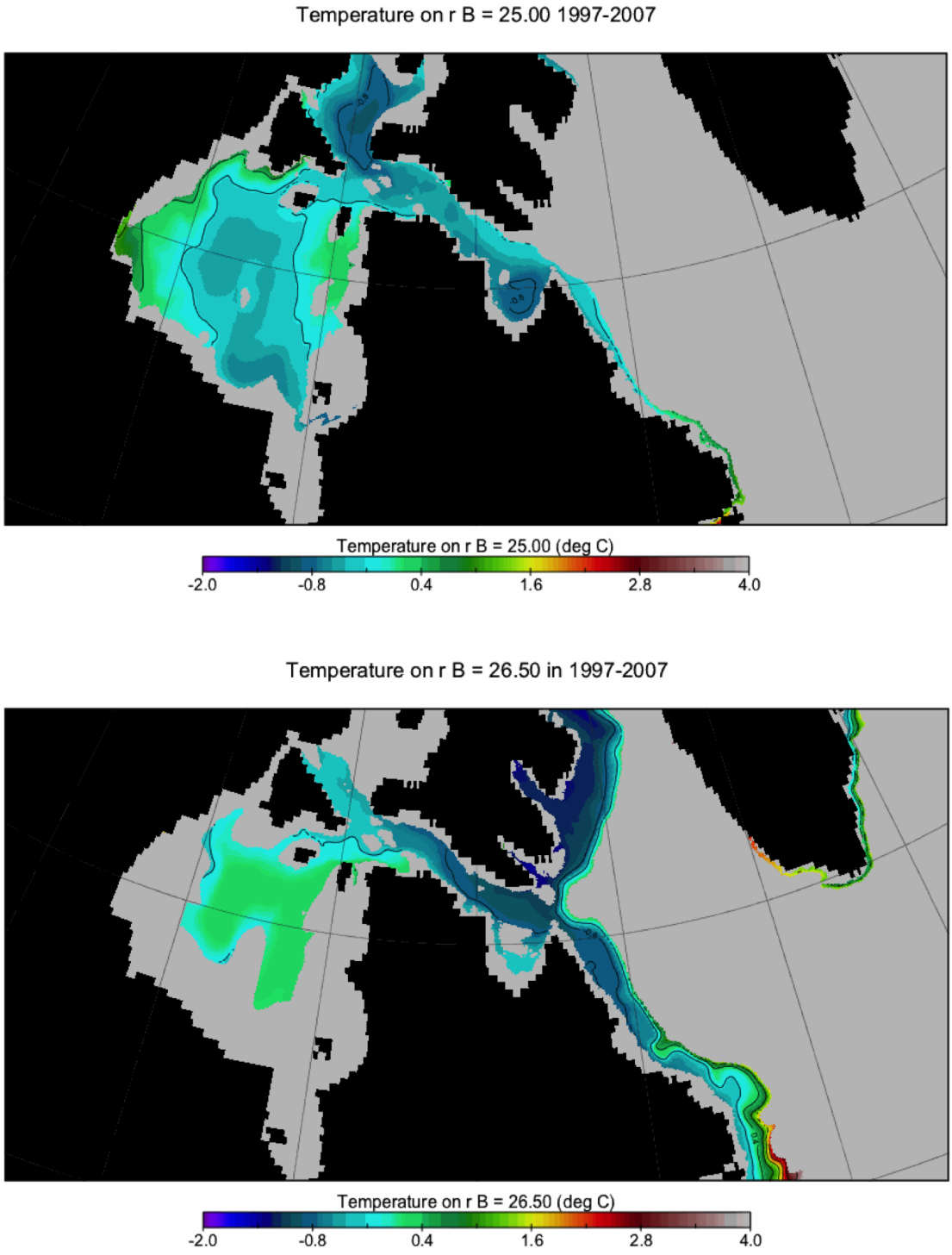

Figure 5.20: Temperature at the inshore front ($r_B = 25.0$ surface, top panel) and the offshore one ($r_B = 26.5$ surface, lower panel).

5.2.4 The Labrador Coastal Current

The coastal jet has been observed before, but it has never been described in detail. It has often been attributed as an inshore component of the Labrador current, whose main branch flows at the shelf edge and slope (e.g. *Smith et al.*, 1937; *Mertz et al.*, 1993). This study, however, has shown that the two currents are not only geographically distinct, but also have different variability (seasonal to multi-annual), different dynamics and different source regions. These results confirm that they are indeed separate currents rather than two branches of the Labrador current. From this point, this thesis will refer to the inner jet on the shelf as the **Labrador Coastal Current**. The naming follows other examples of similar coastal currents, such as the East Greenland Coastal Current (*Bacon et al.*, 2014). A brief description of the Labrador Shelf circulation and the distinction between their components is summarised below, combining previous knowledge with these new results.

The Baffin Island Current, which carries Arctic water southwards through Davis Strait (*Ingram and Prinsenberg*, 1998), splits in two near 63°N (*LeBlond et al.*, 1981). The offshore branch joins the turning West Greenland Current and they form the Labrador Current, flowing southwards along the shelf break and slope (*Smith et al.*, 1937). The inshore branch recirculates outside of the Hudson Strait mouth to then rejoin the offshore branch. Some of it flows in the strait along the north side, but shortly recirculates out setting the offshore boundary of the Hudson outflow. Their degree of mixing remains unknown. The Hudson outflow flows south-east along the south side of the strait (*Drinkwater*, 1988). When it reaches the Labrador shelf, it is deflected by the strong density front with the ambient water and continues south as the Labrador Coastal Current. These dynamics are in agreement with the results by *Straneo and Saucier* (2008), who concluded that the Hudson outflow also responds to buoyancy forcing. At the Seal Island section, both the Labrador Current and the Labrador Coastal Current remain clearly distinct. The Labrador current presents a double core, a baroclinic component on the shelf edge and a barotropic component over the slope. This matches the characteristics of the two currents that precede it; the Baffin and the West Greenland currents. Their limit is set by a distinct front and a characteristic temperature gradient (*Smith et al.*, 1937). The strongly baroclinic Labrador Coastal Current remains in the

first 45 to 60 km of the shelf and traces the front between the Hudson and the shelf waters.

The model suggests that this strong front restricts the Hudson Strait to inshore waters. This allows the Arctic water to fill the shelf between the coastal front and the shelf break one. However, this does not necessarily preclude exchange of water. In order to study the variability of Arctic freshwater on the shelf, it is essential to understand how well this signal is preserved. The next section uses freshwater transports to compare the waters found at the Seal Island section with their source regions. This serves to evaluate their degree of exchange and to conclude whether the variability signal is affected or impacted by variability in other sources.

5.3 Sources and exchange of the shelf waters

As the Arctic-origin water travels south towards the Seal Island section, it is exposed to recirculation, potential mixing with offshore waters, and some additional sources of freshwater (e.g. ice-melt, precipitation). While it is impractical to quantify those processes directly, the continuity of the Arctic water component can be tested in the model by examining the freshwater transport at different locations along the shelf. If mixing, divergence and dilution are small, then the freshwater transport of a current remains almost constant regardless of small changes in volume transport or salinity, and it provides a quasi-conservative tracer tool.

Following the results summarised in the previous section (5.2.4), the long-term means of the Hudson Strait outflow are expected to be consistent with the Labrador Coastal Current. Similarly, the Arctic water export west of Greenland is to be comparable with the mid-shelf water between the Labrador Coastal Current and the shelf edge front. A positive result would further support the hypothesised source regions of the shelf waters. Additionally, their comparability skill will grossly indicate how well preserved the variability signal is at the Seal Island section. This will inform about how the Arctic freshwater exported west of Greenland can be identified on the Labrador shelf and how much it is impacted by other sources. This will allow analysis of Arctic export variability in the following chapter.

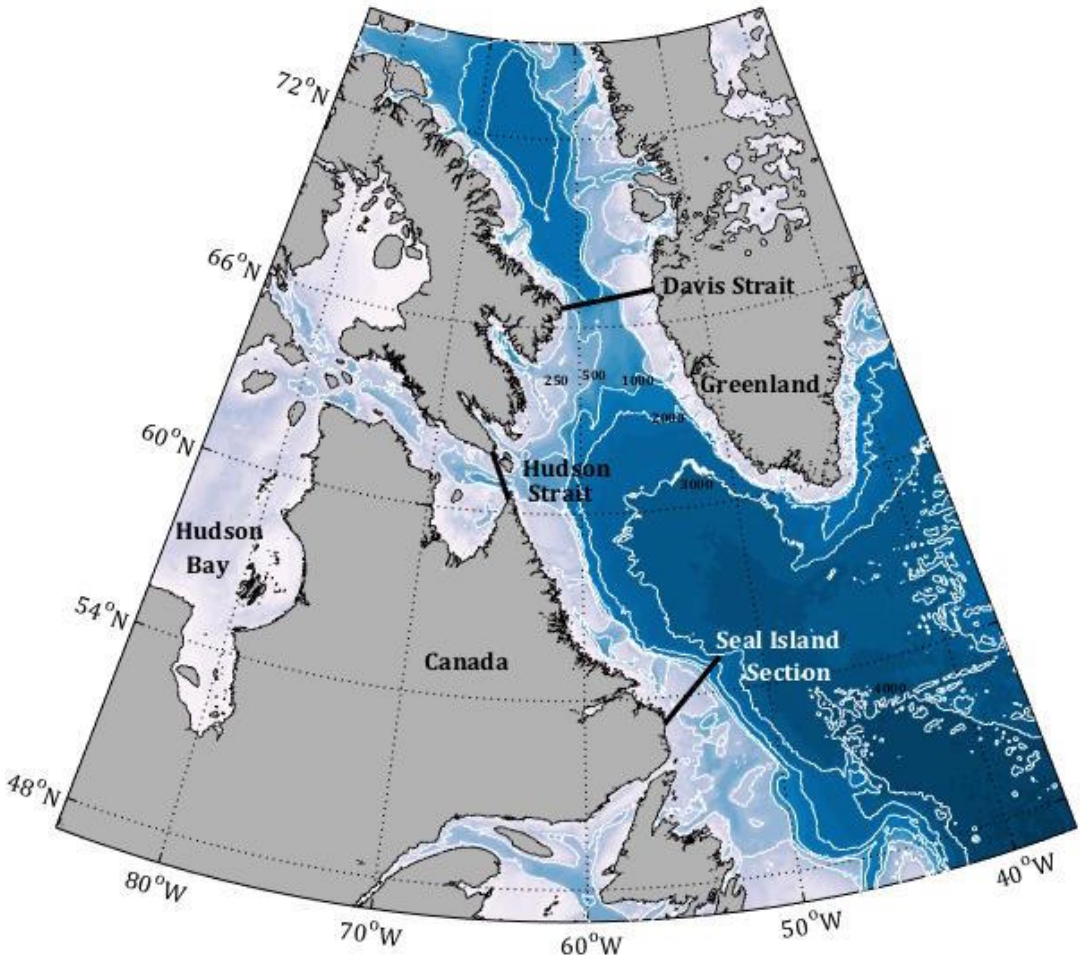

Figure 5.21: Regional map displaying the sections where freshwater transports have been calculated.

Model monthly freshwater transports are calculated at three different sections (figure 5.21): the Seal Island transect, the Hudson Strait opening, and Davis Strait. The net freshwater transport through Davis Strait informs about Arctic water export west of Greenland. The net transport through the Hudson opening accounts for the net outflow of Hudson water. These sections are respectively gateways of the Arctic and Hudson source regions and host observations that allow for comparison. In the coast-to-coast Hudson and Davis Straits, net transports and freshwater export are straightforward to compute from the model. In contrast, the Seal Island section terminates in the open ocean and thus requires care to accurately partition the water masses of interest. Following the dynamics study (section 5.2.2), density gradients are used to distinguish between the Labrador Coastal Current, the open shelf water, and the relatively warm and salty waters of the off-shelf Labrador Sea boundary current. This distinction is done as follows.

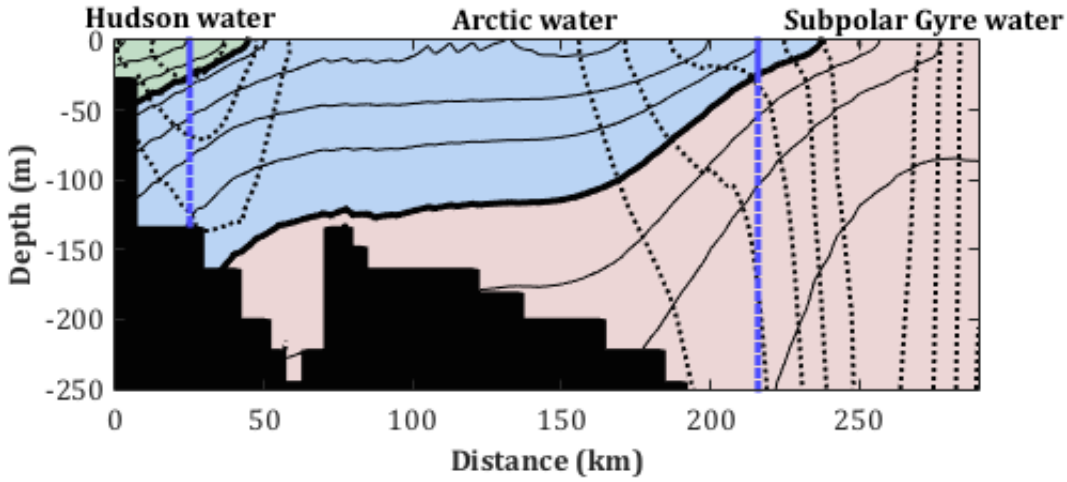

Figure 5.22: Sketch of the methodology followed to separate the different waters at the Seal Island section, using summer (July-August) model data averaged from 1995 to 2010. Filled contours show the resultant partitioning of the waters according to their origin. Dashed black contour lines indicate the average velocity and solid black contours denote salinity (see Fig. 5.3). Density fronts are shown by the blue thick contours, dashed below 25 m deep. The thick black contours show a schematic limit of the different waters, determined by the TS properties of the fronts below the average thermocline (25 m).

The Labrador Coastal Current is supported by the strong density gradient between the very fresh Hudson outflow water and the colder Labrador shelf (Labrador Current) water. The isopycnal at the maximum velocity of the current defines the limit of Hudson outflow water. Similarly, the open shelf water forms another front with the warmer and saltier waters of the Labrador Sea boundary current on the shelf's edge (*Smith et al.*, 1937). This serves to define the eastern limit of the shelf water as the isopycnal at the maximum density gradient in that front. The definition divides the full Labrador Current into the two water types; the cold, fresh and buoyant component over the shelf and shelf break, and the warm and saline recirculating water originating in the West Greenland current, part of the Subpolar Gyre (*Lazier and Wright*, 1993). The Arctic water that fills the open shelf is bounded by these inshore and offshore density limits (figure 5.22).

In order to avoid the surface alteration of the fronts due to summer warming, their densities are computed as found below the thermocline (at 25m deep). The model climatological (1995-2010) density boundaries are 1025 and 1026.5 kg/m^3 for the inshore and offshore fronts respectively. These values are those that have

been used in the Montgomery streamfunction (section 5.2.3). The model average density for the Hudson water at the Seal Island section is 1024.43 kg/m^3, and 1025.93 kg/m^3 for the Arctic open shelf water. These values have been used in the Coastal Current model (section 5.2.2). However, the delimiting isopycnals can, and do, change over time, so they are computed for each model time step. Model monthly averaged freshwater transports have been calculated for 1995 to 2010. The time series and the seasonal variability are presented in figure 5.23.

Model results are first compared with estimates from the literature to assess the performance of the model. In contrast to the salinity reference of 35.0 used in this analysis (see section 3.4), most observation-based studies use the mean Arctic salinity (34.8) as a reference. However, since results appear not to be sensitive to small differences in the reference salinity (*Aagaard and Carmack*, 1989) a gross comparison still remains practical. *Curry et al.* (2014) recorded 93 mSv of net freshwater export through Davis Strait for 2004 to 2010, similar to the 88 mSv estimated here for the same period. Likewise the time series of Hudson net export averaged to 43 mSv, almost coinciding with the 44 mSv of net freshwater addition estimated by *Straneo and Saucier* (2008). To the extent of the available observations, it can be concluded that the model provides a consistent representation of the freshwater sources to the Labrador shelf and is a reliable instrument to investigate the degree to which the Arctic waters are preserved at the Seal Island section.

The long-term mean freshwater transports of the Labrador Coastal Current and the Labrador shelf water at the Seal Island section are in very close agreement with the Hudson Strait Outflow and the Davis Strait transport respectively (figure 5.23). They account for 43 mSv (Hudson) and 45 mSv (Coastal); and for 109 mSv (Davis) and 112 mSv (Labrador open shelf). Additionally, the variability over time, including evidence of seasonal cycles, are in close agreement between each pair. Both pairs show a time lag consistent with the advection time scales expected for the velocity of the currents and the distance between the sections. At a half month resolution, the Hudson-Coastal pair show a maximum correlation ($r = 0.64$) with a lag of two weeks, and the Davis-Arctic pair present a maximum correlation ($r = 0.52$) at a 2.5 months lag. Notably there is little multi-annual trend in the Hudson Outflow and Labrador Coastal Current transports, but in the

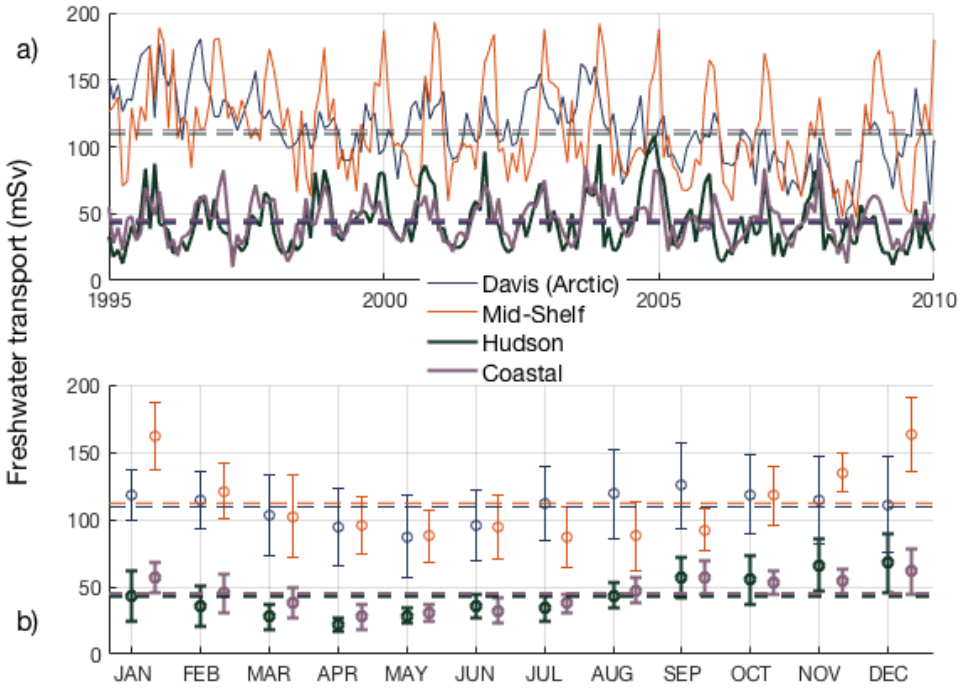

Figure 5.23: Model monthly-averaged freshwater transport time series from 1995 to 2010 (top) and seasonality as monthly means ± the standard deviation indicated by the bars (bottom). The time series show the transport at the Seal Island section, by the Labrador Coastal Current (purple) and the Labrador mid-shelf water (orange), and the transport at the source regions: by the Hudson Strait outflow (green) and through Davis Strait (blue). The dashed lines show the long-term average of the different transports.

Davis Strait and open shelf transports there is a matching long-term trend in the model data.

The closely lying long-term averages are good evidence that there is a high degree of preservation of the water carried by the shelf currents. Such agreement is also shown by matching variability throughout the time-series (from seasonality to multiannual trends). This further supports that, despite recirculation and other local freshwater inputs, the Arctic signal remains preserved at the Seal Island section and it can be identified in the observations.

In summary, the freshwater transports provide further evidence of the origin of the waters within the Labrador shelf as found at the Seal Island section. The Labrador Coastal current is responsible of holding the waters from the bays of

Hudson and Ungava within the first 45 to 60 km of the Labrador shelf with little mixing. This allows Arctic water to fill the open shelf and the signal of changing freshwater export to remain identifiable at the Seal Island section. Therefore, the observations can be confidently used to investigate, for the first time, the multi-decadal variability of Arctic freshwater export to the subpolar North Atlantic.

5.4 Summary

This chapter provided an extensive model analysis of the Labrador shelf circulation. It first tested the skill of the model to represent the regional features. Then, the model was used to complete the gaps in the current knowledge of the circulation. It focused on the two-current system on the shelf, especially in the nature of the inshore jet and the fate of the Hudson outflow once it reaches the Labrador shelf. The main features and findings are:

- The NEMO model provides a reliable representation of the Labrador shelf, as shown by its comparison with available observations.
- The circulation is dominated by two independent and different shelf currents:
  - Cross-sectional velocity at the Seal Island, surface velocity maps and the Montgomery streamfuction show they are geographically separate.
  - Distinct variability and the response to diverse buoyancy changes show they respond to different dynamics.
  - The Montgomery streamfunction shows that they are also provided from separate source regions: Hudson Bay or Arctic export west of Greenland.
- The former "inshore branch" of the Labrador current, as a different current to the main Labrador current, is renamed as the Labrador Coastal current.
- The coastal current is a continuation of the Hudson Strait outflow and yields its water inshore of the shelf.
- The Labrador current has a double component: one is part of the Subpolar Gyre, over the slope. The baroclinic shelf break part carries Arctic water exported west of Greenland, between the coastal and the gyre distinct fronts.
- Freshwater transport shows that the signal of Arctic water remains preserved and identifiable at the Seal Island section.

This new knowledge is used in the following chapter to put the Seal Island observations in context, to isolate the Arctic signal and to provide a multidecadal proxy of Arctic freshwater export west of Greenland.

Chapter 6

A proxy for decadal Arctic freshwater export west of Greenland

The aim of this thesis is to better understand the variability of the Arctic freshwater export west of Greenland in order to better predict its effects on the North Atlantic freshwater budget, to link past variability with changes in the Arctic freshwater budget and to ultimately understand how the current changes will impact global climate. This is now possible with the data and the information provided by previous chapters. This chapter combines the dataset obtained in chapter 4 with the model study from chapter 5 to achieve that goal. Here I study the Arctic freshwater fluxes in the Labrador shelf observations, I compute a proxy that provides insight in long-term variability of the Arctic export west of Greenland for the first time and I analyse the link between the export variability and the fate of the Arctic and North Atlantic freshwater budgets.

A large part of this chapter focuses on obtaining velocity from the observations. It is a fundamental variable, which is not only essential to compute transports, but it is also key to pinpoint the core of the jets and the boundaries of the Arctic water in the model. The different characteristics of the observations require adaptation of the water partitioning method. This chapter further studies the connection between the model and the observations so that the methodology is adjusted to

the observations. As for the transport calculations, the hydrographic data do not include current meter information or other direct measurements of velocity. This hinders their analysis, but it does not prevent estimation of yearly sections of velocity. A fundamental part of this chapter involves obtaining velocity information from the available data. This is possible by computing geostrophic velocities using the hydrographic sections computed in chapter 4. Furthermore, realistic velocity estimates can be achieved by using the model study from chapter 5 to reference them to a level of known motion.

In this chapter, I first separate the shelf waters to isolate the Arctic signal in the observations. To do this, the partitioning method is adapted to reconcile the differences between the model and the observations. I continue computing yearly summer velocity sections from geostrophy, adjusting them to an average barotropic component. With these, I compute the Arctic freshwater transport as found on the Labrador shelf and employ this as a proxy for Arctic freshwater export through Davis Strait. At the end of the chapter, I discuss the main findings and how these relate to the Arctic and North Atlantic freshwater budgets. This will give insight in the interplay between the Arctic freshwater storage, the export and the buoyancy changes in the North Atlantic. This new knowledge will be essential to predict future changes and their implication for climate.

6.1 Partitioning of the shelf waters in the observations

In the model, the velocity data made it possible to pinpoint the centre of the currents in order to define the isopycnals that separate the water of the Labrador Coastal Current, the open shelf (Arctic) water, and the offshore warm saline boundary current water. However, the available hydrographic profiles at the Seal Island do not have velocity information. Additionally, the model provides data on a consistent grid and hence the density fronts present a regular distribution. The observations instead are subject to the yearly spread of the data. The lack of velocity data and the weaker definition of the fronts in the observations challenge

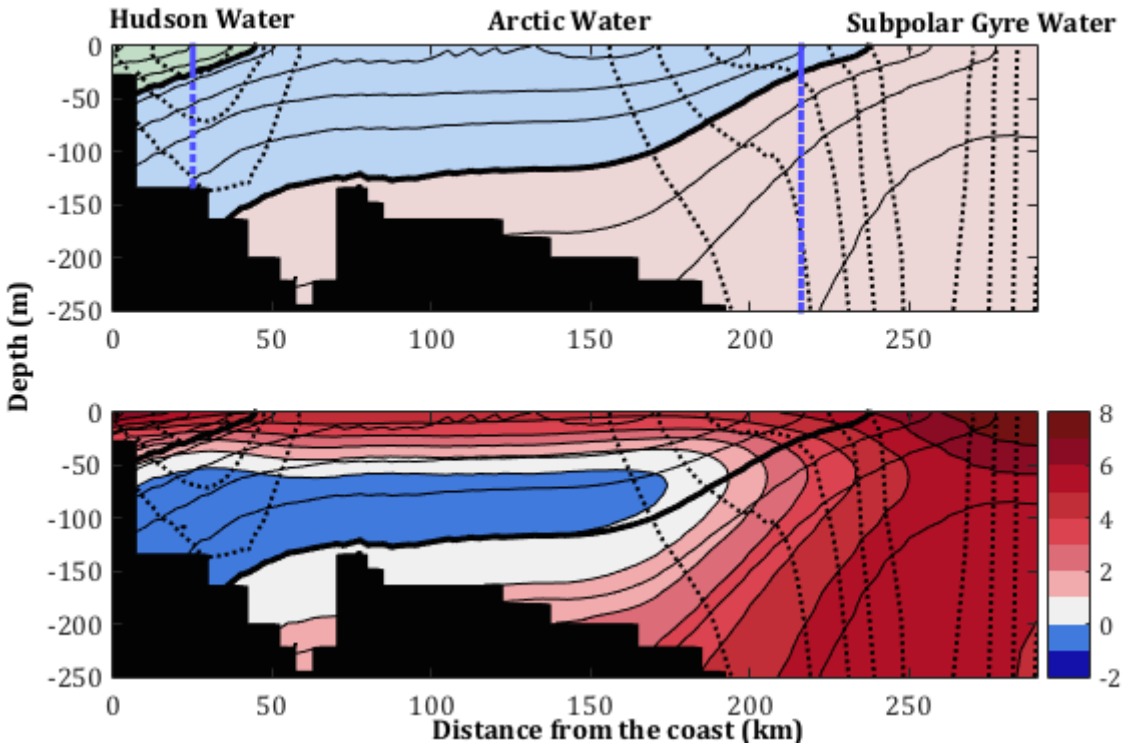

Figure 6.1: Sketch of the methodology followed to separate the different waters at the Seal Island section in the model (upper panel, previous figure 5.22) and its comparison with temperature (lower panel). The latter displays filled contours of model July-August temperature averaged from 1995 to 2010. The overlying dashed contour lines show the velocity and the solid ones denote salinity. Density fronts are shown by the blue thick contours in the upper panel.

the separation of the shelf waters. In order to adapt the partitioning methodology to the observations, this section uses the full model information to describe the relationship between density, velocity and temperature. This way, this relationship can be applied to the observations in order to define the limits of the water types in the Seal Island section data.

Displaying the climatological (1995-2010) model temperature with overlying salinity and velocity helps in linking the different properties of the Arctic water on the shelf. Figure 6.1 shows those variables (lower panel) and compares them to the partitioning method followed in the model (upper panel, from figure 5.22). Temperature is shown by the filled contours at the isotherms indicated by the colour scale. Understanding how it relates to other variables is possible with the overlying contour lines. They display salinity (solid lines), which depict the location of the water fronts; and velocity (dashed lines).

There is a clear relationship between model velocity and mid-depth temperature: the isopycnals coinciding with the highest velocity at the current core also pick out a mid-depth body of very cold water (the Cold Intermediate Layer (*Petrie et al.*, 1988)). This core of water is clearly displayed in the temperature by the negative (blue) temperatures and coincides with the mean observed CIL in July (*Colbourne et al.*, 1995). These authors provide a broad study of this structure, its seasonal evolution and interannual to multidecadal variability. The CIL remains fully formed from June to August, isolated from the surface by strong summer stratification. In late autumn, the vertical temperature stratification disappears and the shelf waters become warmer overall. However, the density fronts remain clearly distinct. The lack of winter data, especially inshore, precludes analysis of its evolution. Overall, the density distribution is linked to the variability of the CIL, especially regarding the position and intensity of the shelf break temperature (and density) front. This supports the use of this structure to adapt the partitioning methodology to the observations and suggests that the Cold Intermediate Layer is the core of the signal of the Arctic water flowing south.

The values of the delimiting isopycnals change slightly from model time step to time step because of the seasonal cycle in salinity and temperature, and because of the changes in mean water mass properties. However, the relationship between the summer Cold Intermediate Layer, the location of density surfaces and the velocity core holds true throughout the model run. This consistent relationship allows us to link the temperature in the observations with the method used to classify the water on the shelf. Thus finding the western and eastern limits of the mid-depth cold layer in the observations and using the isopycnals at those locations serve to distinguish between the three shelf water types.

This new method sets the Arctic boundaries based on the magnitude of the CIL defined by temperature. However, it uses limiting isopycnals rather than temperature directly. This is convenient for two reasons. First because, unlike temperature, the density (determined mainly by salinity here) is not hugely affected by seasonal surface warming. A density-based separation of the water types allows us to include the warm surface layer when computing the freshwater transport. Secondly, density limits make this method consistent with the model, which uses

density limits combined with velocity.

To gain a better understanding of the Arctic water on the shelf, as defined by this method, a TS diagram is shown in figure 6.2. This plot only shows the climatology data (1995 to 2010) in the model (light grey) and the observations (dark grey). The CIL is defined by the water colder than -1°C. The density limits of the CIL (from the observations) are depicted by the blue contours, and the water engulfed by these isopycnals (blue dots) is the water classified as the Arctic water on the shelf. This TS diagram shows how the method incorporates the warmer water above the CIL, without taking in other watermasses, such as the Hudson/-coastal water (clustered at salinities below 32 and relatively high temperatures) or the Atlantic/Subpolar waters (salinities between 34 and 35, at around 4°C). It also avoids the incorporation of most of the mixed water between the different watermasses, depicted by cross-isopycnal tracks between the water types. It is also interesting to note in the TS diagram the previously described differences between the model and the observations climatologies. This is now seen by slightly different TS shapes, where the model underestimates the temperature of the coastal waters, and overestimates the salinity of the waters off the shelf and the temperature of the CIL core.

In order to test the skill of this method, figure 6.3 extracts the summer freshwater transport from the model and compares it to full model variability (as previously shown by figure 5.23). The fundamental differences between the model and the observations, together with the limitations of each method, prevent from providing an in-depth comparison. The model provides monthly freshwater transports, whereas the CIL based method is only applicable when the layer is fully developed (June, July and August). This and the expected variability induced by small variations due to the different methodologies limit this comparison to a gross interannual to multiannual scale only. In order to focus this comparison on the variability at that scale, the figure compares the transport as anomalies from their mean rather than emphasising the differences in their net magnitude. The grey line shows the freshwater transports calculated in the previous chapter, with a monthly resolution. To reduce the effect of the seasonality, the dashed black line displays their annual mean. The overlying orange line displays the summer CIL method with a

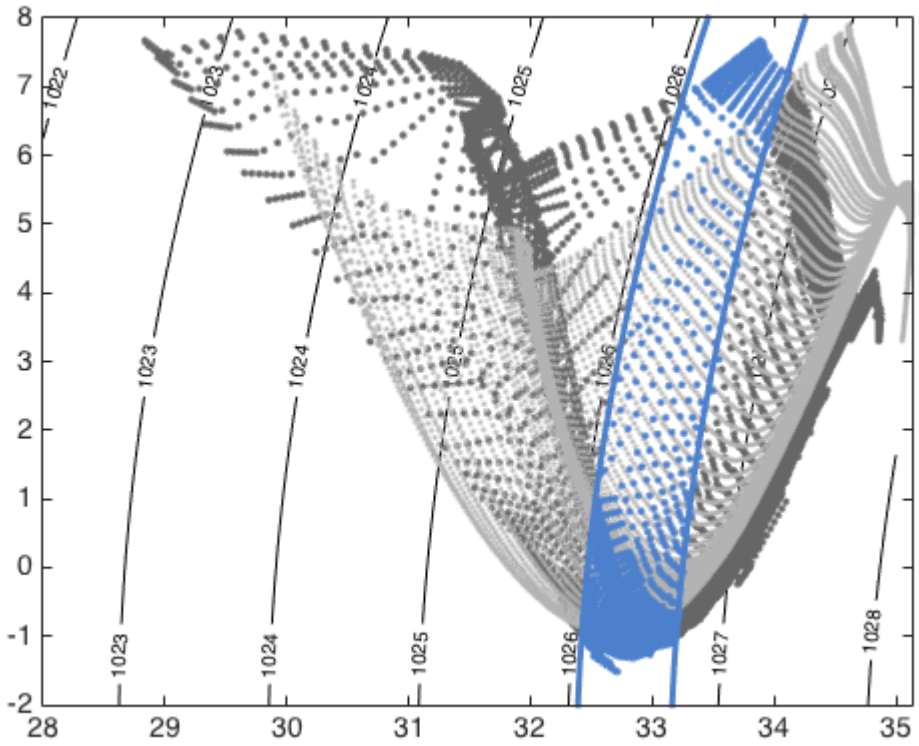

Figure 6.2: Climatological (1995 to 2010) TS diagram at the Seal Island section for the model (light grey) and the observations (dark grey). The CIL core is defined by the water colder than -1°C and, its limiting isopycnals (blue contours), delimit the boundaries of the Arctic water on the shelf (blue scatters). This figure only shows in blue the Arctic water in the observations, not in the model data.

yearly filter (a running average that covers three consecutive data points) in order to emphasise the interannual variability.

As was expected, the seasonal variability in the model freshwater transport has a strong signature in the time series. For this reason, comparing the year to year differences gives a biased view of the variability. The longer term changes, however, can be better represented. The CIL adapted method (orange line) successfully captures the multi-annual to decadal trends and, albeit slight differences in the magnitude, it reproduces the general trend shown by the original method (dashed black line). For instance, the highest transports are found at the beginning of both time series (1995 to 1997). Other peaks are found in 2003-2004 and 2010, a general decrease trend during the late 1990s and a sharp decrease after 2004. The differences in the magnitude and some small offsets are expected due to the different

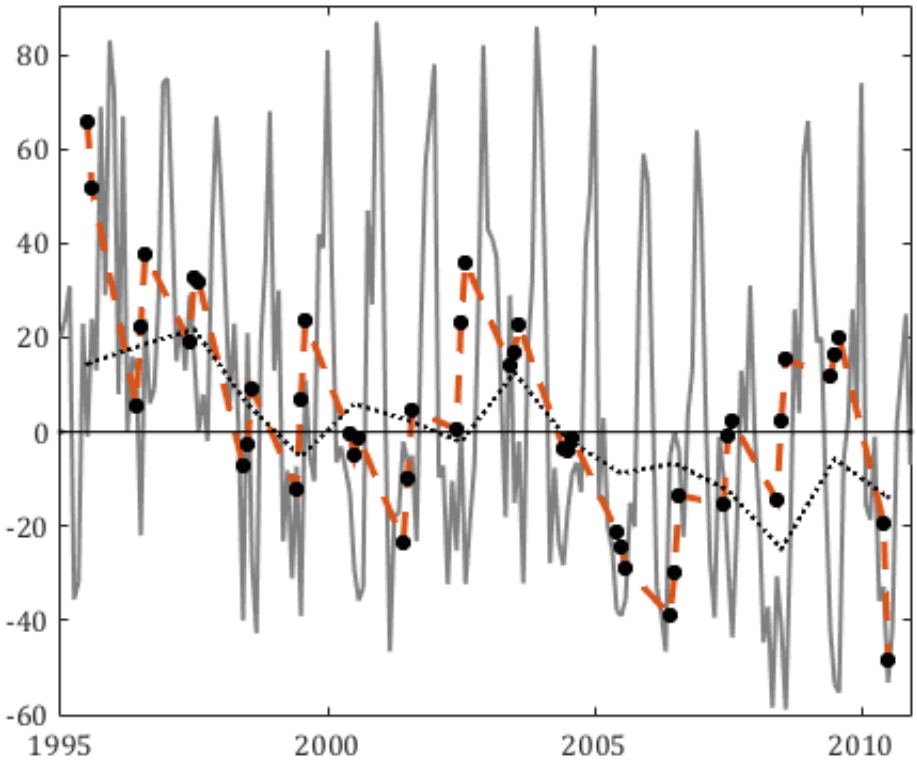

Figure 6.3: Model freshwater transport by the Labrador mid-shelf open water. The monthly transport (using the method defined in section 5.3) is shown by the grey line, the annual mean is displayed by the black dashed line. The overlying orange dashed line shows the model transport for June to August using the adaptation of the method to the observations, filtered with a yearly running average.

specifications of the two methods. However, it is the general trend rather than the net magnitude, which is of greatest interest for this study. The CIL method captures it and provides a reliable method to evaluate the variability of the freshwater export at the Seal Island in the observations. The apparent uncertainty derived from the differences between these two methods invites comparison of eventual calculations of the freshwater transport with the literature. This will help further assess the certainty and it will also help understand whether the magnitude shown by the new method proves reliable.

In order to apply the adapted partitioning method to the observations, the CIL is first identified in each summer temperature section (those shown in annex 1.3). In the literature, this layer is generally defined by an isotherm, either the -1, 0 or +1°C isotherm. The isotherm is often chosen indistinctly without a clear rationale. Here, the isotherm is chosen following some analysis. The sensitivity of this decision will also be evaluated next. The lower limit of the Arctic water, unlike the

surface modified waters, offers a sharp boundary to infer the CIL limit. This will determine the CIL isotherm for this study. In figure 6.1, the bottom of the Arctic water core in the model coincides with the 0°C isotherm. The model, however, overestimates temperature by 1°C as concluded in section 5.1. To account for this, in the observations the CIL will be defined by the -1°C boundary (in appendix 1.3, this is drawn by the dark blue contours). To continue delimiting the Arctic water on the shelf, the lower and higher densities found in this CIL will determine the density boundaries for the Arctic water. These will set the lateral (western and eastern) limits. The water engulfed by those two isopycnals will be considered as the Arctic export signal on the Labrador shelf.

6.1.1 Sensitivity of the temperature limit

The temperature-definition of the sub-surface core of Arctic water may be sensitive to the chosen isotherm. A broader (e.g. +1°C) boundary may lead to larger transports or present a different pattern of variability. To evaluate the sensitivity of the chosen isotherm, the effects of the employing different CIL temperature boundaries (order ±1°C) are compared here. A priori, results are expected not to be greatly sensitive to these changes. For example, *Colbourne et al.* (1995) quantified the magnitude of the Cold Intermediate Layer as the cross-sectional area of the different isotherms (-1, 0 and +1°C), and found that although the average area varied with definition, the interannual variability remained consistent. However, the Arctic layer definition employed in the new temperature method now includes the warmer surface waters and so I re-assess the sensitivity.

In order to evaluate the dependence of the results on the chosen CIL boundary, the cross-sectional area of the layer and its mean salinity are studied in this subsection. These two variables, together with velocity (missing in the observations), are essential determining the freshwater transport. If they remain coherent despite the different temperature limits, this indicates the method is sensitive to the chosen boundary. The overall magnitude of the CIL area is expected to increase with a higher temperature limit. However, it is the year to year variability that we are interested in, so here I focus on anomalies from the time series mean. The net

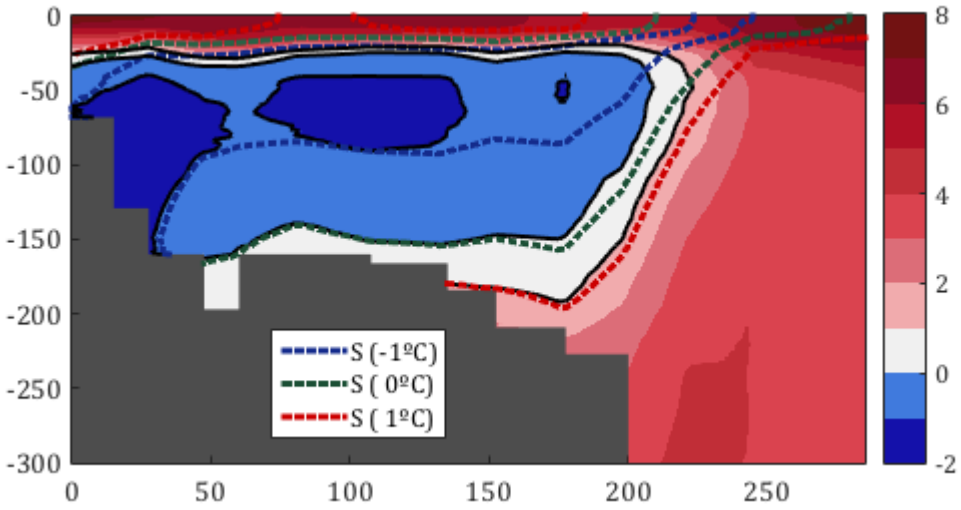

Figure 6.4: Average (1993 to 2014) cold intermediate layer using different temperature limits (-1, 0 and +1°C). Temperature is shown by the coloured contours. Salinity is shown by the dashed contours. These sketch the TS boundaries for the Arctic water on the shelf, according to the different CIL limits.

magnitude of the area may affect the average transport, but this sensitivity can only be evaluated after computing the transport. Section 6.3.2 will cover this.

Figure 6.4 sketches the main differences in the cross-sectional area derived from using the different temperature limits. It displays observed data, averaged from 1993 to 2014 (one observational climatology). Temperature is shown by the filled contours, and the three limiting isotherms (-1, 0 and +1°C) are depicted by the black contours. The overlying salinity (dashed) contours display the isohalines given by each temperature boundary. These TS properties help visualising how the shape and magnitude of the Arctic water vary according to each CIL definition. As expected, warmer (broader) limits yield a greater area. However, this additional area is mostly at the bottom of the mid-shelf, where velocity is lowest (see figure 5.10) and this has a minimal effect on the transport. The location of the Arctic water fronts (lateral limits) remain fairly similar, especially at the coast. This suggests that, although there are differences in the cross-sectional area, these are in weakly variable and low velocity regions and may not have a significant effect on the freshwater transport.

Among the different CIL definitions, the 0°C and 1°C limits appear too large because both incorporate a small fraction of the Hudson and Subpolar gyre waters.

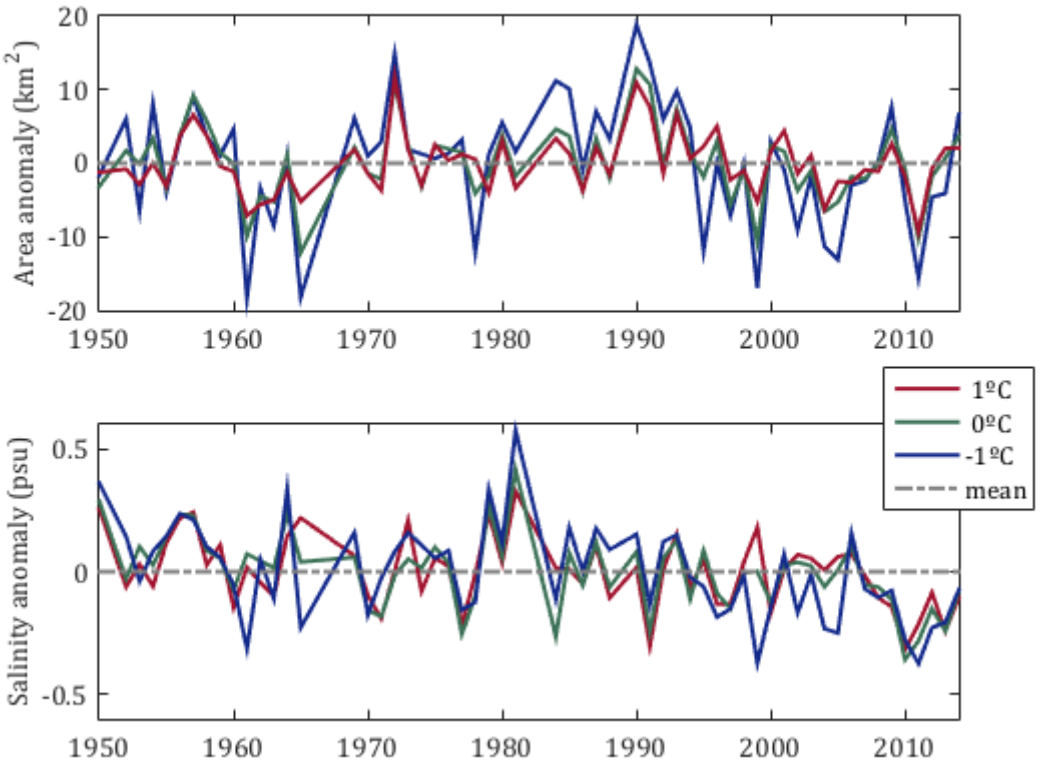

Figure 6.5: Time series (1950 to 2014) of the observed CIL cross-sectional area (top) and its mean salinity (bottom) for the three different temperature limits (-1, 0 and +1°C). Data are shown as the anomaly (or difference) from the time series mean.

The -1°C limit matches more closely with the one defined in the model (figure 6.1), suggesting again this is the optimal approach.

Figure 6.5 further evaluates the method sensitivity by displaying the time series (1950 to 2014) of the CIL cross-sectional area and its mean salinity, for the three different temperature limits. Data are presented as anomalies to focus the attention on the differences in variability rather than in the net value, which is expected to vary. Overall, both time series are coherent between the different temperature limits. The amplitude of the variability changes slightly between the different CIL limits. The -1°C presents the peaks with the largest amplitude (in both high and low anomalies) and therefore more fully captures the year to year variability.

The general agreement between the varied CIL boundaries show that, regardless of the chosen temperature limit, decadal variability is not sensitive to this choice.

A consistent cross-sectional area and salinity allow calculation of reliable freshwater transports, for they are keys factors in this calculation. To complete the transport computation, however, we need to derive velocity. The next section covers the full process to obtain cross-sectional velocities.

6.2 Computing velocity summer sections

The model provides us with full velocity information and this allowed computation of transport and freshwater fluxes. The hydrographic observations, however, only provide temperature, salinity and other properties of the water column that do not include velocity. This section covers the process to derive velocity sections at the Seal Island from the observations.

The analysis presented in chapter 5 showed that the circulation on the shelf is mostly baroclinic; velocity showed a strong shear with near-zero bottom velocities, and varied according to local changes in density. This means that buoyancy, which can be obtained from the temperature and salinity profiles, mostly control the circulation. Additionally, this information can be supplemented with the model, which can be used to estimate the small barotropic velocity in order to add it to the baroclinic observations and hence estimate the total velocity.

This section shows how I derive the net velocity information to compute the transports. First, I compute the geostrophic velocity for the whole time series, from 1950 to 2014, from the observed temperature and salinity sections. Secondly, I use the model to estimate the barotropic component of the circulation on the shelf. This is added to the baroclinic velocities and it is also used to quantify the bartotropic/baroclinic ratio. This will also help to inform about the uncertainty. Finally, the total velocity products are presented following the same structure as chapter 4.

6.2.1 Calculating geostrophic velocities

A flow in geostrophic balance is given when the horizontal pressure gradient is in balance with the Coriolis parameter (equation 3.1 in section 3.3). This means that water will tend to flow from high to low pressure and that it will deflect to the right (left) in the northern (southern) hemisphere because of the Coriolis parameter. This equality allows us to infer the geostrophic velocity from the horizontal pressure gradient. However, directly calculating the horizontal pressure gradient (and hence the velocity) is not yet possible. First, direct pressure measurements would require an unachievable accuracy (a pressure gradient of $1{:}10^5$ would produce a 1 m/s current, requiring a minimum accuracy of at least $1{:}10^7$). Secondly, these measurements should be in reference to the geoid. That is the geopotential surface that defines the mean ocean surface in complete equilibrium (at rest), determined by gravity and rotation alone without any further factors such as wind or tides. Currently, it is not possible to either measure depth independently from pressure nor the slope of the sea surface with respect to the geoid. This hinders the direct calculation of horizontal pressure gradients. However, inferring currents at depth from hydrographic observations is still possible if looking further into the pressure and density relationship.

Pressure (p) can be obtained from the hydrostatic balance equation (equation 3.7, page 30) and it can be re-written as a function of gravity (g), density (ρ) and depth (z), in the form

$$p = \int_{-z}^{\eta} g\rho(z)\mathrm{dz}. \tag{6.1}$$

Here, pressure at a certain depth (-z) is given by the water column above that depth and up to the sea surface (η). Figure 6.6 sketches this relation. It also shows that the water column can be divided into two components: the pressure by the water from a certain depth up to the geoid and that of the water above it and up to the sea surface. That is, respectively,

$$p = \int_{-z}^{0} g\rho(z)\mathrm{dz} + \int_{0}^{\eta} g\rho(z)\mathrm{dz}. \tag{6.2}$$

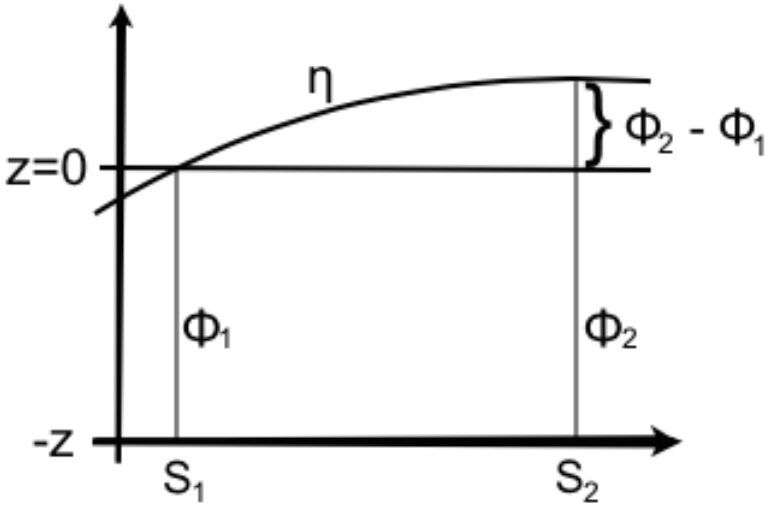

Figure 6.6: Sketch of the geostrophic velocity calculation from hydrographic observations. Two example hydrographic stations (stations S_1 and S_2) present different geopotentials (ϕ_1, ϕ_2), evaluated from a certain depth (-z) up to the sea surface (η).

Finally, this term can be substituted in the geostrophic balance (equation 3.1) to obtain the zonal (u) and meridional (v) velocities:

$$\begin{aligned} u = & -\frac{1}{f\rho}\frac{\partial}{\partial y}\int_{-z}^{0} g\rho(z)\mathrm{dz} - \frac{g}{f}\frac{\partial \eta}{\partial y} \quad ; \\ v = & \underbrace{\frac{1}{f\rho}\frac{\partial}{\partial x}\int_{-z}^{0} g\rho(z)\mathrm{dz}}_{\text{Baroclinic term}} + \underbrace{\frac{g}{f}\frac{\partial \eta}{\partial x}}_{\text{Barotropic term}} \quad . \end{aligned} \tag{6.3}$$

The second term, which accounts for the horizontal pressure gradient due to the sloping sea surface, considers a constant $g\rho$ term and depends only on the horizontal changes of sea surface height.

At this point it is worth noting that the first term of the RHS corresponds to the baroclinic flow, whereas the second term of the RHS is the barotropic one. The barotropic component is given by the pressure gradient associated by the sea surface elevation with respect to the geoid and its effect is constant throughout the whole water column. It is given by pressure surfaces parallel to density ones. Instead, the baroclinic term corresponds to the deviation of the density surfaces with respect to the pressure ones. It is given by internal density changes and its related effects vary (present shear) along the water column. The implications of this are that, in order to calculate geostrophic velocities, it is necessary to calculate the pressure gradient changes from variations in both the stratification and the sea

surface height.

In a perfectly barotropic case (homogeneous ocean; constant density), the baroclinic term is nil and the velocity can be inferred from satellite measurements of sea surface height. In the opposite case, where the ocean is solely baroclinic, the sea surface height coincides with the geoid and the circulation is explained by horizontal density changes. Generally, currents present both components. It is possible to obtain the surface velocity from satellite altimeters. Then, the velocity vertical shear relative to the surface can be estimated from the hydrographic observations. Optionally, when sea surface height information is missing, geostrophic velocity can still be calculated from oceanographic observations by referencing them to a layer of known velocity. However, it has been shown that the circulation on the Labrador shelf is greatly baroclinic and that the velocity at the bottom is near-zero. This information allows calculation of the baroclinic velocity from the observations at the Seal Island section. Here, the observations are used to obtain the baroclinic velocity referenced to a zero bottom velocity. The barotropic component is first approximated to zero, but this component is examined in further detail in the following subsection.

The baroclinic component of the circulation is usually calculated with the dynamic method for gesotrophic velocities. This method estimates the relative magnitude of a current from the dynamic height (or geopotential anomaly). The geopotential anomaly is a measure of the vertical deviation of the pressure field with respect to the geopotential and has units of m^2/s^2. The horizontal variability of the dynamic height is a relative measure of the horizontal pressure gradient, with the advantage that it can be calculated from density rather that direct measurements of pressure. The relative current between stations S_1 and S_2 (figure 6.6) is given by the horizontal difference in geopotential anomaly ($\partial\Phi/\partial x$), or $\Phi_2 - \Phi_1$. The anomalies are obtained by comparing the geopotential between two pressure surfaces. In this case it is the difference of the geopotential at a certain pressure (-z; in this example the pressure coincides with the -z geopotential surface) and at the sea surface (η), or $\Phi = \phi_{-z} - \phi_\eta$.

The geopotential anomaly can be calculated from the specific volume anomaly

(δ, see glossary and equation 3.4) when it is integrated over depth. With the hydrostatic balance, the geopotential anomaly can be related to the steric anomaly in the form $\mathrm{d}\Phi = g\mathrm{dz} = -\delta\mathrm{dp}$ and then substituted in the velocity to obtain

$$\begin{aligned} u = & -\frac{1}{f}\frac{\partial}{\partial y}\int_{p}^{p_{ref}} -\delta\mathrm{dp}; \\ v = & \frac{1}{f}\frac{\partial}{\partial y}\int_{p}^{p_{ref}} -\delta\mathrm{dp}. \end{aligned} \tag{6.4}$$

In this case the steric anomaly is integrated from a pressure surface (p) to a reference pressure (p_{ref}).

With the dynamical method, yearly geopotential anomaly sections at the Seal Island can be obtained from the hydrographic observations. It is common practice to set the reference pressure (p_{ref}) at the surface (atmospheric pressure). This yields a zero geopotential anomaly at surface and, consequently, a zero surface velocity. When the velocity is calculated from the horizontal gradient of the dynamic height, this can be corrected to a zero bottom velocity by subtracting the bottom baroclinic velocity to the whole water column. Because the geostrophic velocity is computed by vertically integrating a gradient, it works best when calculated at individual profiles rather than already interpolated sections. For this reason, the geostrophic velocity is calculated between each pair of consecutive profiles. The resulting velocity profiles are then interpolated along the section.

Figure 6.7 shows the climatological (1993 to 2014) results for the geopotential anomaly referenced to surface atmospheric pressure (upper panel) and the geotrophic baroclinic velocity referenced to a 0 bottom velocity (lower panel). Where the geopotential anomaly isolines are flat, so is their horizontal gradient. This indicates that density surfaces are fairly parallel to pressure ones and the resulting baroclinic velocity is small. The opposite case is found where the isolines are tilted. This generates a horizontal gradient and hence an intensified flow. The relative magnitude of the velocity is stronger where the slope is sharp. The resulting climatological geostrophic baroclinic velocity (lower panel) shows the same two-current system seen in the model. The location of the two jets coincides with the position of the density fronts and remains consistent with the model. The slope component of the Labrador current is the main difference with the net velocity data in the model,

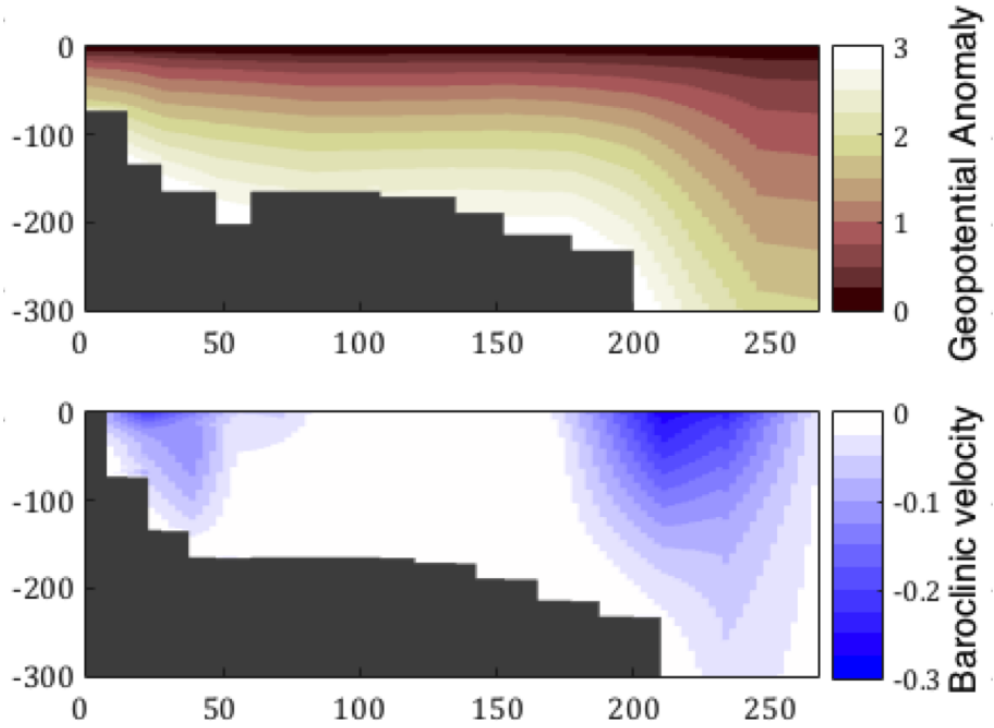

Figure 6.7: Climatological (1993-2014) sections of the geopotential anomaly (m^2/s^2, upper panel) and baroclinic velocity (m/s, lower panel) resulting from the gesotrophic calculations. The geopotential anomaly is referenced to the atmospheric pressure (surface), the velocity is referenced to 0 bottom velocity (before horizontal interpolation).

not being present in the baroclinic velocity derived from the observations. As it was discussed in chapter 5, this component is rather barotropic (constant through the water column and unrelated to density gradients) and its baroclinic velocity is expected to be relatively small.

Regarding the orientation of the flow, velocity is perpendicular to the plane given by each pair of stations. In this case, this means velocity is orthogonal to the section. The direction depends on the reference level. In this case, where velocity is lower at depth (reference velocity is zero at the bottom), it is a general rule that the flow is to the left of the density gradient (northern hemisphere). This is determined by the pressure field (by the direction of the horizontal pressure gradient). Because it is baroclinic, the weight of water above the geoid (z=0) remains constant. To achieve this, sea surface is higher where water is lighter. Thus, the isobaric slopes present the opposite sign to the isopycnal ones. The density field slopes upwards from south-west to north-east, meaning that the flow is south-eastwards (consistent with the model velocity field).

6.2.2 Barotropic correction of the velocity

The geostrophic calculations are based upon a level of no motion; where velocity is assumed zero. This criteria, however, is relatively arbitrary and a reference velocity needs to be added to obtain true net velocities. Albeit the circulation on the shelf has proved to be mostly baroclinic, the barotropic component may be significant when determining the net magnitude of the currents and their transport. For this reason, this subsection finds the average cross-shelf barotropic velocity in order to add to the baroclinic component and obtain net geostrophic velocities.

Section 5.2 covered the circulation and dynamics on the Labrador shelf and provided us with the first estimates of the barotropic component from bottom velocities (shown in figure 5.12). This is continued here with figure 6.8. The 1995-2010 summer average of the model bottom velocity is shown again (black line) and it is compared to the surface velocity (blue line). Because the baroclinic component of the geostrophic velocity has zero bottom velocity, the velocities at the seafloor in the model represent the barotropic part of the circulation. This allows calculation of the barotropic ratio (red line); the barotropic fraction within the net velocity. A higher ratio indicates a larger influence of this component.

This figure shows that the velocity at the bottom is always below 10 cm/s throughout the shelf. Only beyond the shelf break and over the slope does the bottom velocity increase significantly, indicating again the barotropic nature of the Subpolar gyre. The mid-shelf also shows a high barotropic ratio, though this is an artifact produced by the low net velocities there. The importance of this ratio relates to the main circulation features on the shelf. The vertical black lines indicate the mean positions of the Labrador Coastal current (inshore line) and the baroclinic/shelf part of the Labrador current (offshore line). The barotropic components at the core of those currents are, respectively, 15%, and 24% only. So while they are predominantly baroclinic, their barotropic counterpart is significant and it needs to be taken into account in the geostrophic calculations.

The climatological bottom velocity can be used to define the mean barotropic component along the shelf. To compute the absolute velocities this reference velocity is added to the geostrophic velocities computed in the previous section. For

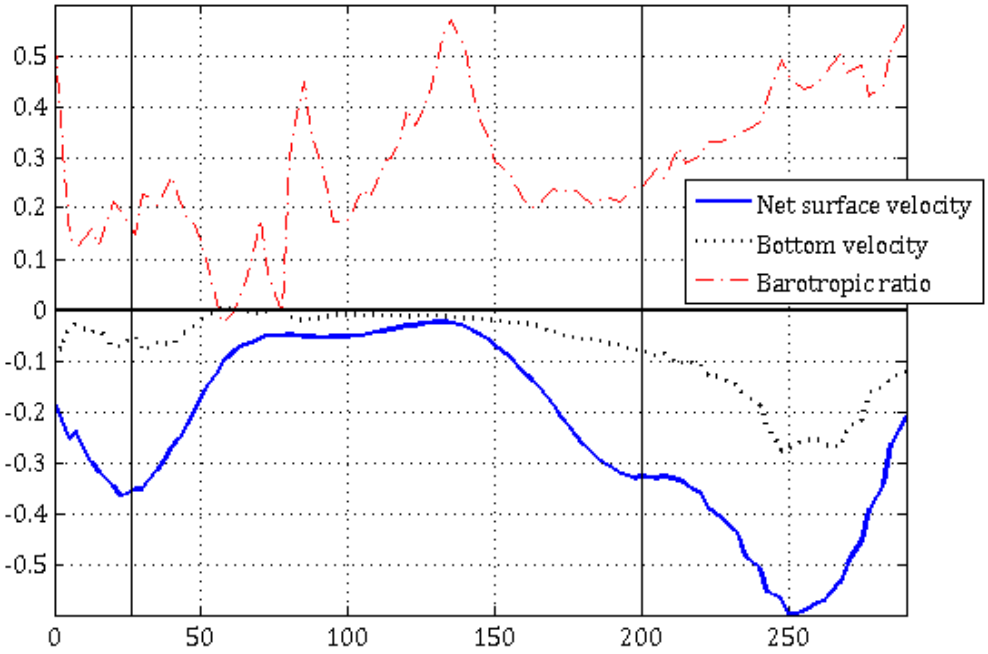

Figure 6.8: Estimation of the mean barotropic component of the Labrador shelf currents in the model. The net surface velocity (m/s, blue line) can be decomposed into a baroclinic component (referenced to a bottom layer of no motion) and a barotropic component, constant along the water column. In this case, the barotropic component corresponds to the velocity at the bottom (black line), as the velocity deviation from the bottom layer of no motion. The baroclinic velocity can be estimated by the difference between the net velocity and the barotropic component. The vertical black lines indicate the average position of the Labrador Coastal current (inshore) and the shelf part of the Labrador current (offshore). The x-axis denotes distance from the coast in km.

each individual station, the model mean bottom velocity is first found at that position. Then, this value is added to the baroclinic velocity over the whole water column. Finally, yearly sections are interpolated from the individual profiles.

The model bottom velocity is a point measure; it is continuous along the section. This allows to correct the velocity sections at individual stations (before their horizontal interpolation) or after, adding the bottom velocity to the whole section. To better preserve the continuity of the data, it is preferred to correct the velocity at a station to station basis. This avoids the introduction of discontinuities due to the changing bathymetry. Figure 6.9 shows the difference between correcting the velocities at each station (upper panel) or at the section as a whole (bottom panel). Although the results are very similar, jumps in the data can be observed when applying the linear bottom velocity as a whole.

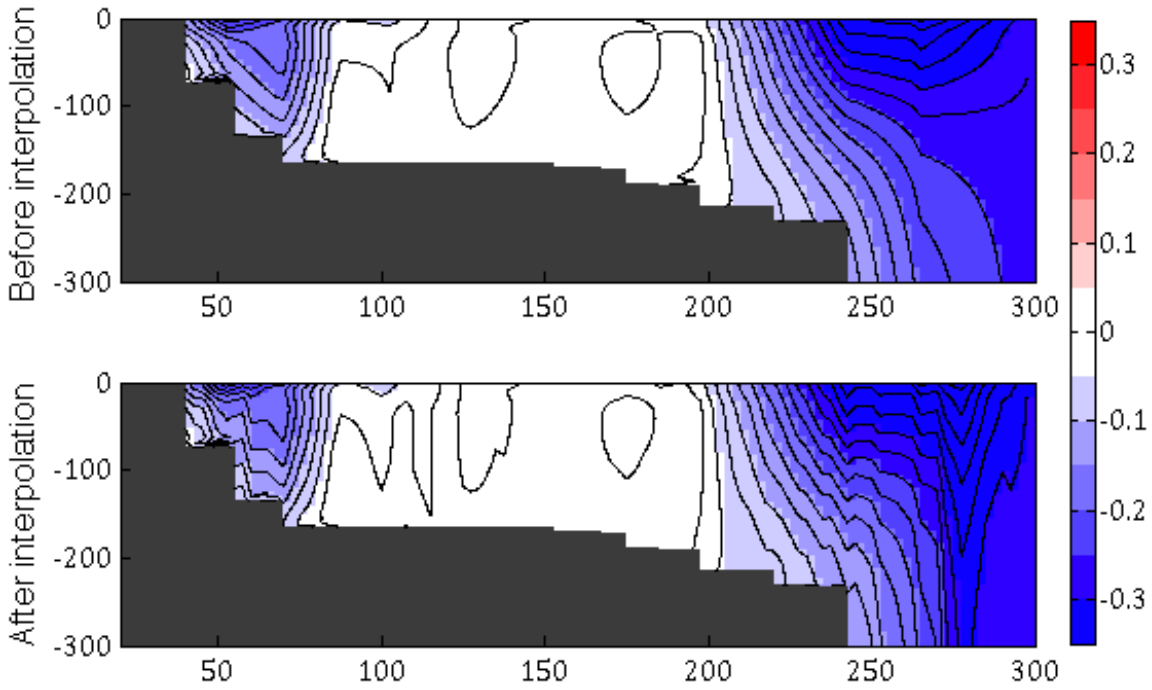

Figure 6.9: Barotropic correction applied at individual stations, before interpolating the velocity (top panel); or applied after the interpolation, to the section as a whole (bottom panel). Velocity in m/s, with black contours every 5 cm/s.

6.2.3 Yearly summer dataset of velocity from the observations

Net geostrophic velocities are calculated for every year with a complete section of summer observations. These are obtained with the dynamical method between each pair of stations and corrected by the barotropic component extracted from the model mean bottom velocity. The velocity transects are completed by horizontal linear interpolation between profiles, following the same method used to compute the temperature, salinity and density sections (see section 4.3). Each resulting yearly section is included in appendix 1.6.

Notwithstanding the sparser distribution of data in the earlier years, all 58 sections display the two jets system on the shelf. The width and intensity of the currents vary from year to year, but in general the Labrador Current accounts for larger speeds than the coastal jet. The mid shelf is characterised by marginal (< 0.05 m/s) velocities, with some years showing weak recirculation. The data coverage is slightly less than the temperature, salinity and density sections because the geostrophic velocity is calculated between station pairs. Discontinuities appear

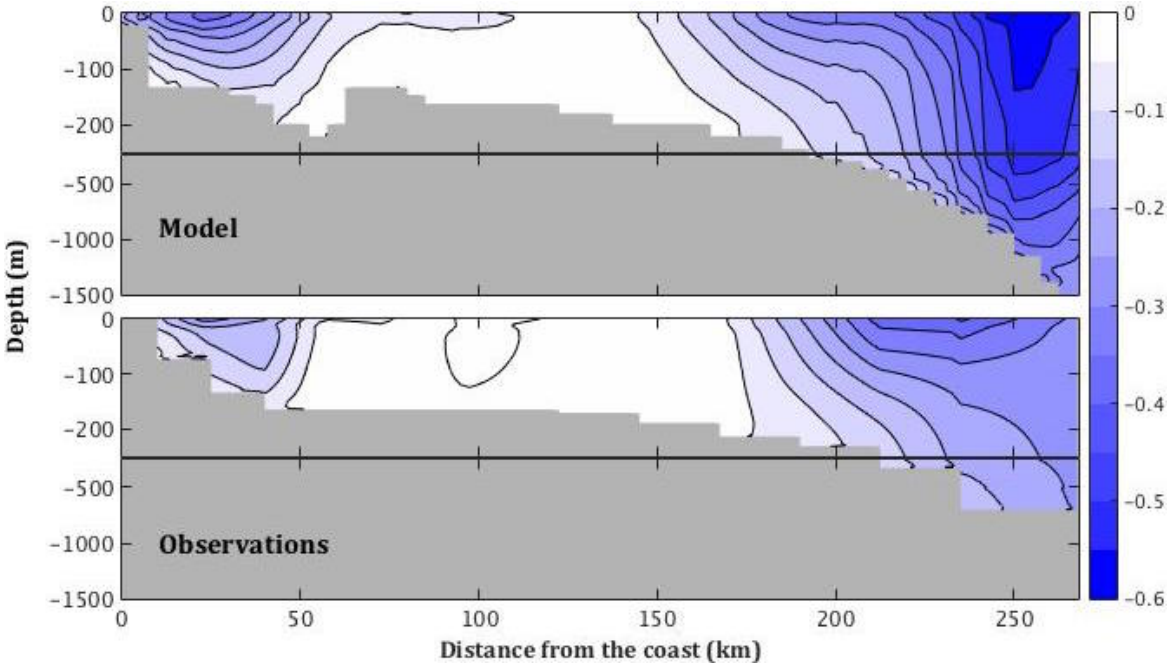

Figure 6.10: Climatological (1995-2010) section of velocity (m/s) in the model (upper panel) and the observations (lower panel). The vertical scale is 5 times stretched at the upper 250 m.

where gaps are replaced with climatological values, in the same way as the previous TS sections. Rather than prioritising the overall visual aspect, filling those regions with background data is essential to achieve equally sized sections. This is required for the transport calculations, which should be integrated over a constant space.

The skill of the geostrophic calculations is evaluated in figure 6.10 by comparing the climatological (1995-2010) velocity in the observations with the model. There is a close agreement in the areas where the baroclinic component of the velocity is important. That is mainly over the shelf, which is the region of interest in this study. There, lies the Labrador Coastal current and the Arctic component of the Labrador current. The slope (or subpolar) part of the Labrador current is weaker in the observations. This can be explained by its larger barotropic component, which is not directly computed from hydrography. The net magnitude of the Labrador Coastal current is smaller in the observations, but that mostly affects the transport of Hudson water. The region where Arctic water is found (as depicted in figure 6.1) has velocities with the same distribution and magnitude in the model and the observations.

The final climatological sections in the model and the observations are shown

together in figure 6.11. This figure summarises the general skill of the model to represent the Seal Island observations. It also serves to test the methods used to interpolate the observations and those to compute the velocity. The overall match of properties, specially on the mid shelf, emphasises the coherence between both tools and their derived results. It also indicates that the calculated geostrophic velocities provide the ability to compute volume and freshwater transports in the observations. Finally, it is interesting to note that climatologies have been calculated for the 1993-2016 and the 1995-2010 periods. The results are almost identical and both climatologies can be used indistinctly.

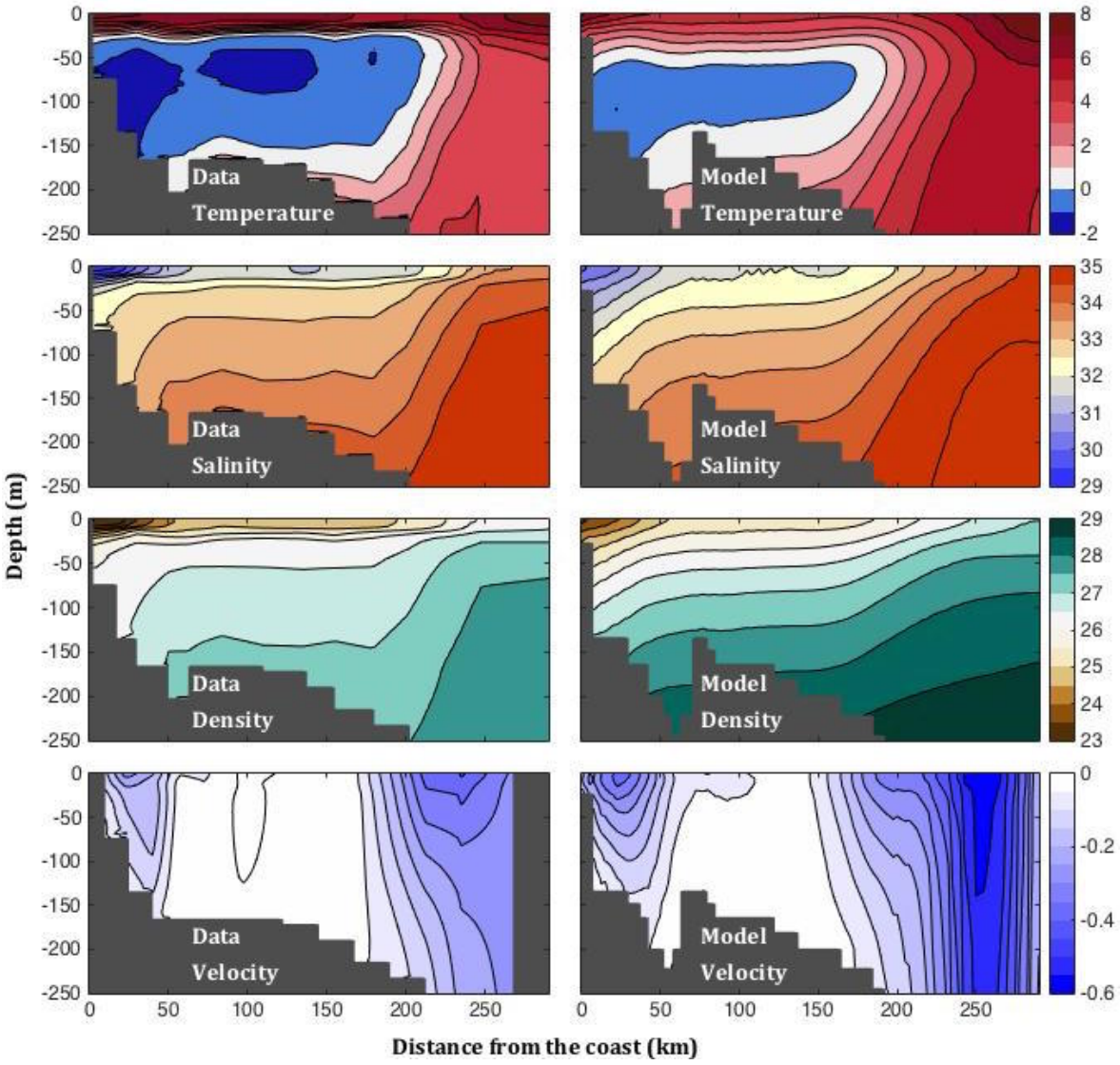

Figure 6.11: Final temperature (1st row), salinity (2nd row), density (3rd row) and velocity (4th row) climatology (1995-2010) sections in the observations (left) and the model (right).

6.3 Arctic freshwater export variability

The model analysis and the sections computed from the hydrography now provide us with the required tools to estimate the Arctic freshwater transport on the Labrador shelf. This transport is a proxy for Arctic freshwater export west of Greenland and will describe its decadal variability from observations for the first time. This section derives this proxy and covers the analysis of the resulting time series. First, the yearly summer sections of temperature and salinity allow identification of the core of Arctic water on the shelf (section 6.1). With the geostrophic velocities from section 6.2 it is possible to compute the volume transport of this water. Finally, combining the transport estimates with the salinity sections, the yearly freshwater fluxes can be obtained for the full length of the observational time series.

Transports are calculated following the method described in section 3.4. The results are shown in figure 6.12. Yearly summer values of freshwater transport are shown by the black crosses, joined by the pointed blue line. The long-term mean transport is displayed by the horizontal dashed line. A running average filter (details below) is applied (black line) to highlight decadal changes. Periods with freshwater transport higher than the mean are indicated by the blue shaded areas. Similarly, years with lower than average transport are shown as red shaded areas. Freshwater transports are given in mSv, where 1 Sv = 10^6 m^3/s.

The observations provide a previously unseen annual time series of freshwater transport of Arctic water on the Labrador Shelf, from 1950 to present. The low-pass filtered view of the data reveals the low frequency variability, with high freshwater transport during the 1950s, 1970s and 1980s, low transport in the 2000s, and a period of rapidly decreasing freshwater transport through the 1990s. The filter's running average has a 7-year period, which approximates to the length of the atmospheric regimes that partly control Arctic halocline water export (*Proshutinsky et al.*, 2015). The average freshwater transport for the whole series is 97 mSv, which is very close to the 93 mSv at Davis Strait obtained by *Curry et al.* (2014) for 2004 to 2010.

Encouragingly, the year to year changes observed at the short time series in

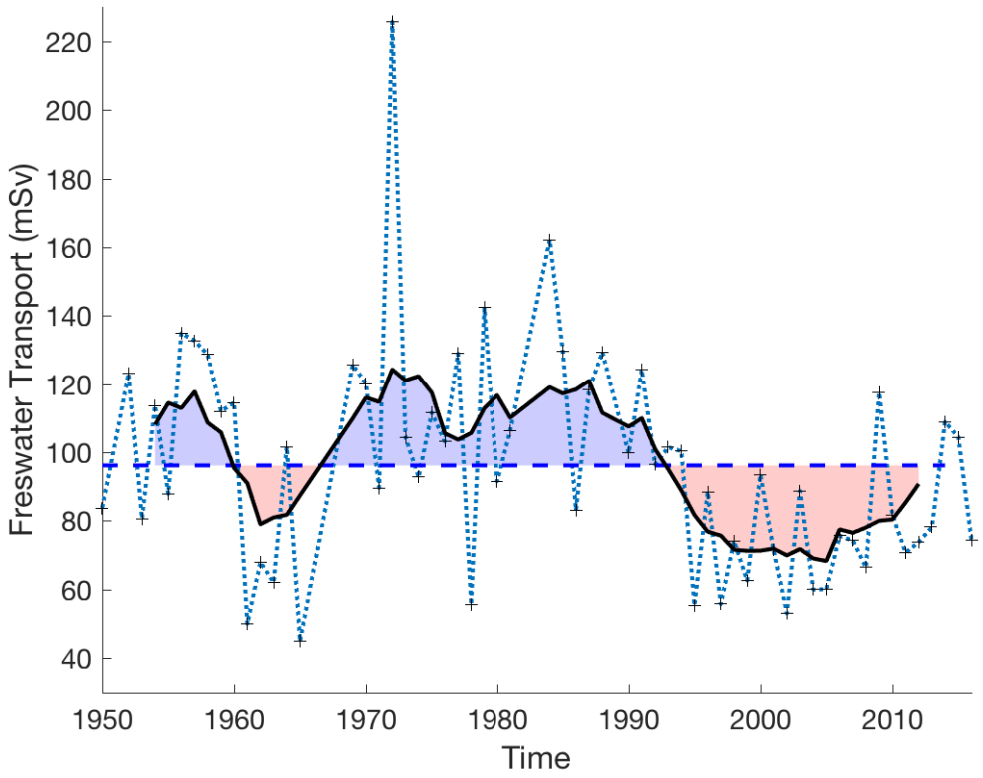

Figure 6.12: Time series of the proxy for Arctic freshwater export west of Greenland. Freshwater transport (FWt) is obtained for those years with available summer sections and are displayed by the black crosses and the dotted line. A 7-year filter (black line) emphasises the multiyear to multidecadal variability. The average transport of the time series (dashed line) limits the periods with a transport that is higher (blue shading) or lower (red shading) than average.

Davis Strait are also apparent in the time series, including lower transport in 2008 and 2010, and higher transport in 2009. There was very high freshwater transport on the Labrador Shelf in 1972 (226 mSv), and in that year an unprecedented magnitude of very cold intermediate water was observed (*Templeman*, 1975), later interpreted as the Great Salinity Anomaly reaching the region (*Dickson et al.*, 1988).

The most notable feature of the time series is the clear multi-decadal signal, which shows distinctive and extended periods of enhanced and decreased Arctic freshwater transport on the Labrador Shelf. The time series shows a high interannual variability; some years display a transport that is double that of previous or following years. This hinders the analysis of year to year changes. However, single data points are generally coherent with the periods in which they are found.

They mostly remain above/below average in their respective enhanced/decreased transport periods. For instance, data from 1995 to present display several values that double or halve consecutively, yet most of them are below average. The opposite case is found in the 1970s to 1994 period, with a majority of years showing transports above the average. This indicates that it is the mutidecadal signal which provides with the clearest signal of Arctic freshwater export west of Greenland and through Davis Strait, yet remaining consistent with inter-annual variability. The distinctive and extended periods of enhanced and decreased Arctic freshwater transport on the Labrador Shelf serve as the proxy for the Arctic export variability. This proxy is used in section 6.4 to evaluate changes in the freshwater budgets of the Arctic and the North Atlantic.

6.3.1 Sensitivity of the infilling of sections with the climatology

Part of the processing of the data into regular sections required the infilling of the outer boundaries with data from the climatology sections. This allowed a regular sectional area for all years, regardless of their completeness degree. Therefore, transport calculations could be based on equal areas. Earlier, it was described that the variability of the sections remained mostly in the mid-shelf and the position of the CIL, and that the outer boundaries to the sides and the bottom of the section presented little variability. This indicates that the infilling of yearly sections with the climatology would not have a significant impact on the result. This subsection quantifies the sensitivity of the results to this part of the processing.

The time series of the proxy for Arctic freshwater export is shown again in figure 6.13 (in orange). The time series is accompanied by the results using the same method on the same dataset, but this time sections have not been filled with the climatology (in blue). The first thing to note is the similarity between both time series. They show the same shape and variability, and the 7-year low pass filter (continuous lines) also agree. The correlation between the two time series is considerably high ($r = 0.94$), indicating that the results are not significantly sensitive to the infilling of sections.

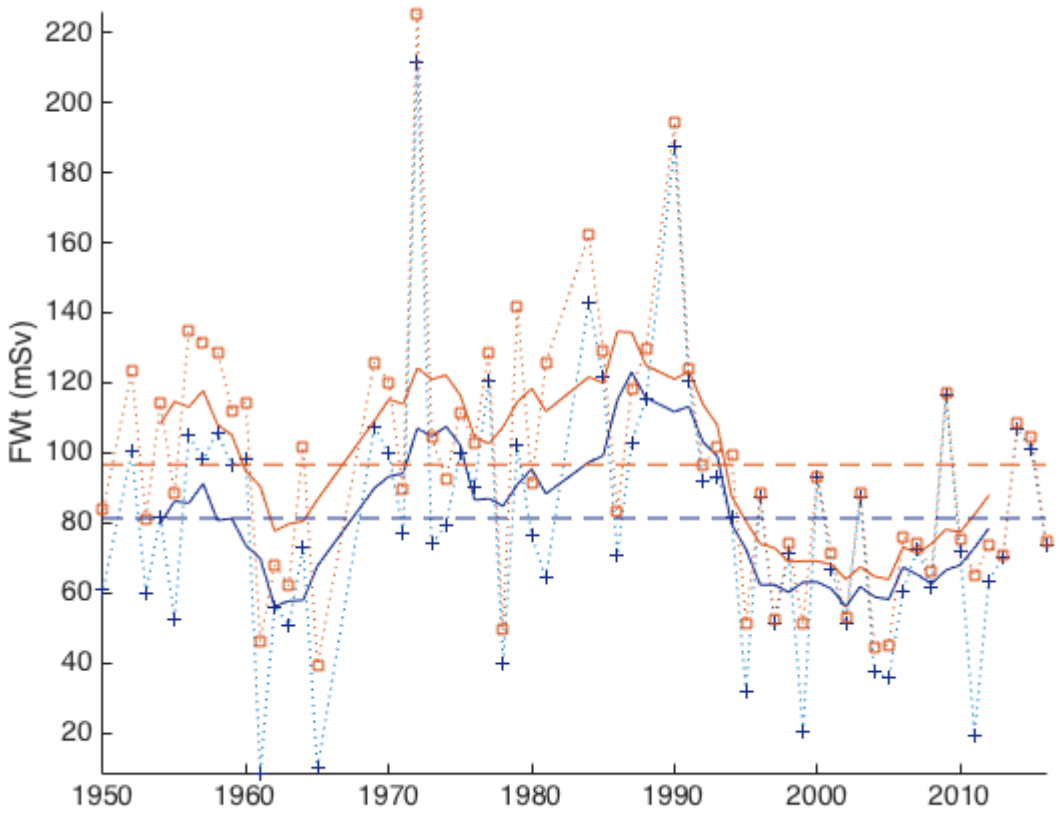

Figure 6.13: Time series of the proxy with the regular method (blue) compared to the same method without infilling of sections (orange). Freshwater transport (FWt) is shown by the dotted line, the 7-year filter is shown by the thick lines and the average transport is displayed by the dashed lines.

The difference between both approaches is noted in the mean. The average transports of both series disagree by 15.3 mSv, with the filled sections showing a larger average equally spread through the time series. That is 15% of the mean transport. This quantity can be considered part of the uncertainty of the mean. This uncertainty is further studied in the following section, where the sensitivity of the method is also investigated.

The filling of the outside boundaries adds a base transport to sections that are incomplete. This is especially seen in the earlier years, before 1965, which present the same trends but showing higher values. This tendency is also observed in years where the transport is unusually low. Incomplete sections with infilling now display transports that are more coherent with the mean (they show deviations from the mean that are of size comparable to other years). Although the data in the last

two decades show more completeness and hence a smaller effect of infilling, some of those years also show increases in the transport that do not alter the trend, they only reduce the amplitude of the inter-annual variability.

In conclusion, the filling of sections allows the computation of transports over equally sized sections (equal cross-sectional area) without compromising the result. This also allows the adjustment of unusually low transports to levels coherent with the standard deviation (35.9 mSv). The caveat is the added uncertainty over the mean transport (15%). However, the agreement between the mean transport of the proxy with that of the Arctic export in the literature (e.g. *Curry et al.*, 2014) indicates that the skill of the proxy to represent the export is accurate. The trends in the time series and the periods of high and low export are nearly identical regardless of the filling of sections (correlation of $r = 0.94$). The study of this decadal variability is the aim of this thesis and therefore this agreement is key for this work.

6.3.2 Sensitivity of the partitioning method

The resulting time series of Arctic freshwater export, as found on the Labrador shelf, is subject to the ability of the water partitioning method to capture the signal of Arctic water. The model analysis and its comparison with the observations has shown before that it is capable to capture this signal. However, the accuracy and reliability of the methodology is not yet fully understood. This section evaluates the sensitivity of the water partitioning method. To do so, different variables (freshwater transport, area, salinity, etc.) are computed for slightly different methods. This sheds light on the estimate of the error and the accuracy of the proxy. Additionally, the freshwater transports are computed for the different temperature limits for the CIL. This serves to estimate the error induced by the subjective selection of the temperature boundary.

The sensitivity is tested for four different approaches used to model the Arctic water on the shelf. All of them are based on the subsurface core of Arctic water; the CIL. However, the boundaries vary between the different methods and they yield different cross sectional areas, as shown in figure 6.14. This will show how

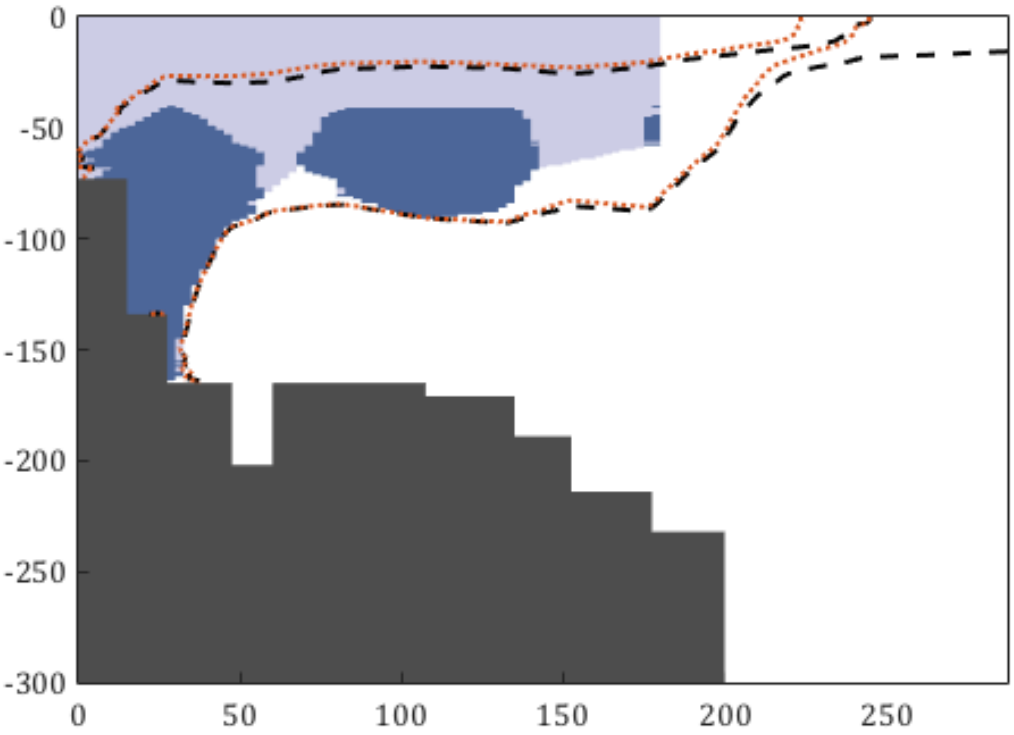

Figure 6.14: Average cross-sectional shapes of the Arctic watermass given by 4 different partitioning methods. The Arctic water is defined by the standard CIL -1°C isotherm (dark blue shading), also by including the water above it (dark and light blue shading), by salinity limits (orange contours) and finally, the standard method, given by the density range (black contours).

dependent the transport is to the accuracy of the water partitioning. The first approach considers the original definition of the CIL as a single isotherm. In this case it is the -1°C isotherm as justified in section 6.1. The resulting average (1995-2014 climatology) shape is given by the dark blue shaded area. This definition, however, precludes the inclusion of the warmed surface layer. The second approach is the CIL extended to the surface, by including the water column above the bottom limit of the -1°C isotherm and interpolating between intermediate gaps. This is shown in the figure by the light blue shading. Finally, the last two methods define the boundaries of the Arctic water by considering further watermass properties. One definition considers the minimum and maximum salinities within the CIL as the limits (orange dotted line). The other is the standard method, which defines the Arctic water by the density range given by the CIL (black dashed line). The latter was derived from the new knowledge provided by the model study and hence stands as the most consistent approach. It is the sensitivity of this standard method that is compared with the other ones.

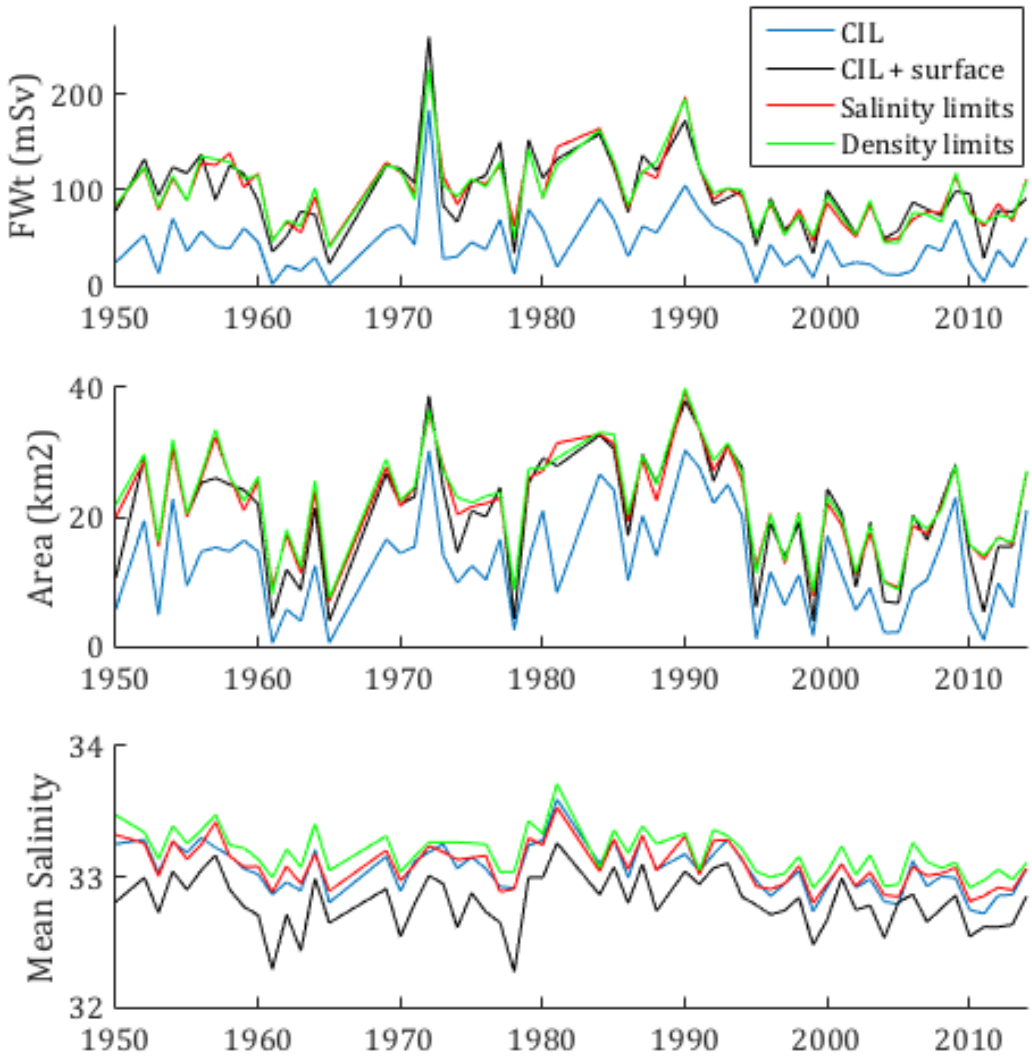

Figure 6.15: Time series of the freshwater transport (top panel), the cross-sectional area (middle panel) and the mean salinity of the Arctic water (lower panel) as defined by the 4 different approaches. These are the CIL as the -1°C isotherm (blue line), the same but including the water column above (black line), the one given by the salinity range (red) and the standard density limits method (green).

The different partitioning methods yield a relatively variable area. This is fundamental to understand the precision required to define the Arctic water. Different shapes are expected to result in differing transports. If the results are similar between the different approaches, this suggests that the methodology is not strongly sensitive to the partitioning precision. This is evaluated by the following set of figures.

First the freshwater transport, the resulting Arctic cross-sectional area and its mean salinity for the 4 approaches are summarised in figure 6.15. This displays the differences in the net magnitude, but most importantly it serves to indicate

	Mean (mSv)	**St. deviation (mSv)**
CIL	42	30
CIL + surface	95	41
S limits	96	36
ρ limits	97	36
3 main methods	96	37

Table 6.1: Summary of the means and standard deviations of the freshwater transport by the different partitioning methods. The CIL extended to the surface, the salinity-limited method and the density-limited method are averaged as the "3 main methods" row.

if the long-term trends are consistent throughout. All three time series show a close agreement in the variability. Years with high or low values are consistent in all methods, and so is the magnitude range of the interannual variability (mean amplitude of 37 mSv shown by the standard deviation of all methods but the simple CIL). This is displayed by lines being fairly parallel. The variability shown by the freshwater transport is summarised in table 6.1. The means by the main methods (those that account for surface waters; that is all but the CIL as a single isotherm) are virtually equal, with a similar amplitude of variability (shown by the standard deviation). The bigger differences are shown by the simple CIL method (the -1°C isotherm). This is especially true when comparing net magnitudes, as it displays a smaller transport (mean of 42 mSv, in comparison with the mean of 96 mSv by the other methods). All the other methods show (surprisingly) similar time series of freshwater transport and cross-sectional area (time-series almost overlie and present comparable means and standard deviations). In contrast, the mean salinity is almost equal ($\sim$33.2) for all approaches except for the one that includes the surface layer directly. As seen in figure 6.14, this method is likely to include the most inshore waters, which are sourced from Hudson Bay. The low salinity of that water decreases the mean, as it is reflected in the time series. Although this method would not be considered valid because it includes the Hudson water, it still provides with a freshwater transport coherent with the standard method (but with a higher variability, as shown by its standard deviation; 41 mSv). This suggests that the influence of mixing or failing to separate the Hudson component does not have a significant effect in the trends shown by the proxy.

The discrepancy shown by a weaker freshwater transport in the simple isotherm method is expected. This approach yields a significantly smaller area and constrains the transport to a limited space. It is also a subsurface structure, so it is below the velocity maxima. Nevertheless, an interesting feature of this approach is that this variability of the CIL area seems to dominate the results by the other methods. Not only do the variability of the other areas follow that of the main CIL, but they also seems to match in the trends and the variability of the freshwater transports.

Table 6.2 shows the correlation of the freshwater transport (by the standard method) with the other variables shown in figure 6.15; the cross-sectional area of Arctic water on the shelf and its mean salinity. The apparent good agreement between the transport and the area is confirmed with a correlation of $r = 0.89$. On the other hand, the correlation between the transport and the mean salinity is much smaller, with $r = 0.52$. Again, this indicates that in the magnitude of the transport, the cross-sectional area plays a much more important role than other properties (such as the salinity and presumably the speed of the shelf currents). This points out the suitability (or representativeness) of the Cold Intermediate Layer to describe the variability of Arctic freshwater export. This will be further discussed later in section 7.4.2.

Freshwater transport is the main variable that we are interested in. The sensitivity of this calculation is essential to understand the certainty of the results. Figure 6.16 displays the freshwater time series for all methods separately. This allows us to look at the interannual and decadal variability in further detail. All methods show the same yearly variability and the trends are coherent throughout the series. The uncertainty of the density-limit method (the standard method of this study) is of 6 mSv. This is given by the standard deviation of the yearly

	Correlation (r)
Freshwater transport & Area	0.89
Freshwater transport & Mean salinity	0.52

Table 6.2: Correlation factors between the Arctic freshwater transport shown by the proxy and the cross-sectional area of the CIL, as well as the correlation between the freshwater transport and the mean salinity of the CIL.

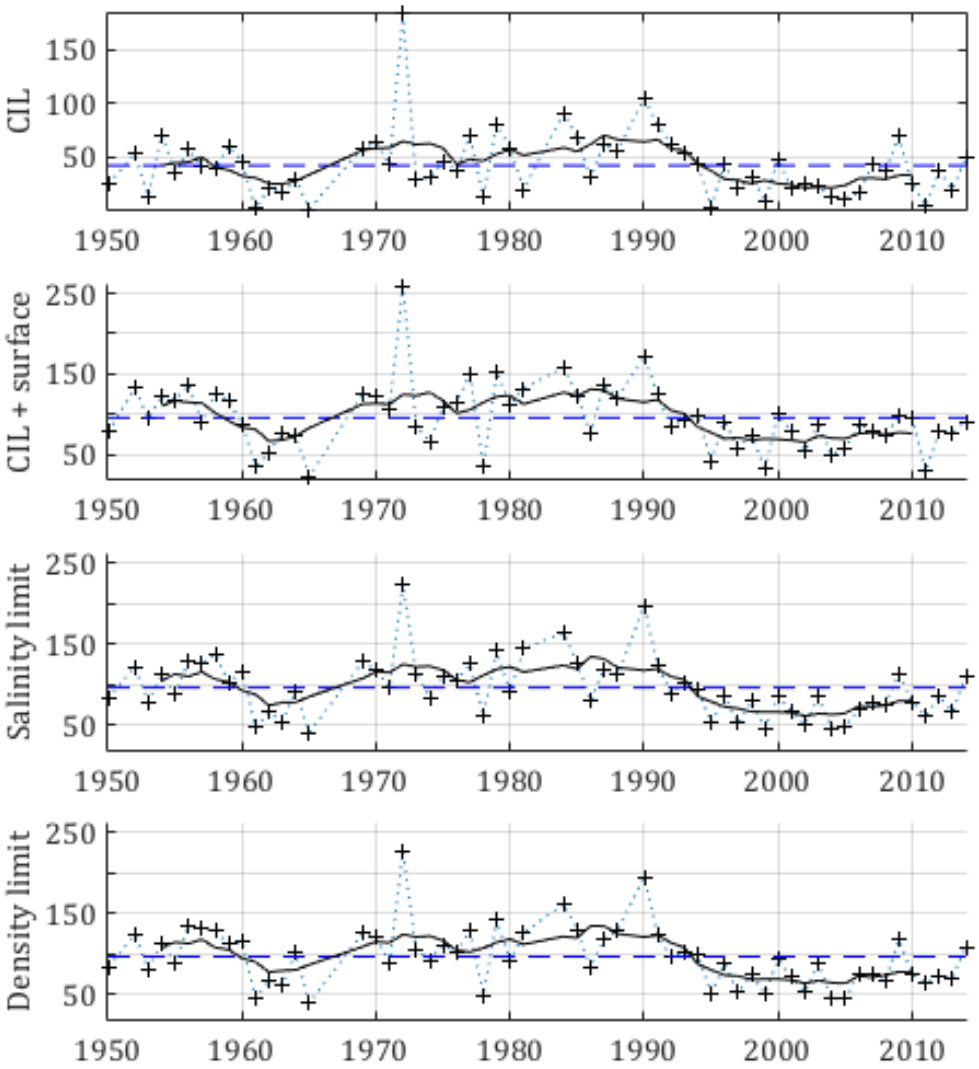

Figure 6.16: Time series of the freshwater transport for the 4 different partitioning methods; the -1°C isotherm (first panel), that with the surface water (second panel), salinity limits (third panel) and the standard method (forth panel). They include the yearly data values (crosses and dotted line) and the 7-year running average (black line).

differences between this standard method and the mean of all methods except of the simple CIL. This is reflected by the low pass filter (black line), which shows the long-term means. The different periods of transports higher or lower than the average (such as the ones displayed by the blue and red shadings in figure 6.12) are equally represented in all methods. This supports the consistency of the results presented earlier in section 6.3. As was also seen in figure 6.15 and table 6.1, this figure shows that the magnitude of the freshwater transport is the same for all methods except for simple CIL isotherm, which displays a smaller area and transport.

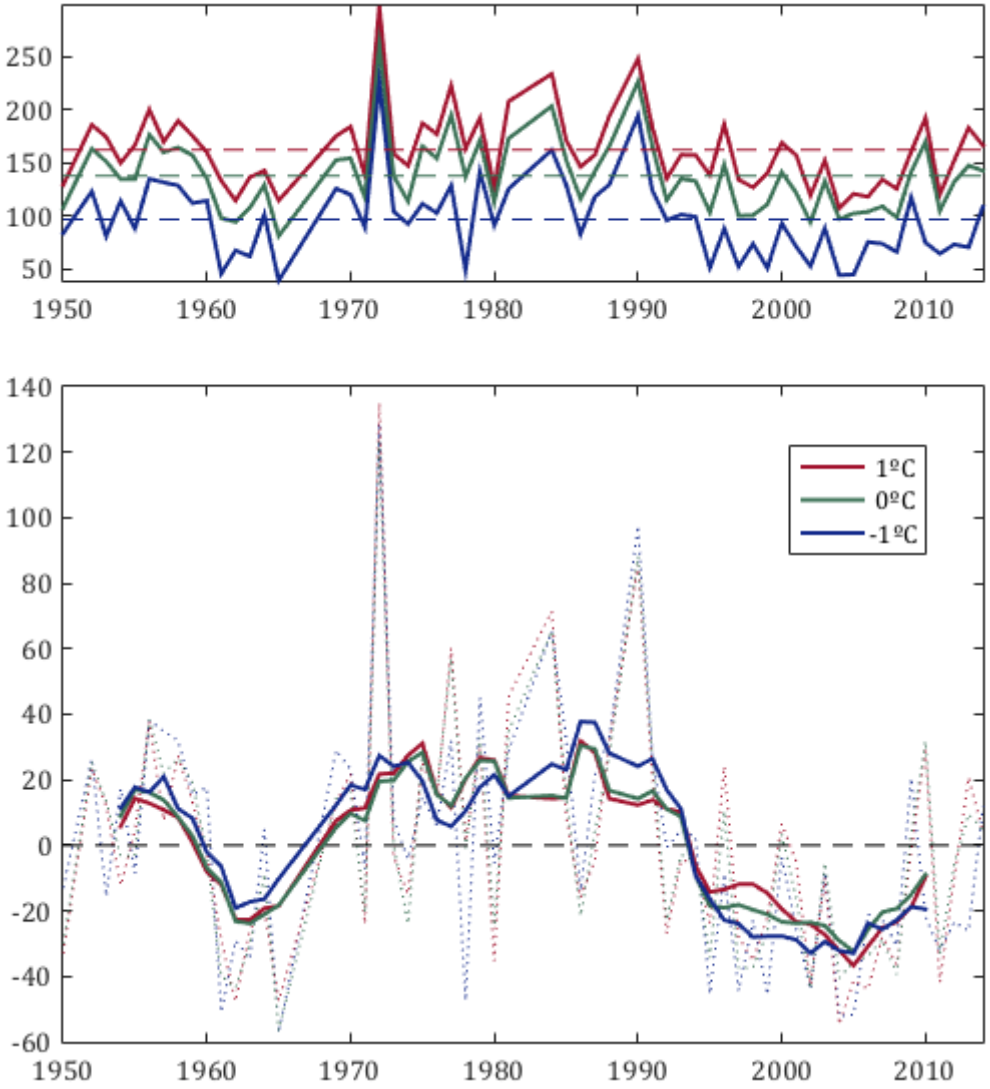

Figure 6.17: Time series of freshwater transport by the standard (density limits) partitioning method for different CIL limiting isotherms (-1, 0 and +1° C). Transports shown as their net magnitude (top panel) and also as the anomaly from their mean (lower panel). The latter includes the 7-year running average.

Overall, the variability and trends of the freshwater transport, the cross-sectional area and the mean salinity of the Arctic water remain consistent for all the different approaches. This is the most important outcome of the sensitivity analysis, for it is the variability or the rate of change that is of most interest in the study of the Arctic freshwater export. Additionally the relatively less important magnitude also appears surprisingly coherent for most methods. The good agreement between the different ways to delimit the Arctic water on the shelf suggests that they are not strongly sensitive to small details of the partitioning. This supports the confidence of the results shown by the proxy.

This has shown that the results are not sensitive to the chosen partitioning method. However, they all rely in the arbitrary selection of the CIL temperature limit. Section 6.1 showed that the area and salinity were not greatly affected by the limiting isotherm (order ±1°C). Figure 6.17 completes this study by comparing the freshwater transport for varying temperature limits. The upper panel shows the magnitude of the transport for each isotherm. As discussed before, a higher temperature allows for a larger core of Arctic water and a resulting higher transport (for fairly similar salinities). The parallel lines show again that the variability remains constant regardless of the chosen temperature. This is further indicated in table 6.3. Regardless of the mean, the range of the variability shown by the standard deviation remains almost equal (∼35 mSv). This is better seen in the lower panel of figure 6.17, where the transports are normalised by the mean (they are shown as anomalies). The yearly values (pointed lines) closely overlap. The long-term trends, depicted by the thick lines, also show that the freshwater transport variability and trends display the same behaviour independent of the temperature limit. This is supported by the uncertainty of the standard method. Again, this is calculated as the standard deviation of the difference between the -1°C method and the mean of all methods. This estimated uncertainty or standard deviation totals to 6 mSV. The enhanced/decreased transport periods (shown as the part of the curves that are above or below 0) are observed in all cases, at the same times and with a similar amplitude as shown by table 6.3. This indicates that, to a reasonable extent, the freshwater transport variability shown by the proxy is neither sensitive to the chosen partitioning method nor to the range of CIL temperature limits.

Finally, there is the question of the representativeness of the summer freshwater transports to the yearly estimates. It is only summer data that can provide decadal insight in the export, not only because data cluster in July and August, but also it is during summer when the CIL is fully formed and isolated from the surface and waters off the shelf. It is only with model data that we can understand how the summer observations fit in the yearly mean. Figure 5.23 showed the model freshwater transport for the Arctic export through Davis strait and the transport on the mid-shelf (the Arctic water in the proxy). The seasonality shows that the transport on the mid-shelf remains fairly constant through most of the year, including

	Mean (mSv)	**St. deviation (mSv)**
+1°C CIL	162	35
0°C CIL	138	34
-1°C CIL	97	36

Table 6.3: Summary of the means and standard deviations of the freshwater transport by the standard method (density-limit) but with different isotherms to define the CIL: -1, 0 and +1°C.

summer. It only increases significantly in autumn, peaking in December-January. This increases the yearly mean, which is slightly higher than the summer one (by 15 mSv, similar to the uncertainty of the mean in the observations). If considering the magnitude of the transport, this difference needs to be taken into account. However, for the study of inter-annual to decadal variability, the trend is rightfully represented by July and August data. From all seasons, summer transport in the mid-shelf shows the closest agreement with the Arctic counterpart (considering the 2.5 months lag, at a correlation of $r = 0.73$) and also with the Arctic export yearly means (correlation of $r = 0.75$).

6.4 The link between the Arctic freshwater export and the freshwater budgets of the Arctic and the North Atlantic

This study has defined a new proxy for a major component of Arctic freshwater export, which has the potential to provide insight into the processes linking the Arctic freshwater budget and North Atlantic salinity. This section discusses in detail how the Arctic export variability relates to significant salinity changes in the North Atlantic and to Arctic freshwater content. In order to do so, the different periods of enhanced and decreased Arctic freshwater export, shown in figure 6.12, are compared to the variability of the Arctic and North Atlantic freshwater budgets. Additionally, this transport is presented again in figure 6.18 as the anomaly from the mean. It also includes the accumulated transport anomaly (red line). This serves to evaluate the expected effect in the North Atlantic freshwater budget

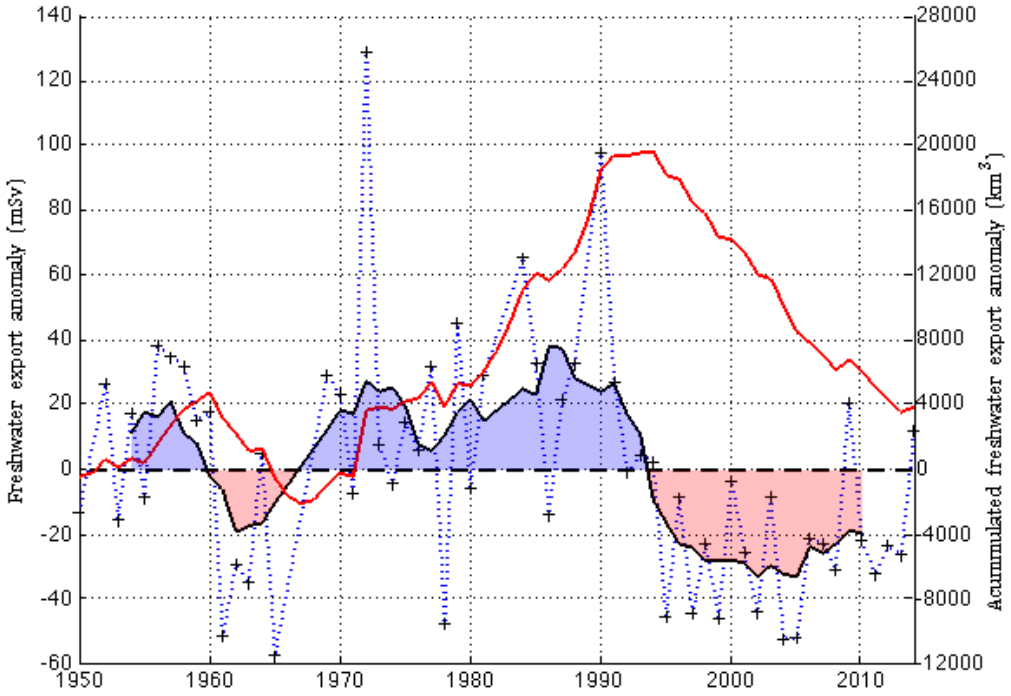

Figure 6.18: Time series of the proxy for Arctic freshwater export west of Greenland. It includes the freshwater volume resulting from the accumulated freshwater export anomalies (red line). Peaks in the curve indicates a long-term accumulation of transports higher than average and are expected to decrease/increase the freshwater budget at the source/sink of the system.

as the result of continuing periods of high or low transport. The accumulated anomaly is calculated as the sum of the export anomalies from the beginning of the time series up to each yearly time step. Years with no transport information are interpolated linearly to provide with a yearly time series. Those values are converted to accumulated transport by considering the transport values constant through the each year and are presented in km^3.

The time series shows two main periods of reduced freshwater transport; in the early 1960s and from the 1990s to present. Two periods of enhanced transport are also seen at the start of the observations (late 1950s) and throughout the 1970s and 1980s. It is expected that prolonged periods of high or low freshwater transport would have a cumulative impact on the salinity of the Subpolar North Atlantic and even in the North Atlantic as a whole (higher export leading to higher subpolar freshwater storage and lower salinity). This cumulative effect is further indicated by the accumulated freshwater export anomaly (red line in figure 6.18). Considering a fairly constant rate of precipitation-evaporation and other freshwater fluxes (so

that the accumulation of freshwater is only dependent on the Arctic export), peaks in this curve suggest favourable conditions for a fresher North Atlantic. Troughs show the opposite conditions and hence a higher average salinity. The slope of this curve is also an indication of the rate or speed of the export; significant pulses like the one in 1972 or 1990 are seen as almost vertical slopes.

The role of the Arctic freshwater export west of Greenland being a dominant factor of the freshwater budgets of its source (the Arctic) and sink (North Atlantic) is supported by existing evidence and it is shown if figure 6.19. The different periods identified in the proxy time series can be related to changes in both budgets. The northern North Atlantic budget experienced a freshwater increase of 15000 km^3 from late 60s to 1990, with most accumulated in just a 5-year period in the early 70s (*Curry and Mauritzen*, 2005). That increase coincided with the clear enhanced Arctic freshwater export shown by the new proxy and also with the largest export record in 1972. Additionally long term salinity changes of the subpolar North Atlantic can be related to the Arctic export variability throughout our whole time series. The same authors observed an increase in the surface salinity from 1955 to 1965, amounting to a freshwater loss of 5000 km3. This coincides with a constant decrease rate in the proxy, the magnitude of which could fully explain the storage minimum observed in 1965. Similarly, another rapid decrease in the Arctic freshwater export proxy in the early 1990s coincides with the increase in salinity of subpolar waters described by *Peterson et al.* (2006). Furthermore, using different methodologies, the accumulated export anomaly shown in figure 6.18 shows the same variability, trend and magnitude to the overall North Atlantic freshwater anomaly estimated by the same authors, as shown in figure 6.19. This is especially true in the North Atlantic combined budget 1965 minimum and the 1995 maximum. The proxy's accumulated export curve (red line) up to 1995 fully accounts for the observed 20000 km^3 of freshwater excess in the North Atlantic. The new proxy serves to extend the North Atlantic freshwater budget beyond 2005. Overall, the relationship between subpolar (or even North Atlantic) salinity and the new proxy for Arctic export variability strongly suggests that the Arctic export west of Greenland has an important role in generating North Atlantic salinity anomalies. Most importantly, the magnitude of these have the potential to affect the buoyancy

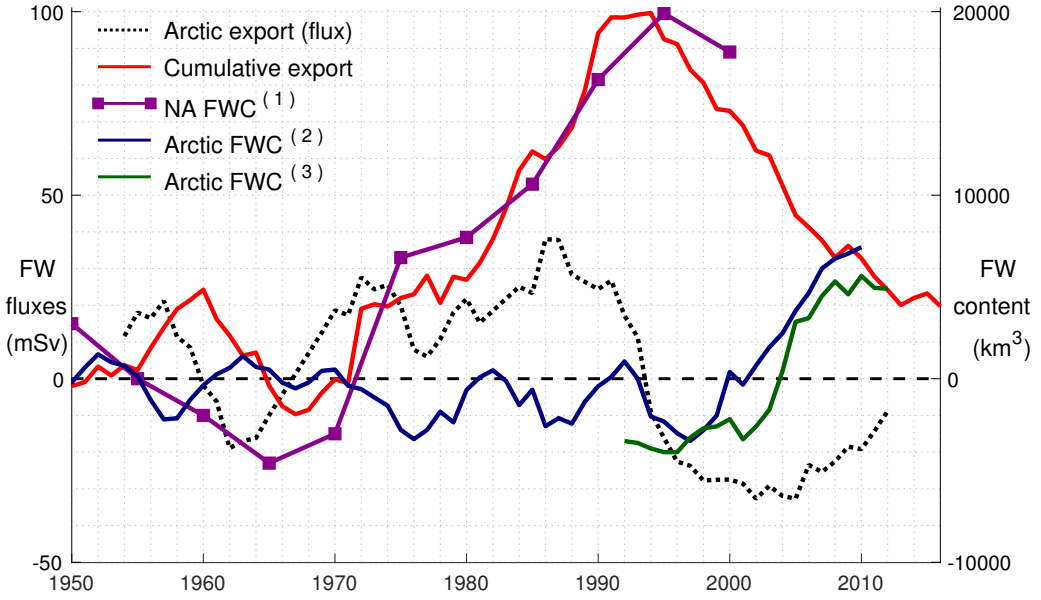

Figure 6.19: Time series of Arctic freshwater export anomaly 7-year running average (black dotted line, left axis) and its cumulative transport (red line, right axis). Estimates of the (1) North Atlantic freshwater budget anomaly (km^3) from Peterson et al. (2006), 5-year means, are shown by the purple line. Estimates of the (2) Arctic freshwater budget anomaly (km^3) are also included, from Polyakov et al. (2013) as a 7-year running average (thick blue line) and (3) from Rabe et al. (2014) as annual means (green line). Anomalies are shown as differences from the mean. Peterson's North Atlantic time series is referenced to the 1955 pentad.

of the subpolar regions where deep-water formation takes place.

The complexity and paucity of observations of Arctic freshwater sources, sinks and storage means that the relationship between Arctic freshwater content and its export to the North Atlantic is still an open question (*Serreze et al.*, 2006). The new proxy allows for the first time to examine whether the estimated Arctic freshwater storage co-varies with the observed Arctic export west of Greenland on decadal timescales. If it was possible to detect a relationship between decadal changes in Arctic freshwater storage and freshwater export through Davis Strait this would confirm the importance to the Arctic of mechanisms influencing changes in freshwater export. Additionally, this would also inform us about the influence of the Arctic on the subpolar North Atlantic and the importance of the Labrador current in the redistribution of freshwater between both basins. This section completes the discussion by linking the export variability shown by the proxy with observed

changes in the Arctic freshwater storage.

If the freshwater transport by the upper Labrador current is a key component of the Arctic freshwater budget, the Arctic freshwater storage would be expected to reduce when the export is high. Similarly, one may hypothesise the opposite effect when the export is low. The few available Arctic observations support this link. *Peterson et al.* (2006) show that the Arctic Ocean accumulated freshwater in the early 1960s, a period of low transports in the proxy. *Polyakov et al.* (2008) described decreasing freshwater storage in the upper Arctic Ocean in the 1970s, coinciding with the sharpest pulse of freshwater export seen in the proxy. The key results by these authors are also presented in figure 6.19 (blue line). Similarly, the rapid decrease in Arctic export in the 1990s observed in the new proxy corresponds with the well-described and unprecedented increase in Arctic freshwater storage at that time (e.g. *Rabe et al.*, 2011). The authors continued that study and estimated an average Arctic freshwater loss rate of 600 $\pm$ 300 km^3/year for the 1992 to 2012 period (*Rabe et al.*, 2014). Their time series is also shown in the figure by the green line. This is in close agreement with the export rate estimated for the same period in this study's proxy, which accounts for a 750 km^3/year rate. This apparent relationship between freshwater export west of Greenland and Arctic freshwater storage points to the importance to the Arctic freshwater budget of the mechanisms controlling this export route.

The hypothesis presented here is also tested with model studies in the literature. *Köberle and Gerdes* (2007) present a multidecadal time series of the Arctic freshwater content. They show a maximum in the freshwater stored in the Arctic at the end of the 1960s, followed by a decreasing trend and a minimum in the late 1990s (a reduction of approximately 16000 km^3). This matches with an opposite minimum and maximum at the same times, as shown by the accumulated transport of the proxy, and accumulates a comparable (if not larger) magnitude (22000 km^3). *Köberle and Gerdes* (2007) show a small reversal of the Arctic freshwater release and a consequent smaller peak in the early 1980s. This temporary reversal to an enhanced storage is also shown by *Lique et al.* (2009) and *Häkkinen and Proshutinsky* (2004) in 1981 and 1988. The accumulated transport shown by the proxy here does not show a reversal in the trend those years, but it does show a contemporary

hiatus where the export rate flattens.

One of the most significant findings here is the observed magnitude of the Arctic freshwater export shown by the upper Labrador current. Its variability alone can fully explain the observed changes in the Arctic and the subpolar North Atlantic freshwater budgets. For instance, the net effect of the increased export from 1965 to 1995 shown by the proxy totals to about 22000 km^3. This could fully account for the changes in the Arctic (decrease of 16000 km^3; *Köberle and Gerdes*, 2007), in the subpolar North Atlantic (increase of 15000 km^3; *Curry and Mauritzen*, 2005) and almost the full North Atlantic (increase of 25000 km^3; *Peterson et al.*, 2006). This is also true for the 1995 to 2012 period. The decrease in the accumulated transport shown by the proxy (approximately 16000 km^3) is enough to account for the changes seen in the Arctic (increase of 10000 km^3; *Rabe et al.*, 2014). This means that the export of freshwater west of Greenland can fully describe the impacts observed in both basins. This is a new view that challenges the previous concept of an export dominated by the transport through Fram strait, or by an alternating transport between both sides of Greenland (*Lique et al.*, 2009). This interesting point will be discussed in detail in the following chapter.

The strong link between the Arctic freshwater export west of Greenland and the freshwater budgets of the Arctic and the North Atlantic has been supported by this study. The importance of this export branch has been generally underestimated in spite of its eastern counterpart, as it was introduced in section 2.2.2. This is further discussed later in section 7.3.3. The study presented here has found evidence that the export west of Greenland, shown as the freshwater transport variability by the upper Labrador current, could account entirely for the subpolar North Atlantic freshwater content changes. It has also shown that it could be large enough to reach the freshening threshold required to significantly affect the North Atlantic circulation and its heat transport (*Curry and Mauritzen*, 2005). The dominant role of the export west of Greenland is only introduced; further observations are required to fully understand this complex system and how it fits with the eastern branch of the export. The evidence shown here, however, remains coherent throughout the time series and clearly shows that the role of the Arctic freshwater export west of Greenland holds a significant role in the system. To predict future North

Atlantic freshening events and the consequences in European climate, it is essential to understand the mechanisms that control the Arctic freshwater export. This will be further discussed in the following chapter.

6.5 Summary

This chapter combined the time series of summer hydrographic sections at the Seal Island section (chapter 4) with the model study (chapter 5) to provide with the first multidecadal analysis of the Arctic freshwater export west of Greenland, from observations. Here I calculated velocity sections from geostrophy, I combined them with the hydrographic sections to obtain the proxy for the Arctic freshwater export and I finally discussed the link between the export and the Arctic and North Atlantic freshwater budgets. The main findings are:

- The Cold Intermediate Layer (CIL) allows adaptation of the watermass partitioning method to the observations. This is not sensitive to the chosen method or the chosen CIL temperature limit.
- Consistent sections of geostrophic velocities can be calculated in the observations by adjusting them with the model average bottom velocity.
- The observed freshwater transport provides a new proxy for over 60 years of freshwater export west of Greenland and through Davis Strait.
- High freshwater export is found during the 1950s, 1970s and 1980s, low export in the early 1960s and 2000s, and a period of rapidly decreasing freshwater transport through the 1990s. The average freshwater transport for the whole series is 97 mSv, consistent with other regional estimates.
- The accumulated effect of the varying freshwater export is linked with the Arctic and North Atlantic freshwater budgets throughout the time series.
- The inverse relationship between subpolar salinity and the new proxy for Arctic export variability suggests that export west of Greenland has a larger role in generating North Atlantic salinity anomalies than previously recognised.
- Likewise the inverse relationship between freshwater export west of Greenland and Arctic freshwater storage points to the importance of mechanisms controlling this export route.

Chapter 7

Discussion

This chapter covers an extensive discussion of the research carried out in this thesis, the main results and conclusions and, especially, it overviews the general implications of this work and future research directions. I first narrate the story line of this thesis; a summary of the work and how the results link my different research directions. I continue listing the main conclusions obtained after interpreting the results. Later, I extend these conclusions to discuss the general implications. I base this around three main topics: the potential role of coastal currents in subpolar freshwater systems, the importance of the Arctic freshwater export as a main control of the Arctic and North Atlantic freshwater budgets, and the relevance of the studied export route in the context of the total Arctic freshwater export. Finally, I include a section to discuss very recent indications of a reversal in the system; an apparent transition to a period of Arctic freshwater release. This also sets the background to explain the additional potential of the Seal Island dataset, as well as to suggest directions for future research.

7.1 Thesis summary

In a rapidly changing climate system, the freshwater budget of the North Atlantic has acquired special attention. This region holds areas of deep water formation that are sensitive to buoyancy fluxes, which can have drastic effects on climate.

The Arctic Ocean directly connects with these regions and has a large potential to generate significant freshwater fluxes. The motivation for the work here was to provide new knowledge about the link between the freshwater budgets of the Arctic and the North Atlantic oceans, through the variability of Arctic freshwater export. This thesis set out to do this, at a multi-decadal time scale and from observations, being a first of its kind. The work carried out and summarised here has successfully described this variability over the past 6 decades and has provided valuable information to better understand the system and to discuss important implications.

After describing the goals and tools, the first scientific chapter of this thesis (chapter 4) thoroughly studied the potential of the Seal Island hydrographic observations. These were taken under many different purposes, over an unusual long time period and with instrumentation that evolved and improved with time. Consequently, the original dataset proved a challenging process to unify the varied profiles into a set of valuable sections. From the original 3864 casts, only 630 were flagged as valid for this study. These allowed computation of a time series of temperature, salinity and density in summer sections at the Seal Island transect, from 1950 to 2014 and almost yearly, with very few years of missing data. The obtained time series provided the observational foundation for the analysis in this thesis.

The second research chapter, chapter 5, provided with a detailed description of the Labrador shelf circulation. The basic features had long been known, but some questions were still open. Two main questions were addressed here: the fate of the very fresh Hudson outflow once it reached the Labrador shelf, and the nature of the usually overlooked coastal jet. The results of this chapter showed that this jet, named the Labrador Coastal current, is a continuation of the Hudson outflow, which is deflected southwards as a buoyant coastal current due to the strong density gradient with the Labrador shelf waters. The circulation and dynamics studied in this chapter allowed identification of the signal of the Arctic freshwater export west of Greenland, on the Labrador shelf. This puts the Seal Island observations in the context of Arctic export.

Finally, the third and last research chapter (number 6) combines the results of

the two previous chapters to compute the first observational estimates of the Arctic freshwater export west of Greenland in a multi-decadal time scale. Two main results could be obtained combining both tools. First, the method to partition Arctic water in the model was adapted to the characteristics of the observations and the Arctic signal was isolated in the latter. Then, the geostrophic velocity was calculated for every hydrographic section and corrected with a barotropic component obtained from the model information. This allowed compution of a time series of Arctic freshwater transport, which served as a proxy for the export west of Greenland linking Arctic and North Atlantic freshwater budgets. The results indicate that this export plays a major role controlling the North Atlantic freshwater budget and also displays significant co-variability with the Arctic freshwater storage. The main conclusions are listed in the following section, which will lead to discussion of the implications of these results.

7.2 Conclusions

This section lists the main conclusions of this thesis. In order to do so, it links back to the objectives (section 2.3, in page 18) and assesses them one by one, in order.

First, about the circulation and waters on the Labrador shelf:

- The Arctic freshwater export west of Greenland circulates southwards as the Baffin Island current, through Davis strait, and fills the mid Labrador shelf as the upper component of the Labrador current.
- On the Labrador shelf, a two-current system dominates the circulation. The Labrador Coastal current lies inshore, as a continuation of the Hudson strait outflow, and the Labrador current circulates independently over the shelf break and slope.
- The coastal current restricts the Hudson water inshore and allows for the upper Labrador current to fill the mid-shelf with Arctic water coming from west of Greenland.

Second, about the Seal Island observations and their skill to capture the Arctic export signal:

- The set of hydrographic observations proves consistent enough to deliver yearly summer sections of temperature, salinity, density and geostrophic velocity at a multi-decadal scale (almost yearly from 1950 to 2014).
- The signal of Arctic water can be identified in these observations. This signal informs about yearly Arctic freshwater transports.
- The variability of the Arctic freshwater transport at the Seal Island is a proxy for the Arctic freshwater export west of Greenland.
- This export is dominated by multi-year to multi-decadal variability, displaying 2 periods of enhanced transport and 2 periods of decreased transport. The frequency of the interannual variability is rather high and noisy, but consistent with the multi-year trends.

Last, about the link between the freshwater budgets of the Arctic and the North Atlantic oceans, through the Arctic export fluxes:

- The variability of the North Atlantic freshwater budget can directly be explained by the accumulated changes in the Arctic freshwater export west of Greenland, since 1950 to present. Rapid increases of the export also explain the salinity anomalies of the North Atlantic.
- The variability of Arctic freshwater content highly anti-correlates with changes in the export west of Greenland, indicating that oceanic advection is a major mechanism regulating the Arctic freshwater budget.
- The magnitude of the export west of Greenland and the coherence with the changes in related budgets point to the significance of this branch to represent the total Arctic freshwater export.

The final objective was to discuss ongoing changes and their implications. This will be done after discussing the main implications of this thesis.

7.3 General Implications

This section covers the main discussion. It provides an interpretation of the main results and conclusions in order to elaborate the implications. This discussion is split into three different topics. The first one reviews the role of the Labrador Coastal current in particular, and of coastal currents in general, in the distribution of freshwater in subpolar regions. The following subsection examines the link between the Arctic and North Atlantic budgets through the export west of Greenland and emphasises the implications of this. Finally, the third and last subsection discusses the importance of the export route west of Greenland in the context of the total Arctic export.

7.3.1 The potential role of subpolar coastal currents

This thesis has provided new knowledge of the Labrador shelf circulation. It emphasised the different nature and dynamics of the generally overlooked coastal jet and established that it is a different current, independent from the main Labrador current. As such it has been given a different name accordingly; the Labrador Coastal current. This current has proved essential in the study of the Arctic freshwater export. It contains the Hudson water inshore and prevents it from fully mixing with the Labrador shelf waters. This permits pinpointing of Arctic water on the Labrador shelf in observations, which displays a fair degree of preservation (little mixing). But beyond the Labrador shelf, what is the role of the Labrador Coastal current in the North Atlantic circulation and its freshwater budget? It would appear that this current has a major role transporting the relatively fresh waters of Hudson Bay, which is a significant watershed of the North American river runoff (*Déry et al.*, 2005). The fate of the Labrador Coastal current after it reaches the Grand Banks of Newfoundland is still unclear. It seems it flows into the Gulf of Saint Lawrence through its northern gate, the Strait of Belle Isle (*Wu et al.*, 2012), and eventually becomes part of the complex circulation system of Nova Scotia and the Atlantic Bight (*Mertz et al.*, 1993).

Coastal currents, generated by plumes of freshwater entering a relatively denser

environment, are not particular to the Labrador shelf and are also found elsewhere in high latitudes. Another coastal current has been modelled and observed on the east Greenland shelf; the East Greenland Coastal Current (*Bacon et al.*, 2002). This current is not only responsible for transporting part of the Arctic freshwater export east of Greenland, but it also collects the meltwater runoff from the island's glaciers.

These coastal currents may play a relevant role in the local distribution of significant quantities of freshwater. Their relative low salinities raise the question of how they interact with the dynamics of the subpolar seas. As *Bacon et al.* (2014) conclude, the large freshwater transport by the East Greenland Coastal current (half of the annual Arctic gain) points out to the need of obtaining further understanding of the sources and continuity of this current. This is specially true in a warming climate. Greenland is the polar ice-sheet that has shown the largest recent melt and contribution of freshwater, exceeding that of the whole Antarctic continent combined (*Shepherd et al.*, 2012). Furthermore, the ice balance of Greenland is rapidly changing and further melting is expected (*Gregory et al.*, 2004). As a current which presumably holds the meltwater runoff from Greenland, it is essential to understand the role of the East Greenland Coastal current in the distribution of this water and its link with those subpolar regions that are sensitive to buoyancy changes. Most studies generally overlook these narrow currents, which occur in the first 50 to 100 kilometres of the subpolar shelves. The magnitude of their freshwater transport, however, means that both model studies and observational programs should take into account the role of coastal currents. Mooring arrays and repeated observations should also consider implementing high resolution on the inshore side of these transects.

7.3.2 The Arctic freshwater export as the link between the Arctic and the North Atlantic freshwater budgets

One of the most important achievements of this thesis has been to provide the first estimates of Arctic export variability from observations, with a time scale that is longer than a decade. The 66 years of information given by the proxy in this study

have proved to be reliable (coherent with existing observations), relatively certain (small sensitivity to the specifications of the method) and highly relevant to the wider region. The most significant finding is the clear link between the Arctic and the North Atlantic freshwater budgets through the export of liquid freshwater west of Greenland. Throughout the whole time series, periods of high transport have been related to a decreasing storage of freshwater in the Arctic and a freshening of the North Atlantic. Similarly, decreased exports have been linked to enhanced storage of freshwater in the Arctic and higher North Atlantic salinities.

This is relevant in regard to the dominant role of the export of liquid freshwater through the Canadian Arctic Archipelago (export route west of Greenland). It is confirming that the oceanic advection is one of the most, if not the most, significant processes by which the Arctic freshwater budget varies. This is in agreement with *Lique et al.* (2009) and *Häkkinen and Proshutinsky* (2004), who pointed out the relevance of these fluxes in the Arctic storage of freshwater, in spite of other processes like Ekman pumping at the Beaufort Gyre or the variability of sea-ice formation. Additionally, this sheds light on the still unravelled mechanisms controlling the storage and export of Arctic freshwater. The processes responsible for the variability of the oceanic advection could prove key to describing the variability of the whole Arctic freshwater system. Trying to better understand the mechanisms behind the circulation of the Arctic surface waters can help with predicting the evolution of its freshwater storage and future impacts on the subpolar North Atlantic and the meridional overturning circulation.

So the question arises: do these observations of varying Arctic freshwater transport measured at the Seal Island section provide new insight into the complex relationship between Arctic and North Atlantic freshwater budgets, and in particular the role of oceanic export? We can address this by examining a two-part hypothesis: firstly that the tendency of the North Atlantic freshwater content is dominated by the Arctic freshwater export component (after *Peterson et al.*, 2006), and secondly that the tendency in Arctic freshwater storage is also dominated by the export component. The hypothesis would be supported by a positive relationship between the Seal Island freshwater transport and North Atlantic freshwater content, and a negative relationship with Arctic freshwater content. We examine

published time series to explore these relationships, and they are illustrated in Figure 6.19.

The Seal Island section time series of cumulative freshwater volume (red curve) represents the additional volume of Arctic freshwater entering the North Atlantic via the Labrador shelf. The curve shows remarkable agreement with an independently estimated time series of North Atlantic freshwater content anomaly (purple curve, adapted from *Peterson et al.*, 2006), both in terms of timing of high vs. low periods and in the magnitude of the anomalies, and even though the content anomalies are estimated for pentads rather than years. That is an accumulated increase in the transport of 22000 km^3, comparable to the 24000 km^3 seen in the North Atlantic by Peterson. Our results are the first observational evidence of the integrated anomalous Arctic freshwater inputs reaching the North Atlantic and support the hypothesis that they dominate North Atlantic freshwater content changes.

The similarity of the Arctic freshwater input time series and the North Atlantic freshwater content time series does not exclude the possibility of other important contributions to the North Atlantic changes. *Yang et al.* (2016) reported a steady increase totalling $\sim$ 20 mSv of freshwater from Greenland glacier melt and CAA and Arctic sea-ice melt during the period of 1980 to 2015, but this has a relative small equivalent cumulative volume of 630 km^3. Over this same period our observations show a net decrease of 40 mSv (smoothed time series in figure 6.19), but with very large decadal variability within this overall change, including a maximum in the mid-1980s followed by a reduction of $\sim$ 70 mSv between 1986 and 2005. In the subpolar North Atlantic the variability in P-E anomaly can be large and appears to reinforce the changes brought by Arctic freshwater transport on the Labrador shelf, with an anomaly of ~ -8000 km^3 in 1970 followed by a steady increase accumulating to +2000 km3 in 2000 (*Peterson et al.*, 2006). This raises the interesting question as to why these two sources of freshwater appear to co-vary, which is an interesting topic for future work.

Peterson et al. (2006) made no link between observations of Arctic freshwater storage and the anomalous freshwater inputs, though other analyses do show changing Arctic freshwater content, and notable a rapid increase from $\sim$ 1995 to

2010 (*Polyakov et al.*, 2013; *Rabe et al.*, 2014). Next I examine the relationship between published time series of Arctic freshwater content and the Seal Island section Arctic freshwater transport (Figure 6.19) for the second part of our hypothesis. First consider the multi-decadal Arctic freshwater content changes (smoothed time series, *Polyakov et al.*, 2013) compared to the smoothed time series of Arctic freshwater transport observed at the Seal Island section. Periods of anomalously low Arctic freshwater storage coincide with periods of high Arctic freshwater transport on the shelf, with highest correlation ($r = 0.73$) at a time lag of 6.5 years. However both the Polyakov and the Rabe time series show a large and rapid increase in Arctic freshwater storage ($\sim$ 8000 km^3) from 1995 to 2010, which follows a decrease in freshwater transport on the Labrador shelf that accumulates to $\sim$ 12000 km^3. The negative relationships between the Arctic freshwater content anomalies and the Arctic freshwater transport on the Labrador shelf support the second part of hypothesis, but with a caveat as follows. The difference in magnitude volume anomalies suggest that changes in export do not fully account for the changes in storage, although there are large uncertainties in the estimates of Arctic freshwater content and change. For example, *Rabe et al.* (2014) estimated an increase in Arctic freshwater content of 600 $\pm$ 300 km^{3}yr^{-1}, which is close to our export estimate of 750 km^{3}yr^{-1} for the same period. The complexity and unknowns of the Arctic freshwater budget are large (*Serreze et al.*, 2006), but we argue that our results provide the first observational evidence that these two components are closely linked.

7.3.3 Relevance of the freshwater export west of Greenland to the total Arctic freshwater export

Aagaard and Carmack (1989) first introduced the importance of the export of Arctic freshwater in the generation of salinity anomalies in the North Atlantic. However, they only acknowledged the relevance of the eastern route of the export; that through Fram Strait. Similarly, other authors attribute the Great Salinity Anomaly (see *Dickson et al.*, 1988) to the export of sea ice through Fram Strait (e.g. *Häkkinen*, 1993; *Karcher et al.*, 2005). The role of the export west of Greenland to

alter the salinity of the North Atlantic is only considered by the latter authors in the most recent salinity low in the early 1990s. Only recently it has been observed that the export through the Canadian Arctic Archipelago is the largest sink of Arctic freshwater in its liquid component (*Prinsenberg and Hamilton*, 2005). Following this line, the work presented in this thesis has strongly indicated that the export west of Greenland is a primary component of the total Arctic export. This export route does not only show the potential to generate further salinity anomalies in the North Atlantic, but it also played a major role in the Great Salinity Anomaly of the early 1970s.

The Great Salinity Anomaly produced an excess of 2200 km^3 in the Labrador Sea, according to *Dickson et al.* (1988). It was later estimated that the total increase in the subpolar North Atlantic and the Nordic Seas between 1965 and 1975 was of 10000 km^3 (*Curry and Mauritzen*, 2005). The accumulated freshening shown by the proxy of this thesis adds up to a total of 6000 km^3 for the same period, with a one year pulse of 4000 km^3 between 1971 and 1972. These export rates are comparable to the magnitude of the North Atlantic freshening observed in the contemporary periods. Furthermore, the total freshening due to the export west of Greenland, between 1965 and 1995, is of approximately 22000 km^3. This falls within the total northern North Atlantic freshening range estimated by *Curry and Mauritzen* (2005); 19000 $\pm$ 5000 km^3. This is a strong indication that the liquid transport of Arctic freshwater through the Canadian Arctic Archipelago has a significant weight in the total Arctic export and in the dilution events of the North Atlantic. It is true that we do not yet fully understand how much and how this exported water reaches the interior of the Labrador Sea and other subpolar basins. However, its close co-variability with the Atlantic freshwater budget throughout the time series strongly supports that this branch is a major source of freshwater to the North Atlantic and fairly representative of the total export.

Continuing with the importance of the Arctic freshwater export west of Greenland to the total export, here I evaluate how representative this route is to the total. *Lique et al.* (2009) described the Arctic export variability as some sort of seesaw. They hypothesised that the volume flux alternated between the east and the west branches, as the transports at the routes display a strong anti-correlation.

Their modelled freshwater transport was mostly determined by the volume transport variability, with salinity playing a larger role only in the route to the east. This implies that the export west of Greenland can only inform about the total Arctic export at the times when this transport occurs through Davis Strait. Hence, it may be relatively hard to represent the full Arctic freshwater export by just one of the branches. However, the results shown in this thesis suggest otherwise. The described co-variability between the export measured here and the freshwater budgets of the basins strongly indicates that this route of the export is fairly representative of the Arctic freshwater export throughout the whole time series (1950 to 2014). This is further supported by the magnitude of the accumulated effect of this export, which is coherent with changes in the North Atlantic salinity balance; it can explain most of the observed freshening. Whether this is true throughout the year or just a seasonal feature (i.e. that the summer transport west of Greenland is representative of the full yearly Arctic transport) is still unclear. *Lique et al.* (2009) captured some clear seasonality in the export through Fram Strait, but further understanding is required.

Here, the relevant role of the west route of the export has been pointed out. However, further research to adequately describe this transport dichotomy would be very interesting to quantify the relative magnitude of both branches to the total export. Describing their seasonality from hydrographic observations would also help test the extent to which these transports are anti-correlated. We now have enough data at the straits of Davis and Fram to compare both routes of the export and to shed light on this open question. Additionally, new observational arrays such as the OSNAP project will soon offer the potential to further analyse the eastern route of the export and, perhaps, to repeat a similar study to the one presented in this thesis.

7.4 An overview of recent changes and indications for future work

The discussion presented here invites a look towards the future, to the analysis of present conditions and to the scope of future work. What is the current state of North Atlantic freshwater budget and that of the Arctic export? How does the new knowledge provided by this thesis relate to any possible changes? The time series presented here contains data up to 2016, but the Seal Island section has continued being measured until present. Data of following years (2017 and 2018) will be soon available. Meanwhile, further observational stations and programs have already introduced the most recent estimates of the North Atlantic salinity and freshwater balance. This section briefly reviews their current state, in anticipation of the update of the Arctic freshwater export proxy. At the end, this section also suggests directions for further additional work, both for the Seal Island dataset and for general research in the topic.

7.4.1 A reversal to a period of Arctic freshwater release?

The latest years in the Arctic export proxy hint a reversal in the multiyear average, from a period of decreased transport (see figure 6.12) to a sequence of yearly increases in the transport. Other than 2016, with relatively low transport, 2009, 2014 and 2015 show the highest transport of the previous two decades. Is this an indication of a reversal in the Arctic freshwater storage trend, which has been locked in this phase since the early 1990s? It is still too early for the time series to inform about this, but further hints can be found in recent results.

The Canadian Science Advisory Secretariat (CSAS) annually updates the oceanographic conditions on the Newfoundland and Labrador shelves. Their report is usually released every June and covers data up to the year prior to the publication. The latest report (*Colbourne et al.*, 2016) summarises the observed changes until 2015. One of their most significant remarks is the continuing positive phase of both the Arctic Oscillation (this favours the release of freshwater by the Beaufort Gyre; *Zhang et al.*, 2003) and the North Atlantic Oscillation, which displayed a record

maximum. The reports by the CSAS also compute a composite climate index that converges the anomalies of many components (including temperature, salinity, ice and CIL anomalies) with the aim to inform about regional climatic conditions and trends (shown as their figure 54). The trend of this climate index (not shown here) displays a rapid decrease towards negative anomalies, in agreement with the apparent changes in 2014 and 2015. This indicates that, in those years, the water in the Labrador and Newfoundland shelves has been colder and fresher than average, with a larger cross-sectional area of the CIL (this can also be seen in their figure 53). Furthermore, the highlight of the report by *Colbourne et al.* (2016) is the anomalous large CIL observed in 2015. Its size on the Grand Banks during the spring is the largest on record since 1970. As shown by this thesis, the cross-sectional area of the CIL is the most relevant variable in determining the magnitude of the Arctic freshwater export, suggesting that a significant input of freshwater into the North Atlantic occurred in 2015.

This raises the question as to whether this has had any impact on the salinity and freshwater budgets of the North Atlantic. Some updated time series in the northern North Atlantic suggest that this is the case. An example is found at some sections in the north-eastern North Atlantic, as shown in figure 7.1 (N. P. Holliday, personal communication). Most salinity time series show an interesting decrease in the trend. This coincides with anomalous fresh values in the last 3 years (2014 to 2016) and specially in 2016 at the Rockall Trough. Additionally, further indications suggest a very recent freshening of the North Atlantic subpolar seas. The salinity of the Icelandic basin has shown a drastic decrease in the last year that is comparable to that observed in this region during the Great Salinity Anomaly (N. P. Holliday, personal communication).

These current observations seem to indicate that a change in the Arctic freshwater storage trend could be possibly occurring now, with a related freshening in the North Atlantic. This is only speculation; it is too early to adequately assess this interpretation. However, it offers an interesting hypothesis to test in the coming years. Additionally, this general apparent freshening does not seem to be related with changes in Fram Strait (salinity anomalies there remain fairly constant and positive, figure 7.1). This confronts the significance of the eastern route of the

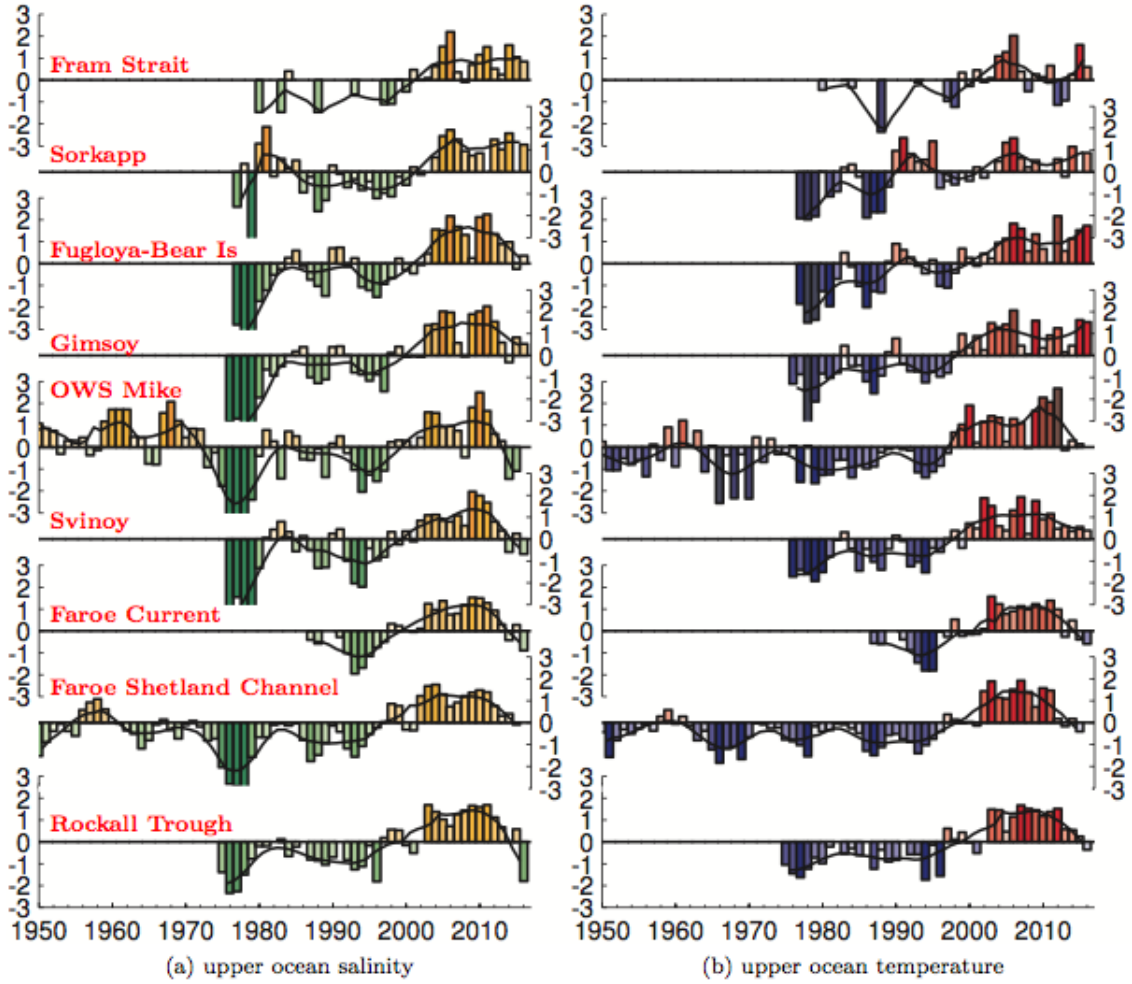

Figure 7.1: Time series of surface salinity (left) and temperature (right) anomalies at several sustained observations sections at the east of the subpolar North Atlantic. This figure is an updated version of figure 2 in Holliday et al. (2008), extended to 2016 (N. P. Holliday, personal communication).

Arctic export and raises the question of which mechanisms are responsible for this freshening. Is it the export west of Greenland? Is it the ice transport through Fram Strait? Does it have to do with other Atlantic fluxes? These are open questions that invite further research.

7.4.2 Additional work and indications for future research

This subsection discusses different lines of potential future work. First, it suggests further analysis that can be carried out with the tools used in this thesis. These include the NEMO model and the observations at the Seal Island section. Finally, it covers some possible directions for eventual research, at a larger scale.

Further work

Regarding the Seal Island dataset, one of the first actions to be done is extending the proxy time series with new observations; including data from 2015 and 2016. These data will be available soon and they will shortly be included in the current time series. This action can be repeated yearly, as new data become available. On the same line, it is possible to extend the time series at its beginning, before 1950. Although data before that year are less frequent and display a lesser standard, they still could provide an idea of earlier variability. Even if salinity data are missing in many of the sections, a similar proxy can still be achieved. The results from this thesis have shown that the cross-sectional area of the CIL is a main indicator of the Arctic freshwater export magnitude, especially if including the surface layer. The size of this area can be obtained from solely temperature profiles. Such a new proxy would be much less precise, but if adequately contrasted with the proxy shown in this thesis, it could provide a very interesting estimate of export during the second quarter of the 20th century.

Another point to analyse with the current observations is the skill of the summer sections to represent the full year. The sections computed in this study only considered summer (July and August) data, but how well do they represent yearly estimates of the export? The Arctic freshwater export proxy has shown a close co-variability with long-term changes in the Arctic and North Atlantic budgets. This indicates that summer export rates are a fair representation of the yearly mean. However, it would be of great interest to better understand the seasonality of the export as seen on the Labrador shelf observations. Data at seasons other than summer are scarce, specially when the shelf is covered with sea-ice during winter. However, there may be enough profiles to at least compute several composite monthly sections. Additionally, it may even be possible to estimate the variability at the Seal Island section during consecutive months within a single year. An example could be found, for instance, in 1973 (see figure 4.3). This year seems to present fairly abundant data during several consecutive months. A detailed analysis of these data can help assessing the skill of the summer-weighted observations to represent the yearly export estimates.

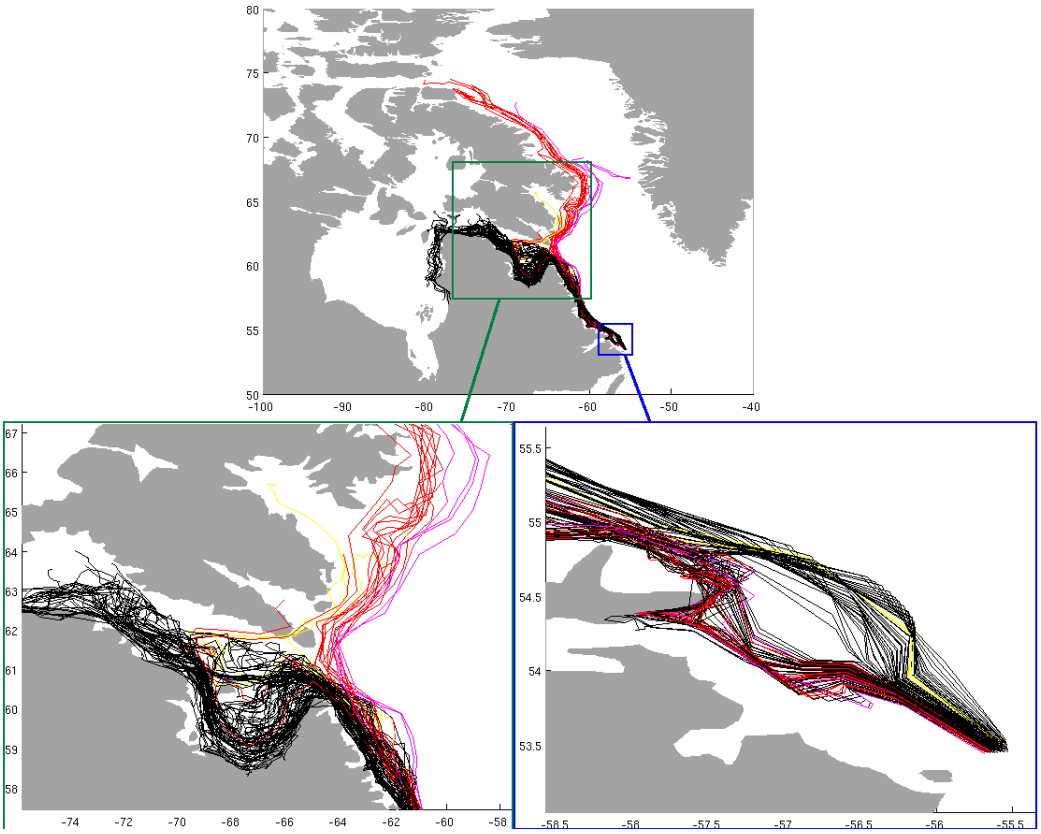

Figure 7.2: Results of a lagrangian experiment test using Ariane. This experiment shows the backwards trajectories of the water carried by the Labrador Coastal Current in the model. It displays the track followed by these waters before reaching the Seal Island section.

Finally, the NEMO model can also be used to expand our knowledge of the export routes and the mixing on the shelf. As part of this work, some preliminary analysis of the trajectories followed by the water on the Labrador shelf was carried out using Ariane. This is a Lagrangian tool that uses the model velocity fields to computes the advection of water. The calculated trajectories can be tracked forward or backwards, allowing us to study the fate or the origins of the tracked particles. Ariane is available at `http://www.univ-brest.fr/lpo/ariane` and is fully described by *Blanke and Raynaud* (1997). An example of Ariane can be seen in figure 7.2, which shows a test experiment to display the potential of this tool.

The details of the preliminary experiment are as follow. Particles were seeded at the Seal Island section, one at each model grid cell on the first 60 km of the shelf (where the Labrador Coastal current sits). One deployment is made in July 2008, and it is tracked backwards (inverted velocities to analyse the origin) for a full year (that is 72 time steps, for 5-day means model files). The trajectories originated

at Hudson Bay are shown in black, those coming from Baffin Bay are in red, and those recirculating from west Greenland are shown in magenta. It is interesting to know that in this preliminary experiment, 94% of the trajectories are sourced in Hudson Bay. This is in agreement with one of the conclusions of this thesis; that the Labrador Coastal current is fed by the Hudson Strait outflow. However, this is just a preliminary experiment that shows the potential of this tool. Full analysis is required in order to investigate this further.

By representing the trajectories of the waters reaching the Seal Island section it is possible to characterise their sources and to quantify their mixing along the way. Furthermore, this can also help inform about seasonality and interannual variability in the model. In a similar way as *Lique et al.* (2010) did in their study, this tool can also serve to better understand the local circulation and the interaction with some of the shelf features (an example can be seen in the lower-right panel in the figure, displaying a separation of trajectories at the Hamilton Bank). Finally, this tool can also prove valuable in studying of the role of the fresh coastal currents in the dynamics of the subpolar seas.

Future research directions

Future research efforts on this topic should consider studying the seasonal and interannual variability of the Arctic export as seen across the two known branches. It is essential to fully understand these dichotomy of the export and to quantify its magnitude through both gateways. By doing this, it will be possible to compare any observed variability with that of the presumed mechanisms that control this variability. This can collectively inform about the evolution of the Arctic freshwater storage and it can help in predicting how fast (and when) the magnitude of the current storage can freshen the North Atlantic. Recent studies have shown that the increase in the freshwater stored in the Arctic (e.g. *Rabe et al.*, 2011) has the potential to produce a North Atlantic freshening large enough to have an impact on the meridional overturning circulation and climate (e.g. *Curry and Mauritzen*, 2005). This thesis has also shown that the advection of this water, at least west of Greenland, can generate significant changes in the salinity of the North Atlantic

on a short time scale. However, the mechanisms behind this and the implications of a divided export route still remain unclear.

Currently, the available observations at Fram and Davis strait span about a decade. They now provide a time series long enough to study the signal of the Arctic freshwater export at both sections and compare synoptically their seasonal and interannual variability. Is it possible to use these data to resolve the relative magnitude and variability of both export branches? Fully characterising the division of the export can be a starting point to study its covariability with other factors (e.g. atmospheric circulation, teleconnections, sea-ice dynamics, river runoff and changes in precipitation). This can shed light on which mechanisms are mostly responsible for the storage and the export of freshwater in the Arctic.

Additionally, can the available transport data at Davis Strait be related to the proxy presented here to a better degree of understanding? It would be greatly interesting to transfer the skill of the proxy informing the export to a section that is closer to the Arctic and that takes measurements throughout the year (as it is the case in the mooring array at Davis strait). Finally, future publications will possibly assess whether the observations at those straits capture the apparent freshening occurring the North Atlantic right now. This will be fundamental information to reply some of the open questions exposed here.

Bibliography

Aagaard, K., and E. C. Carmack, The role of sea ice and other fresh-water in the Arctic circulation, *Journal of Geophysical Research-Oceans*, *94*(C10), 14,485–14,498, times Cited: 669, 1989.

Aksenov, Y., V. V. Ivanov, A. Nurser, S. Bacon, I. V. Polyakov, A. C. Coward, A. C. Naveira-Garabato, and A. Beszczynska-Moeller, The Arctic circumpolar boundary current, *Journal of Geophysical Research: Oceans (1978–2012)*, *116*(C9), 2011.

AMAP, *AMAP assessment report: Arctic pollution issues*, Arctic Monitoring and Assessment Programme (AMAP), 1998.

Arakawa, A., and V. R. Lamb, Computational design of the basic dynamical processes of the UCLA general circulation model, *Methods in computational physics*, *17*, 173–265, 1977.

Bacon, S., G. Reverdin, I. G. Rigor, and H. M. Snaith, A freshwater jet on the east Greenland shelf, *Journal of Geophysical Research: Oceans*, *107*(C7), 2002.

Bacon, S., A. Marshall, N. P. Holliday, Y. Aksenov, and S. R. Dye, Seasonal variability of the East Greenland coastal current, *Journal of Geophysical Research: Oceans*, *119*(6), 3967–3987, 2014.

Bacon, S., Y. Aksenov, S. Fawcett, and G. Madec, Arctic mass, freshwater and heat fluxes: methods and modelled seasonal variability, *Phil. Trans. R. Soc. A*, *373*(2052), 20140,169, 2015.

Blanke, B., and S. Raynaud, Kinematics of the Pacific equatorial undercurrent:

An eulerian and lagrangian approach from GCM results, *Journal of Physical Oceanography*, *27*(6), 1038–1053, 1997.

Brodeau, L., B. Barnier, A.-M. Treguier, T. Penduff, and S. Gulev, An ERA40-based atmospheric forcing for global ocean circulation models, *Ocean Modelling*, *31*(3), 88–104, 2010.

Broecker, W. S., D. M. Peteet, and D. Rind, Does the ocean-atmosphere system have more than one stable mode of operation?, *Nature*, *315*(6014), 21–26, 1985.

Carmack, E. C., The Arctic Ocean's freshwater budget: Sources, storage and export, in *The freshwater budget of the Arctic Ocean*, pp. 91–126, Springer, 2000.

Carmack, E. C., The alpha/beta ocean distinction: A perspective on freshwater fluxes, convection, nutrients and productivity in high-latitude seas, *Deep Sea Research Part II: Topical Studies in Oceanography*, *54*(23), 2578–2598, 2007.

Chapman, D. C., and R. C. Beardsley, On the origin of shelf water in the middle Atlantic Bight, *Journal of Physical Oceanography*, *31*(19), 384–391, 1989.

Colbourne, E., The history of standard hydrographic sections in Newfoundland and Labrador, *The Atlantic Zone Monitoring Program/Le Programme de Monitorage de la Zone Atlantique, p. 2*, p. 29, 2004.

Colbourne, E., J. Craig, C. Fitzpatrick, D. Senciall, P. Stead, and W. Bailey, An assessment of the physical oceanographic environment on the Newfoundland and Labrador shelf during 2010, *Tech. rep.*, Can. Tech. Rep. Hydrogr. Ocean Sci., 2011.

Colbourne, E., J. Holden, D. Senciall, W. Bailey, S. Snook, and J. Higdon, Physical oceanographic conditions on the Newfoundland and Labrador Shelf during 2015, *Canadian Science Advisory Secretariat (CSAS)*, *79*, 2016.

Colbourne, E. B., D. R. Senciall, and K. D. Foote, Temperature, salinity and sigma-t along the standard Seal Island transect, *Tech. Rep. 164: vi + 241 p.*, Can. Tech. Rep. Hydrogr. Ocean Sci., 1995.

Cuny, J., P. B. Rhines, P. P. Niiler, and S. Bacon, Labrador Sea boundary currents and the fate of the irminger sea water, *Journal of Physical Oceanography*, *32*(2), 627–647, 2002.

Curry, B., C. Lee, and B. Petrie, Volume, freshwater, and heat fluxes through Davis Strait, 2004-05*, *Journal of Physical Oceanography*, *41*(3), 429–436, 2011.

Curry, B., C. Lee, B. Petrie, R. Moritz, and R. Kwok, Multiyear volume, liquid freshwater, and sea ice transports through Davis Strait, 2004–10*, *Journal of Physical Oceanography*, *44*(4), 1244–1266, 2014.

Curry, R., and C. Mauritzen, Dilution of the northern North Atlantic Ocean in recent decades, *Science*, *308*(5729), 1772–1774, 2005.

Déry, S. J., M. Stieglitz, E. C. McKenna, and E. F. Wood, Characteristics and trends of river discharge into Hudson, James, and Ungava bays, 1964–2000, *Journal of Climate*, *18*(14), 2540–2557, 2005.

Dickson, R., J. Lazier, J. Meincke, P. Rhines, and J. Swift, Long-term coordinated changes in the convective activity of the North Atlantic, *Progress in Oceanography*, *38*(3), 241–295, 1996.

Dickson, R., B. Rudels, S. Dye, M. Karcher, J. Meincke, and I. Yashayaev, Current estimates of freshwater flux through Arctic and subarctic seas, *Progress in Oceanography*, *73*(3), 210–230, 2007.

Dickson, R. R., J. Meincke, S.-A. Malmberg, and A. J. Lee, The "great salinity anomaly" in the northern North Atlantic 1968–1982, *Progress in Oceanography*, *20*(2), 103–151, 1988.

Drinkwater, K., Physical oceanography of Hudson strait and Ungava Bay, *Elsevier oceanography series*, *44*, 237–264, 1986.

Drinkwater, K., On the mean and tidal currents in Hudson Strait, *Atmosphere-Ocean*, *26*(2), 252–266, 1988.

Dussin, R., B. Barnier, and L. Brodeau, The making of Drakkar forcing set DFS5, *DRAKKAR/MyOcean Rep. 05-10*, *14*, 2014.

Enderlin, E., and G. Hamilton, Estimates of iceberg submarine melting from high-resolution digital elevation models: application to Sermilik fjord, east Greenland, *Journal of Glaciology*, *60*(224), 10841092, doi:10.3189/2014JoG14J085, 2014.

Fahrbach, E., J. Meincke, S. Østerhus, G. Rohardt, U. Schauer, V. Tverberg, and J. Verduin, Direct measurements of volume transports through Fram Strait, *Polar Research*, *20*(2), 217–224, 2001.

Fofonoff, P., and R. Millard Jr, Unesco, algorithms for computation of fundamental properties of seawater, 1983.

Giles, K. A., S. W. Laxon, A. L. Ridout, D. J. Wingham, and S. Bacon, Western Arctic Ocean freshwater storage increased by wind-driven spin-up of the Beaufort Gyre, *Nature Geoscience*, 2012.

Glover, W., *Charting Northern Waters: Essays for the Centenary of the Canadian Hydrographic Service*, McGill-Queen's Press-MQUP, 2004.

Gregory, J. M., P. Huybrechts, and S. C. Raper, Climatology: Threatened loss of the Greenland ice-sheet, *Nature*, *428*(6983), 616–616, 2004.

Haine, T. W., et al., Arctic freshwater export: Status, mechanisms, and prospects, *Global and Planetary Change*, *125*, 13–35, 2015.

Häkkinen, S., An Arctic source for the great salinity anomaly: A simulation of the Arctic ice-ocean system for 1955–1975, *Journal of Geophysical Research: Oceans*, *98*(C9), 16,397–16,410, 1993.

Häkkinen, S., and A. Proshutinsky, Freshwater content variability in the Arctic Ocean, *Journal of Geophysical Research: Oceans*, *109*(C3), 2004.

Hawkins, E., R. S. Smith, L. C. Allison, J. M. Gregory, T. J. Woollings, H. Pohlmann, and B. De Cuevas, Bistability of the Atlantic overturning circulation in a global climate model and links to ocean freshwater transport, *Geophysical Research Letters*, *38*(10), 2011.

Holliday, N., S. Cunningham, C. Johnson, S. Gary, C. Griffiths, J. Read, and T. Sherwin, Multidecadal variability of potential temperature, salinity, and trans-

port in the eastern subpolar North Atlantic, *Journal of Geophysical Research: Oceans*, *120*(9), 5945–5967, 2015.

Holliday, N. P., A. Meyer, S. Bacon, S. G. Alderson, and B. de Cuevas, Retroflection of part of the east Greenland current at Cape Farewell, *Geophysical Research Letters*, *34*(7), 2007.

Holliday, N. P., et al., Reversal of the 1960s to 1990s freshening trend in the northeast North Atlantic and Nordic seas, *Geophysical Research Letters*, *35*(3), 2008.

Ingram, R., and S. Prinsenberg, Coastal oceanography of Hudson Bay and surrounding eastern Canadian Arctic waters, *The sea*, *11*(29), 835–859, 1998.

IOC, SCOR, and IAPSO, *The international thermodynamic equation of seawater–2010: Calculation and use of thermodynamic properties*, Intergovernmental Oceanographic Commission, Manuals and Guides No. 56, UNESCO (English), 196 pp. Available from http://www.TEOS-10.org, 2010.

Iselin, C., A report on the coastal waters of Labrador, based on explorations of the "Chanc" during the summer of 1926, in *Proceedings of the American Academy of Arts and Sciences*, vol. 66, pp. 1–37, JSTOR, 1930.

Jahn, A., B. Tremblay, L. A. Mysak, and R. Newton, Effect of the large-scale atmospheric circulation on the variability of the Arctic Ocean freshwater export, *Climate dynamics*, *34*(2-3), 201–222, 2010.

Jones, E., J. Swift, L. Anderson, M. Lipizer, G. Civitarese, K. Falkner, G. Kattner, and F. McLaughlin, Tracing Pacific water in the North Atlantic ocean, *Journal of Geophysical Research: Oceans*, *108*(C4), 2003.

Jones, E. P., L. G. Anderson, and J. H. Swift, Distribution of Atlantic and Pacific waters in the upper Arctic Ocean: Implications for circulation, *Geophysical Research Letters*, *25*(6), 765–768, 1998.

Karcher, M., R. Gerdes, F. Kauker, C. Köberle, and I. Yashayaev, Arctic Ocean change heralds North Atlantic freshening, *Geophysical Research Letters*, *32*(21), L21,606, 2005.

Köberle, C., and R. Gerdes, Simulated variability of the Arctic Ocean freshwater balance 1948–2001, *Journal of physical oceanography*, *37*(6), 1628–1644, 2007.

Koenigk, T., U. Mikolajewicz, H. Haak, and J. Jungclaus, Arctic freshwater export in the 20th and 21st centuries, *Journal of Geophysical Research: Biogeosciences*, *112*(G4), 2007.

Large, W. G., and S. G. Yeager, *Diurnal to decadal global forcing for ocean and sea-ice models: the data sets and flux climatologies*, National Center for Atmospheric Research Boulder, 2004.

Lazier, J. R., and D. G. Wright, Annual velocity variations in the Labrador current, *Journal of Physical Oceanography*, *23*(4), 659–678, 1993.

LeBlond, P. H., T. Osborn, D. Hodgins, R. Goodman, and M. Metge, Surface circulation in the western Labrador Sea, *Deep Sea Research Part A. Oceanographic Research Papers*, *28*(7), 683–693, 1981.

Lecointre, A., J.-M. Molines, and B. Barnier, Definition of the interannual experiment ORCA12. L46-MAL95, 1989-2007, 2011.

Lentz, S., Buoyant coastal currents, *Buoyancy-Driven Flows. Cambridge University Press, Cambridge*, pp. 164–202, 2012.

Lentz, S. J., and K. R. Helfrich, Buoyant gravity currents along a sloping bottom in a rotating fluid, *Journal of Fluid Mechanics*, *464*(1), 251–278, 2002.

Levitus, S., Interpentadal variability of temperature and salinity at intermediate depths of the North Atlantic Ocean, 1970–1974 versus 1955–1959, *Journal of Geophysical Research: Oceans (1978–2012)*, *94*(C5), 6091–6131, 1989.

Lique, C., A. M. Treguier, M. Scheinert, and T. Penduff, A model-based study of ice and freshwater transport variability along both sides of Greenland, *Climate Dynamics*, *33*(5), 685–705, 2009.

Lique, C., A.-M. Treguier, B. Blanke, and N. Grima, On the origins of water masses exported along both sides of Greenland: A lagrangian model analysis, *Journal of Geophysical Research: Oceans*, *115*(C5), 2010.

Lique, C., M. M. Holland, Y. B. Dibike, D. M. Lawrence, and J. A. Screen, Modeling the arctic freshwater system and its integration in the global system: Lessons learned and future challenges, *Journal of Geophysical Research: Biogeosciences*, 2015.

Loder, J. W., B. Petrie, and G. Gawarkiewicz, The coastal ocean off northeastern North America: A large-scale view, *The sea*, *11*, 105–133, 1998.

Lozier, M. S., et al., Overturning in the Subpolar North Atlantic Program: a new international ocean observing system, *Bulletin of the American Meteorological Society*, 2016.

Macdonald, R., Arctic estuaries and ice: A positive—negative estuarine couple, in *The freshwater budget of the Arctic Ocean*, pp. 383–407, Springer, 2000.

Madec, G., *NEMO ocean engine*, vol. 27, Note du Pole de modélisation, Institut Pierre-Simon Laplace (IPSL), France, 2008.

Manabe, S., and R. J. Stouffer, Simulation of abrupt climate change induced by freshwater input to the North Atlantic Ocean, *Nature*, *378*(6553), 165–167, 1995.

Marzocchi, A., J. J.-M. Hirschi, N. P. Holliday, S. A. Cunningham, A. T. Blaker, and A. C. Coward, The North Atlantic subpolar circulation in an eddy-resolving global ocean model, *Journal of Marine Systems*, *142*, 126–143, 2015.

McDougall, T. J., Streamfunctions for the lateral velocity vector in a compressible ocean, *Journal of Marine Research*, *47*(2), 267–284, 1989.

McDougall, T. J., and A. Klocker, An approximate geostrophic streamfunction for use in density surfaces, *Ocean Modelling*, *32*(3), 105–117, 2010.

McPhee, M., A. Proshutinsky, J. H. Morison, M. Steele, and M. Alkire, Rapid change in freshwater content of the Arctic Ocean, *Geophysical Research Letters*, *36*(10), L10,602, 2009.

Meredith, M., K. Heywood, P. Dennis, L. Goldson, R. White, E. Fahrbach, U. Schauer, and S. Østerhus, Freshwater fluxes through the western Fram Strait, *Geophysical research letters*, *28*(8), 1615–1618, 2001.

Mertz, G., S. Narayanan, and J. Helbig, The freshwater transport of the Labrador current, *Atmosphere-Ocean*, *31*(2), 281–295, 1993.

Montgomery, R., A suggested method for representing gradient flow in isentropic surfaces, *Bull. Am. Meteorol. Soc*, *18*(2), 10–2, 1937.

Myers, P. G., C. Donnelly, and M. H. Ribergaard, Structure and variability of the West Greenland current in summer derived from 6 repeat standard sections, *Progress in Oceanography*, *80*(1), 93–112, 2009.

Nansen, F., *The oceanography of the north polar basin*, vol. 3, Longmans, Green, and Company, 1902.

Peterson, B. J., J. McClelland, R. Curry, R. M. Holmes, J. E. Walsh, and K. Aagaard, Trajectory shifts in the Arctic and subarctic freshwater cycle, *Science*, *313*(5790), 1061–1066, 2006.

Petrie, B., S. Akenhead, S. Lazier, and J. Loder, The cold intermediate layer on the Labrador and northeast Newfoundland shelves, 1978–86, *NAFO Sci Counc Stud*, *12*, 57–69, 1988.

Polyakov, I. V., U. S. Bhatt, J. E. Walsh, E. P. Abrahamsen, A. V. Pnyushkov, and P. F. Wassmann, Recent oceanic changes in the Arctic in the context of long-term observations, *Ecological Applications*, *23*(8), 1745–1764, 2013.

Polyakov, I. V., et al., Arctic Ocean freshwater changes over the past 100 years and their causes, *Journal of Climate*, *21*(2), 364–384, 2008.

Prinsenberg, S., and J. Hamilton, Monitoring the volume, freshwater and heat fluxes passing through Lancaster Sound in the Canadian Arctic Archipelago, *Atmosphere-Ocean*, *43*(1), 1–22, 2005.

Prinsenberg, S., and I. Peterson, Sea-ice properties off Labrador and Newfoundland during LIMEX 89, *Atmosphere-Ocean*, *30*(2), 207–222, 1992.

Proshutinsky, A., D. Dukhovskoy, M.-L. Timmermans, R. Krishfield, and J. L. Bamber, Arctic circulation regimes, *Phil. Trans. R. Soc. A*, *373*(2052), 20140,160, 2015.

Proshutinsky, A. Y., and M. A. Johnson, Two circulation regimes of the wind-driven Arctic Ocean, *Journal of Geophysical Research: Oceans*, *102*(C6), 12,493–12,514, 1997.

Rabe, B., M. Karcher, U. Schauer, J. M. Toole, R. A. Krishfield, S. Pisarev, F. Kauker, R. Gerdes, and T. Kikuchi, An assessment of Arctic Ocean freshwater content changes from the 1990s to the 2006–2008 period, *Deep Sea Research Part I: Oceanographic Research Papers*, *58*(2), 173–185, 2011.

Rabe, B., M. Karcher, F. Kauker, U. Schauer, J. M. Toole, R. A. Krishfield, S. Pisarev, T. Kikuchi, and J. Su, Arctic Ocean basin liquid freshwater storage trend 1992–2012, *Geophysical Research Letters*, *41*(3), 961–968, 2014.

Rabe, B., et al., Liquid export of Arctic freshwater components through the Fram Strait 1998–2011, *Ocean Science*, *9*(1), 91–109, 2013.

Rignot, E., I. Velicogna, M. R. van den Broeke, A. Monaghan, and J. T. Lenaerts, Acceleration of the contribution of the Greenland and Antarctic ice sheets to sea level rise, *Geophysical Research Letters*, *38*(5), 2011.

Roach, A. T., K. Aagaard, C. H. Pease, S. A. Salo, T. Weingartner, V. Pavlov, and M. Kulakov, Direct measurements of transport and water properties through the Bering Strait, *Journal of Geophysical Research: Oceans*, *100*(C9), 18,443–18,457, doi:10.1029/95JC01673, 1995.

Rodwell, M. J., D. P. Rowell, and C. K. Folland, Oceanic forcing of the wintertime North Atlantic Oscillation and European climate, *Nature*, *398*(6725), 320–323, 1999.

Scheinert, M., A. Biastoch, and C. Böning, The global ocean model NEMO-ORCA12: Documentation of the Kiel DRAKKAR experiment setup, *Tech. rep.*, Technical report, IFM-Geomar, Kiel, Germany, 2010.

Schiller, A., U. Mikolajewicz, and R. Voss, The stability of the North Atlantic thermohaline circulation in a coupled ocean-atmosphere general circulation model, *Climate Dynamics*, *13*(5), 325–347, 1997.

Serreze, M. C., et al., The large-scale freshwater cycle of the Arctic, *Journal of Geophysical Research: Oceans (1978–2012)*, *111*(C11), 2006.

Shepherd, A., et al., A reconciled estimate of ice-sheet mass balance, *Science*, *338*(6111), 1183–1189, 2012.

Smeed, D., G. McCarthy, D. Rayner, B. Moat, W. Johns, M. Baringer, and C. Meinen, Atlantic meridional overturning circulation observed by the RAPID-MOCHA-WBTS (RAPID-Meridional Overturning Circulation and Heatflux Array-Western Boundary Time Series) array at 26n from 2004 to 2015, 2016.

Smith, E. H., The Marion expedition to Davis Strait and Baffin Bay, *US Coast Guard Bulletin*, *19*, 221, 1931.

Smith, E. H., F. M. Soule, and O. Mosby, *The Marion and General Greene Expeditions to the Davis Strait and Labrador Sea Under the Direction of the United States Coast Guard, 1928-1931-1933-1934-1935. Scientific Results Part 2, Physical Oceanography*, US Government Printing Office, 1937.

Smith, P. C., and F. B. Schwing, Mean circulation and variability on the eastern Canadian continental shelf, *Continental Shelf Research*, *11*(8-10), 977–1012, 1991.

Steele, M., D. Thomas, D. Rothrock, and S. Martin, A simple model study of the Arctic Ocean freshwater balance, 1979–1985, *Journal of Geophysical Research: Oceans*, *101*(C9), 20,833–20,848, doi:10.1029/96JC01686, 1996.

Steele, M., R. Morley, and W. Ermold, PHC: A global ocean hydrography with a high-quality Arctic Ocean, *Journal of Climate*, *14*(9), 2079–2087, 2001.

Steele, M., J. Morison, W. Ermold, I. Rigor, M. Ortmeyer, and K. Shimada, Circulation of summer Pacific halocline water in the Arctic Ocean, *Journal of Geophysical Research: Oceans*, *109*(C2), 2004.

Stepanov, V., and K. Haines, Mechanisms of Atlantic meridional overturning circulation variability simulated by the NEMO model, *Ocean Science*, *10*(4), 645–656, 2014.

Stommel, H., *Thermohaline convection with two stable regimes of flow*, *224-230*, vol. 13, Tellus, 1961.

Straneo, F., and F. Saucier, The outflow from Hudson Strait and its contribution to the Labrador Current, *Deep Sea Research Part I: Oceanographic Research Papers*, *55*(8), 926–946, 2008.

Sutton, R. T., and D. L. Hodson, Atlantic Ocean forcing of North American and European summer climate, *science*, *309*(5731), 115–118, 2005.

Tang, C. C., C. K. Ross, T. Yao, B. Petrie, B. M. DeTracey, and E. Dunlap, The circulation, water masses and sea-ice of Baffin Bay, *Progress in Oceanography*, *63*(4), 183–228, 2004.

Taylor, J. R., K. K. Falkner, U. Schauer, and M. Meredith, Quantitative considerations of dissolved barium as a tracer in the Arctic Ocean, *Journal of Geophysical Research: Oceans*, *108*(C12), 2003.

Templeman, W., Comparison of temperatures in july-august hydrographic sections of the eastern Newfoundland area in 1972 and 1973 with those from 1951 to 1971, *INTERNATIONAL COMMISSION*, 1975.

Thomson, R. E., and W. J. Emery, *Data analysis methods in physical oceanography*, Newnes, 2014.

Tsubouchi, T., et al., The Arctic Ocean in summer: A quasi-synoptic inverse estimate of boundary fluxes and water mass transformation, *Journal of Geophysical Research: Oceans (1978–2012)*, *117*(C1), 2012.

Wagner, T. J., and I. Eisenman, How climate model biases skew the distribution of iceberg meltwater, *Geophysical Research Letters*, *44*(8), 3691–3699, 2017.

Weaver, A. J., et al., Stability of the Atlantic meridional overturning circulation: A model intercomparison, *Geophysical Research Letters*, *39*(20), 2012.

Woodgate, R. A., and K. Aagaard, Revising the Bering Strait freshwater flux into the Arctic Ocean, *Geophysical Research Letters*, *32*(2), n/a–n/a, doi:10.1029/2004GL021747, l02602, 2005.

Woodgate, R. A., K. Aagaard, and T. J. Weingartner, Interannual changes in the Bering Strait fluxes of volume, heat and freshwater between 1991 and 2004, *Geophysical Research Letters*, *33*(15), L15,609, 2006.

Wu, Y., C. Tang, and C. Hannah, The circulation of eastern Canadian seas, *Progress in Oceanography*, 2012.

Yang, Q., T. H. Dixon, P. G. Myers, J. Bonin, D. Chambers, M. Van Den Broeke, M. H. Ribergaard, and J. Mortensen, Recent increases in Arctic freshwater flux affects Labrador Sea convection and Atlantic overturning circulation, *Nature communications*, *7*, 10,525, 2016.

Yankovsky, A. E., and D. C. Chapman, A simple theory for the fate of buoyant coastal discharges, *Journal of Physical oceanography*, *27*(7), 1386–1401, 1997.

Zhang, X., M. Ikeda, and J. E. Walsh, Arctic sea ice and freshwater changes driven by the atmospheric leading mode in a coupled sea ice–ocean model, *Journal of Climate*, *16*(13), 2159–2177, 2003.

Appendix A

Additional figures

Appendix A contains a set of supplementary figures, part of the results and/or used during the analysis. These are mostly information about the Seal Island section and the resulting dataset of summer sections. First, appendix 1.1 presents the positions of all the different profiles each year. Secondly, section 1.2 shows the yearly location of summer stations after unsuitable profiles have been removed. Then, appendixes 1.3 to 1.5 include the final summer sections of temperature, salinity and density from 1950 to 2014. Finally, last section of the appendix (1.6) shows sections of the calculated velocity across the transect.

1.1 Yearly distribution of stations at the Seal Island

The following figures display the yearly positions (longitude × latitude) of all available profiles around the Seal Island area. These are all the originally available files before any data cleansing, from 1928 to 2014. Missing years do not contain any data. The black line displays the standard transect. Markers, described in the legend, are different for every month. This is to depict the seasonal spread of data. Winter (blue colours), spring (greens), summer (yellow to red) and autumn (purple shades).

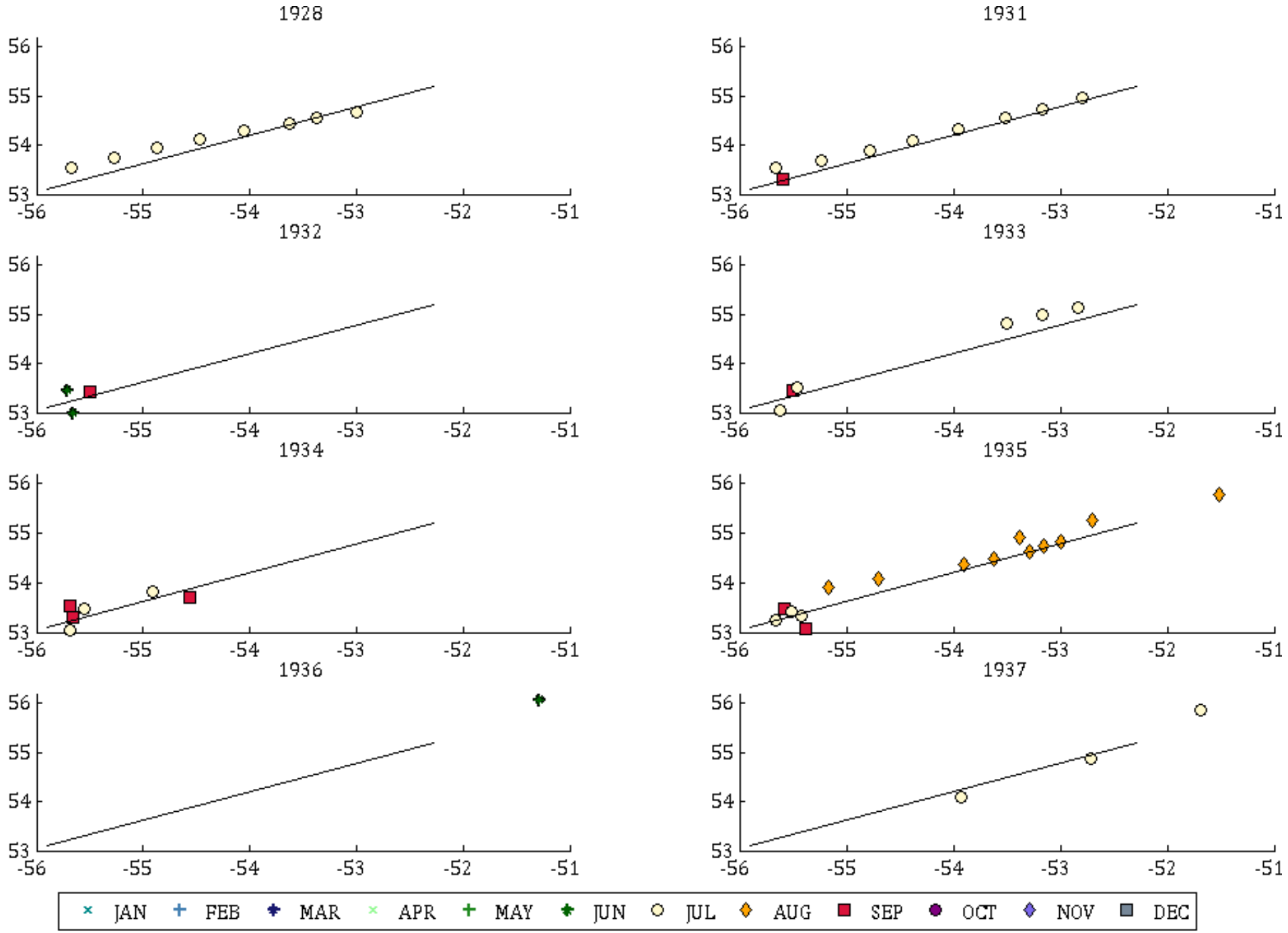
1928
1931
1932
1933
1934
1935
1936
1937
56
55
54
53
-56
-55
-54
-53
-52
-51
JAN
FEB
MAR
APR
MAY
JUN
JUL
AUG
SEP
OCT
NOV
DEC

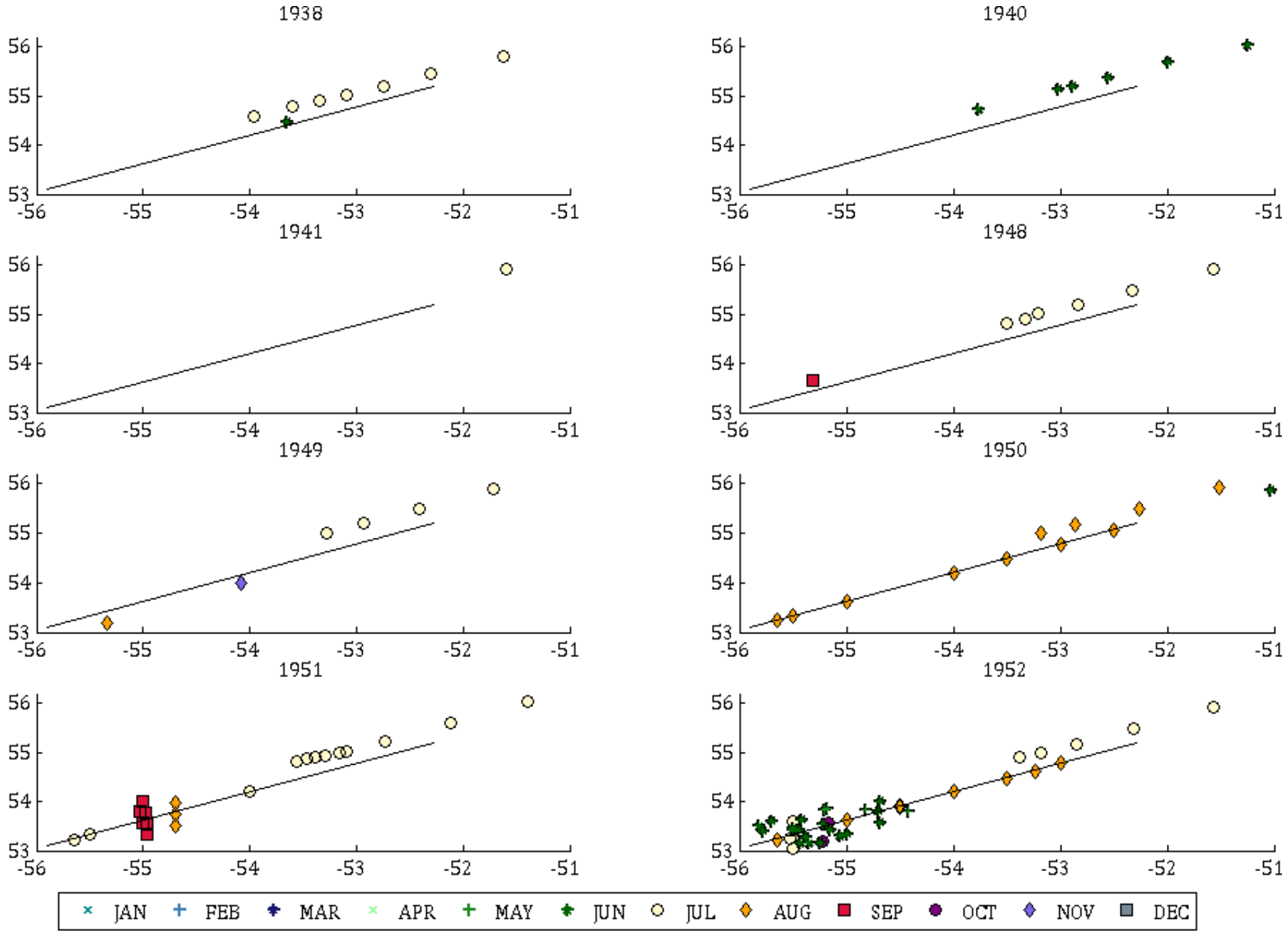
1938
1940
1941
1948
1949
1950
1951
1952
56
55
54
53
-56
-55
-54
-53
-52
-51
JAN
FEB
MAR
APR
MAY
JUN
JUL
AUG
SEP
OCT
NOV
DEC

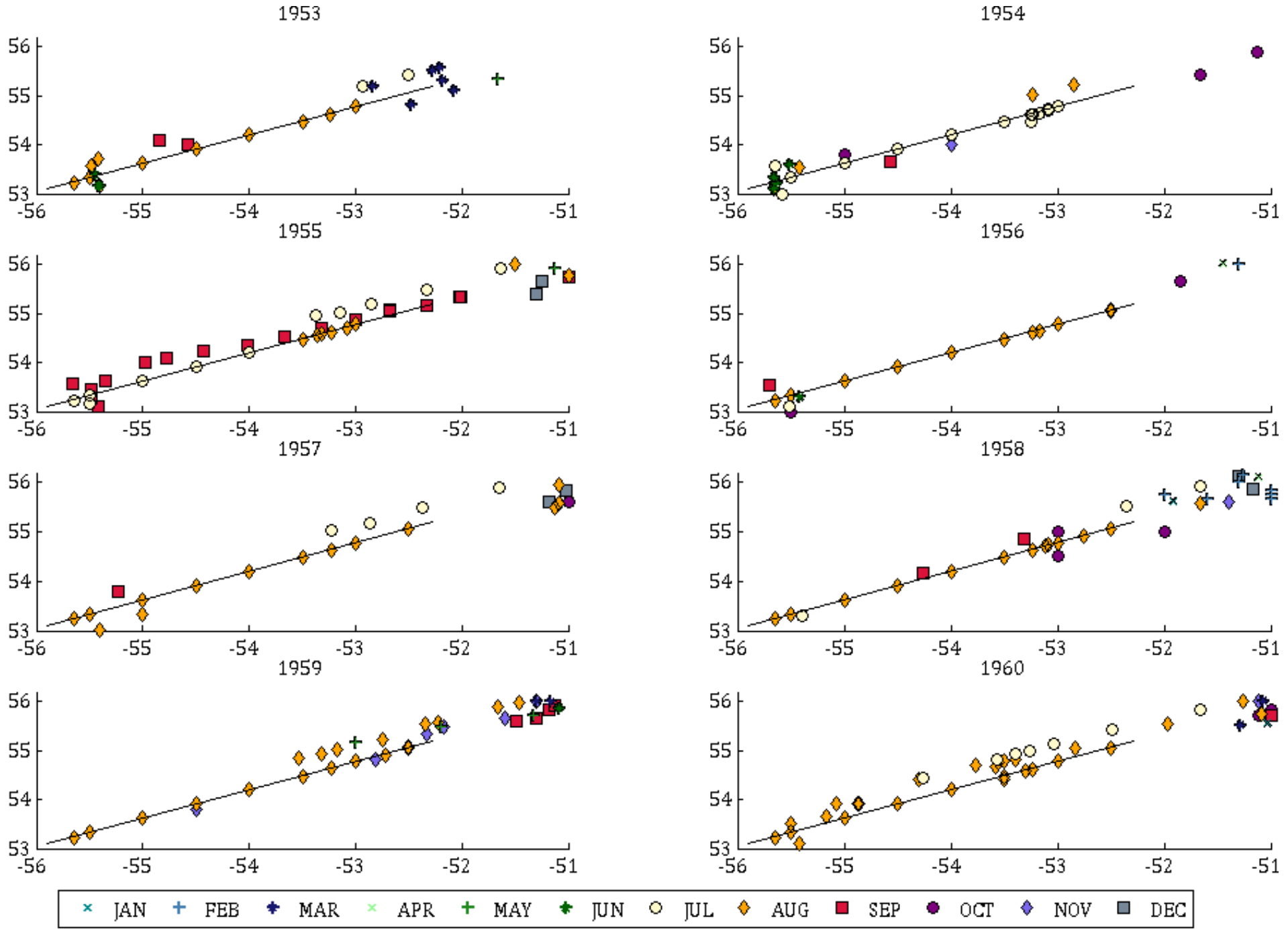
1953
1954
1955
1956
1957
1958
1959
1960
56
55
54
53
-56
-55
-54
-53
-52
-51
JAN
FEB
MAR
APR
MAY
JUN
JUL
AUG
SEP
OCT
NOV
DEC

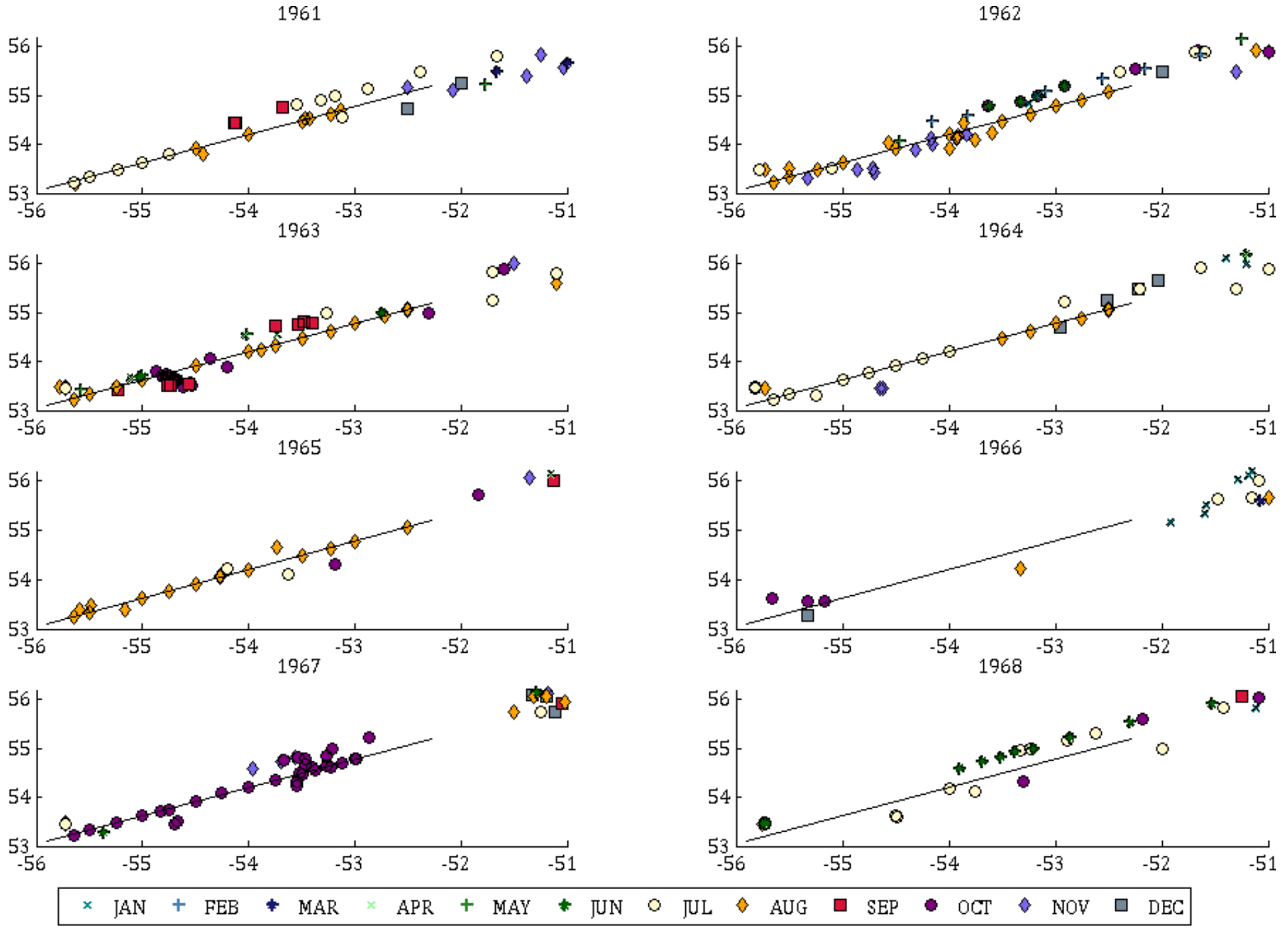
1961
1962
1963
1964
1965
1966
1967
1968
56
55
54
53
-56
-55
-54
-53
-52
-51
JAN
FEB
MAR
APR
MAY
JUN
JUL
AUG
SEP
OCT
NOV
DEC

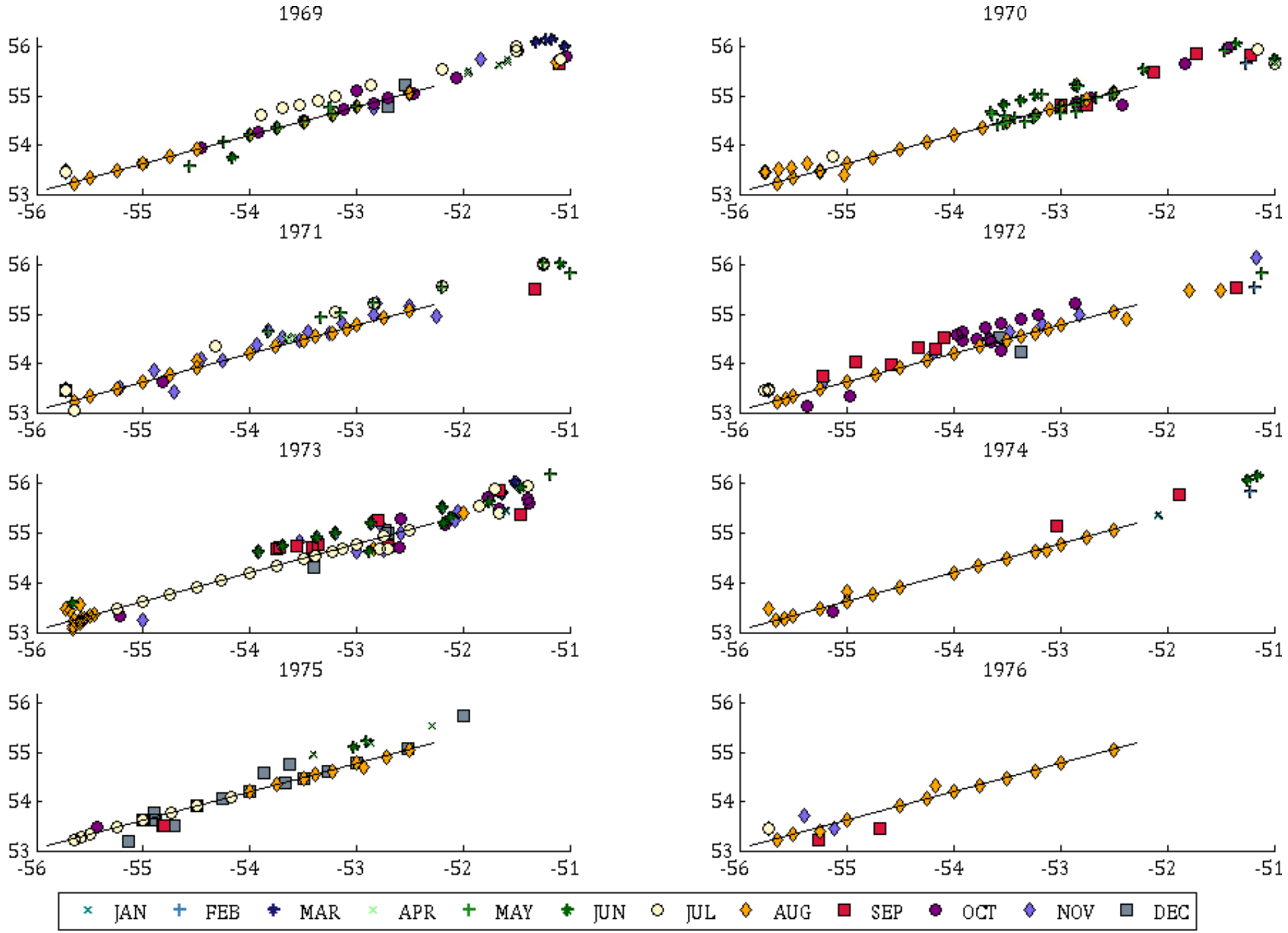
1969
1970
1971
1972
1973
1974
1975
1976
56
55
54
53
-56
-55
-54
-53
-52
-51
JAN
FEB
MAR
APR
MAY
JUN
JUL
AUG
SEP
OCT
NOV
DEC

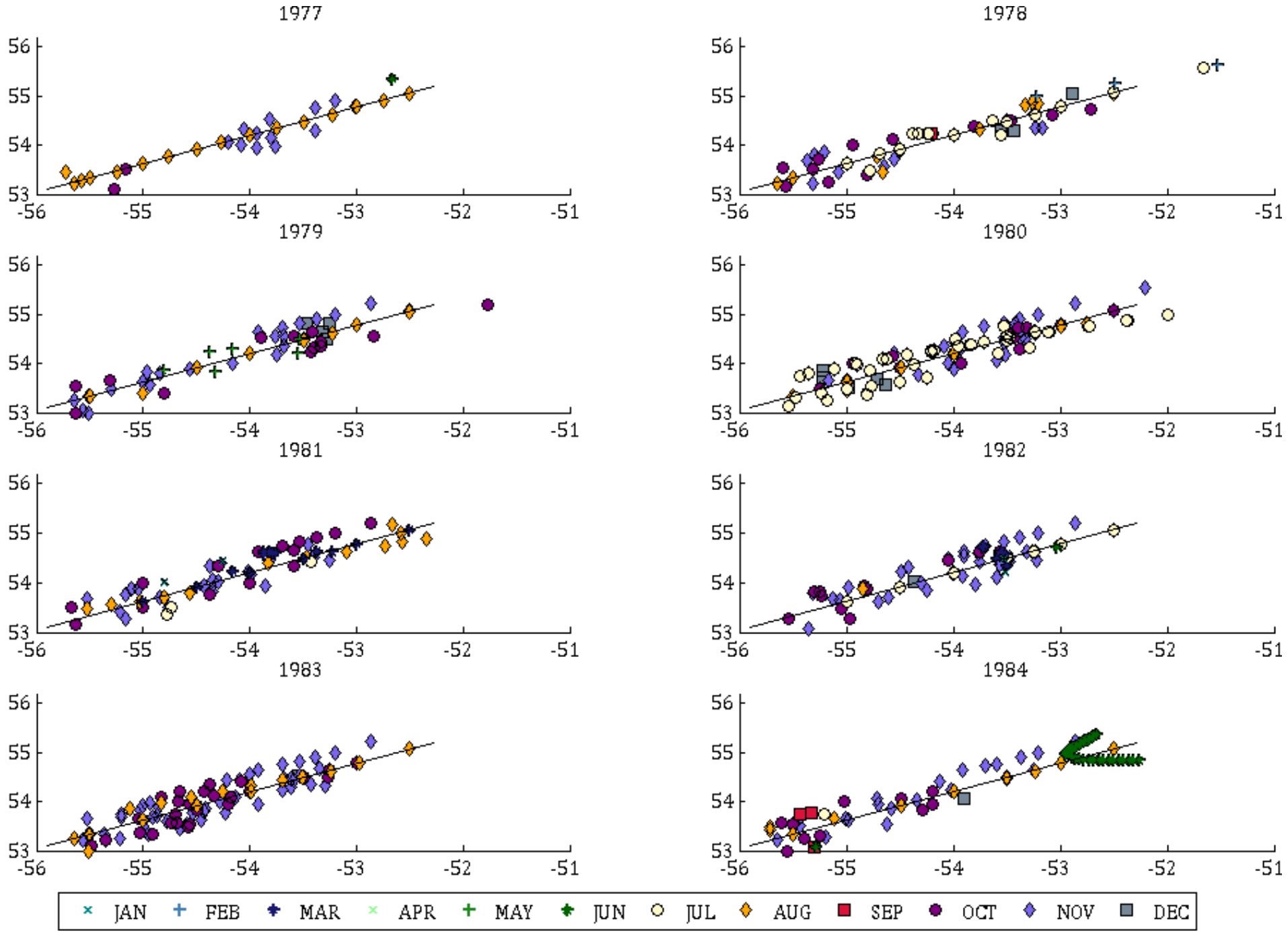
1977
1978
1979
1980
1981
1982
1983
1984
56
55
54
53
-56
-55
-54
-53
-52
-51
JAN
FEB
MAR
APR
MAY
JUN
JUL
AUG
SEP
OCT
NOV
DEC

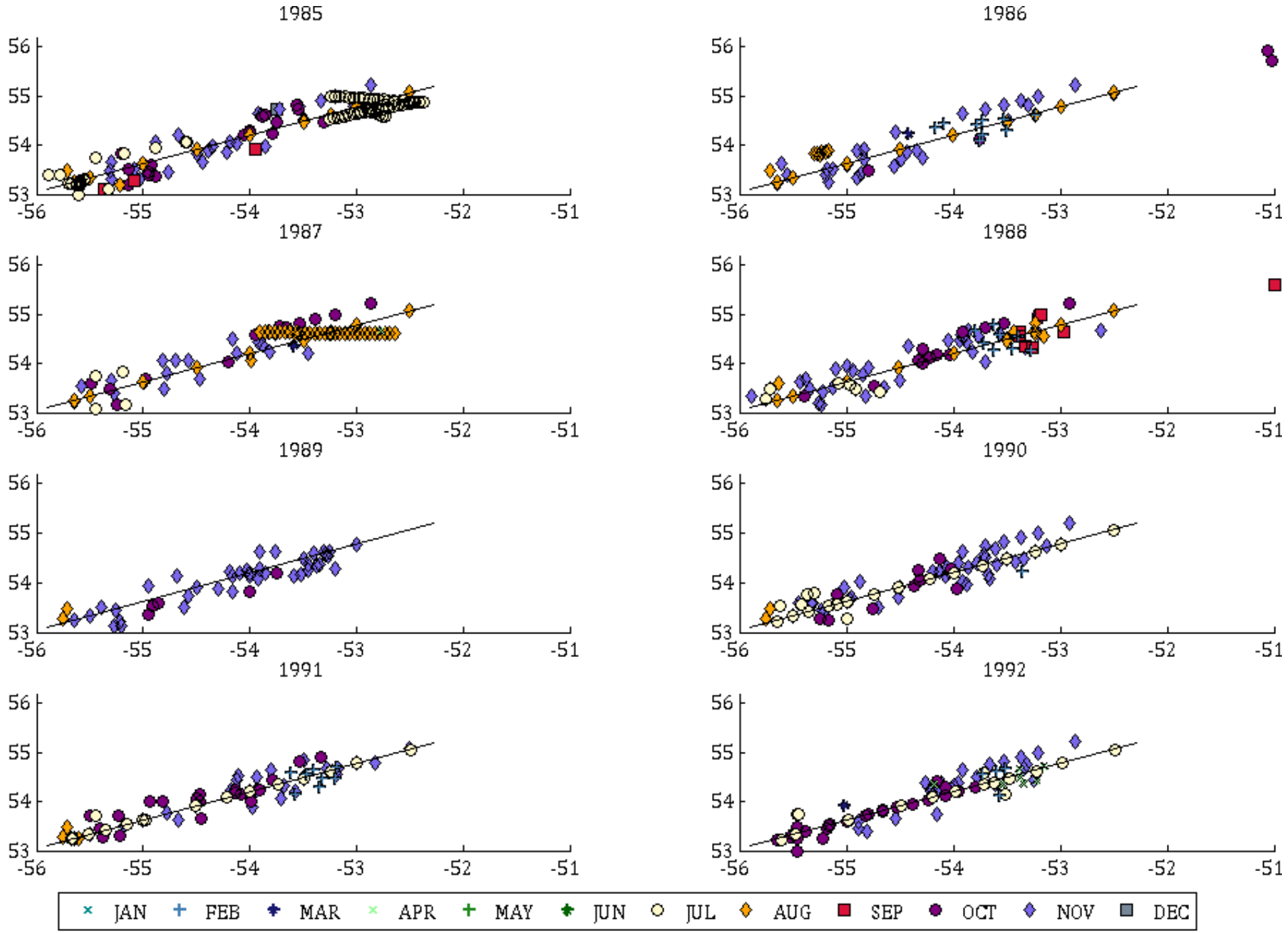
1985
1986
1987
1988
1989
1990
1991
1992
56
55
54
53
-56
-55
-54
-53
-52
-51
JAN
FEB
MAR
APR
MAY
JUN
JUL
AUG
SEP
OCT
NOV
DEC

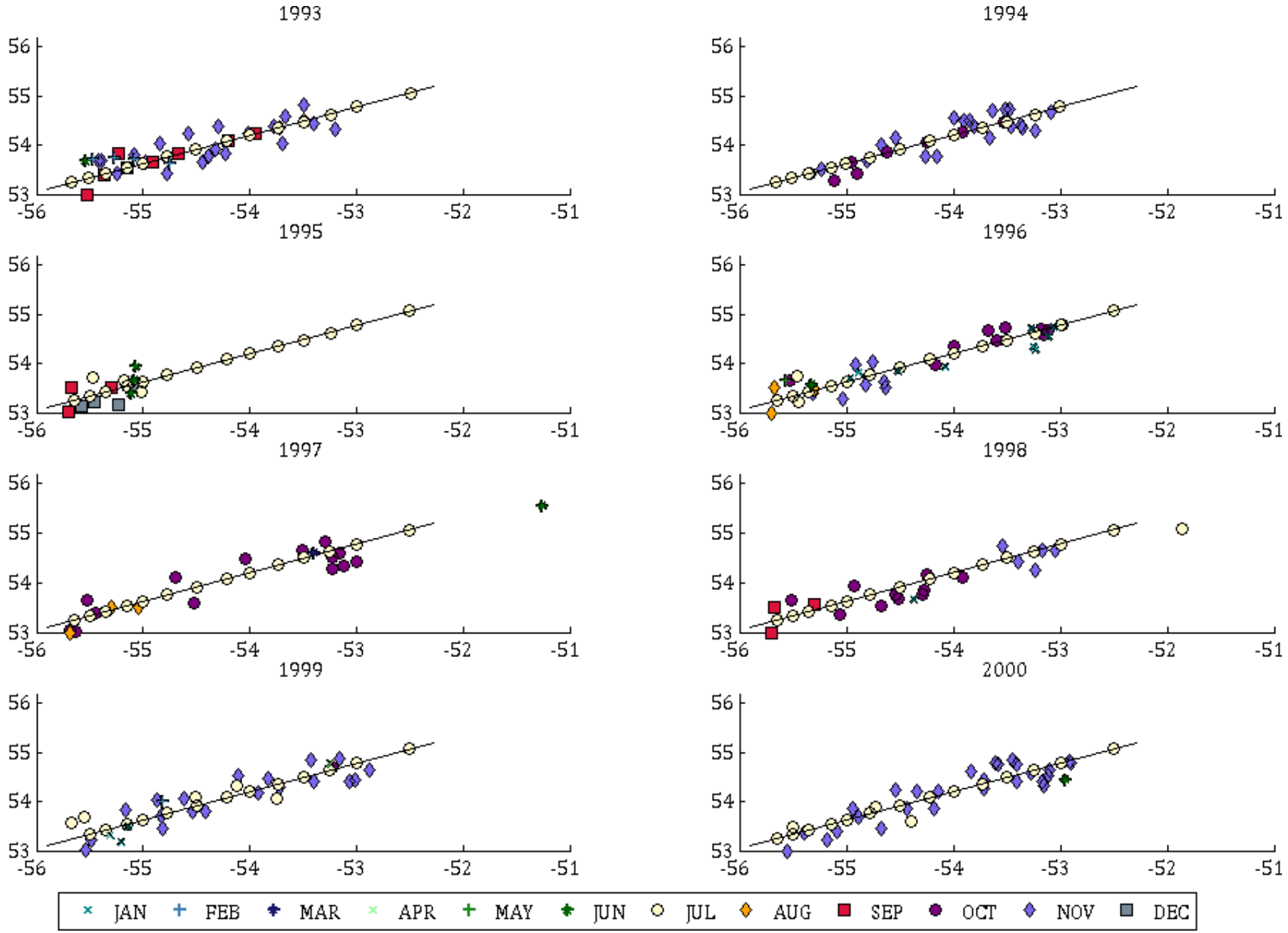
1993
1994
1995
1996
1997
1998
1999
2000
56
55
54
53
-56
-55
-54
-53
-52
-51
JAN
FEB
MAR
APR
MAY
JUN
JUL
AUG
SEP
OCT
NOV
DEC

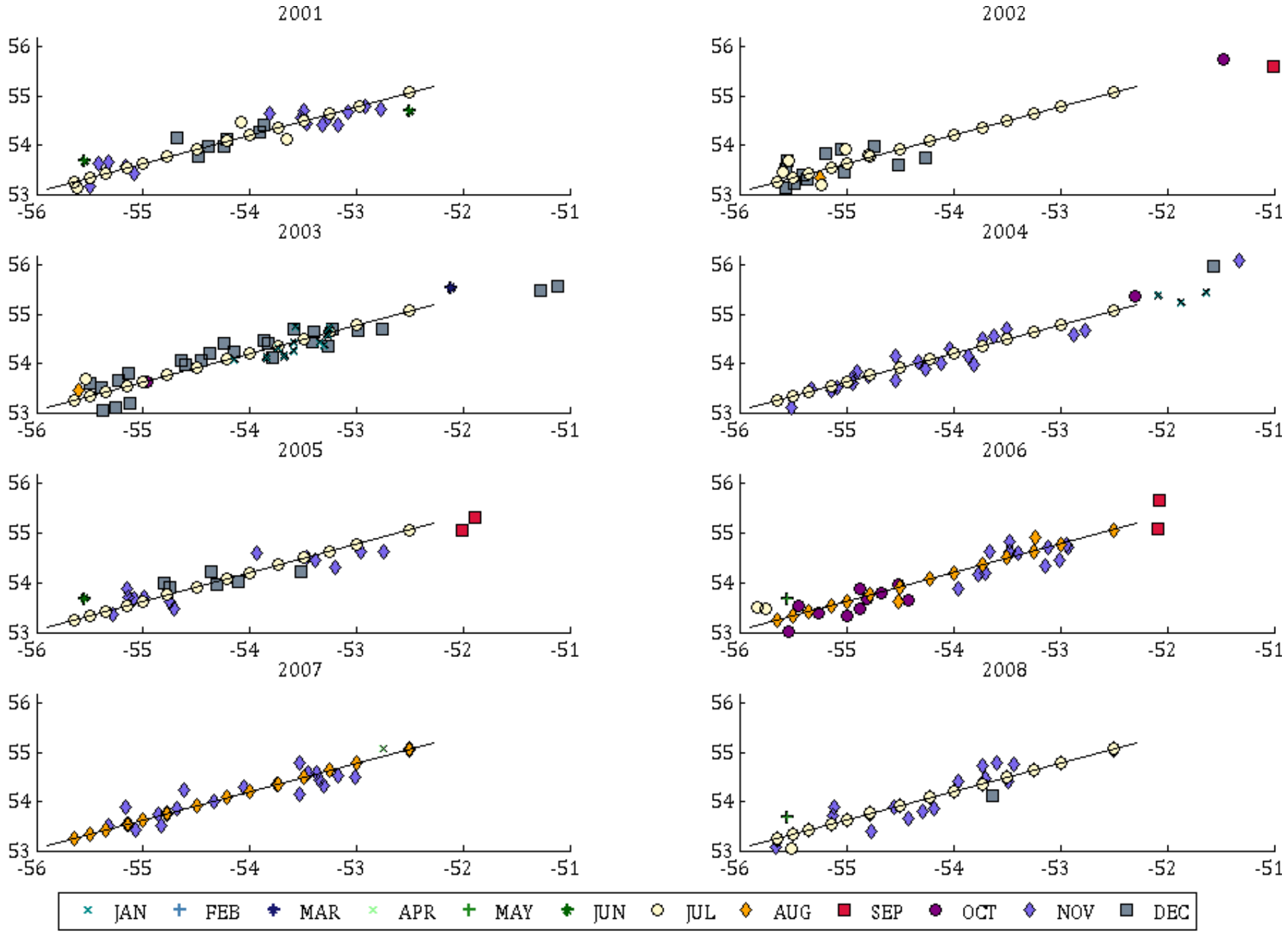
2001
2002
2003
2004
2005
2006
2007
2008
56
55
54
53
-56
-55
-54
-53
-52
-51
JAN
FEB
MAR
APR
MAY
JUN
JUL
AUG
SEP
OCT
NOV
DEC

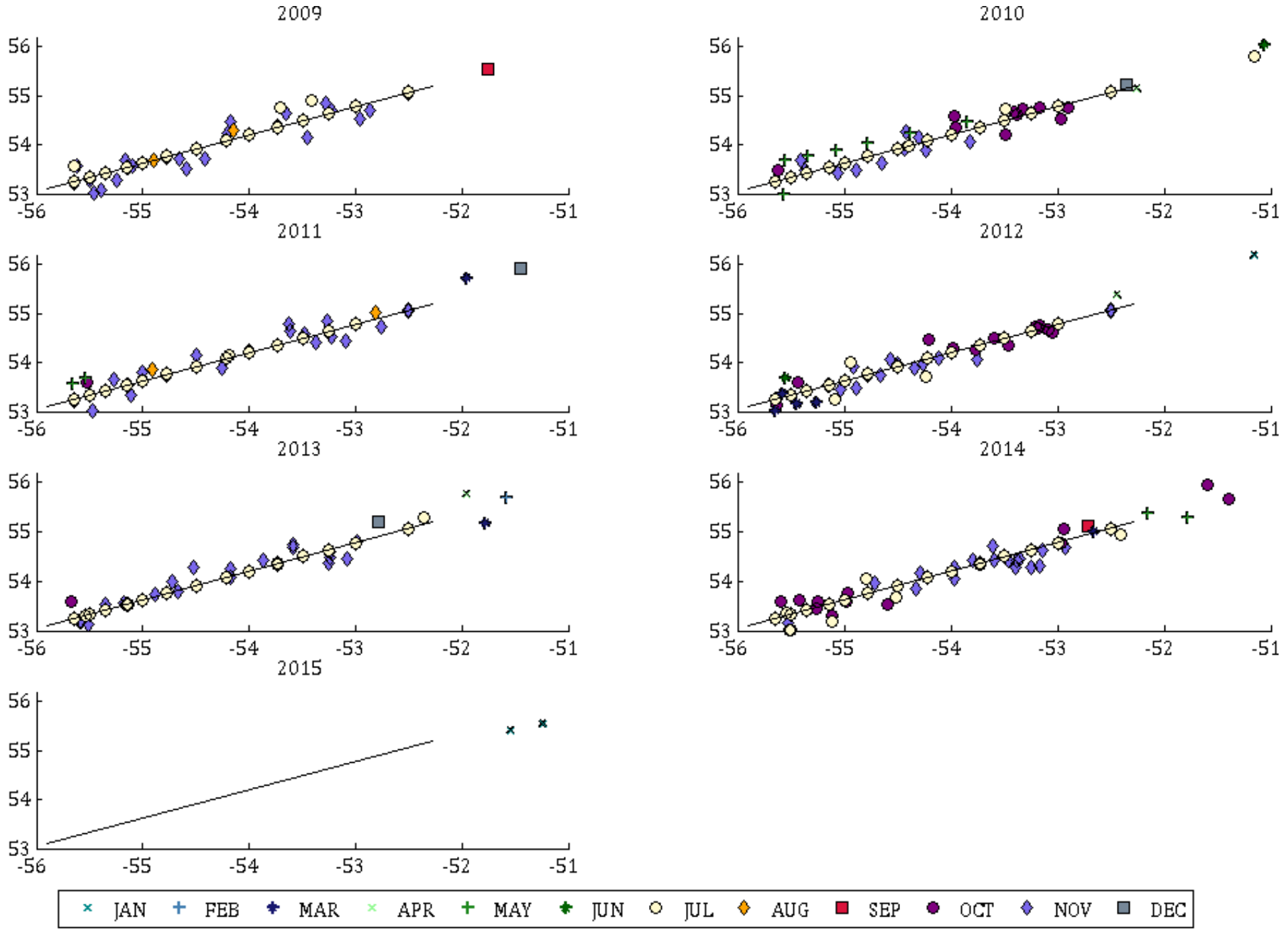
2009
2010
2011
2012
2013
2014
2015
56
55
54
53
-56
-55
-54
-53
-52
-51
JAN
FEB
MAR
APR
MAY
JUN
JUL
AUG
SEP
OCT
NOV
DEC

1.2 Final distribution of summer stations at the Seal Island

This appendix shows the final distribution of stations after suitable profiles have been selected. Missing years do not contain enough information across the shelf to make a section. The Seal Island standard stations are shown by the grey circles and the official transect, given by the best fitting line across the stations, is shown by the overlying line. The positions of the final yearly available observations is shown by the black diamonds.

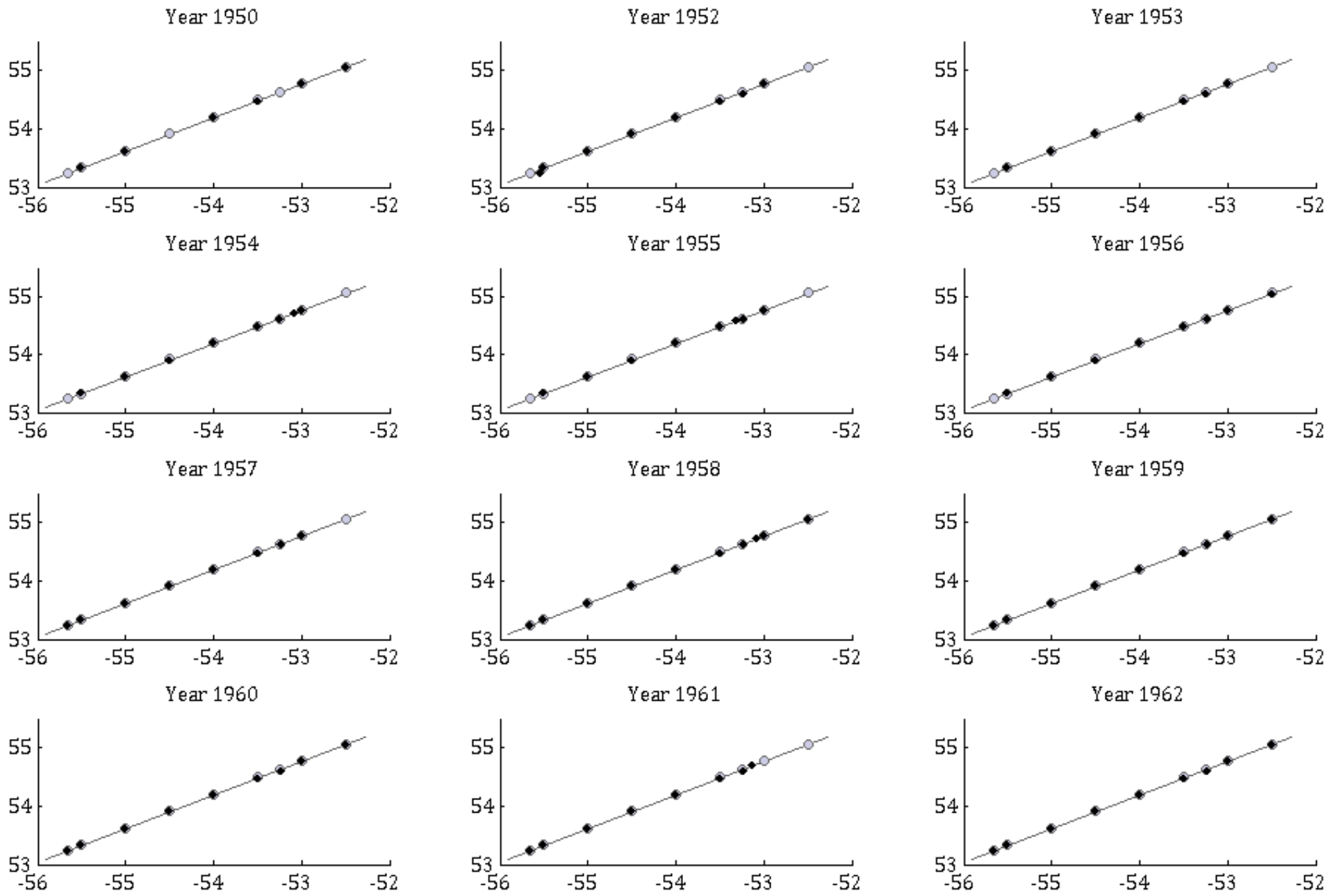
Year 1950
Year 1952
Year 1953
Year 1954
Year 1955
Year 1956
Year 1957
Year 1958
Year 1959
Year 1960
Year 1961
Year 1962
55
54
53
-56
-55
-54
-53
-52

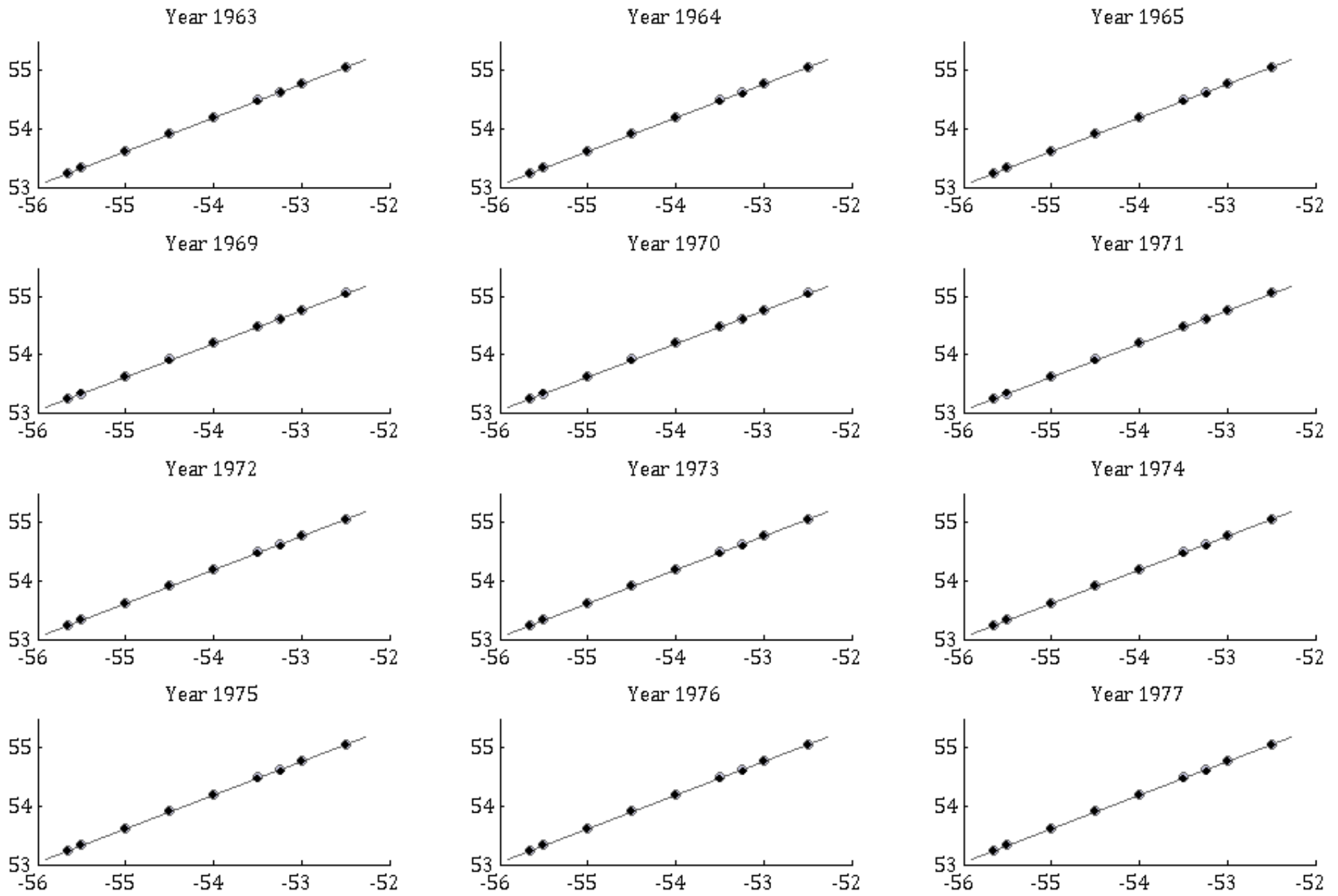
Year 1963
Year 1964
Year 1965
Year 1969
Year 1970
Year 1971
Year 1972
Year 1973
Year 1974
Year 1975
Year 1976
Year 1977
55
54
53
-56
-55
-54
-53
-52

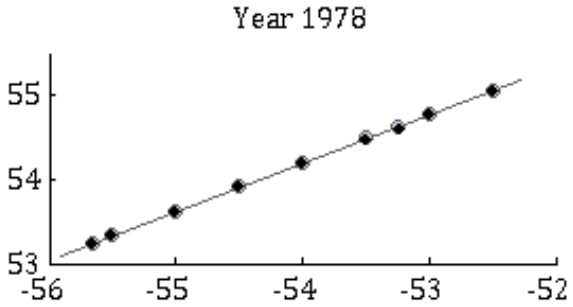
Year 1978
55
54
53
-56
-55
-54
-53
-52

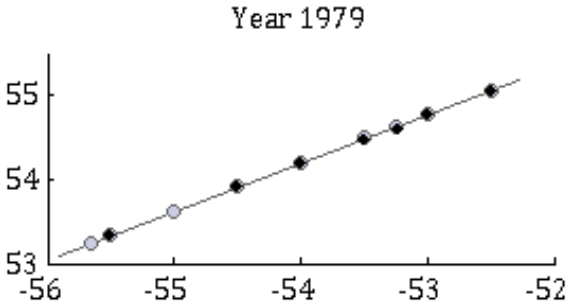
Year 1979
55
54
53
-56
-55
-54
-53
-52

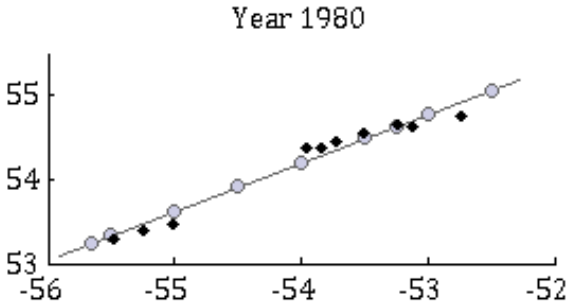
Year 1980
55
54
53
-56
-55
-54
-53
-52

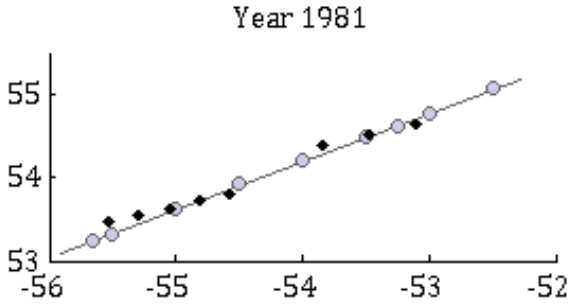
Year 1981
55
54
53
-56
-55
-54
-53
-52

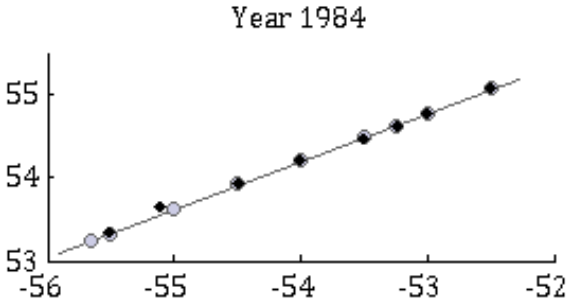
Year 1984
55
54
53
-56
-55
-54
-53
-52

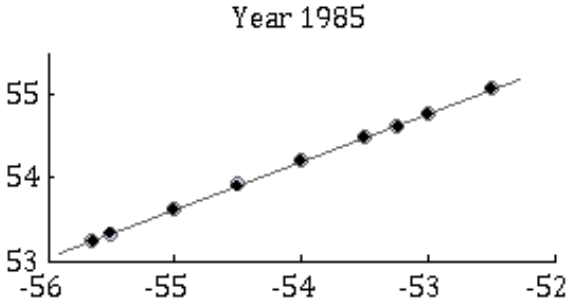
Year 1985
55
54
53
-56
-55
-54
-53
-52

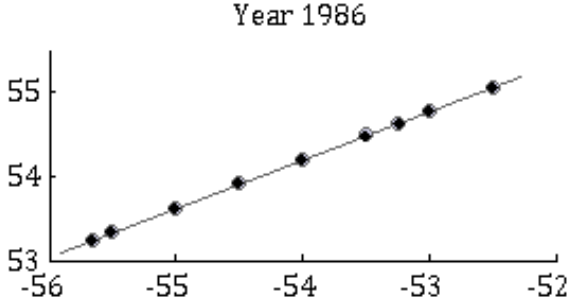
Year 1986
55
54
53
-56
-55
-54
-53
-52

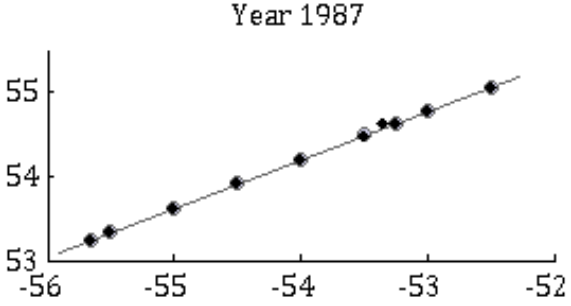
Year 1987
55
54
53
-56
-55
-54
-53
-52

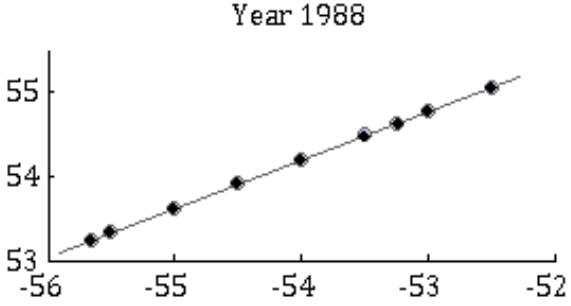
Year 1988
55
54
53
-56
-55
-54
-53
-52

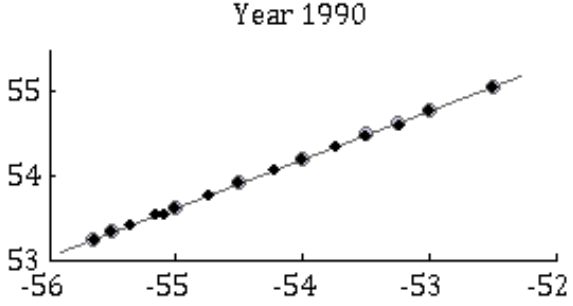
Year 1990
55
54
53
-56
-55
-54
-53
-52

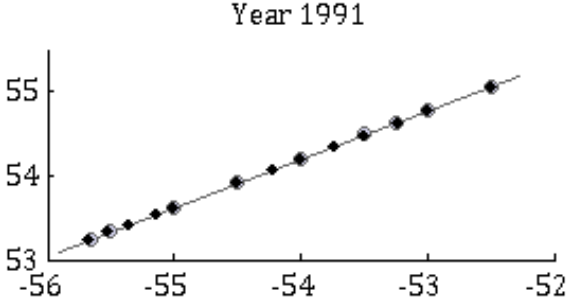
Year 1991
55
54
53
-56
-55
-54
-53
-52

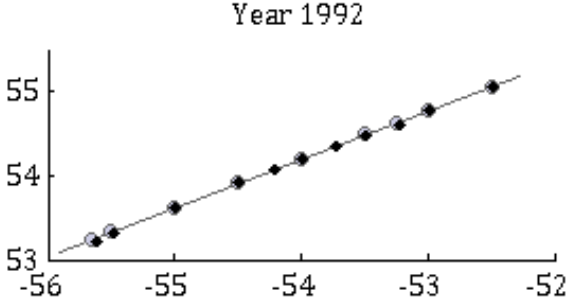
Year 1992
55
54
53
-56
-55
-54
-53
-52

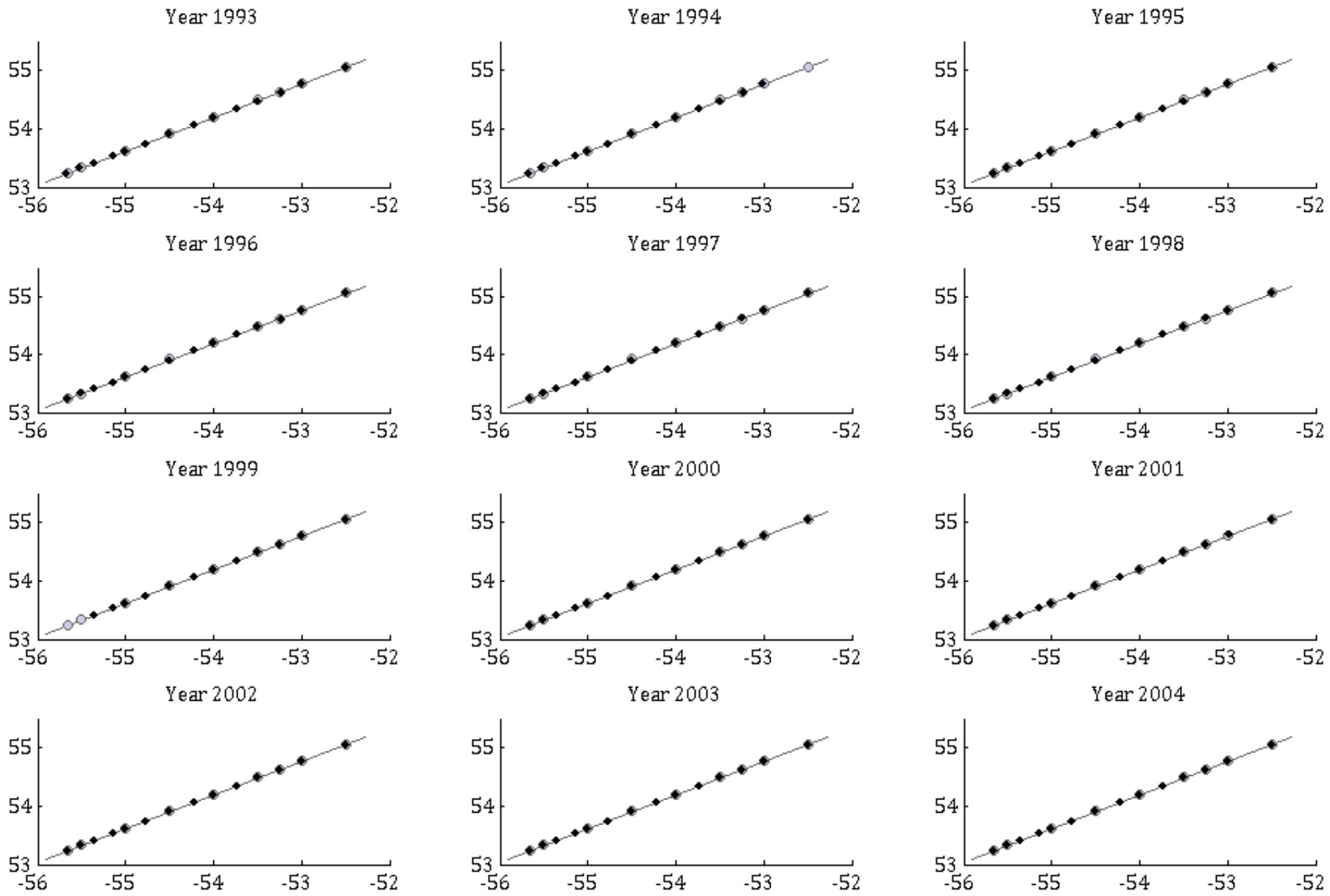
Year 1993
Year 1994
Year 1995
Year 1996
Year 1997
Year 1998
Year 1999
Year 2000
Year 2001
Year 2002
Year 2003
Year 2004
55
54
53
-56
-55
-54
-53
-52

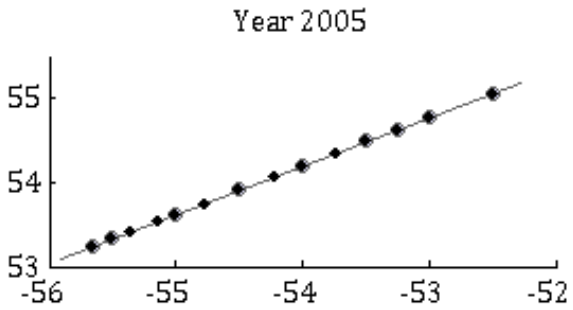
Year 2005
55
54
53
-56
-55
-54
-53
-52

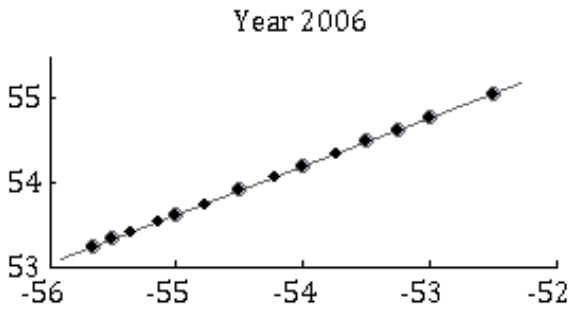
Year 2006
55
54
53
-56
-55
-54
-53
-52

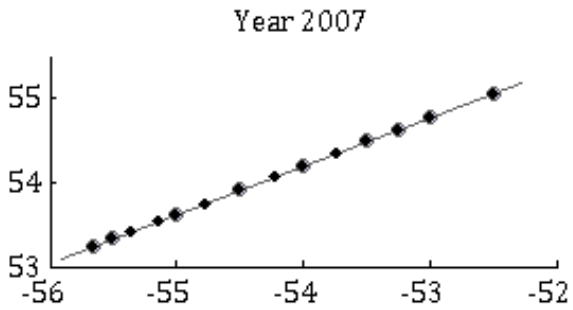
Year 2007
55
54
53
-56
-55
-54
-53
-52

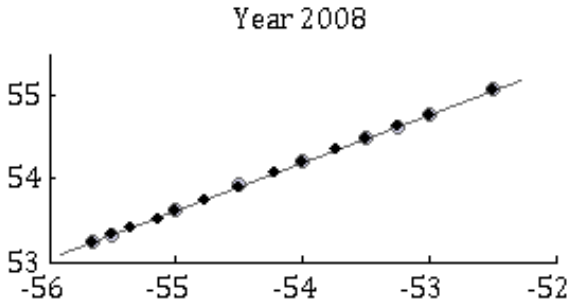
Year 2008
55
54
53
-56
-55
-54
-53
-52

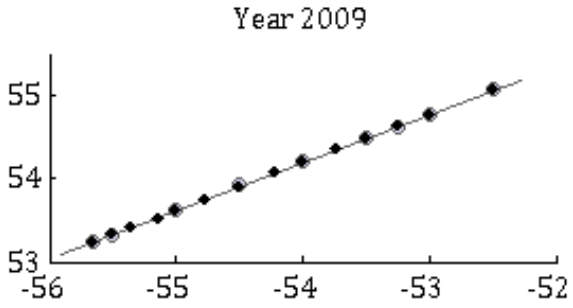
Year 2009
55
54
53
-56
-55
-54
-53
-52

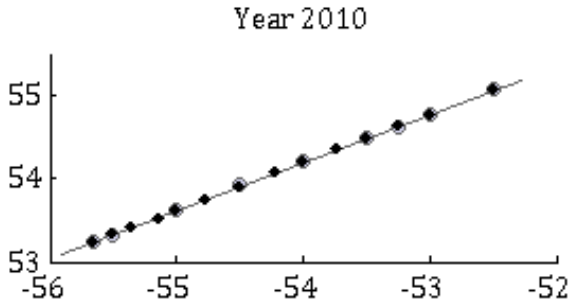
Year 2010
55
54
53
-56
-55
-54
-53
-52

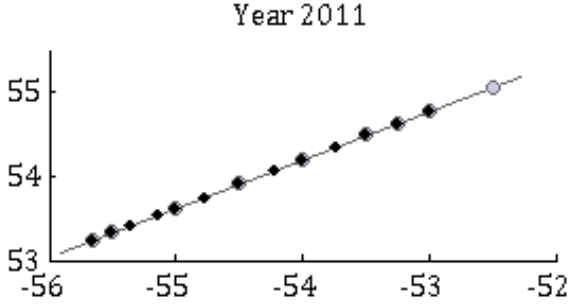
Year 2011
55
54
53
-56
-55
-54
-53
-52

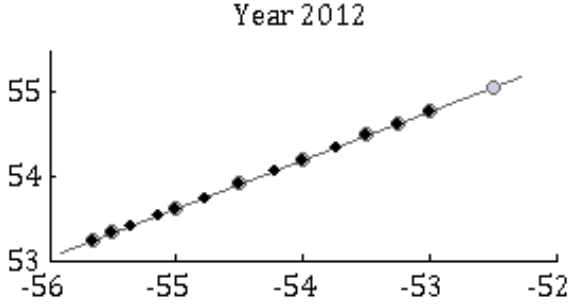
Year 2012
55
54
53
-56
-55
-54
-53
-52

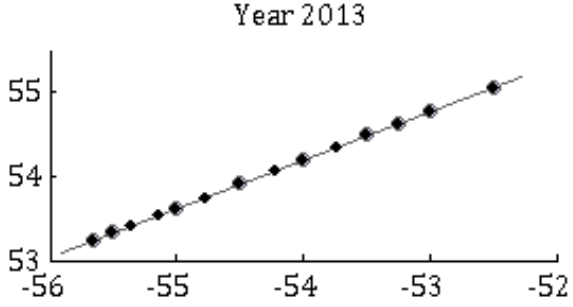
Year 2013
55
54
53
-56
-55
-54
-53
-52

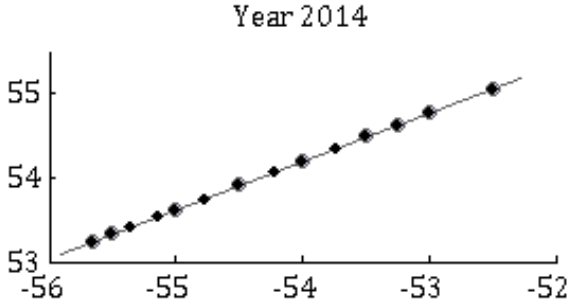
Year 2014
55
54
53
-56
-55
-54
-53
-52

1.3 Final temperature summer sections at the Seal Island

The computed temperature summer sections from 1950 to 2014 are shown here. Missing years do not contain enough information for a section. The shelf is shown in dark grey and computed from the maximum depth reached by the profiles. The reference ($x = 0$) is given by the most inshore profile. The x-axis shows the distance in km from the reference. The vertical axis displays depth (in m). The position of profiles and their depth bins are shown by the black dots. Data have bin vertically binned to 1 m and interpolated horizontally onto a 2.5 km grid. Missing information at the bottom and the sides have been completed with climatological values. The color scale, shown below, displays temperature in °C.

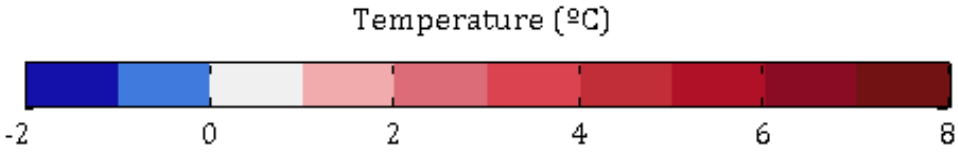

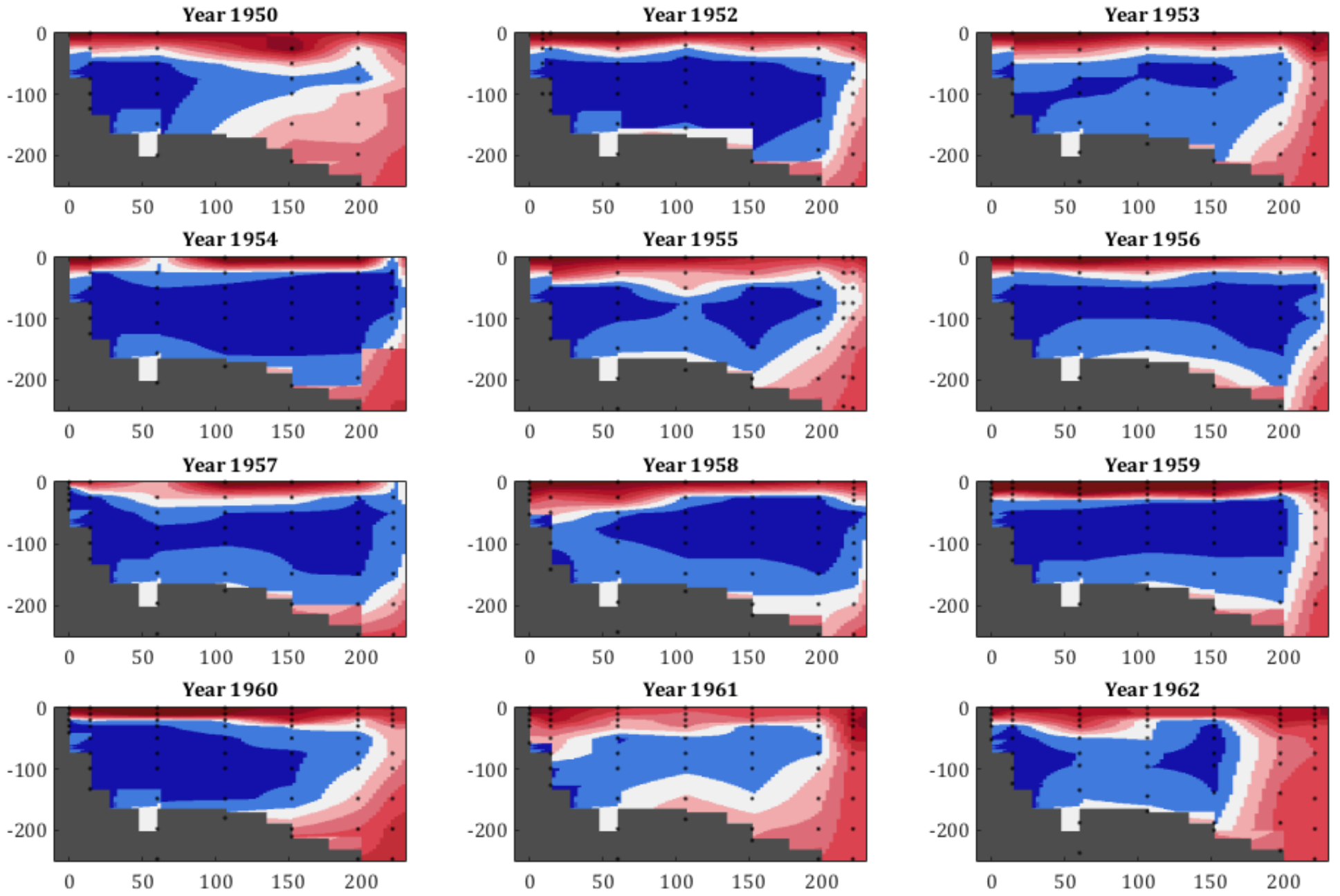
Year 1950
Year 1952
Year 1953
Year 1954
Year 1955
Year 1956
Year 1957
Year 1958
Year 1959
Year 1960
Year 1961
Year 1962
0
-100
-200
0
50
100
150
200

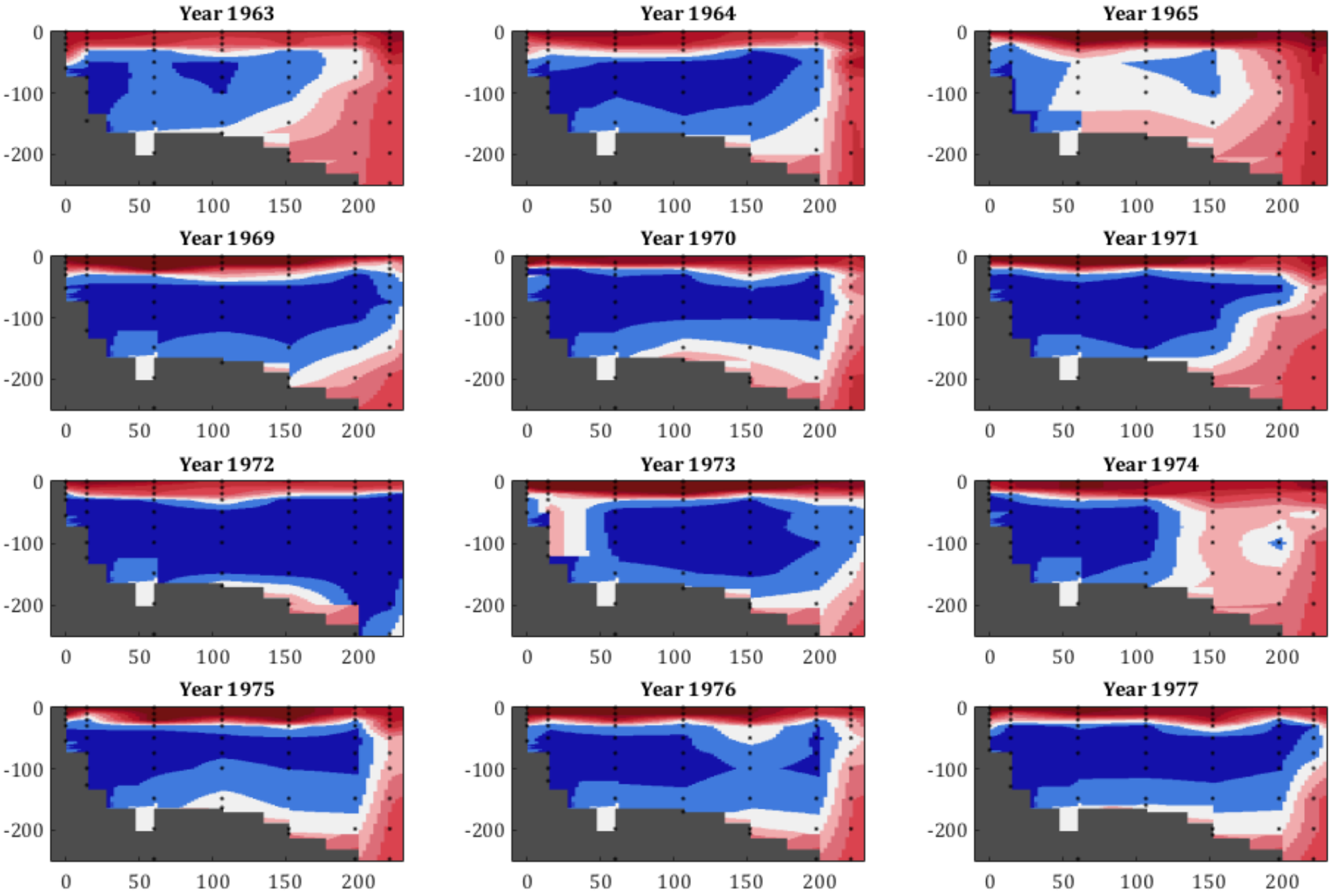
Year 1963
Year 1964
Year 1965
Year 1969
Year 1970
Year 1971
Year 1972
Year 1973
Year 1974
Year 1975
Year 1976
Year 1977
0
-100
-200
0
50
100
150
200

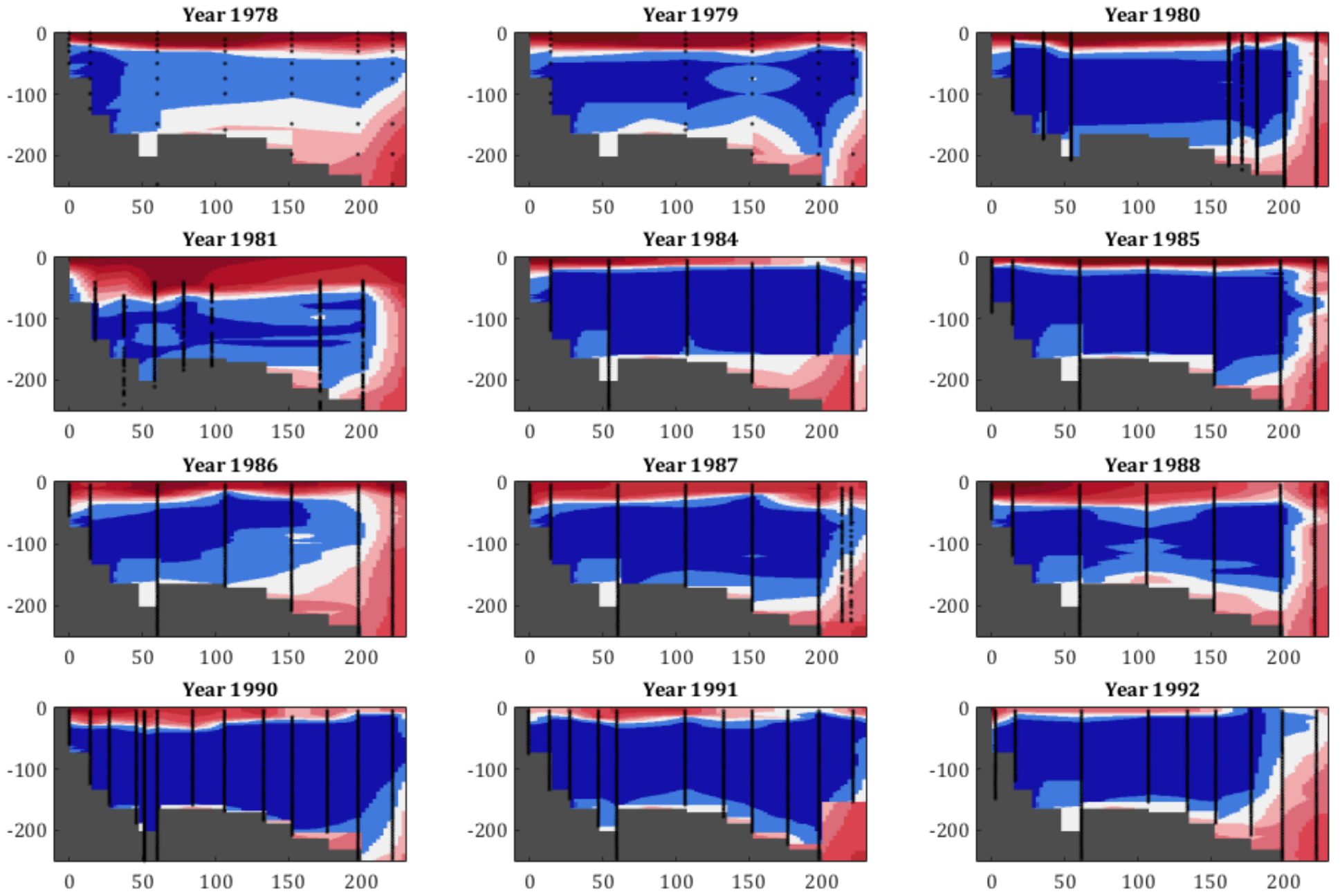
Year 1978
Year 1979
Year 1980
Year 1981
Year 1984
Year 1985
Year 1986
Year 1987
Year 1988
Year 1990
Year 1991
Year 1992
0
-100
-200
0
50
100
150
200

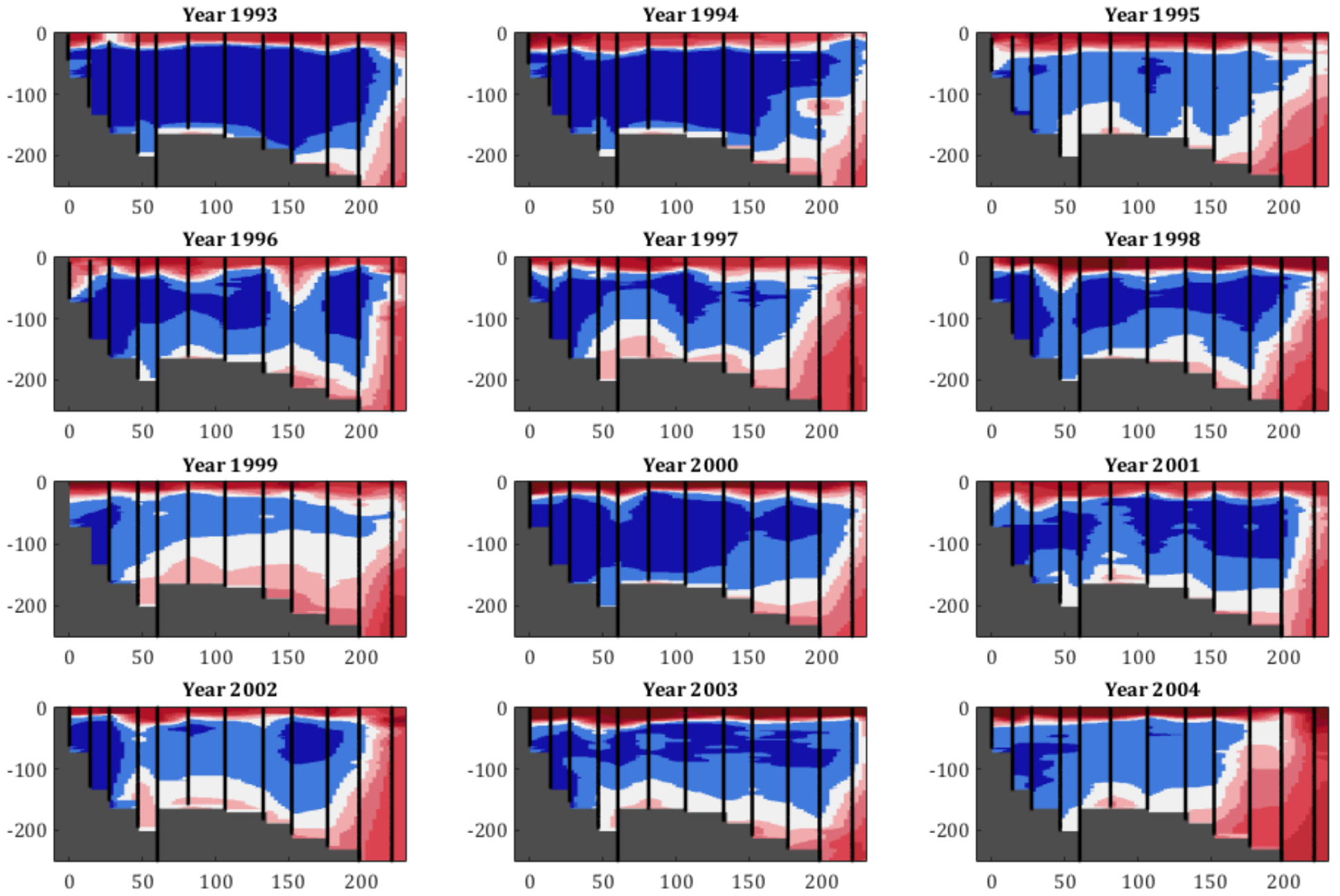
Year 1993
Year 1994
Year 1995
Year 1996
Year 1997
Year 1998
Year 1999
Year 2000
Year 2001
Year 2002
Year 2003
Year 2004
0
-100
-200
0
50
100
150
200

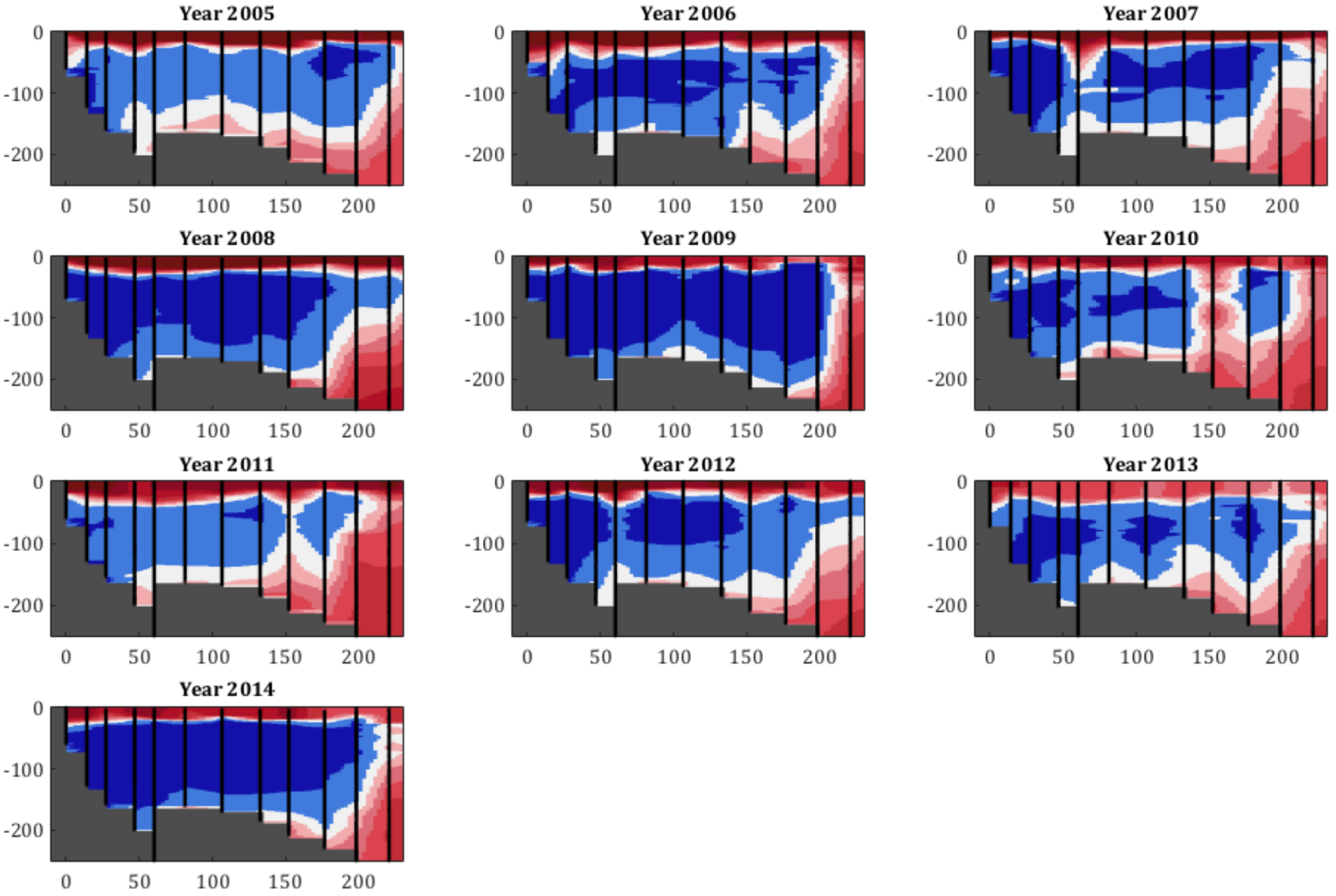
Year 2005
Year 2006
Year 2007
Year 2008
Year 2009
Year 2010
Year 2011
Year 2012
Year 2013
Year 2014
0
-100
-200
0
50
100
150
200

1.4 Final salinity summer sections at the Seal Island

The computed salinity summer sections from 1950 to 2014 are shown here. Missing years do not contain enough information for a section. The shelf is shown in dark grey and computed from the maximum depth reached by the profiles. The reference ($x = 0$) is given by the most inshore profile. The x-axis shows the distance in km from the reference. The vertical axis displays depth (in m). The position of profiles and their depth bins are shown by the black dots. Data have bin vertically binned to 1 m and interpolated horizontally onto a 2.5 km grid. Missing information at the bottom and the sides have been completed with climatological values. The color scale, shown below, displays salinity.

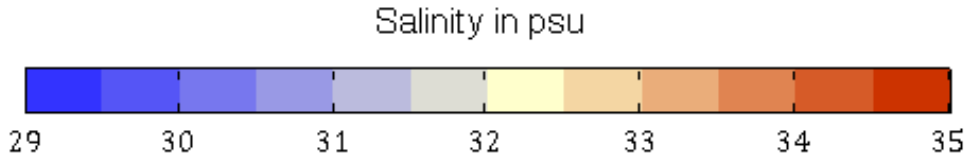

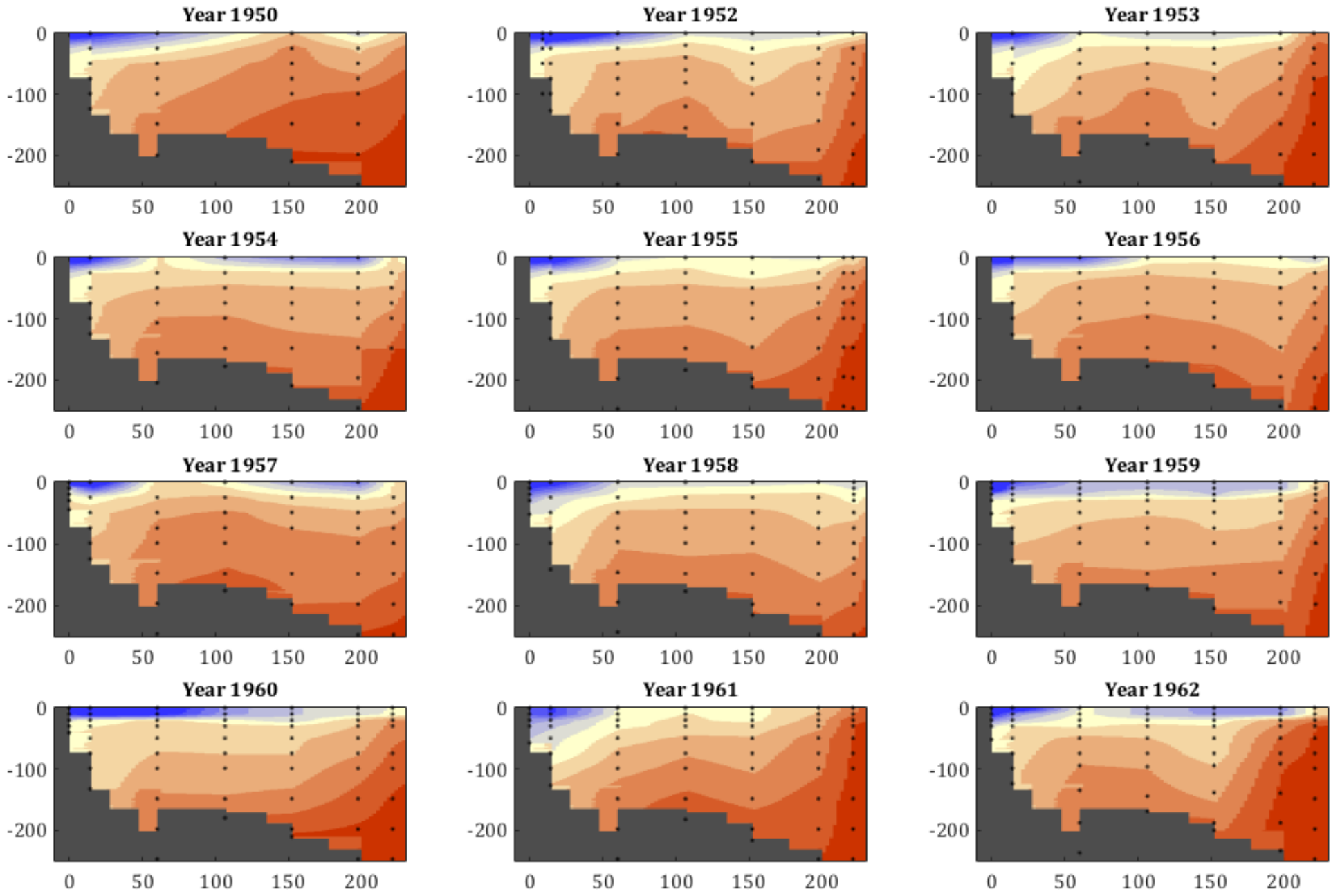
Year 1950
Year 1952
Year 1953
Year 1954
Year 1955
Year 1956
Year 1957
Year 1958
Year 1959
Year 1960
Year 1961
Year 1962
0
-100
-200
0
50
100
150
200

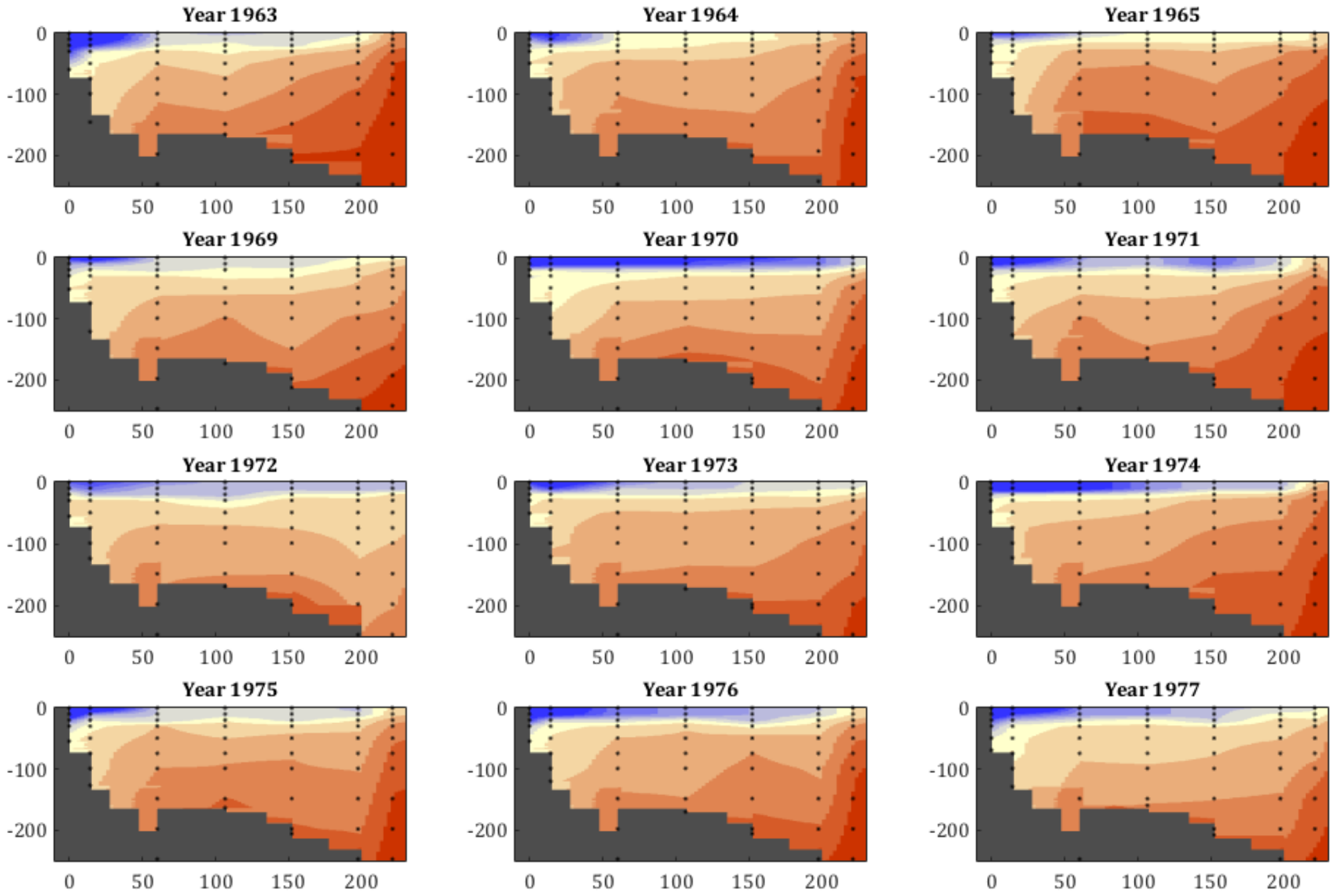
Year 1963
Year 1964
Year 1965
Year 1969
Year 1970
Year 1971
Year 1972
Year 1973
Year 1974
Year 1975
Year 1976
Year 1977
0
-100
-200
0
50
100
150
200

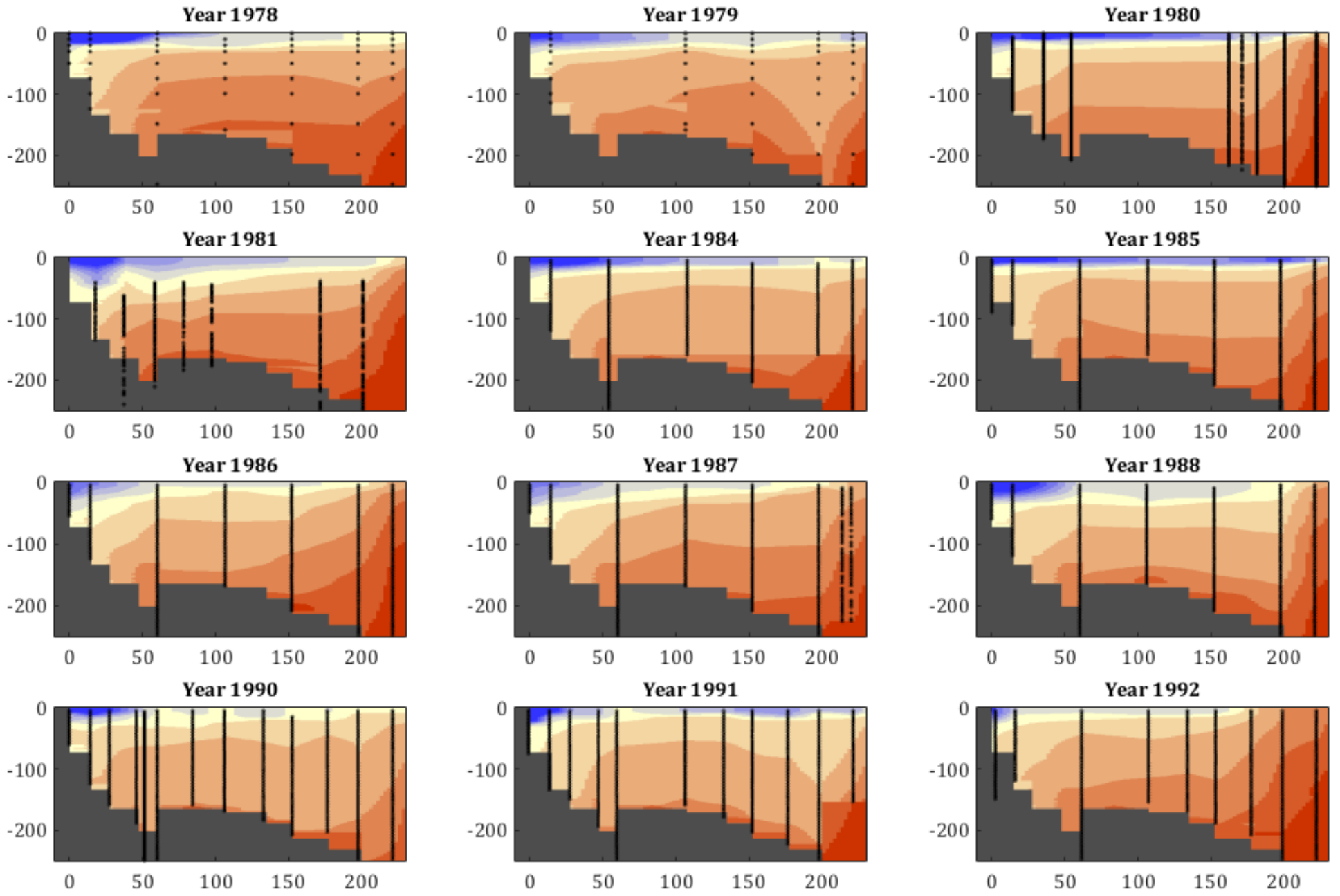
Year 1978
Year 1979
Year 1980
Year 1981
Year 1984
Year 1985
Year 1986
Year 1987
Year 1988
Year 1990
Year 1991
Year 1992
0
-100
-200
0
50
100
150
200

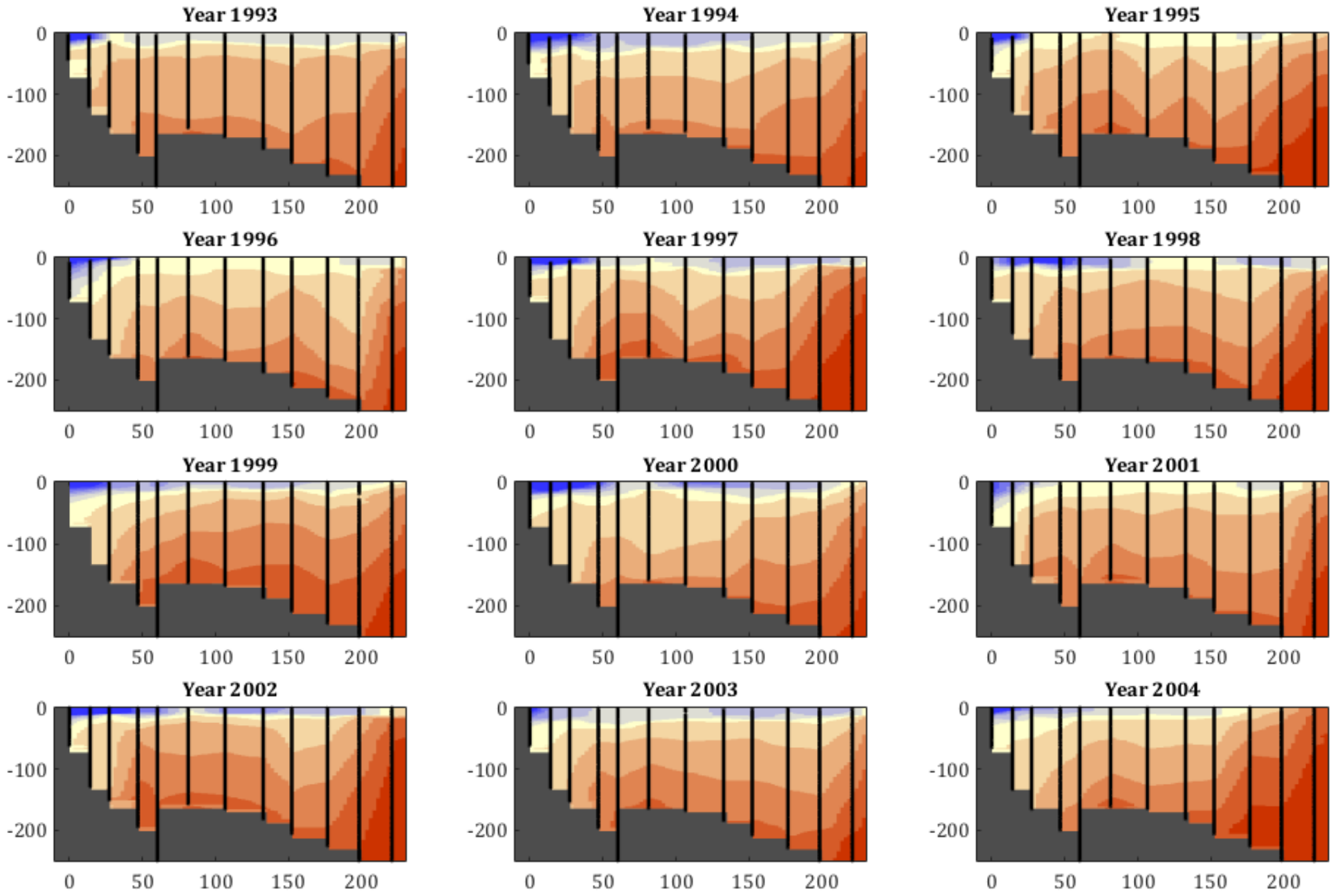
Year 1993
Year 1994
Year 1995
Year 1996
Year 1997
Year 1998
Year 1999
Year 2000
Year 2001
Year 2002
Year 2003
Year 2004
0
-100
-200
0
50
100
150
200

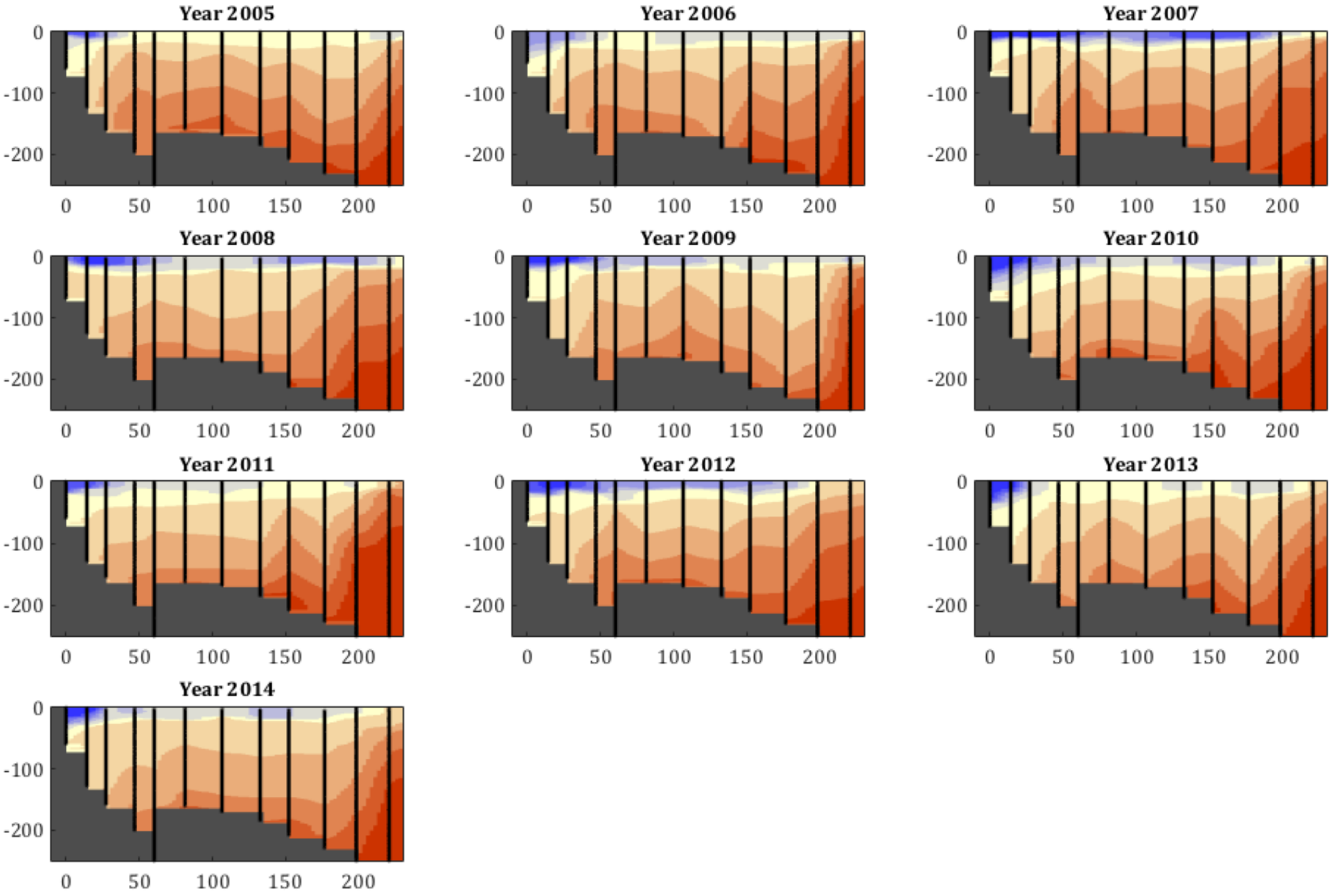
Year 2005
Year 2006
Year 2007
Year 2008
Year 2009
Year 2010
Year 2011
Year 2012
Year 2013
Year 2014
0
-100
-200
0
50
100
150
200

1.5 Final density summer sections at the Seal Island

The calculated density summer sections from 1950 to 2014 are shown here. Missing years do not contain enough information for a section. The shelf is shown in dark grey and computed from the maximum depth reached by the profiles. The reference ($x = 0$) is given by the most inshore profile. The x-axis shows the distance in km from the reference. The vertical axis displays depth (in m). The position of profiles and their depth bins are shown by the black dots. Data have bin vertically binned to 1 m and interpolated horizontally onto a 2.5 km grid. Missing information at the bottom and the sides have been completed with climatological values. The color scale, shown below, displays density (σ_0) referenced to surface, in kg/m^3 and subtracting 1000.

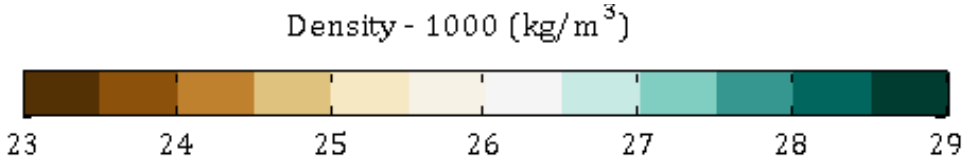

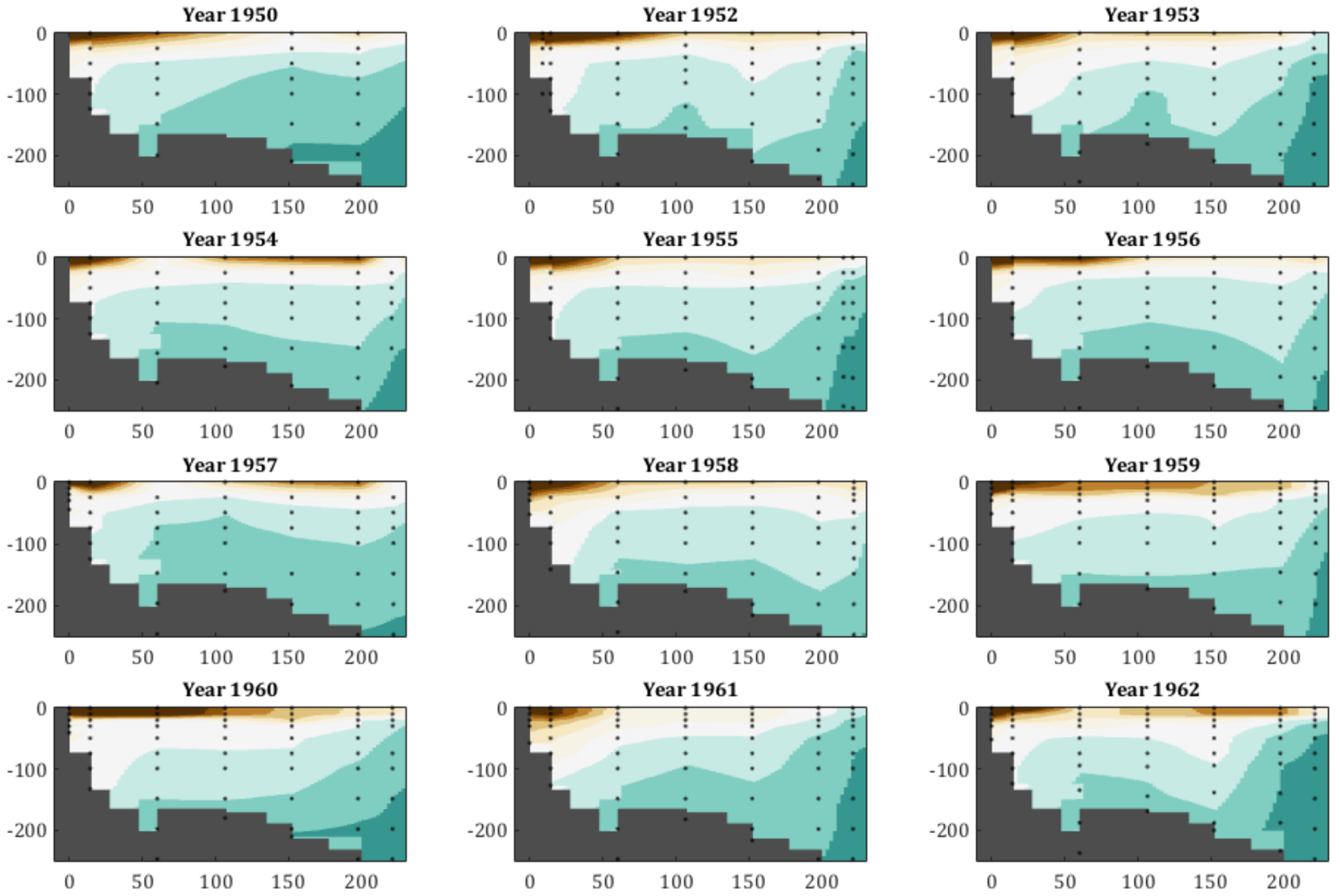
Year 1950
Year 1952
Year 1953
Year 1954
Year 1955
Year 1956
Year 1957
Year 1958
Year 1959
Year 1960
Year 1961
Year 1962
0
-100
-200
0
50
100
150
200

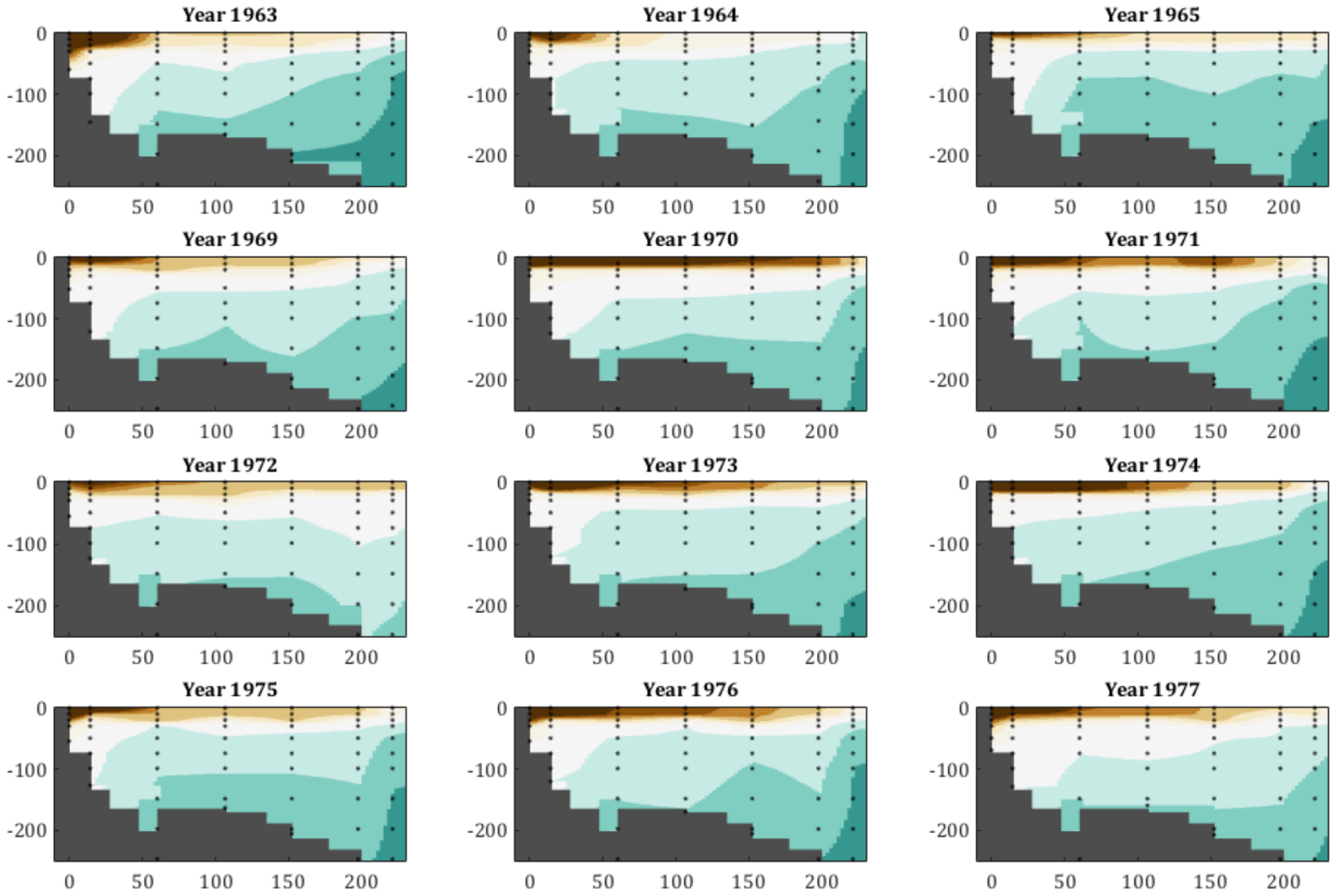
Year 1963
Year 1964
Year 1965
Year 1969
Year 1970
Year 1971
Year 1972
Year 1973
Year 1974
Year 1975
Year 1976
Year 1977
0
-100
-200
0
50
100
150
200

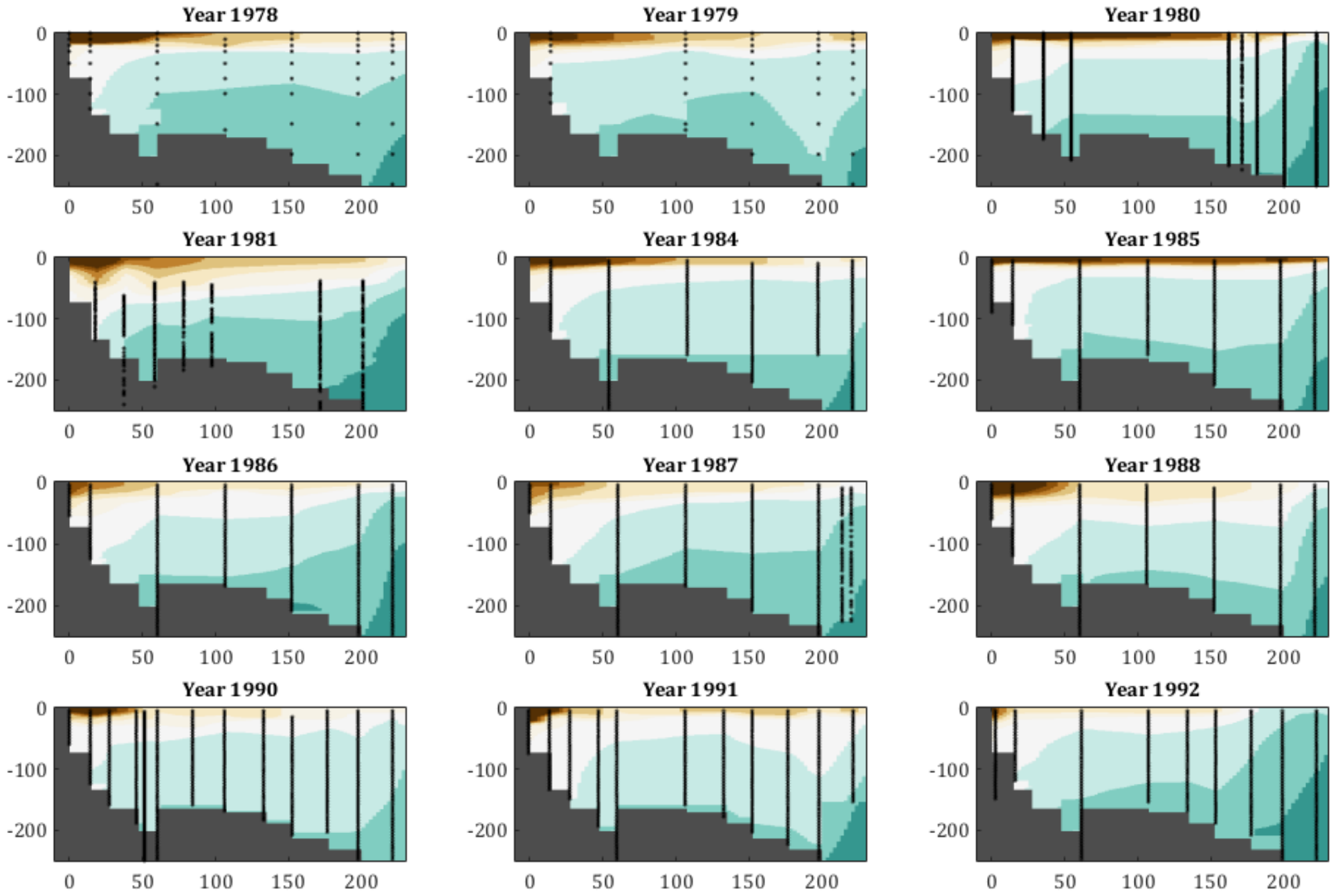
Year 1978
Year 1979
Year 1980
Year 1981
Year 1984
Year 1985
Year 1986
Year 1987
Year 1988
Year 1990
Year 1991
Year 1992
0
-100
-200
0
50
100
150
200

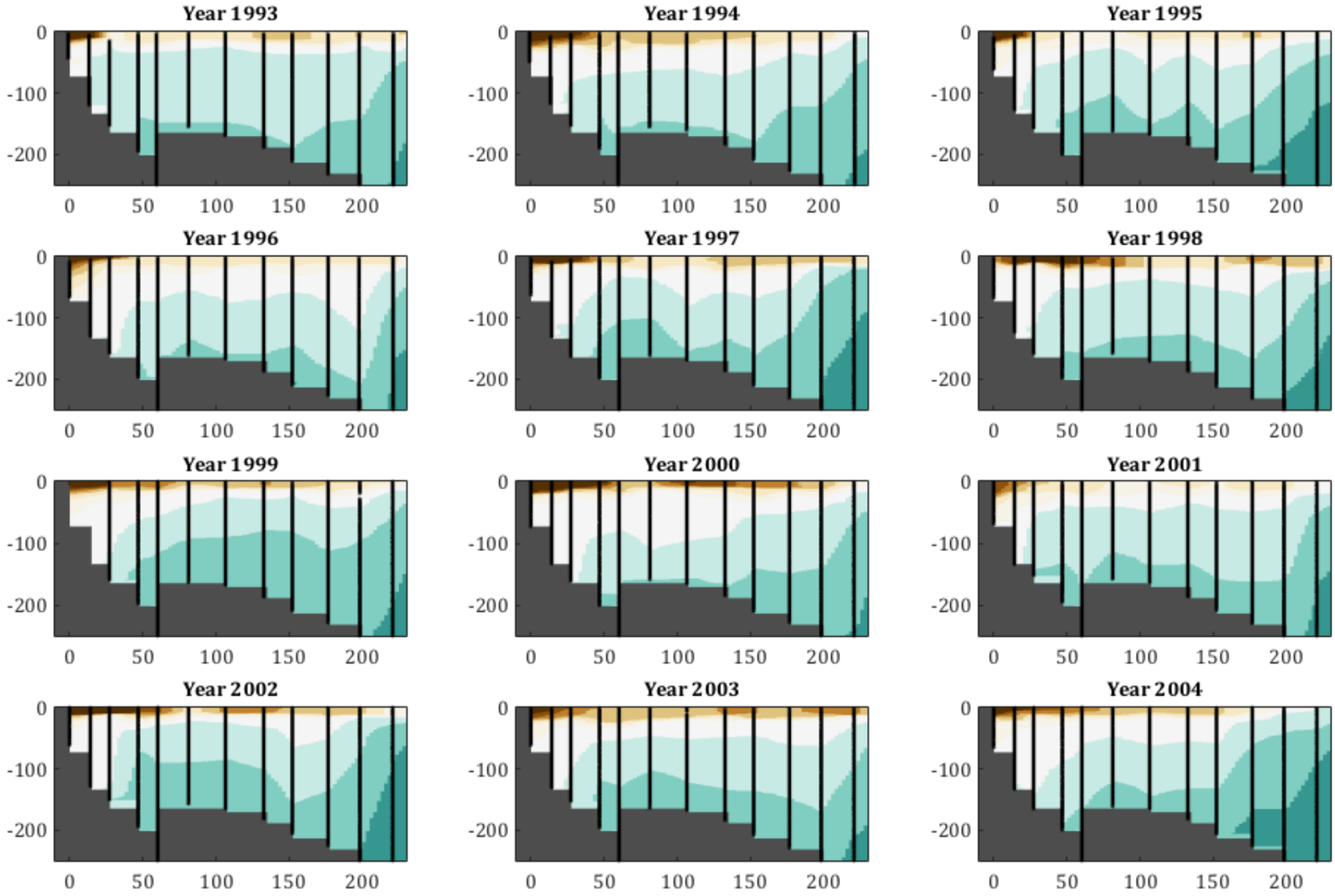
Year 1993
Year 1994
Year 1995
Year 1996
Year 1997
Year 1998
Year 1999
Year 2000
Year 2001
Year 2002
Year 2003
Year 2004
0
-100
-200
0
50
100
150
200

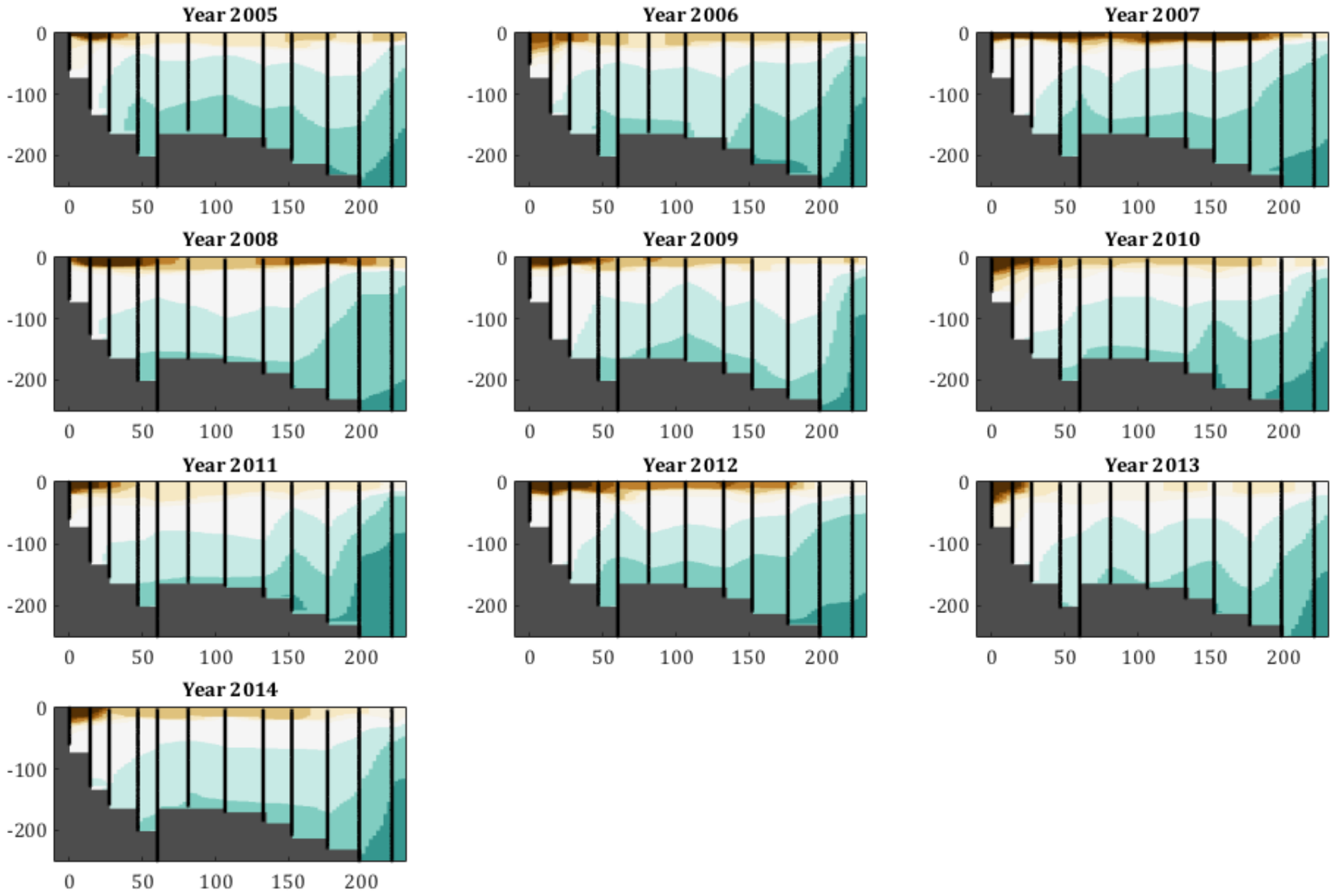
Year 2005
Year 2006
Year 2007
Year 2008
Year 2009
Year 2010
Year 2011
Year 2012
Year 2013
Year 2014
0
-100
-200
0
50
100
150
200

1.6 Final geostrophic velocity summer sections at the Seal Island

The calculated geostrophic velocity summer sections from 1950 to 2014 are shown here. Missing years do not contain enough information for a section. The shelf is shown in dark grey and computed from the maximum depth reached by the profiles. The reference ($x = 0$) is given by the most inshore profile. The x-axis shows the distance in km from the reference. The vertical axis displays depth (in m). The position of profiles and their depth bins are shown by the black dots. Data have bin vertically binned to 1 m and interpolated horizontally onto a 2.5 km grid. Missing information at the bottom and the sides have been completed with climatological values. The color scale, shown below, displays velocity in m/s.

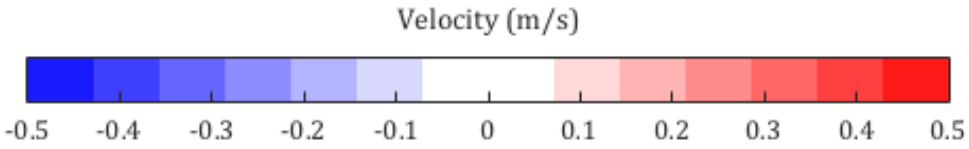

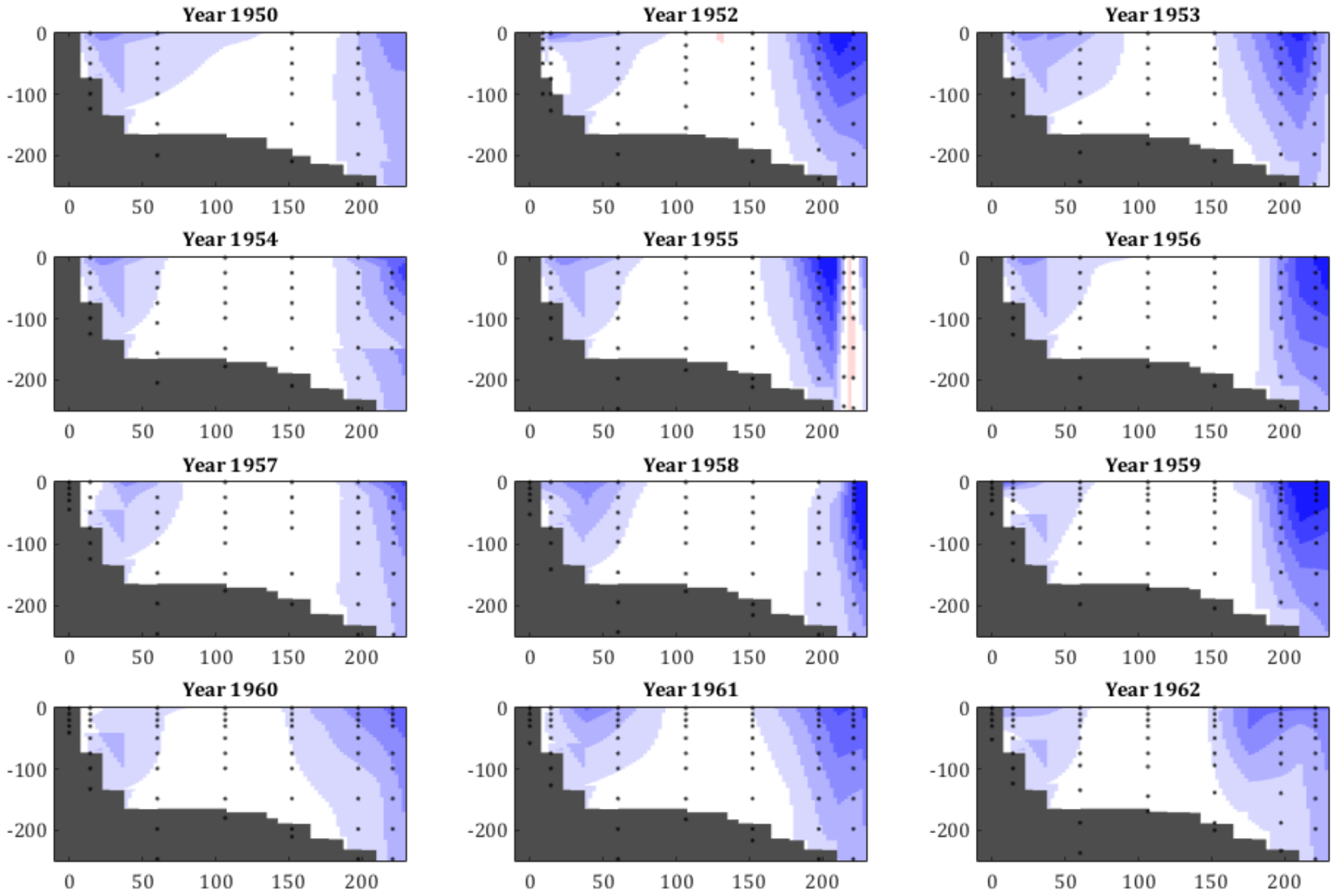
Year 1950
Year 1952
Year 1953
Year 1954
Year 1955
Year 1956
Year 1957
Year 1958
Year 1959
Year 1960
Year 1961
Year 1962
0
-100
-200
0
50
100
150
200

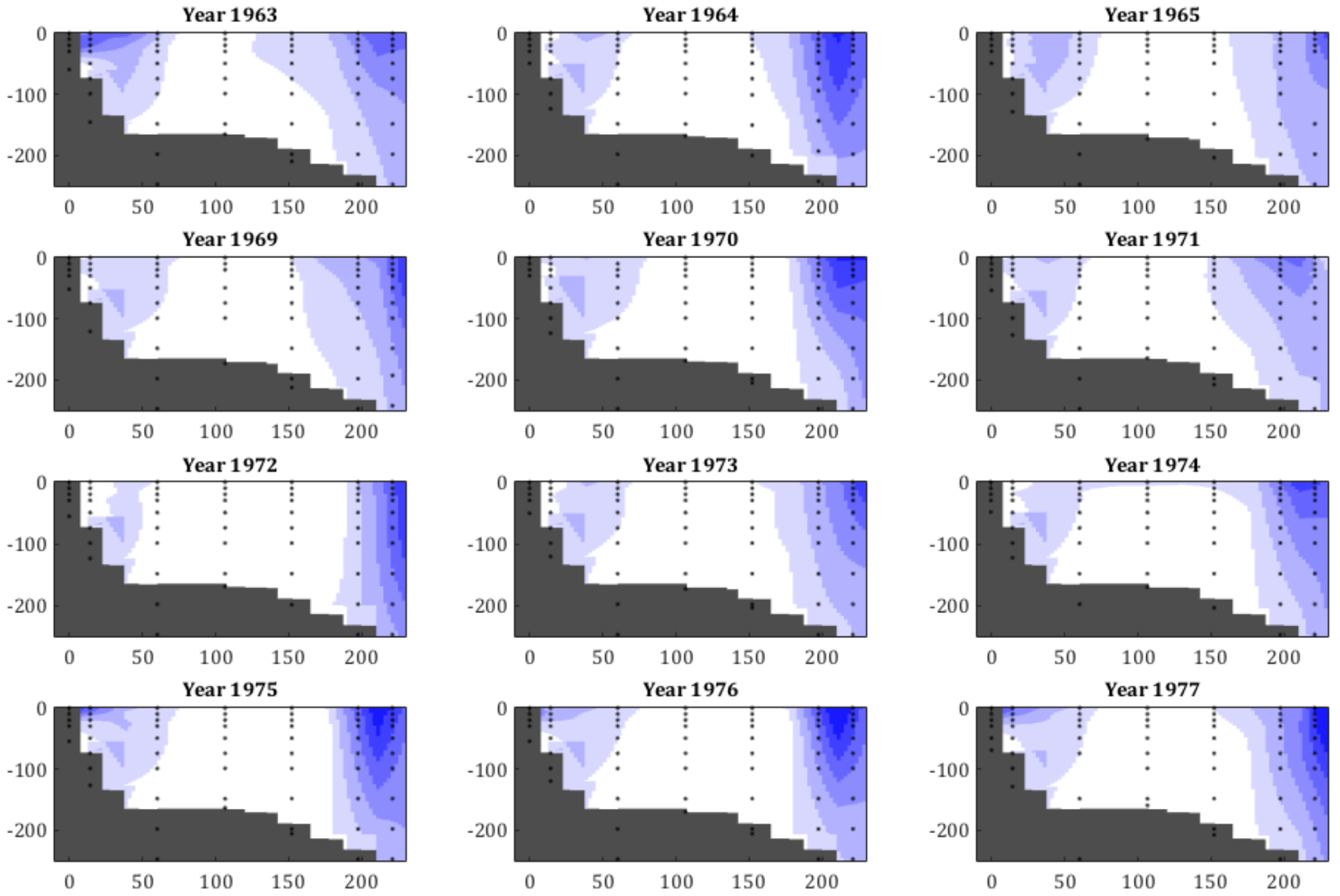
Year 1963
Year 1964
Year 1965
Year 1969
Year 1970
Year 1971
Year 1972
Year 1973
Year 1974
Year 1975
Year 1976
Year 1977
0
-100
-200
0
50
100
150
200

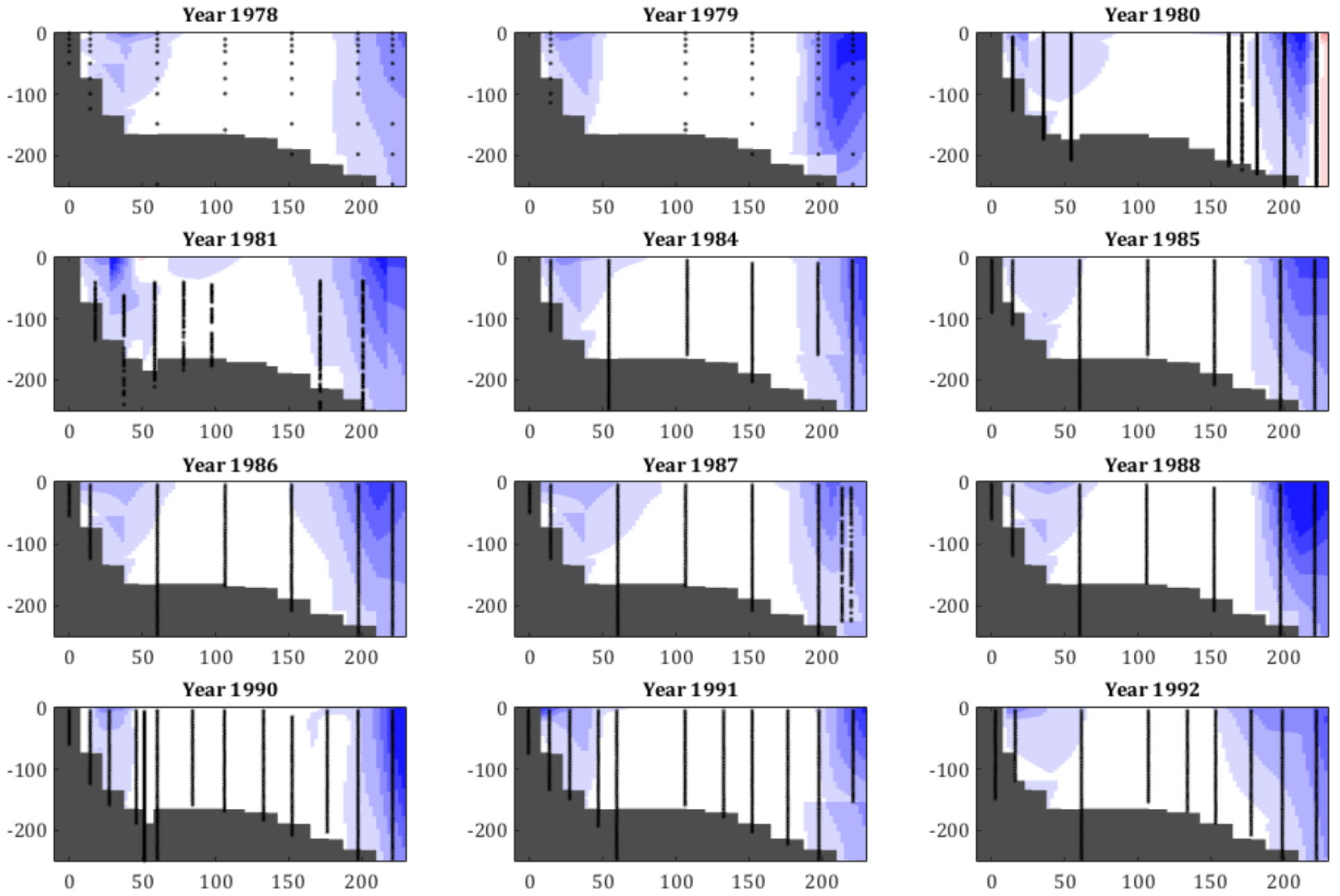
Year 1978
Year 1979
Year 1980
Year 1981
Year 1984
Year 1985
Year 1986
Year 1987
Year 1988
Year 1990
Year 1991
Year 1992
0
-100
-200
0
50
100
150
200

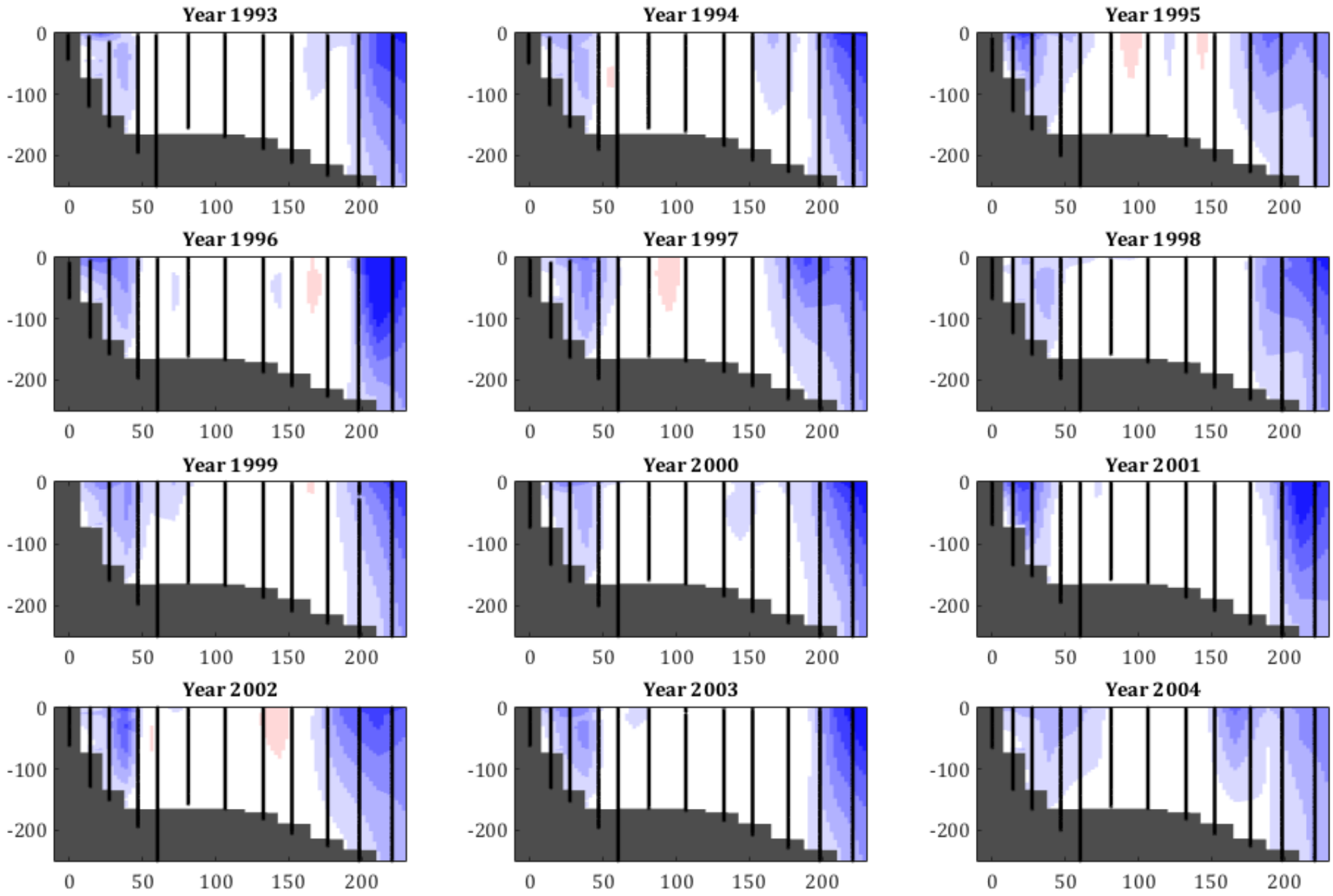
Year 1993
Year 1994
Year 1995
Year 1996
Year 1997
Year 1998
Year 1999
Year 2000
Year 2001
Year 2002
Year 2003
Year 2004
0
-100
-200
0
50
100
150
200

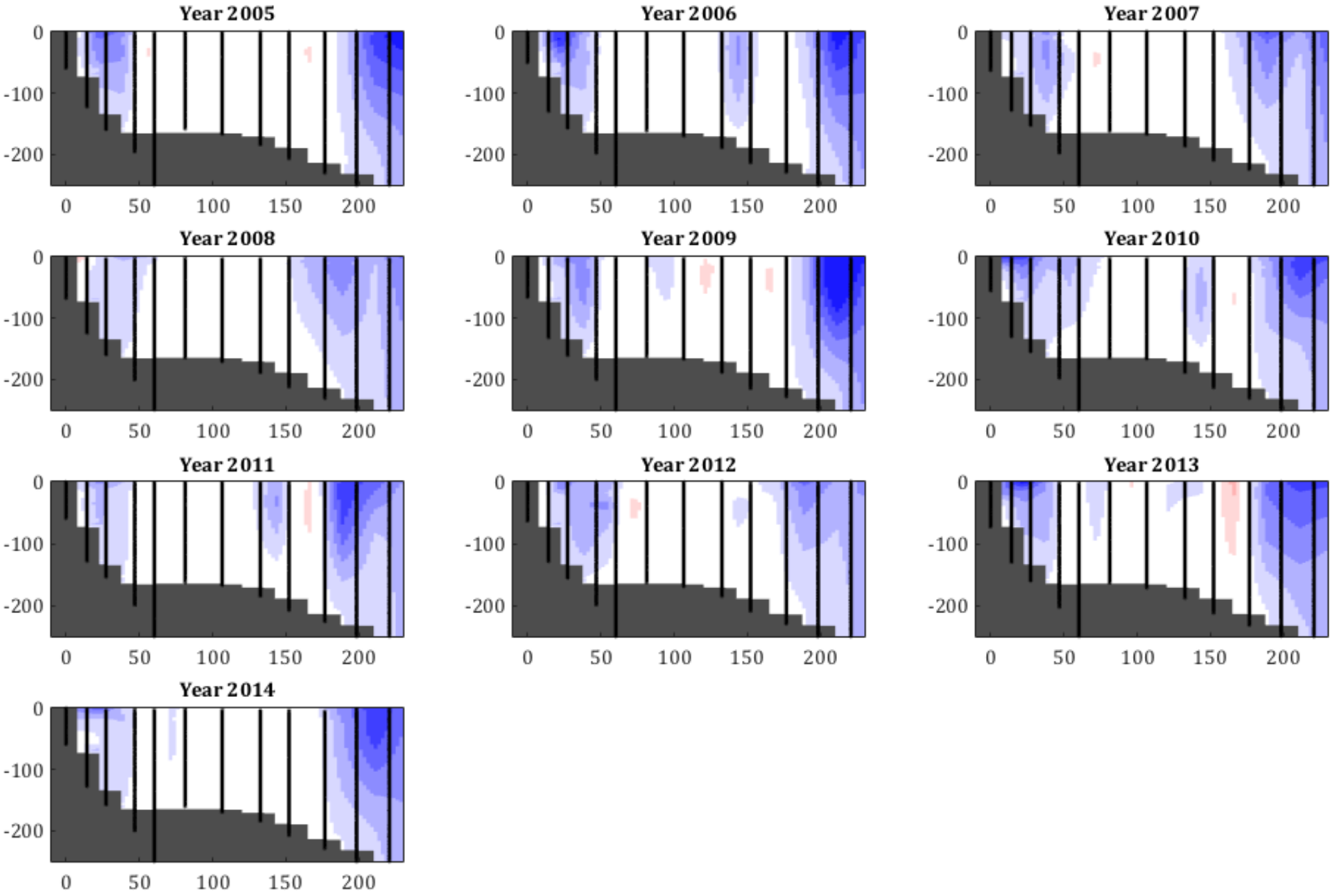
Year 2005
Year 2006
Year 2007
Year 2008
Year 2009
Year 2010
Year 2011
Year 2012
Year 2013
Year 2014
0
-100
-200
0
50
100
150
200